

University of Alberta

**Physiochemical and biological controls on barite precipitation and
petrography – Insights from subaerial barite-precipitating springs**

by

Sandy Marie Bonny



a thesis submitted to the Faculty of Graduate Studies and Research
in partial fulfillment of the requirements for the degree of

Doctor of Philosophy

Department of Earth and Atmospheric Sciences

Edmonton, Alberta
Fall 2007



Library and
Archives Canada

Bibliothèque et
Archives Canada

Published Heritage
Branch

Direction du
Patrimoine de l'édition

395 Wellington Street
Ottawa ON K1A 0N4
Canada

395, rue Wellington
Ottawa ON K1A 0N4
Canada

Your file *Votre référence*
ISBN: 978-0-494-32922-1
Our file *Notre référence*
ISBN: 978-0-494-32922-1

NOTICE:

The author has granted a non-exclusive license allowing Library and Archives Canada to reproduce, publish, archive, preserve, conserve, communicate to the public by telecommunication or on the Internet, loan, distribute and sell theses worldwide, for commercial or non-commercial purposes, in microform, paper, electronic and/or any other formats.

The author retains copyright ownership and moral rights in this thesis. Neither the thesis nor substantial extracts from it may be printed or otherwise reproduced without the author's permission.

AVIS:

L'auteur a accordé une licence non exclusive permettant à la Bibliothèque et Archives Canada de reproduire, publier, archiver, sauvegarder, conserver, transmettre au public par télécommunication ou par l'Internet, prêter, distribuer et vendre des thèses partout dans le monde, à des fins commerciales ou autres, sur support microforme, papier, électronique et/ou autres formats.

L'auteur conserve la propriété du droit d'auteur et des droits moraux qui protègent cette thèse. Ni la thèse ni des extraits substantiels de celle-ci ne doivent être imprimés ou autrement reproduits sans son autorisation.

In compliance with the Canadian Privacy Act some supporting forms may have been removed from this thesis.

Conformément à la loi canadienne sur la protection de la vie privée, quelques formulaires secondaires ont été enlevés de cette thèse.

While these forms may be included in the document page count, their removal does not represent any loss of content from the thesis.

Bien que ces formulaires aient inclus dans la pagination, il n'y aura aucun contenu manquant.


Canada

The Earth herself is thought alive, and all
Within; which living power can endow
The very stones with life: they crystallize
In forms quite regular with lines and sides,
In straight or curved angles sharp or flat.

Each growing from their original germs,
As plants from buds and seeds, while stony gems
From molecules arise: and altogether
In elements the stream of life imbibe.

C.S. Rafinesque (1836)

Excerpt from *THE WORLD, OR INSTABILITY*

ABSTRACT

Investigation of barite (BaSO_4) precipitation at three North American springs demonstrated that biological and physiochemical parameters assert combined, environmentally specific influences on the textural development of ambient temperature barite.

At Flybye Springs, NWT, anoxic, 8.5°C , pH circumneutral, barium-rich (12 ppm) waters precipitate inorganic barite microcrystals upon exposure to atmospheric oxygen. Downstream, dysoxic waters precipitate barite among sulphide-tolerant microbes. Passive adsorption of barium to microbial cells and extracellular polymeric substances (EPS) mediates barite precipitation at redox boundaries in floating mats, around individual microbial cells, and in the outer cell walls of *Beggiatoa*, and *Oscillatoria*. Active barium bioaccumulation and metabolic sulphur oxidation induce barite precipitation inside *Beggiatoa*, *Thiothrix*, and *Chromatium*, and outside fungal hyphae. Holocene to Recent precipitation at Flybye Springs has produced a weakly radioactive barite tufa mound that contains 'inorganic' raft, undulatory sheet, ooid coated grain, and detrital conglomerate lithotypes, as well as 'biogenic' coated bubble, oncoid coated grain, and microfossiliferous stromatolitic lithotypes.

At Stinking Springs, Utah, saline, 48°C , pH circumneutral, barium-enriched (7.8 ppm) spring water precipitates calcite in and on microbial mats, producing calcite tufas that contain calcified cyanobacteria and sulphate reducing bacteria, and weakly radioactive diagenetic barite cements. Release of bioaccumulated barium from putrefying diatoms mediates barite saturation in the lithifying microbial mats, producing primary

barite that forms haloes around diatoms, lines diatom frustules, forms internal diatom casts, and replaces diatom silica.

At Twitya Spring, NWT, CO₂-degassing and oxidation of 24 °C, pH circumneutral, calcium- (65 ppm) and barium- (≥ 0.78 ppm) bearing spring water induces precipitation of barium-enriched dendritic calcite travertine that contains barite as: (1) intergrown tabular crystals formed in solution, (2) tabular and rhombic crystals nucleated on calcite, and (3) sub-anhedral crystals nucleated on microbes and EPS. The formation and distribution of the three types of barite are controlled by physiochemical gradients, calcite precipitation rates, and adsorption of barium to microbial biomass, all of which vary seasonally and episodically.

Experimental precipitation of barite among streamers of sulphur oxidizing bacteria showed that barium adsorption to microbial cells and EPS promotes localization of barite on microbes, and that sulphate-limiting conditions favour the development of biogenic textures in barite.

ACKNOWLEDGEMENTS

Many thanks to the Canadian Circumpolar Institute of the University of Alberta, Northern Science Training Program of the Department of Indian Affairs and Northern Development, the Alberta Ingenuity Fund, and the National Science and Engineering Research Council of Canada, who provided essential funding for my doctoral studies and research.

I would also like to thank Brian Jones for his academic and research guidance, editorial skills, and faith in my choice of thesis topic (especially when the Flybye Springs became temporarily misplaced). Robert Blackett (Utah Geological Survey) provided reconnaissance and background information for fieldwork in Utah, and data, reconnaissance and hospitality provided by Richard Popko and Alasdair Veitch (Environment and Natural Resources, Sahtu Region) and pilots Flynd Horn and Guy Thibeault (Sahtu Heli) were crucial to the success of fieldwork in the Northwest Territories. Alex MacNeil, Jeff Baker, and Dustin (Pukey) Rainey were fantastic field assistants.

This research would not have been possible without the expertise of many individuals in the Department of Earth and Atmospheric Sciences — special thanks go to George Braybrook for assistance with the SEM and advice on sample preparation, to Sergei Mateev for assistance with the electron microprobe, to Alex Wolfe for consulting on diatom identification, to Karlis Meuhlenbach for advice on gas collection and sample analysis, to Don Resultay and Mark Labbe for preparing thin sections, to John Duke for conducting nuclear activation analyses, and to Diane Caird for all her help with X-ray diffraction, radiometric measurements and disposal of putrefying microbial samples.

Finally, I would like to thank my family (especially Jeff, Julius and Evelyn), the Carbonate Springs Research Group (Alex, Hilary, Michelle, Rachel, Dustin and Breanna), and my friends in Edmonton for their support during the completion of this thesis.

TABLE OF CONTENTS

| | <i>page</i> |
|---|-------------|
| CHAPTER 1 | |
| Introduction | 1 |
| Field sites | 5 |
| Previous research | 8 |
| Rationale and objectives | 12 |
| References | 15 |
| CHAPTER 2 | |
| Barite biomineralisation at Flybye Springs | 20 |
| Study site | 21 |
| Methods | 21 |
| Spring water physiochemistry | 24 |
| Spring biology | 27 |
| Mineral precipitates | 31 |
| Discussion | 43 |
| Conclusions | 53 |
| References | 55 |
| CHAPTER 3 | |
| Petrography and textural development of inorganic and biogenic lithotypes in barite tufa at Flybye Springs | 62 |
| Methods | 65 |
| Terminology | 66 |
| Geologic setting | 66 |
| Relict barite tufa composition | 67 |
| Relict barite tufa lithotypes | 71 |

| | | |
|-----------|--|-----|
| | Barite tufa diagenesis | 91 |
| | Discussion | 95 |
| | Conclusions | 102 |
| | References | 104 |
| CHAPTER 4 | Diatom-mediated barite precipitation in microbial mats calcifying at Stinking Springs | 111 |
| | Study site | 112 |
| | Methods | 114 |
| | Results and interpretation | 115 |
| | Discussion | 136 |
| | Conclusions | 140 |
| | References | 142 |
| CHAPTER 5 | Controls on the precipitation of barite crystals in calcite travertine at Twitya Spring | 148 |
| | Study site | 149 |
| | Methods | 151 |
| | Results | 152 |
| | Interpretation | 164 |
| | Discussion | 171 |
| | Conclusions | 174 |
| | References | 176 |
| CHAPTER 6 | Experimental precipitation of barite among streamers of sulphur oxidizing bacteria | 182 |

| | | |
|------------|--|-----|
| | Methods | 183 |
| | Results | 187 |
| | Interpretation and discussion | 189 |
| | Conclusions | 196 |
| | References | 197 |
| CHAPTER 7 | Conclusions | 201 |
| APPENDIX 1 | Chemical and mineral analyses of NWT spring water and mineral precipitates with field notes | 213 |
| APPENDIX 2 | Description and evaluation of analytical methods and modelling in biologically colonised systems | 214 |
| APPENDIX 3 | Thesis sample collection inventory | 217 |

LIST OF TABLES

| | | <i>page</i> |
|------------------|---|-------------|
| Table 2-1 | Chemistry of the Flybye Spring water | 27 |
| Table 2-2 | Characteristics used to identify microbes at Flybye Springs | 29 |
| Table 4-1 | Chemistry of the Stinking Springs water | 115 |
| Table 5-1 | Characteristics used to identify microbes as Twitya Spring | 153 |
| Table 5-2 | Chemistry of the Twitya Spring water | 154 |

LIST OF FIGURES

| | <i>page</i> |
|---|-------------|
| Figure 1-1 Location of field sites | 2 |
| Figure 1-2 Location of barite-precipitating springs around the world | 4 |
| Figure 1-3 General views of field sites | 7 |
| Figure 1-4 Radioactive springs and barite in popular culture | 10 |
| Figure 2-1 Location and overview of Flybye Springs | 22 |
| Figure 2-2 Flybye Springs physiochemistry and microbes | 26 |
| Figure 2-3 Microbes from Flybye Springs | 30 |
| Figure 2-4 Fresh precipitates | 32 |
| Figure 2-5 Inorganic barite | 34 |
| Figure 2-6 Barite laminae in microbial mats | 35 |
| Figure 2-7 Barite coating and encrusting microbes | 37 |
| Figure 2-8 Barite encrusting microbes | 38 |
| Figure 2-9 Barite permineralising microbes | 39 |
| Figure 2-10 Intracellular barite in filamentous microbes | 41 |
| Figure 2-11 Intracellular and extracellular spherical barite | 42 |
| Figure 3-1 Location and overview of Flybye Springs | 63 |
| Figure 3-2 Compositional variation of relict barite tufa | 68 |
| Figure 3-3 Compositional variation of relict barite tufa | 69 |
| Figure 3-4 Coated bubble barite tufa lithotype | 72 |
| Figure 3-5 Raft barite tufa lithotype | 75 |

| | | |
|--------------------|--|-----|
| Figure 3-6 | Undulatory sheet barite tufa lithotype | 77 |
| Figure 3-7 | Stromatolitic barite tufa lithotype | 80 |
| Figure 3-8 | Barite strings from stromatolitic barite tufa | 81 |
| Figure 3-9 | Microfossils from stromatolitic barite tufa | 83 |
| Figure 3-10 | Coated grain barite tufa lithotype | 88 |
| Figure 3-11 | Detrital lithoclast barite tufa lithotype | 90 |
| Figure 3-12 | Barite tufa cements | 92 |
| Figure 3-13 | Artefacts preserved in barite tufa | 94 |
| Figure 3-14 | Schematic comparison of barite and carbonate spring deposi | 96 |
| Figure 4-1 | Location and overview of Stinking Springs | 113 |
| Figure 4-2 | Schematic diagram of flow path, Stinking Springs biology | 117 |
| Figure 4-3 | Diatoms from Stinking Springs | 118 |
| Figure 4-4 | Mineralizing microbial mats and calcite tufa | 119 |
| Figure 4-5 | Mineral precipitates | 121 |
| Figure 4-6 | Barite surrounding diatom frustules | 123 |
| Figure 4-7 | Barite lining diatom frustules | 126 |
| Figure 4-8 | Barite diatom casts | 129 |
| Figure 4-9 | Barite replacing diatom frustules | 132 |
| Figure 4-10 | Diagenetic barite crystals | 135 |
| Figure 5-1 | Location and overview of Twitya Spring | 150 |
| Figure 5-2 | Schematic diagram of flow path | 155 |
| Figure 5-3 | Twitya Spring biology | 156 |

| | | |
|--------------------|---|-----|
| Figure 5-4 | Elemental sulphur and calcite from Twitya Spring | 158 |
| Figure 5-5 | Dendritic calcite from Twitya Spring | 160 |
| Figure 5-6 | Compositional variation between calcite dendrites and ceme | 161 |
| Figure 5-7 | Compositional variation between calcite dendrites and ceme | 162 |
| Figure 5-8 | Travertine growth bands | 163 |
| Figure 5-9 | T1 and T2 'inorganic' barite crystals | 165 |
| Figure 5-10 | T3 microbe-associated barite crystals | 166 |
| Figure 6-1 | Sample location and experiment set-up | 184 |
| Figure 6-2 | Microbial samples | 186 |
| Figure 6-3 | Experimentally precipitated barite | 188 |
| Figure 6-4 | Iron oxides, sulphides and FeS/BaSO ₄ 'sandwiches' | 190 |

Chapter 1 Introduction

This study focuses on barite-precipitation at subaerial springs, a globally rare phenomenon, which has only recently gained the attention of geobiologists (e.g. Senko et al., 2004; Tazaki and Watanabe, 2004). In contrast, springs that precipitate calcium carbonate, opaline silica, and iron oxide are globally abundant, and the relative importance of biological versus inorganic controls on the precipitation of these minerals has been debated for centuries (Pliny, 77; Darwin, 1839). Petrographic and geobiological investigation of mineral precipitation in springs has been pivotal to the development of low temperature geochemistry, and to reconstruction of Earth history from chemical sediments, by providing important information on the geochemical and textural response of carbonates, silica and iron oxides to specific physiochemical variables (e.g. Folk et al., 1985; Chafetz et al., 1991; Andrews et al., 1997; Jones and Renault, 2006), microbial processes (e.g. Folk et al., 1985; Walter and DesMarais, 1993; Jones and Renault, 1998; Arp et al., 1999; Kawano and Tomita, 2001; Konhauser et al., 2003), and plant and animal biomineralisation (e.g. Riding and Awramik, 2000; Pentecost, 2005; Fortin and Langley, 2005). A lack of similar referential data from contemporary barite-precipitating environments currently handicaps interpretation of barite in the geologic record (McManus et al. 1998; Aharon, 2000; Torres et al., 2003; Riedinger et al., 2006), including putative Precambrian (Buick et al., 1981) and Paleozoic stromatolites (Graber, 1988; Carroue, 1996). This thesis explores the potential of barite-precipitating springs for providing information on the textural response of barite to physiochemical and biological influences.

In-depth petrographic and geobiological investigations were carried out at three North American springs: the cold Flybye and warm Twitya Springs in Canada's Northwest Territories, and hot Stinking Springs, Utah (Fig. 1-1). Barite-precipitating springs are rare and remain poorly documented. Younger (1986), for example, located only three citations for *barite*-precipitating springs. In a more recent review of spring deposits around the world, Pentecost (2005) stated that, globally, there are 'several'

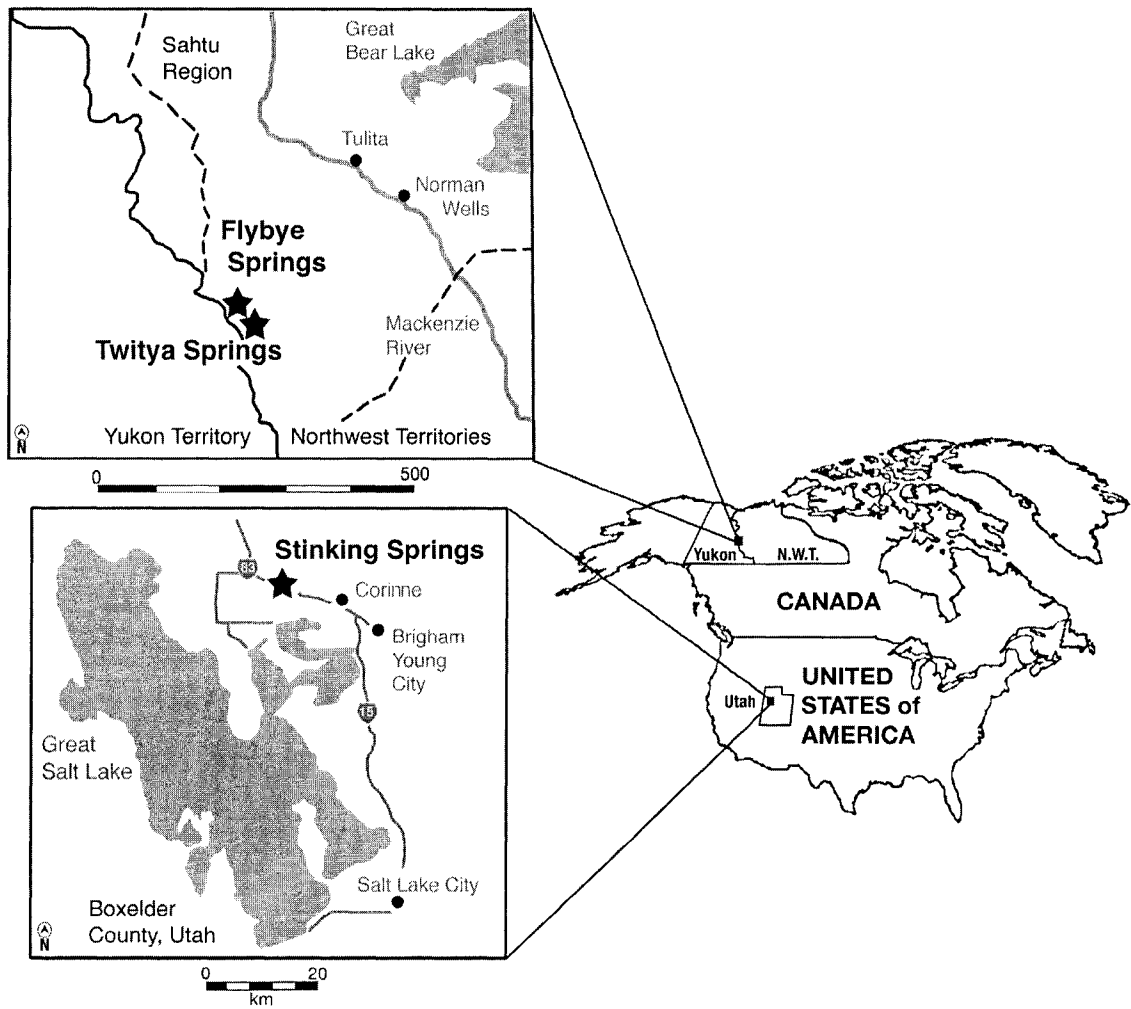


Figure 1-1. Location map for the Flybye, Twitya and Stinking Springs.

baryte-precipitating springs. Searches of the ISI Web of ScienceSM and GeoRef databases conducted in 2007, using both the British and American spellings, as well as the terms *radiobarite* and *radiobaryte* (for radium-rich barite), *hepatite* (for 'fetid' barite), and the Asian *hokutolite* (for lead-rich barite), located eight springs that precipitate barite as a dominant mineral phase (> 50% of the spring deposit by volume). The number rises to sixteen if those springs that have barite as an accessory mineral hosted in calcium carbonate, silica, and/or iron oxide are included, and two further barite-precipitating springs, Twitya and Sc lupin Springs, NWT (Appendix 1) were discovered in the course of this study (Fig. 1-2). For comparison, searching ISI Web of ScienceSM for 'silica spring' produces 513 citations, 'carbonate spring' produces 535 citations, and 'iron spring' produces 708 citations. The global scarcity of barite-precipitating subaerial springs is explained by the low solubility of barium in oxygenated, sulphate-bearing solutions ($\log K_{sp} \approx -10.3 @ 25^\circ$), which both restricts dissolution of barium from aquifer strata and requires that spring waters remain anoxic to shallow depth (Hanor, 2000).

Barite's low solubility also places restrictions on other geological environments in which it is deposited. Most economically important barite deposits were formed during the Precambrian and early Paleozoic, when oxidation of Earth's ocean and atmosphere progressively increased the global availability of sulphate and reduced the solubility of barium (Jewell, 2000; Huston and Logan, 2004). Interfaces between barium-rich anoxic and oxygenated solutions in organic-rich sediments and around deep-sea hydrothermal vents and cold methane seep fields are the most important depositional settings for barite today (Hanor, 2000). Accumulation rates can be rapid in those environments; for example, Neogene to recent cold methane seepage in the Derugin Basin, Sea of Okhotsk, has produced a deposit that covers 22 km² and contains over 5 million tons of barite (Greinert et al., 2002; Aloisi et al., 2004). These barites form among chemosynthetic microbial communities (Aharon, 2000; Aloisi et al., 2004) and may be good analogues for the interpretation of putative biogenic textures in low temperature Paleozoic barites (Graber, 1988; Fu et al., 1994; Torres et al., 2003). Unfortunately, logistic difficulties involved with submarine sample collection hinder examination of cold seep barite precipitation *in situ*, complicating analysis of mineral-microbe interactions (cf. Riedinger et al., 2006).

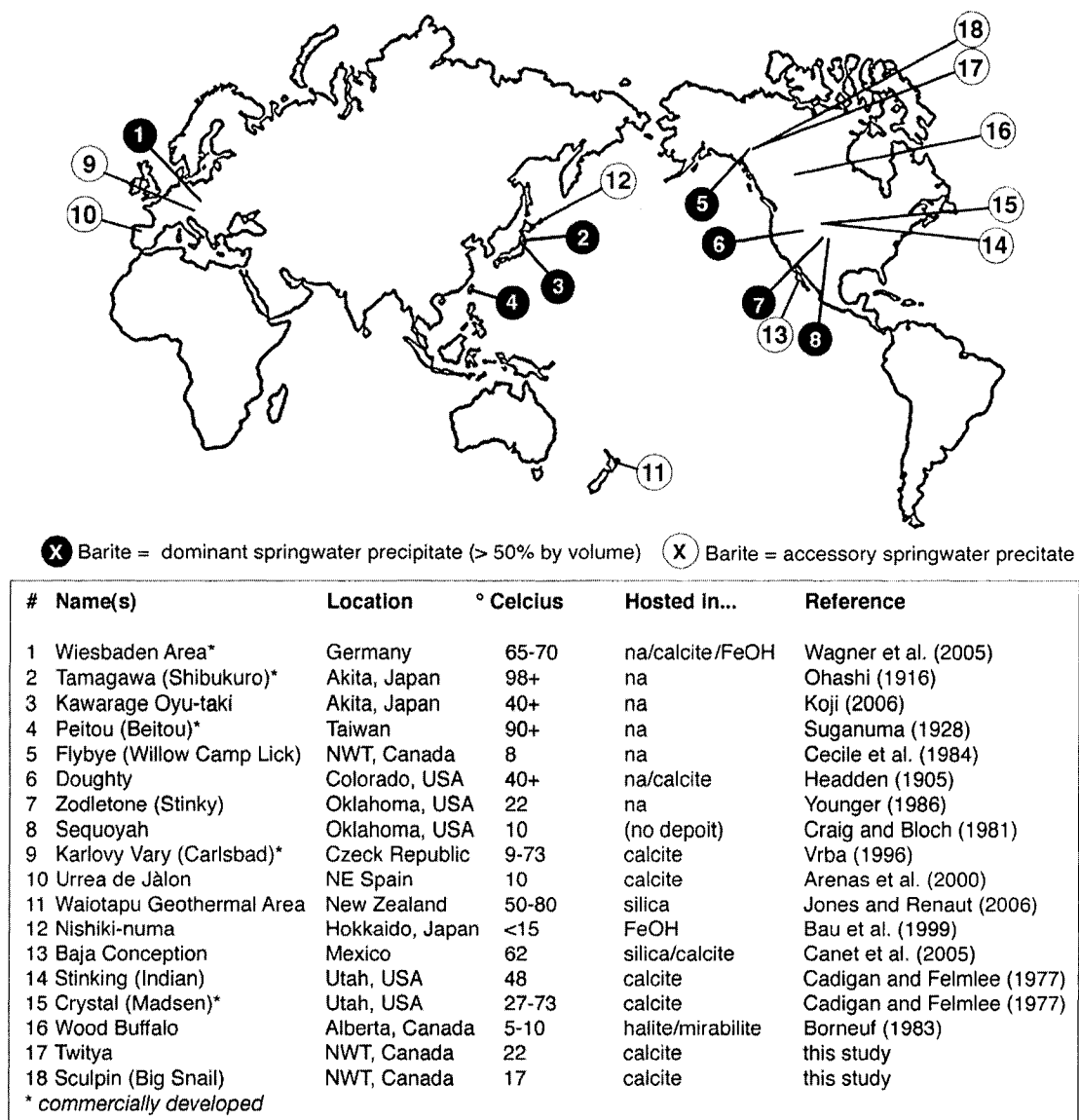


Figure 1-2. Location map for documented barite-precipitating springs around the world (na= 'not applicable').

Barite precipitation among planktonic biomass in the upper marine water column is another important component of the global barium cycle (Bishop, 1988). Accumulation of this barite as particulate 'rain' in siliclastic and carbonate sediments is correlated to marine productivity (Paytan et al., 1993; Lu et al., 2004) and may provide a refractory record of palaeoseawater $\delta^{34}\text{S}$, $^{87}\text{Sr}/^{86}\text{Sr}$ and Ba/Sr ratios (Martin et al., 1995; Kiipli et al., 2004). Investigations of contemporary particulate marine barite formation and preservation are required to maximize its utility for palaeoenvironmental reconstruction (McManus et al., 1998), but are complicated by the impossibility of collecting planktonic material without disrupting chemical microenvironments, and by local dissolution of barite crystals during sedimentation (Bishop, 1988; Paytan et al., 1993).

In contrast to marine depositional environments, terrestrial springs are readily accessible, allowing *in situ* investigation of inorganic mineral precipitation and mineral-microbe interactions, as well as assessment of early diagenetic changes between fresh and lithified precipitates. Each barite-precipitating spring provides an opportunity to determine the controls on barite precipitation in a unique physiochemical and biological context, and thus has potential to contribute new insight and understanding to the interpretation of barite in the geological record. Field sites for this study were selected because each: (1) has a substantial lithified spring deposit that contains barite, (2) has ongoing spring water flow and mineral precipitation, (3) is accessible from Edmonton, Alberta, and (4) has not been commercially developed.

Field Sites and Methods

The Flybye and Twitya Springs are located in the Sahtu region of the Northwest Territories where research is licensed by the Territorial Government through the Aurora Research Institute. Both sites are accessible by helicopter from Norman Wells, or, traditionally, by foot or canoe along tributaries of the Mountain River, and fall within the Bonnet Plume and Sekwi Mountain Map Areas. Regional meta-sedimentary strata contain local barite-rich horizons and dispersed particulate barite crystals whose dissolution contributes to elevated barium concentrations in ground and stream waters (Cecile et al., 1984; Cecile, 2000; Day et al., 2004). The Flybye Springs are globally unique as the only location where a substantial relict mound of barite has formed by cold

spring activity. It therefore provides a rare opportunity to examine both contemporary precipitation and early diagenesis of cold subaerial barite (Fig. 1-3A). Locally, however, the Flybye Springs are valued as a watering hole for migratory caribou and are known to outfitters (who use a grassy knoll opposite the flow path as a hunting screen) as ‘Willow Camp Lick’.

The Flybye Springs are the only location in the Sahtu where barite precipitates as a dominant mineral phase (Appendix 1), but it precipitates as accessory mineral at Twitya Spring, ~ 35 km to the south. ‘Twitya’ is the Dene name for a river system that passes near the spring site, and has various phonetic spellings, including Tuitya, Tuitye, and Twitcha. This study uses ‘Twitya’ following the preference of the Sahtu Renewable Resource Board. At Twitya Spring, barite is hosted among dendritic calcite crystals in a layered travertine mound, and thus provides an opportunity to examine barite precipitation and preservation in inorganic carbonates (Fig. 1-3B). Game trails crossing the flow path indicate that Twitya Spring is also used as a watering hole, but it is not a hunting destination. Rather, it is considered a heritage site by the Sahtu Dene and has traditionally been visited for therapeutic purposes (R. Popko, pers. comm.).

The third field site investigated, Stinking Springs, located on private and Land Bureau holdings near Brigham Young City, Utah, also has a history of therapeutic use. Construction of a highway between the spring vents and the spring flow path has not reduced their appeal. Fieldwork at Stinking Springs coincided with the opening of a duck hunt in marshland fed by the spring and, despite continuous gunfire, bathing tubs carved into the spring flow path were in continual use. The bathing area, parking lot, and current flow path of the Stinking Springs are underlain by an extensive deposit of relict barite-bearing carbonate tufa, and barite and calcite precipitation continue among living microbial mats (Fig. 1-3C). This spring provided a unique opportunity to examine the formation, preservation, and early diagenesis of barite in microbial carbonates.

Fieldwork conducted at Flybye Springs in August, 2004 and July 2005, at Twitya Spring in July 2005, and at Stinking Springs in October 2003 included collection of water, gas, microbes, fresh precipitates and relict barite samples, physiochemical measurements, and documentary drawing and photography. Glass slides installed at Stinking Springs for 24 hours and at Flybye Springs for 10 months provided a means of

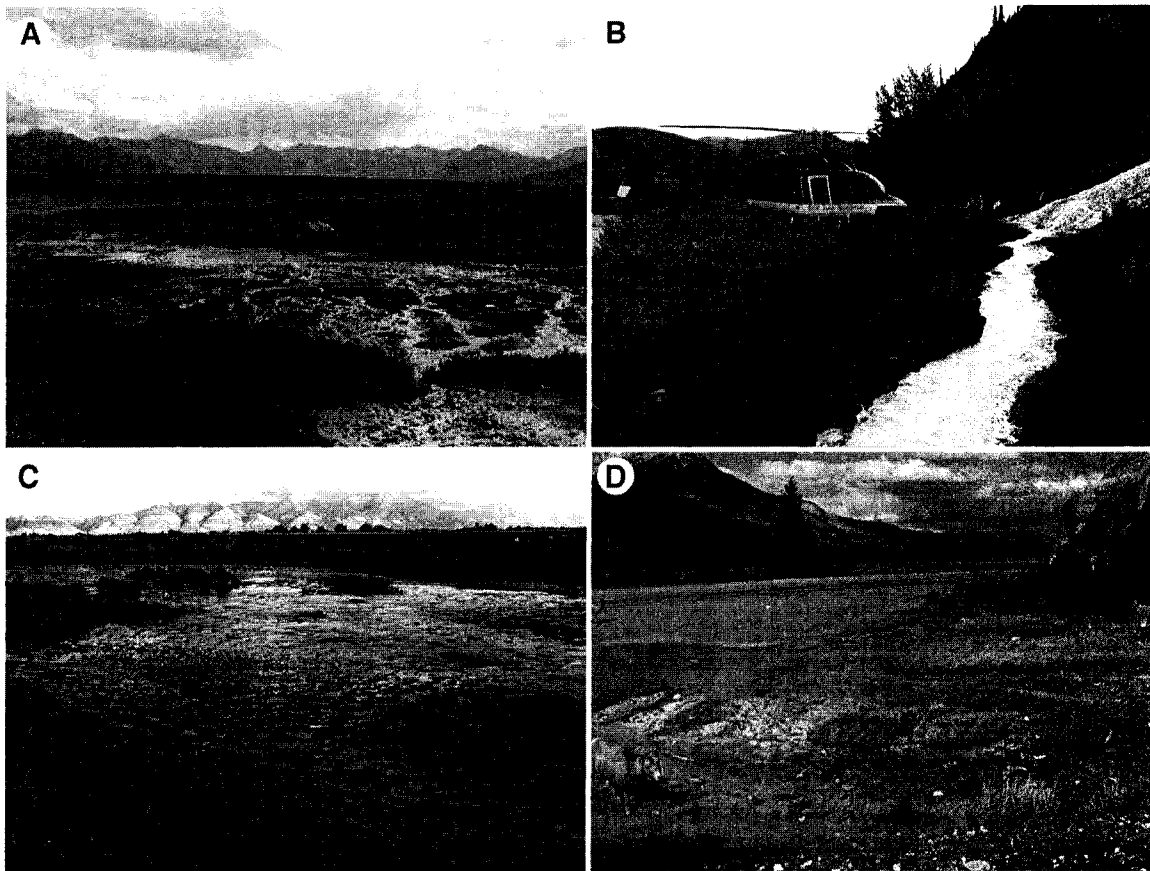


Figure 1-3. Photographs of field sites. (A) View from the top of the Flybye Springs, NWT, tufa mound; drainage streams run towards a caribou wallow, a grassy knoll and the Selwyn Mountains are visible beyond the helicopter. (B) View of bright green stream draining from Twitya Springs, NWT. (C) View of microbially colonised terraces at Stinking Springs, Utah, with the Wasatch Mountains in the background. (D) View of the Jasper Cold Sulphur Springs, Alberta, flow path with mountain sheep.

assessing precipitation rates and preservation biases between fresh precipitates, lithified, and relic spring deposits. Experimental barite precipitation was also initiated among microbial samples collected from a fourth spring site in Jasper National Park, Alberta (Fig. 1-3D). The fine textural influences of microbes on mineralisation are best resolved by examining samples at a variety of scales; thus, comprehensive field and sample descriptions, supplemented by thin section petrography, light and scanning electron microscopy, and electron microprobe, comprise most of this study. Qualitative and quantitative analyses of select samples (including elemental characterization of water and gas samples, stable isotope analysis, x-ray diffraction, energy dispersive x-ray analysis and neutron activation analysis) supplement descriptive data and inform the interpretations and conclusions forwarded. Details of specific methods, and the operative conditions of analytical instruments, are provided in subsequent chapters.

Previous Research

Barite's high specific gravity (4.5-5) has ensured its popularity as a weighting agent since ancient times, when the Greeks named it after their word *barys*, meaning 'heavy'. The first scientific references to barite focus, however, on its 'lightness'. In 1602, Vincenzo Casciarolo, an amateur alchemist, discovered barite near Bologna, Italy, which both glowed in the dark and acted as a powerful depilatory when carried against skin. The phosphorescence of Casciarolo's 'solar', later known as 'Bolognian' or 'Bologna Stone', caught the attention of notable scientists of the day, including Galileo Galilei (1564-1642), who hypothesized that the rock absorbed and emitted light and heat, "much like a sponge" (Roda et al., 1998). Ovidio Montalbani (1601-1671) and Fortunius Licetus (1577-1657) forwarded a contrary explanation that the glow arose from a 'burning' inside the rock, a phenomenon they also invoked to explain light 'emitted' by the moon. Indeed, Montalbani and Licetus adopted the Bolognian stone as 'evidence' for their phosphorescent moon theory, and thus persuaded many of Galileo's contemporaries to dismiss his hypothesis that the moon reflects the light of the sun (Roda et al., 1998). Despite this early role in retarding the progress of astronomy, barite has been extremely important to the progress of chemical and mineralogical theory.

Following Carl Scheele's discovery of barium in 1774, and Marie Skłodowska-Curie's discovery of radium in 1898, the luminescence of the Bolognian Stone was revealed to arise by excitation of both barium and radium. Radium cannot precipitate as a separate phase in most geologic environments because of the limiting solubility of radium salts (Ames et al., 1983). It is, however, readily substituted into the barite crystal lattice, commonly in high enough abundance to imbue barite above background radiation (Cecile et al., 1984; Oddo et al., 1993). Indeed, the depilatory power of the Bolognian Stone was likely an effect of radiation poisoning derived by decay of ^{226}Ra (cf. Ames et al., 1983).

Unfortunately, the dangers of radiation-poisoning were not fully realized until the 1930's, and radiation therapies, including drinking and bathing in radium-enriched spring water, were lauded in the 19th and early 20th centuries as a cure for diseases as varied as psoriasis, depression, pleurisy, and hirsutisity (Fig. 1-4A; Evans, 1933). Prospectors for naturally therapeutic radioactive springs produced the first scientific descriptions of barium-rich spring waters and their 'radiotherapeutic' precipitates. Crystalline deposits of lead-rich barite, or hokutolite, first discovered in 1912 during development of spas at the Peitou (Beitou) Springs in Japanese-annexed Taiwan, were described in detail (Suganuma, 1928) and later enshrined as the national mineral of Japan (Fig. 1-4B-D). Headden (1905) provided the first North American report of subaerial barite and barytocalcite [$\text{BaCa}(\text{SO}_4)_2$] precipitation at Doughty Springs, Colorado during a radiometric survey of regional ground waters. Barite precipitation at several other springs in Oklahoma and Utah was discovered in the 1970's when the Geological Society of America, by then aware of the hazards of environmental radium exposure, began gathering regional water-quality data (Cadigan and Felmlee, 1977).

A significant body of literature exists pertaining to the physiological effects, crystallography and trace element chemistry of hokutolite (e.g. Suganuma, 1928; Sasaki and Minato, 1982; Momoshima et al., 1997; Tomita et al., 2006). Geologic research at other barite spring-deposits has mainly been cursory, or limited to investigations of aquifer hydrology and precipitate radioactivity or crystallography (e.g. Craig and Bloch, 1981; Bove and Felmlee, 1982; Cecile et al., 1984; Sanders, 1998). Indeed,



Figure 1-4. (A) Radio-therapy water container circa 1900. (B) Government of Taipei tourism poster for the Peitou (Beitou) Hot Springs Festival 2006. (C) Bath wipes with radiotherapeutic effect available for purchase at Tamagawa Hot Springs, Japan, as of 2005. (D) Hokutolite postage stamp issued by the Chinese government of Taiwan. (Images A and C are used with the permission of the Oak Ridge Associated Universities Health Physics Historical Instrumentation Museum website).

the first publications pertaining to the Flybye Springs (Cecile et al., 1984) and Stinking Springs (Cadigan and Felmlee, 1977; Blacket and Wakefield, 2004) focus solely on the origins of radium in the spring waters and the slight radioactivity of the mineral deposits.

Biological influences on mineral precipitation at carbonate and silica springs were readily apparent to early scientists because of the abundance of plant fossils preserved in carbonate tufas and travertines, and silica sinters (e.g. Weed, 1889a, b; Roddy, 1915; Emig, 1917). Awareness of microorganisms that biomineralized carbonate (ostracodes, forams, mollusks) and silica (diatoms, radiolarians) no doubt facilitated early identification of biological influences on carbonate and silica precipitation (Weed, 1889a). The most famous barite-precipitating springs, however, either emerged at superheated temperatures and formed crystalline deposits that lack evidence for microbiological influences (Suganuma, 1928), or contained mixed deposits of calcite and barite in which 'biogenic' textures could be explained by carbonate-microbe interactions (Headden, 1905; Lindgren, 1933). To this day, few geologists are aware of barite biomineralisation in molluscs (Lowell et al., 1990), marine xenophyophores (Gooday and Nott, 1982), the common desmid *Closterium*, or the freshwater algae *Chara fragilis* and *Spirogyra* (Brooks et al., 1980), with the result that barite is usually interpreted as an inorganic precipitate, even when found among microbes or hosted in biogenically precipitated carbonate and/or silica (Arenas et al., 2000; Canet et al., 2005; Aloisi et al., 2006). In fact, Cecile et al. (1984) interpreted barite tufa from Flybye Springs, NWT, as 'inorganic' despite the fact that it contains so many biogenic textures (including microbial streamers and stromatolitic layering) that they initially mistook it for microbial carbonate tufa (Cecile, pers. comm.).

Although the ability of sulphur metabolizing microbes to mediate saturation gradients for sulphide and sulphate minerals has been stressed by numerous authors (e.g. Tazaki et al., 1997; Aharon, 2000; Senko et al., 2004), the role of microbes in barium cycling remains unconstrained (Torres et al., 2003; Aloisi et al., 2004; Riedinger, et al., 2006). Recent investigations of barite precipitation among microbes in laboratory settings has demonstrated the ability of various microbes to host and organize the distribution of barite precipitates, not by sulphur metabolism, but by adsorbing and bioaccumulating barium (Gonzalez-Munoz et al., 2003; Ganeshram et al., 2003). Barite precipitation

resulting from microbial barium-fixation is also hinted at in several reports from barite-precipitating springs: Younger (1986) makes passing mention of 'white barium-rich frostings' around cyanobacteria at Doughty Springs, Colorado, as well as fossilized 'vegetable tubes' in relict barite from Zodletone Springs, Oklahoma; and Tazaki and Watanabe (2004) speculate that barium-enriched microbial mats may promote hokutolite precipitation at Tamagawa Springs, Japan. Current descriptions of barite precipitation at springs lack important details, however, regarding how microbial influences on barium and/or sulphur cycling are translated into barite texture, and thus have limited applicability to the interpretation of geologic barite.

Rationale and Objectives

Although previous studies at barite-precipitating springs have provided valuable information regarding barite mineralogy, regional aquifer hydrology, and the mobility of barium and radium in ground water, they have not provided information on mineral-microbe interactions that is comparable to the breadth and depth of information obtained by ongoing research at carbonate, silica, and iron oxide springs. In addition to inhibiting interpretation of geologic barite, the current lack of data regarding subaerial barite-precipitation represents a failed opportunity to evaluate hypotheses formulated to explain the textural development of other chemical sediments.

A broadening of the geochemical context of springs research is also required to resolve the relative influences of precipitate mineralogy, crystallography, and microbial metabolism on the taphonomy of microfossils. Although extracellular precipitation of silica is not considered to be metabolically controlled, photosynthetic withdrawal of CO₂ has been implicated in creating pH elevated microniches that favour calcite precipitation around microbial cells (Arp et al., 2001), and sulphur- and iron-metabolising species are capable of mediating saturation gradients for sulphate/sulphide and iron oxide minerals (Shen et al., 2001; Popa et al., 2004; Senko et al., 2004). Comparison of mineral-microbe interactions in barite springs with those in carbonate, silica, and iron oxide springs may help to determine which features of microfossil preservation are biologically vs. physiochemically controlled.

This study presents the first combined petrographic and geobiological analysis of ambient temperature subaerial barite precipitation, with the aim of providing new information that will improve the interpretative potential of sedimentary barite in the geologic record and contribute the general knowledge regarding the textural and microtextural development of chemical sediments. Specific objectives of this thesis include (1) providing comprehensive descriptions of three physiochemically distinct barite-precipitating subaerial springs, (2) describing mineral-microbe interactions in these natural settings, (3) documenting the textural products of these interactions, (4) assessing their potential for diagenetic persistence, and (5) experimentally constraining the conditions under which barite-precipitation is localized on microbial cells, and hence most likely to preserve biogenic textures.

This thesis is presented in 'paper-format' — each chapter has been written to stand alone and has been published, accepted, or is under review, in a peer-reviewed publication:

Chapter Two describes the physiochemistry and microbiology of the modern Flybye Springs, focusing on the textural products of microbe-barium-sulphate interactions. Differences in barite biomineralisation between microbial genera are discussed with reference to their environmental preference, metabolism, and cellular structure.

(Published as Bonny, S. and Jones, B. Barite (BaSO₄) biomineralisation at Flybye Springs, a cold sulphur spring system in Canada's Northwest Territories, Canadian Journal of Earth Sciences, 44: 835-856.)

Chapter Three provides a comprehensive petrographic description and analysis of relict barite tufa from Flybye Springs, highlighting unexpected congruencies with thermogene carbonate spring deposits.

(Accepted as Bonny, S. and Jones, B. Petrography and textural development of inorganic and biogenic lithotypes in a relict barite tufa deposit at Flybye Springs, Northwest Territories, Canada, by Sedimentology.)

Chapter Four describes the physiochemistry and microbiology of the Stinking Springs flow path, documenting barite precipitation in and around diatoms entombed in calcite tufa. Implications for the efficacy of particulate marine barite as a palaeoproductivity proxy are discussed.

(*Published as* Bonny, S. and Jones, B. 2007. Diatom-mediated barite precipitation in microbial mats calcifying at Stinking Springs, a warm sulphur spring system in Northwestern Utah, USA, *Sedimentary Geology*, 194. 223-244.)

Chapter Five examines physiochemical and biological controls on the distribution of three types of barite crystals found among calcite dendrites in travertine from Twitya Spring.

(*Submitted as* Bonny, S. and Jones, B. Controls on the precipitation of barite (BaSO₄) crystals in calcite travertine at Twitya Spring, a warm sulphur spring in Canada's Northwest Territories *to Sedimentary Geology*.)

Chapter Six documents the morphology and substrate selectivity of barite experimentally precipitated among streamers of sulphur oxidizing bacteria collected from Jasper Cold Sulphur Springs.

(*Submitted as* Bonny, S. and Jones, B. Experimental precipitation of barite (BaSO₄) at ambient temperature among streamers of sulphur oxidizing bacteria *to the Journal of Sedimentary Research*.)

Chapter Seven presents the conclusions of this thesis.

References

- Aharon, P. 2000. Microbial processes and products fueled by hydrocarbons at submarine seeps. In: Riding, R., Awramik, S.M. (Eds.), *Microbial Sediments*, Springer-Verlag, Heidelberg Germany, pp. 270-281.
- Aloisi, G., Wallmann, K., Bollwerk, S.M., Derkachev, A., Bohrmann, G. and Suess, E. 2004. The effect of dissolved barium on biogeochemical processes at cold seeps. *Geochimica et Cosmochimica Acta*, 68: 1735-1748.
- Ames, L.L., McGarrah, J.E., and Walker, B.A. 1983. Sorption of trace constituents from aqueous solutions onto secondary minerals II. radium. *Clays and Clay Minerals*, 31: 335-342.
- Andrews, J.E., Riding, R. and Dennis, P.F. 1997. The stable isotope record of environmental and climatic signals in modern terrestrial microbial carbonates from Europe. *Palaeogeography, Palaeoclimatology, Palaeoecology*, 129: 171-189.
- Arenas, C., Gutierrez, F., Osacar, C., and Sancho, C., 2000. Sedimentology and geochemistry of fluvio-lacustrine tufa deposits controlled by evaporite solution subsidence in the central Ebro Depression, NE Spain. *Sedimentology*, 47: 883-909.
- Arp, G. Theil, V., Reimer, A. Michaelis, W., and Reitner, J. 1999. Biofilm exopolymers control microbialite formation at thermal springs discharging into the alkaline Pyramid Lake, Nevada, USA. *Sedimentary Geology*, 126: 159-176.
- Arp, G., Reimer, A., and Reitner, J. 2001. Photosynthesis-induced biofilms calcification and calcium concentrations in Phanerozoic oceans. *Science*, 292: 1701-1704.
- Bau, M., Usui, A., Pracejus, B., Mita, N., Kanai, Y., Irber, W., Dulski, P. 1998. Geochemistry of low-temperature water-rock interaction: evidence from natural waters, andesite, and iron-oxyhydroxide precipitates at Nishiki-numa iron-spring, Hokkaido, Japan. *Chemical Geology*, 151: 293-307.
- Bishop, J.K.B., 1988. The barite-opal-organic carbon association in oceanic particulate matter. *Nature*, 332: 341-343.
- Blacket, R.E. and Wakefield, S. 2004. Geothermal resources of Utah: A digital atlas of Utah's geothermal resources. Utah Geological Survey Open-File Report 431.
- Borneuf, D. 1983. Earth Sciences Report 82-3: Springs of Alberta. Alberta Research Council, National Resources Division, Groundwater Development.
- Bove, D. and Felmlee, J.K. 1982. Mineralogy and autoradiography of selected mineral-spring precipitates in the western United States. US Geological Survey, Open-file Report 82-792, 74 pp.
- Brooks, A.J., Fotheringham, A., Bradly, J. and A. Jenkins. 1980. Barium accumulation by desmids of the genus *Closterium* (Zygnemaphyceae). *British Phycological Journal*, 15: 261-164.
- Cadigan, R.A. and Felmlee, J.K., 1977. Radioactive springs geochemical data related to uranium exploration. *Journal of Geochemical Exploration*, 8: 381-395.
- Canet, C., Prol-Ledesma, R.M., Torres-Alvarado, I., Gilg, H.A., Villanueva, R.E. and Cruz, R. L-S. 2005. Silica-carbonate stromatolites related to coastal hydrothermal venting in Baia Concepcion, Baja California Sur, Mexico. *Sedimentary Geology*, 174: 97-113.

- Carroue, J-P. 1996. Une presentation originale de la barytine ou des stromatolithes de poids. *Mineraux et Fossiles*, 246: 21-22.
- Chafetz, H.S., Rush, P.F. and Utech, N.M. 1991. Microenvironmental controls on mineralogy and habit of CaCO₃ precipitates: an example from an active travertine system. *Sedimentology*, 38: 107-126.
- Cecile, M.P. 2000. Geology of the Northeastern Nidderly Lake Map Area, East-central Yukon and adjacent Northwest Territories. Geological Survey of Canada Bulletin 553, 120 pp.
- Cecile, M.P., Goodfellow, W.D., Jones, L.D., Krouse, H.R. and M.A. Shakur. 1984. Origin of radioactive barite sinter, Flybye springs, Northwest Territories, Canada. *Canadian Journal of Earth Sciences*, 21: 383-395.
- Craig, S. and Bloch, R.L. 1981. Radioactive springs in the watershed of a proposed reservoir in Sequoyah County, Oklahoma; origin and environmental effect. *Geology*, 9: 195-199
- Darwin, C.R., 1839. *The Voyage of the Beagle*.
- Day, S.J.A., Lariviere, J.M., Friske, P.W.B., Gochnauer, K.M., MacFarlane, K.E., McCurdy, M.W., and McNeil, R.J., 2005. National Geochemical Reconnaissance, Regional Stream Sediment and Water Geochemical data, Macmillan Pass – Sekwi Mountain Northwest Territories (NTS 105O east and 105 P). Geological Survey of Canada Open File 4949/Northwest Territories Geoscience Office Contribution 0014. 1 CD-ROM.
- Donovan, R.N. and C. Ditzell. 1986. Stop 3: Geologic highlights at Zedletone (“Stinking Mountain”). *Oklahoma Geological Survey Guidebook*, 24: 96-100.
- Emig, W.H. 1917. Travertine deposits of Oklahoma. *Oklahoma Geol. Surv. Bull.*, 76 pp.
- Evans, R.D. 1933. Radium poisoning – a review of present knowledge. *American Journal of Public Health*, 23: 1017-1023.
- Frasier, M.L., and F.A. Corsetti. 2003. Neoproterozoic carbonate shrubs: interplay of microbial activity and unusual environmental conditions in post-Snowball Earth oceans. *Palaios*, 18:378-387.
- Folk, R.L., Chafetz, H.S., and Tiezzi, P.A. 1985. Bizarre Forms of depositional and diagenetic calcite in Hot-spring travertines, central Italy. In: Schneidermann, N. and Harris, P.M. (Eds.) *Carbonate Cements*, SEPM Special Publication, 36: 349-369.
- Fortin, D., and Langley, S. 2005. Formation and occurrence of biogenic iron-rich minerals. *Earth-Science Reviews*, 71: 1-19.
- Fu, B., Aharon, P., Byerly, G.R., and Roberts, H.H., 1994. Barite chimneys on the Gulf of Mexico slope; initial report of their petrography and geochemistry. *Geo-Marine Letters*, 14: 81-87.
- Ganeshram, R.S., Francois, R., Commeau, J., and Brown-Leger, L., 2003. An experimental investigation of barite formation in seawater. *Geochimica et Cosmochimica Acta*, 67: 2599-2605.
- Gonzalez-Munoz, M.T., Fernandez-Luque, B., Martinez-Ruiz, F., Chekroun, K.B., Arias, J.M., Rodriguez-Gallego, M., Martinez-Canamero, M., de Linares, and C., Paytan, A., 2003. Precipitation of Barite by *Myxococcus xanthus*: Possible Implications for the

- Biogeochemical Cycle of Barium. *Applied and Environmental Microbiology*, 69: 5722-5725
- Gooday, A.J., and J.A. Nott. 1982. Intracellular barite crystals in two Xenophyophores, *Aschemonella ramuliformis* and *Galatheaammin* sp. (Protozoa: Rhizopoda) with comments on the taxonomy of *A. ramuliformis*. *Journal of the Marine Biological Association of the U.K.*, 62: 595-605.
- Graber, K.K. 1988. Stratigraphy and petrography of bedded barite in phosphatic Devonian Slaven chert, Toquima Range, Nye County, central Nevada [Unpublished MSc Thesis]: Houston, Texas, University of Houston, 294 pp.
- Greinert, J., Bollwerk, S.M., Derkachev, A., Bohrmann, G., and Suess, E. 2002. Massive barite deposits and carbonate mineralisation in the Derugin Basin, Sea of Okhotsk: Precipitation processes at cold seep sites. *Earth and Planetary Science Letters*, 203: 165-180.
- Headden, W.P. 1905. The Doughty Springs, a group of radium bearing springs on the North fork of the Gunnison River, Delta County, Colorado. *Proceedings of the Collective Science Society*, 8: 1-30.
- Hanor, J.S. 2000. Barite-celestine geochemistry and environments of formation. *Reviews in Mineralogy and Geochemistry*, 40: 193-275.
- Huston, D.L., and Logan, G.A. 2004. Barite, BIFs and bugs - evidence for the evolution of the Earth's early hydrosphere. *Earth and Planetary Science Letters*, 220: 41-55.
- Jewell, P.W. 2000. Bedded barite in the geologic record. *SEPM Special Publication*, 66: 147-161.
- Jones, B., and Renaut, R.W., 2006. Growth of siliceous spicules in acidic hot springs, Waiotapu Geothermal Area, North Island, New Zealand. *Palaios*, 21: 406-423.
- Jones, B., Renaut, R.W. and Rosen, M.R. 1998. Microbial biofacies in hot-spring sinters: a model based on Ohaaki Pool, North Island, New Zealand. *Journal of Sedimentary Research*, 68: 413-434.
- Kawano, M., and Tomita, K. 2001. Geochemical modeling of bacterially induced mineralization of schwertmannite and jarosite in sulfuric acid spring water. *American Mineralogist*, 86: 1156-1165.
- Kiipli, E., Kiipli, T., and Kallaste, T., 2004. Bioproductivity rise in the east Baltic epicontinental sea in the Aeronian (Early Silurian). *Palaeogeography, Palaeoclimatology, Palaeoecology*, 205: 255-272.
- Koji, S. 2006. Acid spring waters of high temperature in Taiwan and Japan. *Onsen Kagaku*, 55: 188-194.
- Konhauser, K.O., Jones, B., Reysenbach, A-L., and R.W. Renaut. 2003. Hot spring sinters: keys to understanding Earth's earliest life forms. *Canadian Journal of Earth Sciences*, 40: 1713-1724.
- Lindgren, W., 1933. *Mineral deposits*, 4th edition. McGraw-Hill Publishers, New York, 930 pp.
- Lowell, W.F., Ragone, L.M., Lutz, R.A., and Swapp, S. Biomineralization of barite in the shell of the freshwater Asiatic clam *Corbicula fluminea* (Mollusca: Bivalvia). *Limnology and Oceanography*, 35: 756-762.

- Lu, Z.C., Liu, C.Q., Liu, J.J., and Wu, F.C., 2004. The bio-barite in witherite deposits from Southern Qinling and its significance. *Progress in Natural Science*, 14: 889-895.
- Momoshima, N., Nita, J., Maeda, Y., Sugihara, S., Shinno, I., Matsuoka, N. and Huang, C.-W., 1997. Chemical composition and radioactivity in Hokutolite (plumbian barite) collected at Peito Hot Springs, Taiwan. *Journal of Environmental Radioactivity*, 37: 85-99.
- Martin, E.E., Macdougall, J.D., Herbert, T.D., Paytan, A., and Kastner, M., 1995. Strontium and neodymium isotopic analyses of marine barite separates. *Geochimica et Cosmochimica Acta*, 59: 1353-1361.
- McManus, J., Barelson, W.M., Klinkhammer, G.P., Johnson, K.S., Coale, K.H., Anderson, R.F., Kumar, N., Burdige, D.J., Hammond, D.E., Brumsack, H.J., McCorkle, D.V., and Rushdi, A., 1998. Geochemistry of barium in marine sediments: implications for its use as paleoproxy. *Geochimica et Cosmochimica Acta*, 62: 3454-3473.
- Oddo, J.E., Al-borno, A., Ortiz, I., Anthony, R., Pope, D.H., Hill, D.G., Linz, D.G., Frank, J., Becker, D.M., and Tomson, M.B. 1993. The chemistry, prediction and treatment of scale containing naturally occurring radioacting martials (NORM) in Antrim gas fields, Michigan. *Production Operations Symposium*, Oklahoma City, OK, (21/03/1993), p. 695-704.
- Ohashi, R. 1916. Note on radioactive barites from Shibukuro, Prefecture of Akita, Japan. *Journal of the Geological Society of Tokyo*, 23: 477.
- Paytan, A., Kastner, M., Martin, E.E., Macdougall, J.D., and Herbert, T., 1993. Marine barite as a monitor of seawater strontium isotope composition. *Nature*, 366: 445-449.
- Pentecost, A., 2005. *Travertine*. Springer-Verlag, Heidelberg, 429 pp.
- Pliny the Elder, 77. *Naturalis Historia*.
- Popa, R., Kinkle, B.K., and A. Badescu. 2004. Pyrite framboids as biomarkers for iron-sulfur systems. *Geomicrobiology Journal*, 21: 193-206.
- Riedinger, N., Kasten, S., Groger, J., Franke, C., and Pfeifer, K., 2006. Active and buried authigenic barite fronts in sediments from the Eastern Cape Basin. *Earth and Planetary Sciences Letters*, 241: 876-887.
- Riding, R.E. and Awramik, S.M. 2000. *Microbial Sediments*, Springer-Verlag, Berlin, 331 pp.
- Roda, A., Pazzagli, M., Kricka, L.J. and Sanley, P.W. 1998. *Bioluminescence and Chemiluminescence: Perspectives for the 21st Century*, Chichester, UK, John Wiley and Sons, 625 pp.
- Roddy, H.J. 1915. Concretions in streams formed by the agency of blue green algae and related plants. *Proceedings of the American Philosophical Society*, 54: 246-258.
- Sanders, W.E. 1998. Rate and mechanism of barite mineralization at Zodletone Mountain, Southwestern Oklahoma. M. Sc. Thesis, University of Oklahoma.
- Sasaki, N., and Minato, H., 1982. Relationship between lattice constants and strontium and calcium contents of hokutolite. *Mineralogical Journal*, 11: 62-71.

- Senko, J.M., Campbell, B.S., Henriksen, J.R., Elshahed, M.S., Dewers, T.A., and Krumholz, L.R. 2004. Barite deposition resulting from phototrophic sulfide-oxidizing bacterial activity. *Geochimica et Cosmochimica Acta*, 68: 773-780.
- Shen, Y., Buick, R. and D.E. Canfield. 2001. Isotopic evidence for microbial sulphate reduction in the early Achaean era. *Nature*, 410: 77-81.
- Suganuma, I. 1928. On the constituents and genesis of a few minerals produced from hot springs and their vicinities in Japan. I. The Akita Hokutolite. *Journal of the Chemical Society of Japan*, 3: 69-73.
- Tazaki, K., Webster, J., and Fyfe, W.S. 1997. Transformation processes of microbial barite to sediments in Antarctica. *Japanese Journal of Geology*, 26: 63-68.
- Tazaki, K. and Watanabe, H. 2004. Biomineralization of radioactive sulfide minerals in strong acidic Tamagawa Hot Springs. *Science Reports of the Kanazawa University*, 49: 1-24.
- Tomita, J., Sakaguchi, A. and Yamamoto, M. 2006. Hokutolite collected from riverbed at Peitou Hot Spring in Taiwan: with emphasis on radiochemical studies. *Journal of Radioanalytical and Nuclear Chemistry*, 270: 1588-2780.
- Torres, M.E., Bohrmann, G., Dube, T.E., and Poole, F.G., 2003. Formation of modern and Paleozoic stratiform barite at cold methane seeps on continental margins. *Geology*, 31: 897-900.
- Vrba, J. 1996. Thermal mineral water springs in Karlovy Vary. *Environmental Geology*, 27: 1432-1495.
- Wagner, T., Kimbauer, T., Boyce, A.J., and Fallick, A.E. 2005. Barite-pyrite mineralization of the Wiesbaden thermal spring system, Germany: a 500-kyr record of geochemical evolution. *Geofluids*, 5: 124-139.
- Walter, M.R. and D.J. Des Marais. 1993. Preservation of biological information in thermal spring deposits: developing a strategy for the search for fossil life on Mars. *Icarus*, 101-129-143.
- Weed, W.H. 1889a. The diatom marshes and diatom beds of the Yellowstone National Park. *Botanical Gazette*, 14: 117-120.
- Weed, W.H. 1889b. Formation of travertine and siliceous sinter by the vegetation of hot springs. *US Geological Survey Annual Report*, 9: 613-676.
- Younger, P. 1986. Barite travertine from southwestern Oklahoma and west-central Colorado. M.Sc. Thesis, Oklahoma State University, Stillwater, 163 pp.

Introduction

Mineral springs that precipitate calcite, aragonite, silica and iron oxides in microbially colonized flow paths are globally abundant. Research at these springs has provided insight into the controls on mineral solubility, crystallography, and microfossil preservation (Walter and Des Marais, 1993; Westall, 1999; Jones et al., 2000; Konhauser et al., 2003), improving the interpretative potential of chemical sediments in the geologic record (e.g. Arp et al., 2001; Kaufman and Xiao, 2003). In contrast, springs that precipitate barite (BaSO₄) as a dominant mineral phase are rare (Cadigan and Felmler, 1977; Sasaki and Minato, 1982; Younger, 1986), and the influence of microbes on barite precipitation has only recently come under investigation (Senko et al., 2004).

The Flybye Springs in Canada's Northwest Territories are unique as the only known location where barite precipitates as a dominant mineral phase from cold spring water. The Flybye spring water is barium-rich (up to 12 ppm), contains high levels of dissolved sulphide, and supports a microbial community dominated by sulphur-oxidising bacteria, sulphur-tolerant cyanobacteria, and fungi. These microbes assert microenvironmental influence on redox and ionic concentration gradients and, thus, mediate barite solubility in, on, and around microbial mats, cells and intracellular inclusions. Barite precipitated through microbial mediation, or biomineralisation, at Flybye Springs commonly produces microfossils that preserve the dimensions of microbial cells and cellular inclusions. Though the geochemical cycling of barium is strongly linked to organic productivity (Bertram and Cohen, 1997; Ganeshram et al., 2003), and the influence of sulphur metabolizing microbes on barite saturation gradients is well established (Baldi et al., 1996; Senko et al., 2004), the textural products of barite biomineralisation have not been documented outside of laboratory experiments (e.g. Sakorn et al., 2002; Gonzalez-Munoz et al., 2003).

This paper uses a combined geochemical and microscopic approach to describe the unique physiochemical and microbiological characteristics of the Flybye Springs flow

* *A version of this chapter has been published.*
Bonny S. and Jones, B. 2007. Barite (BaSO₄) biomineralisation at Flybye Springs, a cold sulphur spring system in Canada's Northwest Territories. *Canadian Journal of Earth Sciences*, 44: 835-856.

path that combine to facilitate what is, to the best knowledge of the author, the first account of 'natural' barite biomineralisation and its microtextural artefacts.

Study Site

The Flybye Springs sit at a southwesterly dipping contact between massive Devonian limestone and black, pyritic shale (Cecile, 2000) exposed on the north side of a terraced valley between the Selwyn and Mackenzie mountain ranges in the Sahtu Region of Canada's Northwest Territories (Fig. 2-1A). There are numerous mineral springs in the area (Cecile, 2000) but the Flybye Springs are the only ones known to precipitate barite as a dominant mineral phase. Barium in the Flybye spring water is thought to be derived from dissolution of barite microcrystals and barium-enriched feldspars dispersed in Paleozoic marine aquifer strata (Cecile et al., 1984; Orberger et al., 2005).

The Flybye spring water emerges through a sparsely vegetated crescent-shaped mound, 200 m² in area and up to 5 m high, which is composed of relict barite tufa formed by past activity at the springs. There are ten active spring vents and numerous small seeps concentrated on the south-eastern side of the mound, and spring water flows downhill towards a mud wallow frequented by caribou and other wildlife (Fig. 2-1B). This study focuses on microbes and mineral precipitates found in the flow paths of the four largest spring vents, D1-4 (Fig. 2-1C). Located just south of the Arctic Circle, the Flybye Springs experience harsh winters that precluded year-round observation of the field site – all data pertain to summer (July-August) conditions.

Methods

Fieldwork

The pH, conductivity, and dissolved oxygen content of the Flybye spring water were measured across the spring site in July 2004 and August 2005 using a portable accumet AP62 pH/mV meter and an Orion Model 1230 D.O./pH/mV probe, both of which yield data adjusted to contemporaneous temperature measurements. Water samples were collected from vents D1-4 through a 0.45 µm pore size FisherBrand water-testing membrane, and stored in sterile 250 ml Nalgene containers for isotopic and elemental analysis. H₂S_(g) dissolved in the spring water was collected from the flow path beneath

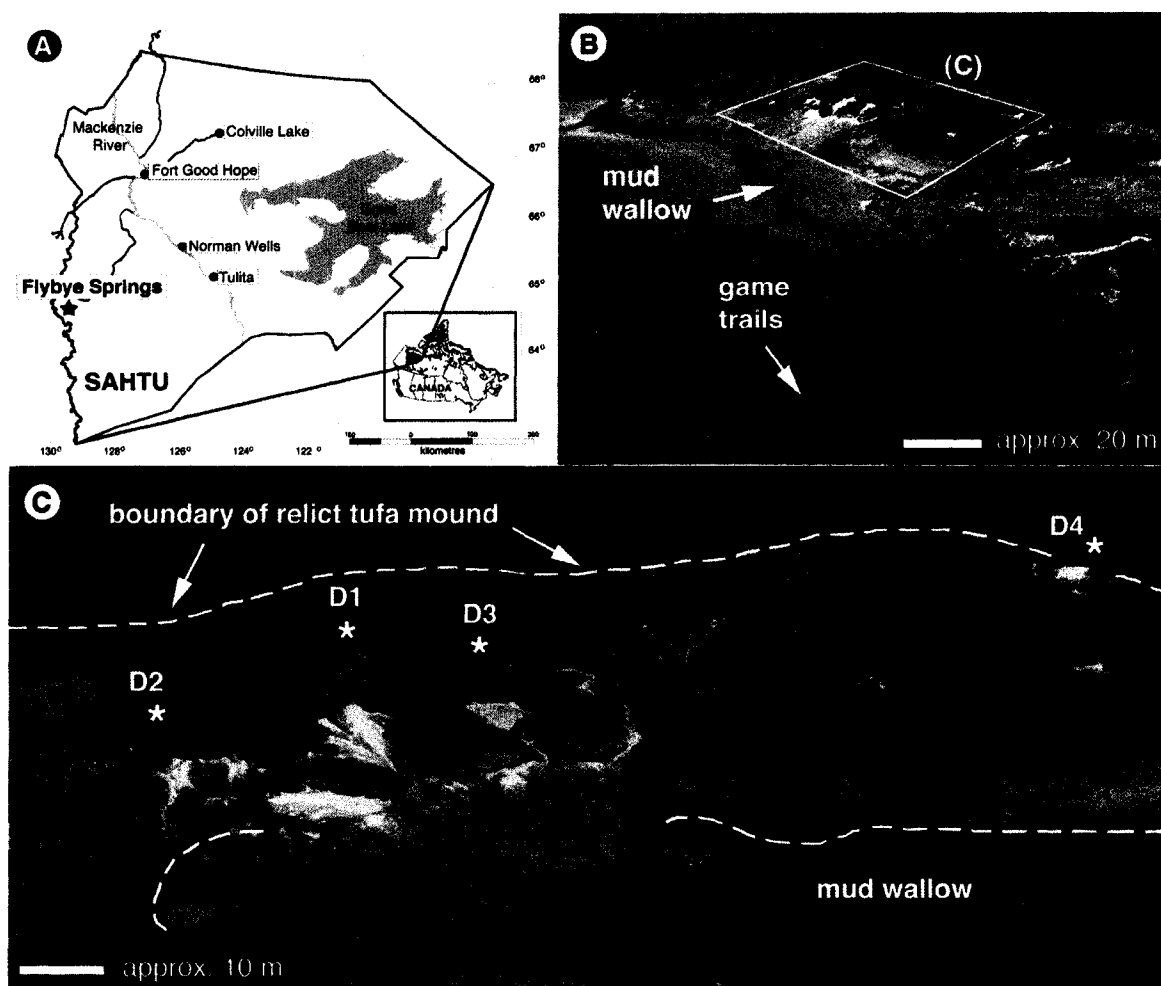


Figure 2-1. Study area. (A) Location of the Flybye Springs. (B) Aerial view of Flybye Springs site. (C) Aerial view of boxed area in image B showing spring vents D1 to D4.

vent D1 by mixing with soluble CdCl_2 in sterile 250 ml Nalgene containers to prompt precipitation of insoluble CdS. Vent waters were channeled into the containers gravimetrically through tygon tubing to prevent oxidation prior to precipitation. Gases exsolving from a vent-fed pool below D2 were collected by filling a sterile Nalgene bottle with spring water, inverting it above a spring vent, and trapping the rising gas bubbles in the bottle.

Fresh mineral precipitates and microbial samples were collected in sufficient number to represent the textural and chromatic variability observed in the field. One half of each microbial sample was stored in spring water and the other was preserved in a 6:3:1 solution of water, 95% alcohol and formalin with 5 ml of glycerol added per 100 ml. Twelve glass slides were placed in the proximal flow paths of vents D1-4 in early July, 2004. Despite careful flagging, only three slides were retrieved 10 months later, and two of these were fractured. Caribou hair, antlers and hoof prints on the spring mound indicate that the site was disturbed repeatedly over the course of the year.

Laboratory Analyses

Elemental spring water chemistry was determined by inductively coupled mass spectrometry (ICP-MS) or four vent water samples at the University of Saskatchewan (see Appendix 2). Barium measured significantly lower than data reported by Cecile et al. (1984), which may be explained by inadvertent oxidation of the water samples during collection (resulting in removal of Ba^{2+} as BaSO_4 prior to water analyses), or by the fact that the ICP-MS method is calibrated to detect trace quantities of Ba^{2+} in groundwater, and yielded spurious results for higher concentrations in Flybye Spring water. Select 'whole container' samples (i.e. dissolved and potentially precipitated elements) were re-analyzed by neutron activation analysis (NAA) at the University of Alberta's SLOWPOKE Facility (following Al-Jundi, 2001). SOLMINEQ88 was used to evaluate the saturation state of the spring water with respect to relevant mineral phases (see Appendix 2). The gas sample was analysed on a Finnigan Mat 252 mass spectrometer to determine the gas type, and qualitatively assess the relative abundance of gaseous components. Peak detection criteria were set as start slope 0.090 mV/s, end slope 0.010 mV/s, with a minimum detection amplitude of 0.020 V. $\delta^{34}\text{SCDT}$ of 4 H_2S gas samples

(precipitated as CdS and converted to AgS) and 9 dissolved sulphate samples were determined by elemental analysis and isotope ratio mass spectrometry (EA-IRMS) at the University of Calgary Isotope Science Laboratory. Data are reported relative to the Vienna Canon Diablo Triolite standard, with precision of +/- 0.4 ‰.

Mineral precipitates and retrieved glass slides were examined by petrographic microscope, X-ray diffraction (XRD), scanning electron microscopy (SEM), and energy dispersive X-ray analysis (EDX). SEM samples were desiccated, mounted on steel stubs with carbon tape, sputter coated with gold and examined in secondary electron and backscattered electron mode on a JEOL 6301 field emission scanning electron microscope at accelerating voltages of 5 – 30 kV. In backscattered electron SEM images, variations in atomic weight are reflected in image brightness – barium (with an atomic mass of 137.3) is very bright in contrast to increasingly dark sulphur (32.1), silicon (28.1), and organic material (~12.0).

Microbial samples were examined by light microscopy and SEM. Diatoms were identified to species-level following Simonsen (1987). Where possible, soft-bodied microbes were identified by morphological criteria following Rippka et al. (1979), Reichenback (1981), Larkin and Strohl (1983), Schlegel and Bowien (1987), and Wher and Sheath (2003). The Flybye Springs filamentous microbes were identified to genus-level with a high degree of confidence, but species-assignments were not possible on the basis of morphology (cf. Douglas and Douglas, 2001; Teske and Nelson, 2005). A variety of sub-micron sized unicellular microbes and actinomycetes were found in SEM, but as these forms are not volumetrically dominant, or commonly mineralised, they were not identified. Powdered samples of microbes and detrital organics were also investigated by neutron activation analysis to assess barium, radium and strontium enrichment in biomass submerged in the Flybye spring water.

Spring water physiochemistry

The Flybye spring water emerges with an average vent temperature of 8.5°C and is heated by sunlight to 14°C before entering the mud wallow. pH is circumneutral at the vents and increases downstream to a maximum value of 8.4. The spring water is anoxic

to dysoxic on emergence, containing ≤ 0.54 mg/L dissolved oxygen, and exsolves fragrant H_2S gas.

Water emerging from vent D1 and nearby seeps has $\delta^{34}\text{S}_{\text{sulphide}}$ values ranging from 13.7 – 15.8 ‰, which agree with a sulphur source in Paleozoic marine strata (Cecile et al., 1984; Canfield, 2001; Allen et al., 2002). $\delta^{34}\text{S}_{\text{sulphate}}$ increases downstream in the D1 flow path, shifting from 17.3 ‰ at 1 m, to 19.0‰ by 5 m, then reverses the trend, dropping to a minimum of 14.7 ‰ in the distal flow path.

Flybye spring water becomes oxygenated (van Everdingen, 1972) an average distance of 8 m from its source; however, re-mixing with anoxic or dysoxic waters emerging from seeps in the lower mound complicate the dissolved oxygen profile of many spring water tributaries (Fig. 2-2). Stream fed pools on the lower Flybye Spring mound are redox stratified, with anoxic, organic rich bottom waters, and clear, oxygenated surface waters. Vent fed pools on the upper mound are also redox stratified, with anoxic bottom waters and dysoxic surface waters (Fig. 2-2).

Gas bubbles exsolving from a vent fed pool were found to contain methane, propane, ethane and iso- and normal butane, in a ratio consistent with a source in a medium maturity natural gas seep (Meuhlenbachs, per. comm.). The gas also contains carbon dioxide, which probably originated from CO_2 dissolved in the spring water and microbial respiration amongst organic detritus accumulated in the pools.

The spring water contains high concentrations of sodium and chloride, and is anomalously enriched in barium relative to regional surface waters (Cecile et al., 1984) (Table 2-1).

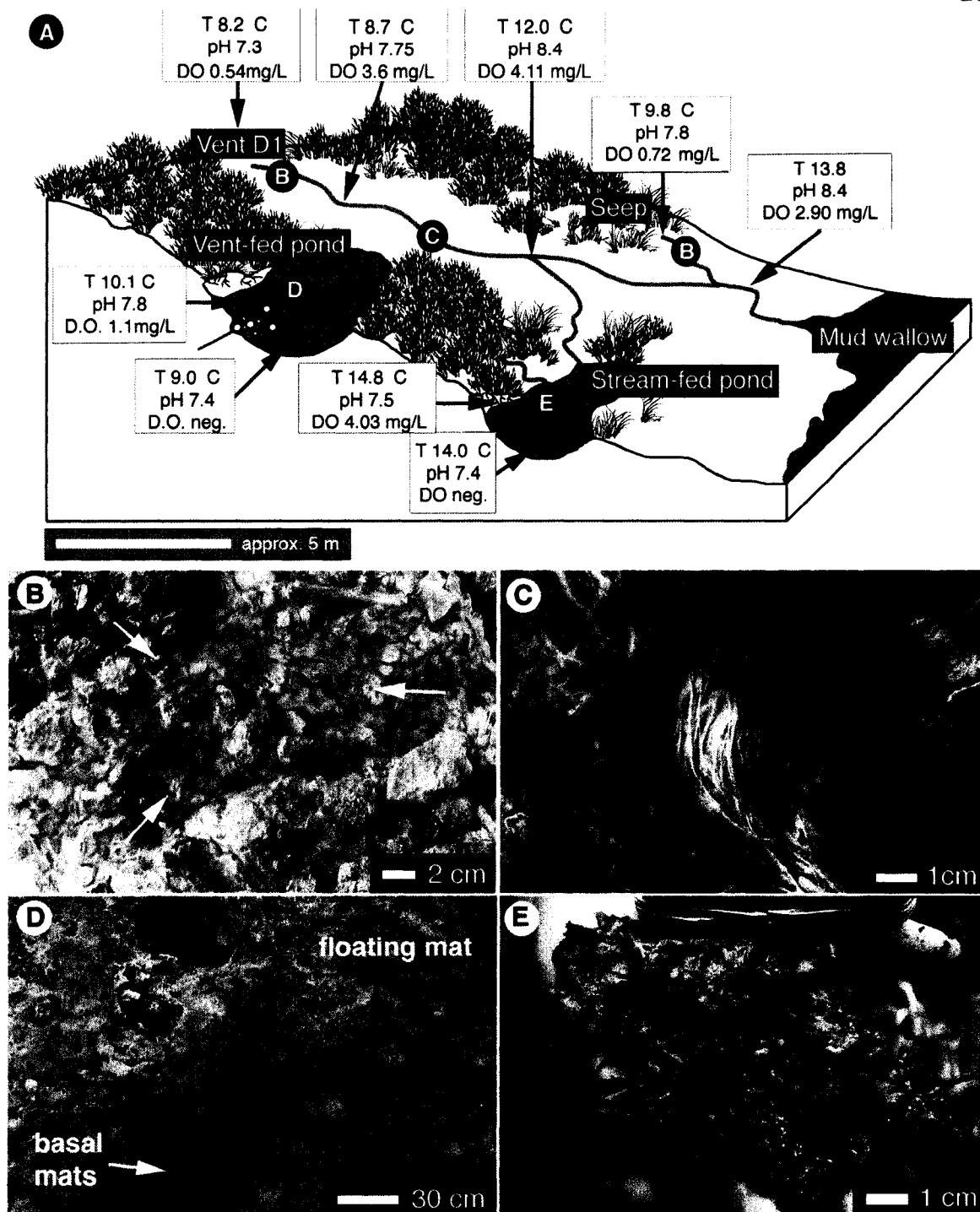


Figure 2-2. Schematic representation of flow path beneath vent D1. (A) Idealized profile of flow path below vent D1 showing physiochemical data and distribution of microbial communities. (B) Fringes of *Thiothrix*. (C) Streamers composed of *Thiothrix* and filaments. (D) Tiered microbial mats in a vent-fed pond. (E) Bubbly microbial mat from stream-fed pond (pocket knife is 10 cm long).

| | Cecile et al. (1984) | ICP-MS (2004) | ICP-MS (2005) | NAA (2005) |
|--------------------------------|----------------------|-------------------|---------------|------------|
| Ca ²⁺ | 38 | 47 | 42 | |
| Mg ²⁺ | 18 | 11.7 | 15.6 | |
| Mn ²⁺ | | | | 0.016 |
| K ⁺ | 3.3 | 2.6 | 3.2 | |
| Na ⁺ | 6.2 | 52.6 | 56.7 | |
| Ba ²⁺ | 112 [†] | 0.57 [*] | 3.38 | 12 |
| Sr ²⁺ | | 0.02 [*] | 1.06 | |
| Fe ²⁺ | <0.025 | 0.08 | 0.007 | |
| Pb ²⁺ | 0.013 | 0.018 | | |
| Cl ⁻ | 110 | 72.9 | 61 | 72.4 |
| HCO ₃ ²⁻ | 245 | | 192 | |
| SO ₄ ²⁻ | 36 | 53.4 | 53.3 | |
| NO ₃ ⁻ | | | 2.2 | |
| UO ₂ | 0.007 | 0.001 | | |
| SiO ₂ | 7.4 | 4.9 | 3.7 | |
| Ra (pCi/L) | 41.5 | | | |

all values in ppm

Table 2-1. Average chemical composition of Flybye Springs vent waters. ICP-MS = inductively coupled plasma mass spectrometry; NAA = neutron activation analysis; data from Cecile et al. (1984) were generated by atomic absorption mass spectrometry.

[†] May have been estimated from charge balance calculations rather than measured directly
^{*} Anomalously low values may reflect difficulties with the ICP-MS method for measuring these elements (cf. Al Jundi 2001)

Solutions are saturated with respect to mineral phases for which [$\log(\text{ion activity product/solubility constant})$] is ≥ 0 . Upon emergence, the Flybye spring water is near saturation with respect to calcite (-0.16 to 0.00), aragonite (-0.31 to -0.01), and chalcedony (-0.02 to 0.10), undersaturated with respect to witherite (-2.48 to -0.82), and supersaturated with respect to barite (0.99 to 2.32)(SOLMINEQ88 – see Appendix 2).

During the summer months, all inundated parts of the Flybye flow path are microbially colonized and desiccated mat samples were found to be up to three times enriched in strontium compared to surrounding spring water, and contain up to 36.5 wt % barium. This corresponds to roughly 14 wt.% barium in hydrated mats, or 24.8 wt. % barite if all mat-bound barium were precipitated with sulphate.

Spring Biology

Microbes inhabit all inundated parts of the Flybye Spring mound. Good correlation was found between the macroscopic appearance of microbial colonies, their

constituent microbial genera, and spring water physiochemistry (Table 2-2; Fig. 2-2). The flow paths of springs D1, D2, and D3 share a downstream progression of microbial genera (Fig. 2-2).

In proximal dysoxic flow paths, white fringes, 1-3 cm long (Fig. 2-2A), composed of *Thiothrix* (Figs. 2-3A, B) are established within 1.5 - 2 m of most vents and seeps. In dysoxic eddies and pools downstream, filaments of *Beggiatoa* (Fig. 2-3C) are intertwined with *Thiothrix* in streamers up to 5 cm long, which also contain abundant mucus, or extracellular polymeric substances (EPS)(Fig. 2-2B).

Redox stratified vent-fed ponds have tiered microbial communities (Fig. 2-2C). *Thioploca* (Figs. 2-3D, E) forms black-green, EPS-rich drapes with sulphur-reducing bacteria and *Chromatium* (Fig. 2-3F) amongst degrading organic detritus in anoxic bottom waters. Diatoms (including *Achnanthes minutissima*, *Achnanthes flexella*, *Cymbella microcephala* and species of *Amphora* and *Navicula*), *Oscillaotoria* (Figs. 2-3G, H, I) and *Beggiatoa* cohabitate in green-brown microbial mats floating in dysoxic waters 3-10 cm below the surface of the ponds.

Ponds fed by spring water tributaries have oxygenated surface waters with floating bubbly, laminated green-orange mats (Fig. 2-2D). The top layer of these mats is dominated by cyanobacteria including *Oscillatoria*, *Planktothrix*, and an *Anabaena*-like cyanobacterium that lacks heterocysts (Figs. 2-3I, J), and diatoms. Basal layers of the mats contain patches of *Beggiatoa* filaments, degrading cyanobacteria, and *Chromatium*. Sulphate reducing bacteria colonize detrital organics accumulated at the bottom of the ponds.

Substrates bordering spring water tributaries are commonly encrusted by yellow films composed of sulphur and fungal hyphae (Figs. 2-3K, L). Although it cannot be certain that samples were not contaminated after collection, SEM analysis of these films showed that they are dominated by *Penicillium* sp. *Thiothrix* filaments were found intertwined with fungal hyphae in several areas, which indicates that the fungi are endemic to the edges of the spring flow path. Fungal diversity may be limited by the high sulphur

Table 2-2. Morphological and environmental details of the dominant microbial genera at the Flybye Springs. ISD = 'intracellular sulphur deposition'; ST = 'sulphide tolerant' (after Rippka et al. 1979; Reichenback 1981; Larkin & Strohl 1983; Wher & Sheath 2003; Teske & Nelson 2005).

| Genus | Morphology | ISD | ST | Habitat | Flybye Field Appearance |
|-----------------------------------|---|------------|-----------|--|--|
| <i>Sulphur Oxidising Bacteria</i> | | | | | |
| <i>Thiothrix</i> | Colourless cylindrical filaments; 1-2 µm wide; septa every 0.5-1 µm; unsheathed; occur in rosettes; adhere to filaments of <i>Beggiatoa</i> | Yes | Yes | Flowing dysoxic water | White fringes; streamers |
| <i>Beggiatoa</i> | Colourless cylindrical filaments; 3-5 µm wide; septae every 1-2 µm; unsheathed; occur singly; form hormogonia; gliding movement | Yes | Yes | Oxic/anoxic interface, low current conditions | Streamers; basal layers of floating mats; occasionally top layers of floating mats |
| <i>Thioploca</i> | Up to 15 <i>Beggiatoa</i> -like filaments within a common sheath up to 20 µm in diameter; sheath has sub-regular constrictions and sometimes longitudinal wrinkles; macroscopic green-blue colour | Yes | Yes | Bottom of dysoxic/anoxic lakes, ponds and springs with elevated sulphide | Stringy drapes amongst organic detritus at the base of vent-fed ponds |
| <i>Purple Sulphur Bacteria</i> | | | | | |
| <i>Chromatium</i> | Motile; oval to bean shaped cells 1-3 µm long; pink in light microscope | Yes | Yes | In photic zone with hydrogen sulphide and organic carbon | Magenta patches on 'leafy mats'; mid-lower layers of floating mats |
| <i>Cyanobacteria</i> | | | | | |
| <i>Oscillatoria</i> | Olive-green filaments; 5 µm wide; septa every 1 µm (or less); unsheathed; non refractory internal granules; form hormogonia by necrotic cell development; gliding movement | No | Yes | Flowing or stagnant oxygenated to dysoxic water, wide chemical and thermal tolerance | Abundant in orange-green top-mid layers of floating mats |
| <i>Planktothrix</i> | Green filaments; 4-5 µm wide; septa every 1.5 µm; slightly constricted at cross walls; unsheathed; slightly expanded terminal cells | No | No | Cool to warm freshwater lakes and ponds | Top green layer of mats floating in stream-fed ponds |
| <i>Anabaena (?)</i> | Blue-green filaments; 3 µm wide; septa every ~ 4 µm; deep constrictions at cross walls; no heterocysts observed in filaments from Flybye Springs | No | No | Cool to warm freshwater lakes, ponds, and streams | Top green layer of mats floating in stream-fed ponds; mud wallow hoof prints |

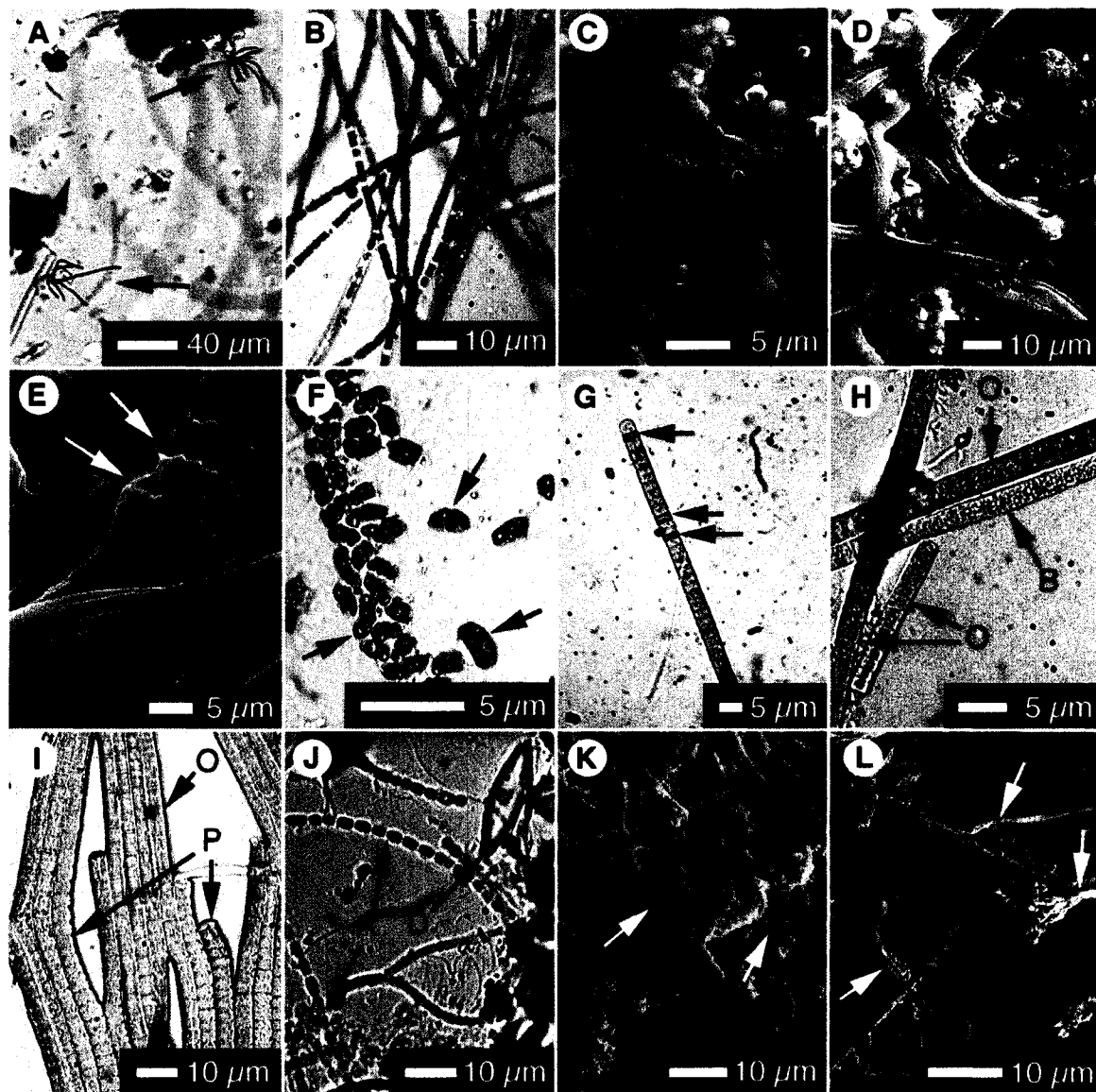


Figure 2-3. Light microscope and SEM images of microbes from Flybye Springs. (A) Rosettes of *Thiostrix*. (B) *Thiostrix* filaments with internal sulphur globules. (C) *Beggiatoa* filaments with internal sulphur globules. (D) Ensheathed *Thioploca* filament bundles. (E) Detail view of *Thioploca* bundle with deep sheath constriction points (arrows). (F) *Chromatium* with internal sulphur globules. (G) Filament of *Oscillatoria* with necrotic cells (arrows). (H) Filaments of *Oscillatoria* (O), with nonrefractory granular inclusions and *Beggiatoa* (B) with refractory sulphur globules. (I) Aligned filaments of *Oscillatoria* (O) and *Planktothrix* (P). (J) *Anabaena* (?) filaments and a diatom (d). (K) Branching fungal hyphae among elemental sulphur rhombs and beads. (L) Detail of *Penicillium* conidiophores.

content of the spring water, which is inhibitory to many fungal species (Gadd 1993; Rajashekhar and Kaveriappa 2003).

Fungal hyphae are also present in organic detritus in the spring flow path. Beneath overhanging shrubbery, many 'microbial' mats floating in vent and stream fed ponds contain up to 80% degrading leaves, by volume. The air-exposed surfaces of these 'leafy mats' are heavily colonized by fungi. Submerged leafy mat surfaces are commonly magenta due to dense colonization by *Chromatium*.

Mineral Precipitates

Glass slides left in the proximal flow paths for 10 months developed mineral encrustations 50 – 250 μm thick, suggesting a very slow rate of mineral precipitation from the spring water (Fig. 2-4A). Rocks, desiccating microbial mats and streamers, and detrital organics submerged in spring water tributaries, however, bear yellow films of elemental sulphur and yellow-gray mineral encrustations that are up to 5 mm thick (Fig. 2-4B). The yellow-gray crusts are composed of microbial cells and EPS, microcrystalline barite, amorphous silica in the form of diatom frustules and algal cysts, and elemental sulphur (Figs. 2-4C, D).

Sulphur is found as microcrystalline rhombic crystals and spherical globules (Fig. 2-4E). Crystalline elemental sulphur is a typical product of inorganic redox reactions in oxygenating spring water (Douglas and Douglas, 2000). The spherical globules, however, are identical in size and shape to those produced by sulphur metabolizing bacteria (Figs. 2-3B, C, F) and are most likely biogenic (cf. Douglas and Douglas 2001).

Barite is the most abundant and least soluble mineral precipitating from the Flybye Spring water. The Flybye barite is relatively pure, containing < 0.3% calcium and < 0.5% strontium, but is radioactive (up to 8 $\mu\text{Sv/hr}$, or three times background levels) due to co-precipitation of radium (Cecile et al. 1984).

Inorganic Barite Precipitation

The Flybye spring water is supersaturated with respect to barite with even slight oxidation of vent waters (SOLMINEQ88). Proximal to the spring vents, barite

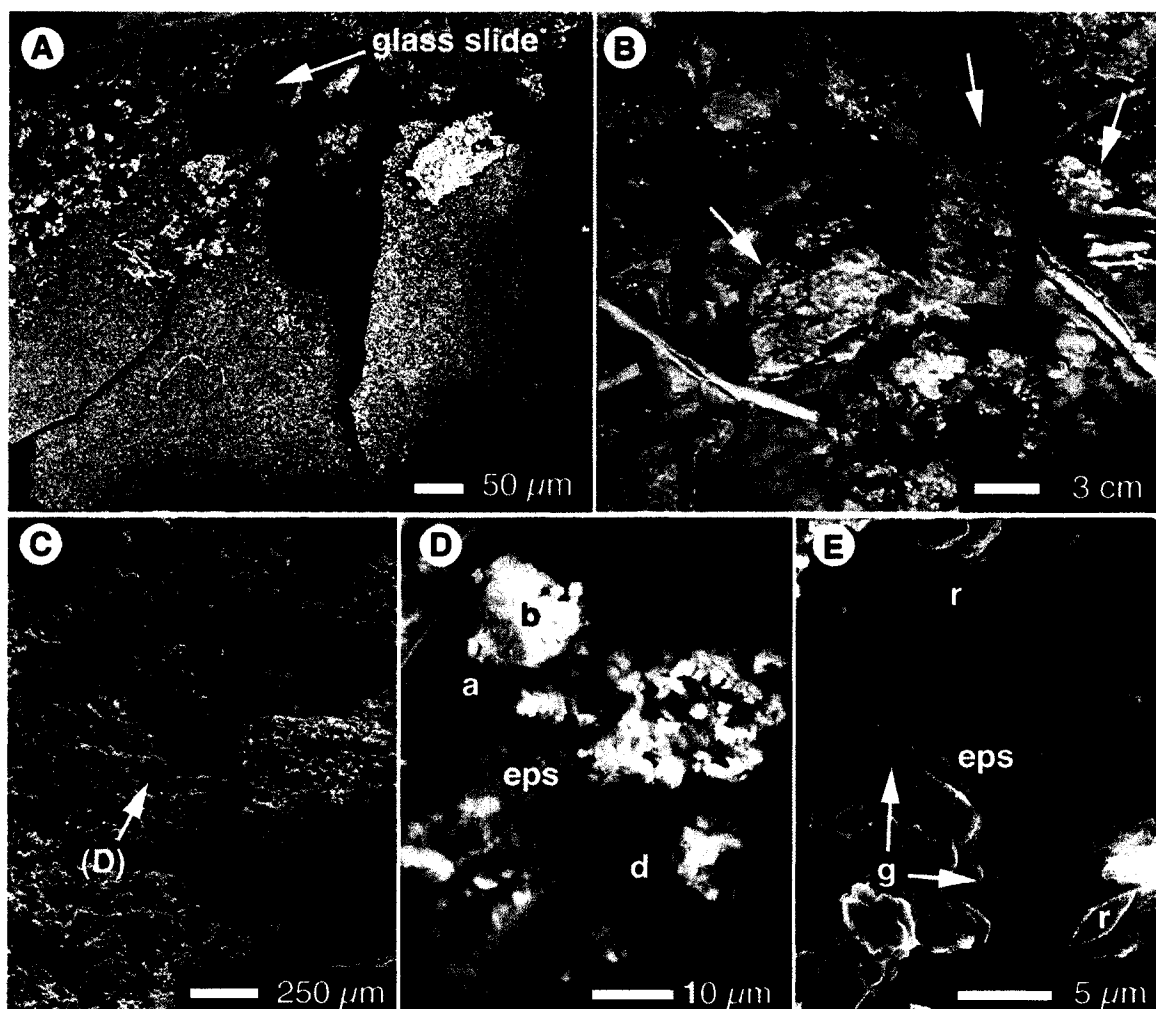


Figure 2-4. Fresh mineral precipitates from Flybye Springs. (A) Mineral encrustation on glass slide retrieved from below spring D2. (B) Mineral encrustations on rocks and detrital organics proximal to spring D2 (arrows). (C) SEM image of sample collected from image B. (D) Detail backscattered electron SEM image of previous sample showing an algal cyst (a), diatoms (d), EPS (eps) and detrital barite (b). (E) Elemental sulphur rhombs (r) and globules (g) trapped in EPS (eps).

precipitates in suspension as stellate microcrystals, 4-10 μm in diameter (Fig. 2-5A); scalloped platy microcrystals, 0.5 to 1 μm long, that are composed of subhedral platy microcrystals ≤ 200 nm wide (Figs. 2-5B, D); and intergrown tabular microcrystals 0.5-3 μm wide (Figs. 2-5C, D). These barite crystals accumulate amongst microbial mats and streamers bordering the flow paths, and continued crystal growth commonly envelops microbial cells or EPS strands (Figs. 2-5C, D). Microbial cells are also enveloped by balls of blocky barite microcrystals, up to 40 μm in diameter, found amongst porous clumps of detrital plant material and animal hair in proximal flow path tributaries (Figs. 2-5E, F). Spontaneous precipitation of barite from the spring water ceases beyond ~ 5 m of most spring vents and inorganic barite crystals are found only as scattered, presumably detrital, grains.

Barite Laminae in Microbial Mats

Mats in the proximal flow path entrap randomly distributed detrital barite microcrystals, but elsewhere on the spring mound, most mat-bound barite is concentrated in narrow laminae. Mats floating in spring water ponds commonly contain one or more barite lamina ≤ 10 μm thick (Figs. 2-6A, B). These laminae are sandwiched between lower *Beggiatoa*-rich and upper *Oscillatoria*/diatom-rich mat layers in dysoxic, vent-fed ponds, and between lower *Beggiatoa*-rich and upper *Oscillatoria/Anabaena* (?)/diatom-rich layers in surface oxygenated, stream-fed ponds (Figs. 2-6C, D). The barite laminae are composed of tightly packed anhedral to subhedral granular microcrystalline barite surrounded by EPS with few to no visible microbial cells (Figs. 2-6C, D).

'Leafy' microbial mats contain distinct barite laminae localized beneath the cuticular layers of degrading leaves. These laminae are composed of loosely packed composite barite spherules 0.8 to 5.0 μm in diameter (Fig. 2-6E). There is a gradational change in the habit of the composite microcrystals with spherule size: spherules ≤ 1 μm are composed of radially-arranged anhedral barite rods (Fig. 2-6F); intermediate-sized spherules have an outer-layer of subhedral platy crystals ≤ 100 nm long (Fig. 2-6G); and large spherules are coated by subhedral plates that are up to 0.5 μm long (Fig. 2-6E).

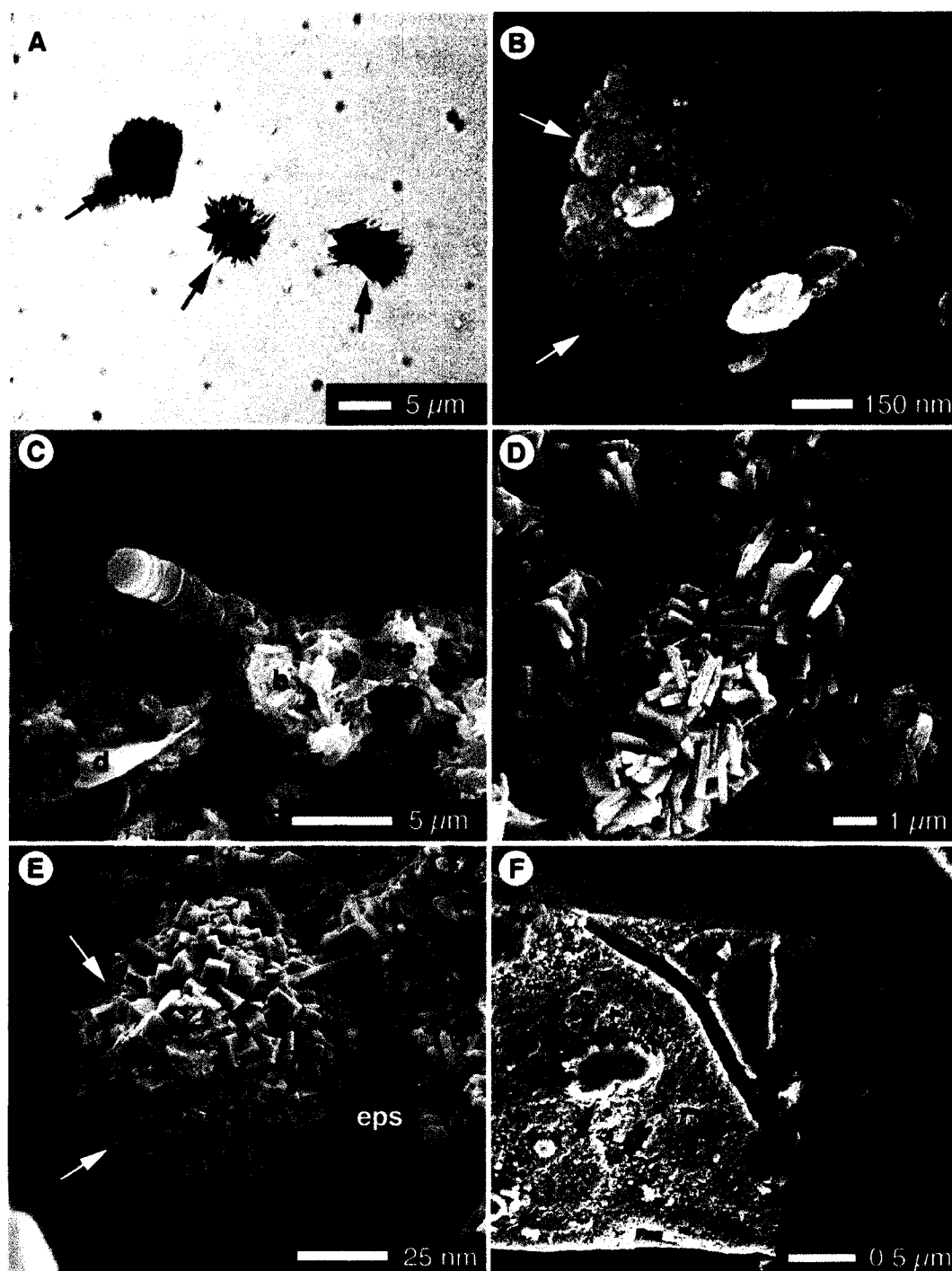


Figure 2-5. Inorganic barite precipitated from Flybye Springs. (A) Stellate barite microcrystals (arrows) among elemental sulphur globules. (B) Scalloped platy barite microcrystal (arrow). (C) Tabular barite microcrystals surrounded by EPS (eps) and microbial filament. (D) Close view of tabular barite microcrystals. (E) Composite blocky barite ball (arrows) trapped in EPS (eps). (F) Microbial cells forming casts (arrows) in blocky barite crystal.

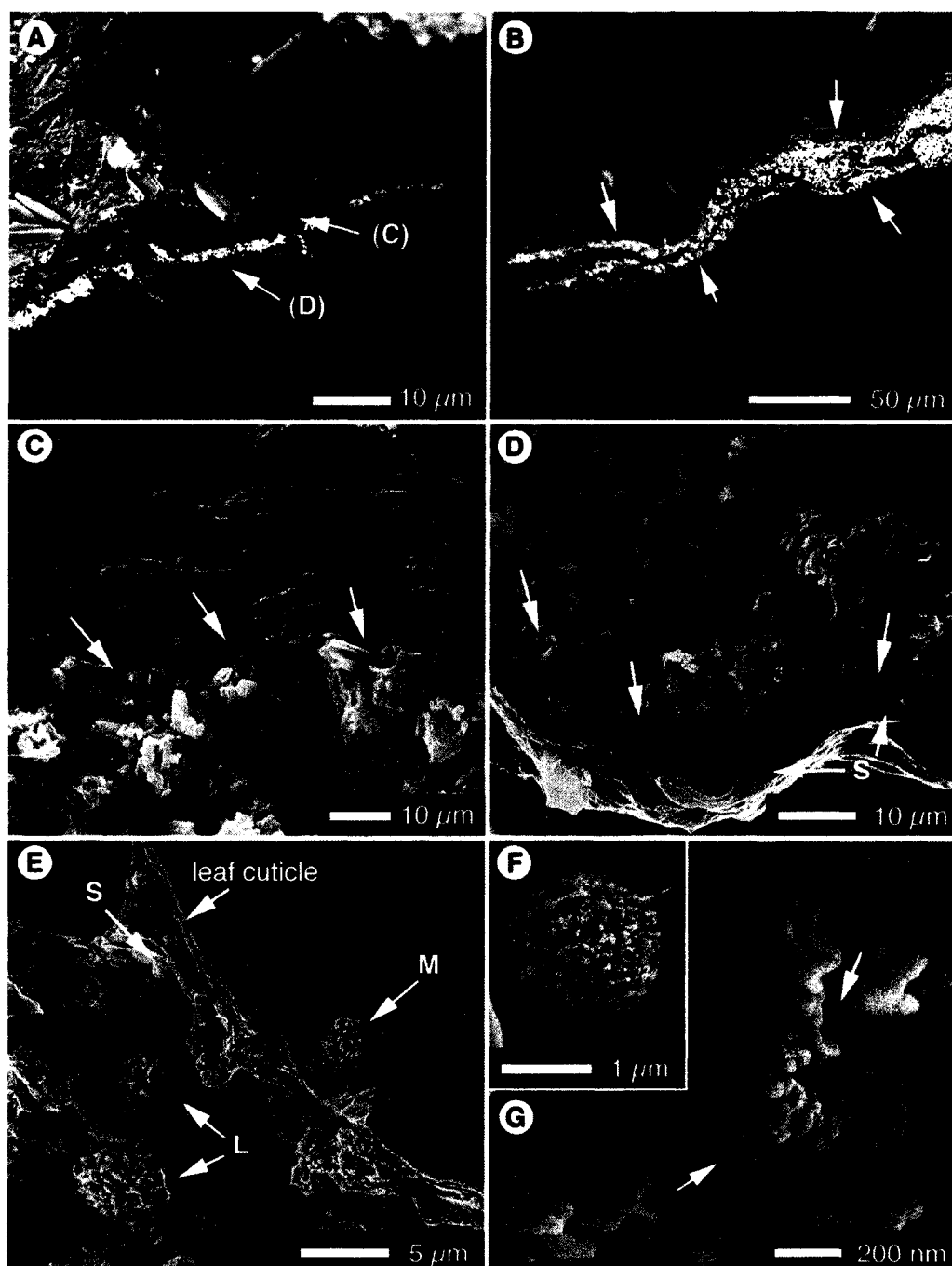


Figure. 2-6. Barite laminae in floating microbial mats. (A) BSE-SEM image of barite lamina in stream-fed pond mat (arrows). (B) BSE-SEM image of barite laminae in vent-fed pond mat (arrows). (C) Upper boundary of barite lamina from A (arrows) with filamentous cyanobacteria and diatom above, granular barite below. (D) Lower boundary of barite lamina from A (arrows) with detrital diatoms, organics and sulphur-metabolizing microbes (S-arrow shows sulphur inclusions) below, granular barite above. (E) Sparse barite lamina below leaf cuticle in floating 'leafy mat' – barite spherules are large (L), medium (M-image F) and small (S- image G).

Barite Coated and Encrusted Microbes

Barite is found coating the outer surfaces of diverse microbial genera throughout the Flyby spring system. Initial barite precipitation involves the deposition of globules of barite, <100 nm in diameter, on outer cell surfaces. Early globule precipitation is spatially specific in fungi, with globules concentrated at hyphal tips (Fig. 2-7A), but appears random in other microbial groups (Fig. 2-7B). Progressive globule precipitation forms cell-encompassing coatings (Figs. 2-7C, D).

Globular barite coatings are common on *Thioploca* bundles growing in anoxic ponds, where they adhere to the exterior of *Thioploca*'s thick EPS sheath (Figs. 2-7D, E), and are basal to secondary encrustations. Unicellular bacteria (most likely SRB) attached to the *Thioploca* sheaths are enveloped by these barite encrustations and preserved as ovoid molds (Fig. 2-7F).

Secondary encrustations can triple the diameter of coated microbes (Figs. 2-8A, B). They are composed of subhedral to euhedral platy barite crystals that precipitate *in situ* (Fig. 2-8C) and/or detrital grains trapped by EPS films (Fig. 2-8D). Fragmentation of coated and encrusted microbial filaments generates tunnel-shaped detrital grains (Fig. 2-8D).

Barite Permineralised Cell Walls

The outer cell layers of *Thiothrix* and *Beggiatoa* growing as streamers in flow path tributaries, and *Beggiatoa* and *Oscillatoria* in the upper layers of mats floating in vent-fed ponds, are commonly impregnated, rather than coated, by nanometric barite globules (Figs. 2-9A, B, C). Permineralised cell walls are basal to secondary encrustations of anhedral and subhedral barite microcrystals in many specimens (Figs. 2-9D, E, F). Degradation of the cell contents following permineralisation of the cell wall creates tunnel shaped grains that, most commonly, are not only externally encrusted, but also filled by barite microcrystals (Figs. 2-9D, E). Fragmentation of these microfossils generates three-layered detrital grains (Fig. 2-9F).

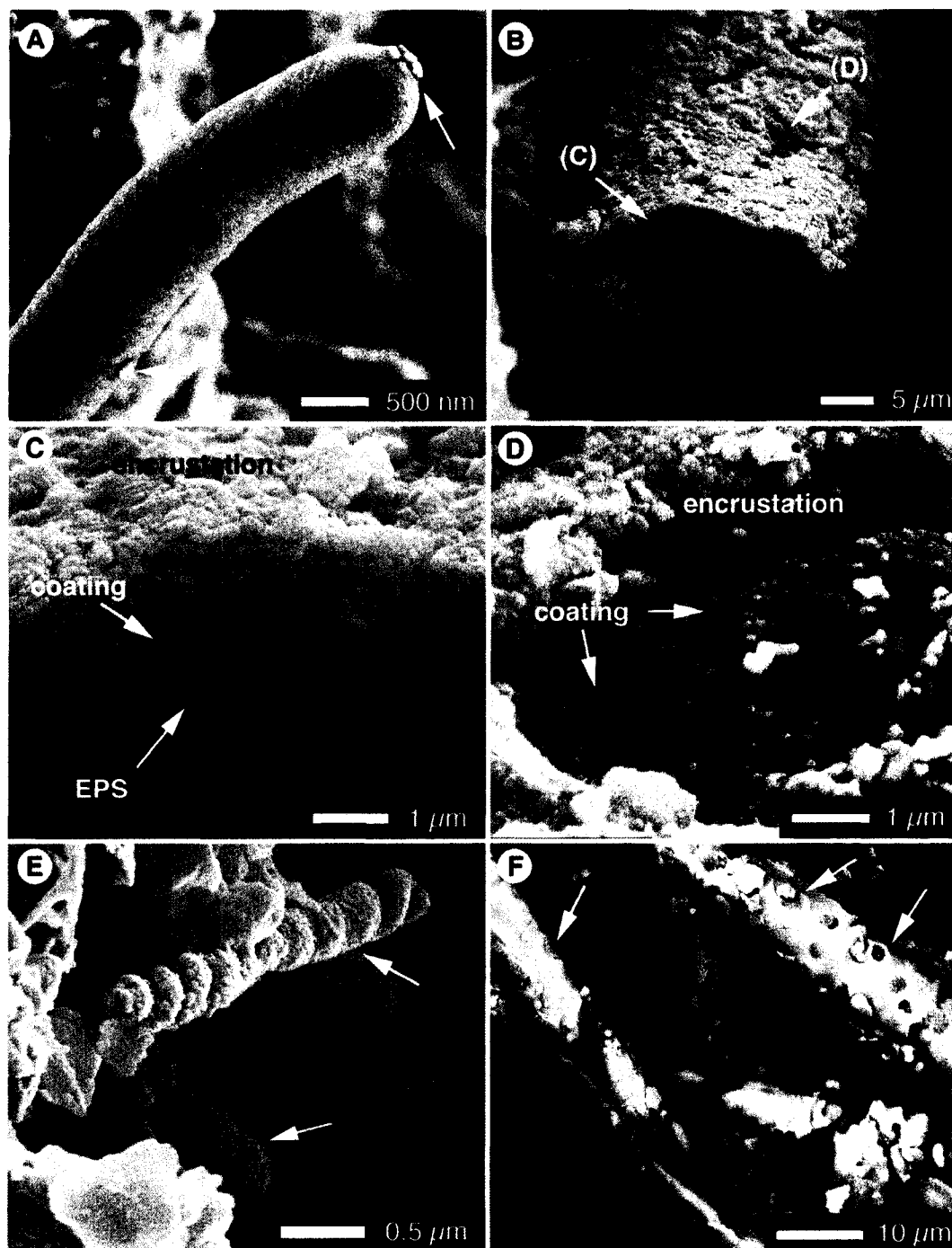


Figure 2-7. Barite coating and encrusting microbial cells. (A) Nanometric barite globules (arrows) concentrated near tip of fungal hypha. (B) Barite coated and encrusted *Thioploca* sheath. (C) Cross-section of *Thioploca* filament in B. (D) Detail of sparsely mineralised part of *Thioploca* filament showing random arrangement of nanometric barite globule coating. (E) Two single-celled bacteria (arrows) with cell encompassing globular barite coatings. (F) BSE-SEM image of barite encrusted *Thioploca* filaments with casts of SRB (arrows).

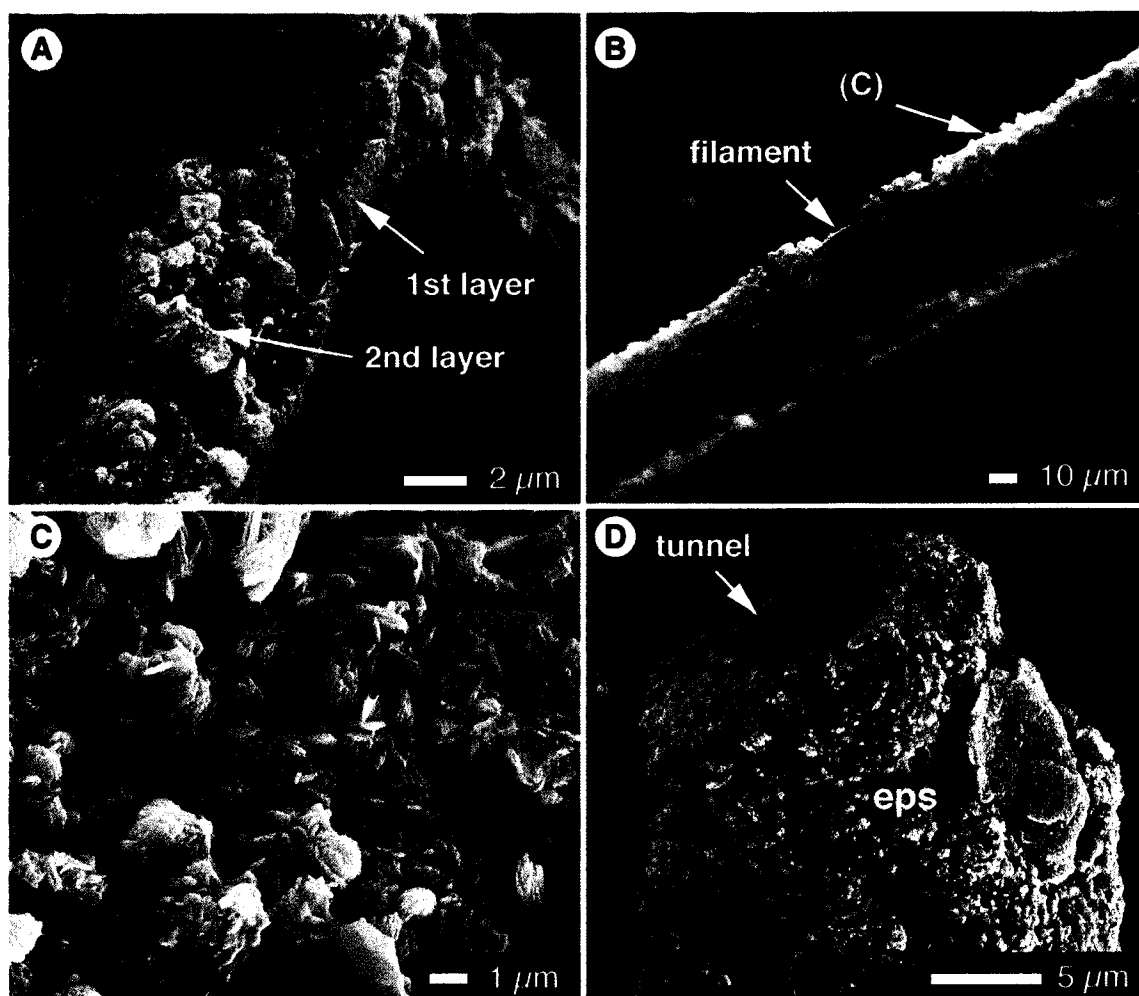


Figure 2-8. Barite encrusting microbial cells. (A) Thioploca filament with subhedral crystals (2nd layer) on top of anhedral encrustation (1st layer). (B) Heavily encrusted filament. (C) Detail of surface of encrusted filament in B showing intergrown subhedral platy crystals. (D) Detrital tunnel-shaped grain with outer layer of detrital barite trapped in EPS (eps).

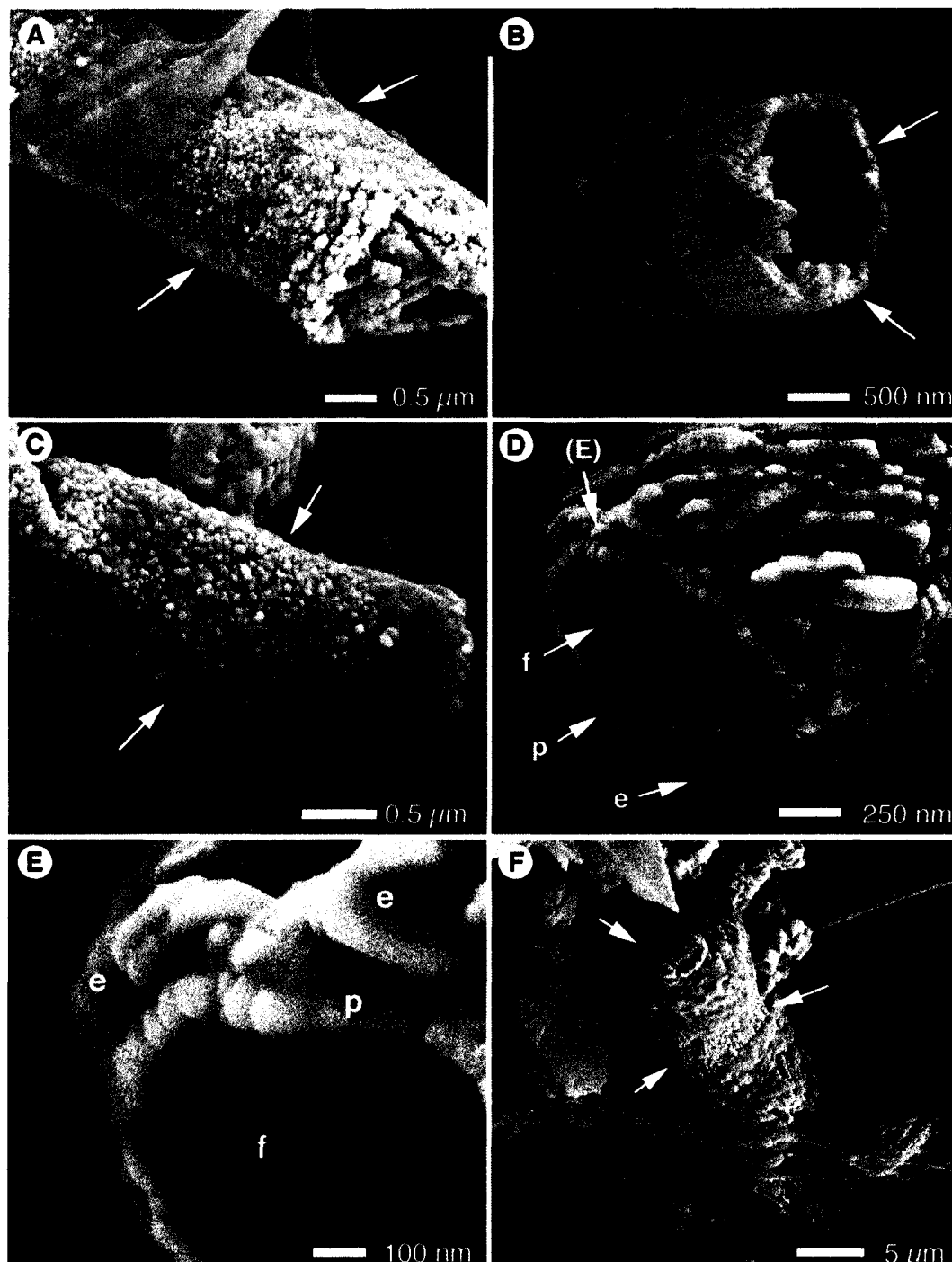


Figure 2-9. Barite permineralised microbial cell walls. (A) Side view of permineralised filament with diameter corresponding to *Beggiatoa* or *Oscillatoria*. (B) Cross-section of permineralised filament. (C) Detail of surface of permineralised cell with diameter corresponding to *Thiostrix*. (D) End of filament showing encrusting barite (e), permineralised cell wall (p), and infilling precipitates (f). (E) Detail of filament in D showing distinction between permineralising barite globules (p) and encrusting platy crystals (e). (F) Three layered detrital grain.

Intracellular barite precipitation

A distinct mode of baritisation was found in *Beggiatoa* and *Thiothrix* filaments growing near the top of a glass slide ~ 4 m from vent D2, and in *Beggiatoa* filaments from the bottom layer of mats floating in stream-fed ponds. These filaments have cellular compartments that are locally filled by barite (Fig. 2-10). Chains of neighbouring cells are sometimes baritised together (Figs. 2-10A, B), but it is also common to find filaments of *Beggiatoa* or *Thiothrix* in which only one cell, or several adjacent cells, are barite-filled, and surrounding cells appear viable (Figs. 2-10C, D, E). Barite precipitation is limited to the cell cavity, or cytoplasmic chamber, and does not appear to affect septae, nor cell walls (Figs. 2-10A, B). In no instance was a filament found that was both filled and coated/permineralised by barite. Indeed, in many instances barite-filled filaments were found among completely non-mineralised filaments (e.g., Fig. 2-10A).

It is difficult to assess the crystal morphology of the cell-filling barite because it is surrounded by intact cell walls (Fig. 2-10E). Detrital, unimodal cylindrical grains, composed of nanometric anhedral barite are locally abundant among desiccating *Beggiatoa* streamers, however, and may represent cell-filling barite released from degrading filaments (Fig. 2-10F).

In the sulphide-rich proximal spring flow path, *Beggiatoa* and *Thiothrix* filaments are commonly packed with $\leq 1.5 \mu\text{m}$ spherical inclusions identifiable as sulphur globules by their refractory appearance in crossed polar light microscopy and EDX analysis. Detrital chains of intergrown, sub-crystalline sulphur spheres are released upon cell lysis (Fig. 2-11A). Morphologically analogous chains of intergrown sub-spherical barite were also found among desiccating streamer colonies and are dispersed in *Beggiatoa*-rich mats in stream-fed ponds (Figs. 2-11B, C). In some specimens barite spheres are aligned along lysed filaments (Figs. 2-11D, E), indicating that they may have formed intracellularly. A cluster of *Chromatium* found on the slide retrieved from the D2 flow path was found to contain both intracellular sulphur globules and barium-enriched intracellular inclusions (Fig. 2-11F).

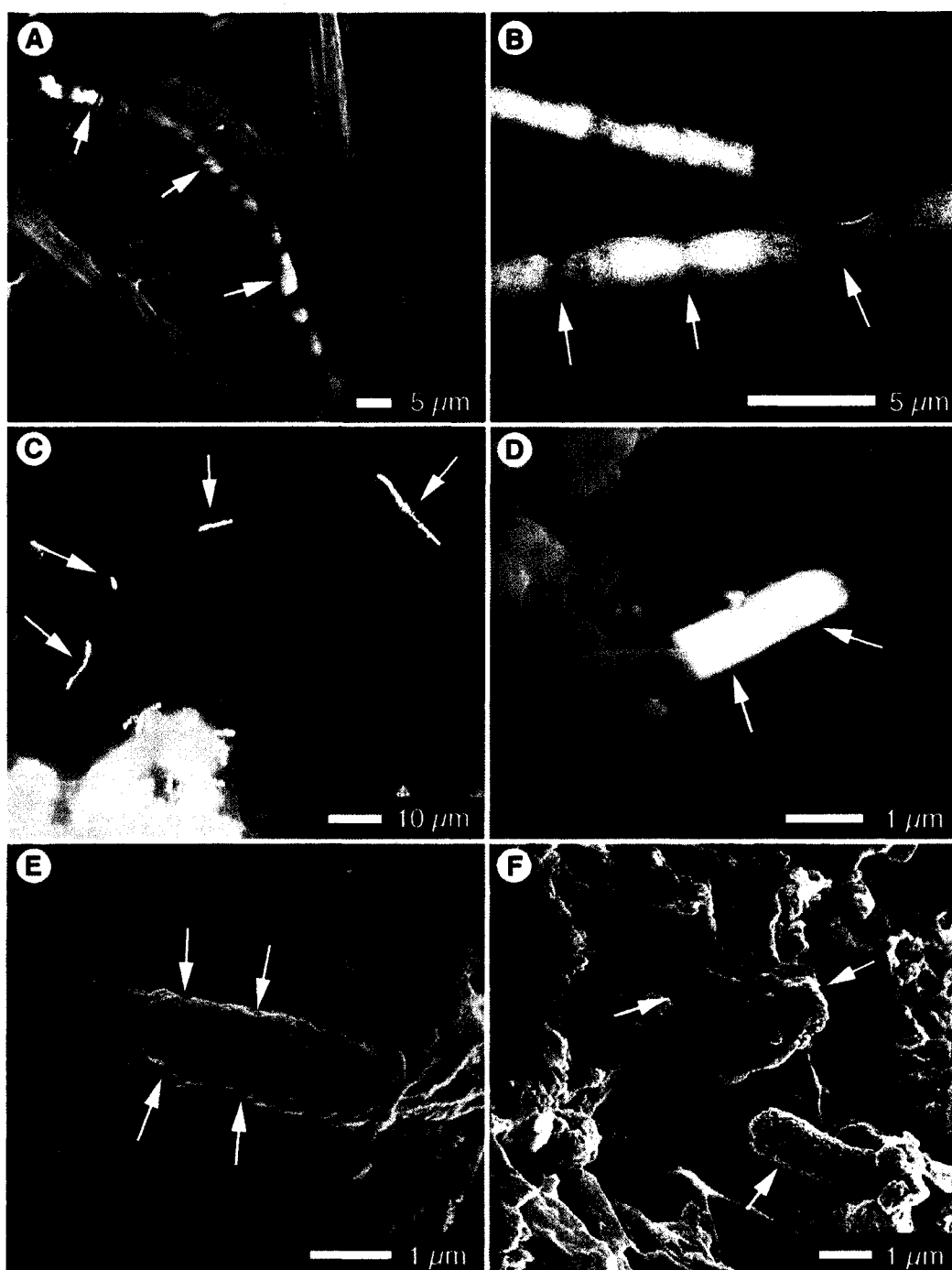


Figure 2-10. Barite filled microbial cells. (A) Barite filled *Beggiatoa* filament among non-mineralised filaments. (B) BSE-SEM image of barite filled cells in *Beggiatoa* and *Thioploca* filaments – note that cell walls and septae are not mineralised (arrows). (C) Crossed polar light microscope image of *Thiothrix* filaments with isolated groups of barite filled cells. (D) Two barite filled cells in *Thiothrix* filament (arrows). (E) Chain of barite filled cells embedded in EPS (arrows indicate septal breaks). (F) Unimodal detrital grains may represent barite released from degrading filaments (arrows).

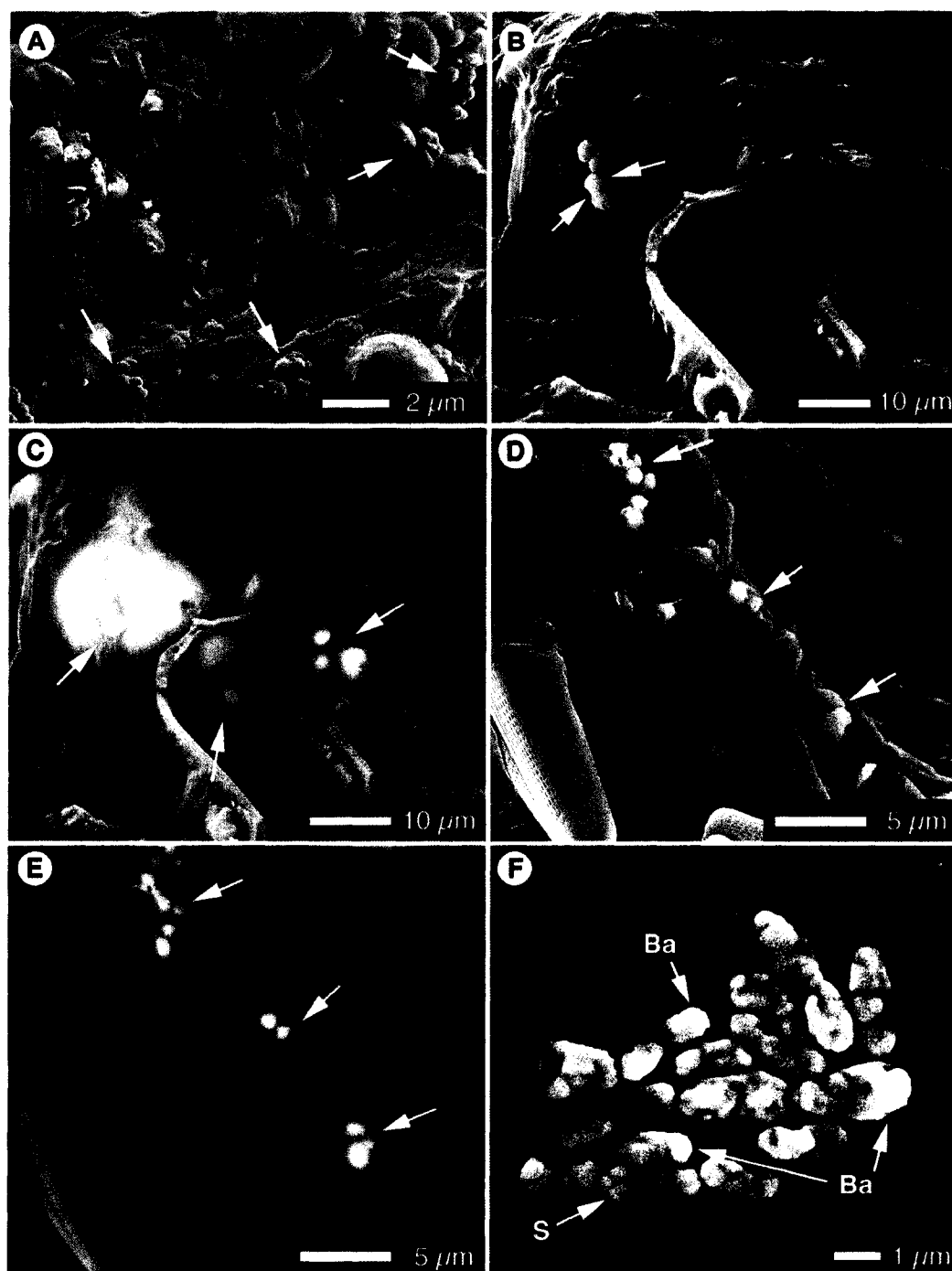


Figure 2-11. Bacteriogenic sulphur and barite globules. (A) Detrital elemental sulphur chains (arrows). (B, C) Detrital barite spheres in secondary electron and BSE- SEM images (arrows). (D, E) Detrital barite spheres aligned along a lysed filament in secondary electron and BSE- SEM images (arrows). (F) BSE-SEM image of *Chromatium* cells with elemental sulphur (s-arrow) and barium-enriched inclusions (Ba-arrow).

Discussion

Barite crystal habit varies as a function of the degree of saturation (Torres et al., 2003), the chemistry, and the viscosity of the precipitating solutions (Sasaki and Minato, 1982; Radanovic-Guzvica et al., 1999; Su et al., 2002). The wide array of barite crystal forms found in fresh precipitates reflects the physiochemical and biological diversity of the Flybye Springs flow paths. Barite precipitates through three potential mechanisms at the Flybye Springs: (1) inorganically, from barite supersaturated solutions, (2) by passive biologic mediation, in the presence of living or dead biomass, and (3) by active biologic mediation, in the presence of fungi and sulphur-metabolising bacteria.

Proximal to the vents, spring water achieves barite supersaturation via rapid oxidation of H_2S to SO_4 , and stellate and tabular barite microcrystals form in solution. Beyond ~ 5 m of the spring vents and seeps, inorganic barite nucleation is likely inhibited by a combination of lower barium concentrations (due to upstream barite precipitation), decreasing pCO_2 (cf. Lindgren, 1933; Bolze et al., 1974), the presence of organic leachates derived from surrounding vegetation (cf. Smith et al., 2004), and sequestration of barium and sulphate in microbial biomass.

The stellate barite crystals found at the Flybye Springs are typical of those precipitated at the air-water interface in barite supersaturated solutions (Sermon et al., 2004); whereas platy barites are more typical of precipitation at interfaces between oxidized and reduced solutions (Stark et al., 2004; Wagner et al., 2005). Scalloped crystals (Fig. 2-5B) usually form by very rapid precipitation where precipitation of new nuclei competes with extension of pre-existing barite lattices (Stark et al., 2004) and likely formed in more strongly barite supersaturated Flybye spring water than the euhedral, tabular crystals shown in Fig. 2-5D (cf. Shikazono, 1994; Greinert et al., 2002).

Though the composite blocky barite balls form in close contact with microbial cells (Fig. 2-5F), they are also thought to form inorganically. They are found only among porous debris (most commonly, clumps of caribou hair) in proximal flow path tributaries at Flybye Springs. Turbulence incited by such obstacles drives rapid oxidation of spring water flowing through them, and probably facilitates precipitation of the composite barite balls. Analogous balls of blocky calcite have been described from a hot sulphur spring

flow path at Miette Springs in Jasper National Park, Alberta, where they are associated with high rates of CO₂ degassing (Bonny and Jones, 2003).

Despite the lack of textural evidence for a microbial influence on 'inorganic' barite precipitation, barite solubility in the proximal flow paths may be subvertly influenced by bacterial metabolism. Biological sulphur oxidation may contribute to the production of dissolved sulphate for barite precipitation (Senko et al., 2004), and the ~4‰ fractionation between $\delta^{34}\text{S}_{\text{sulphide}}$ and $\delta^{34}\text{S}_{\text{sulphate}}$ in the proximal D1 flow path probably arises from bacterial sulphate reduction which (because bacterial preferentially reduce the lighter ³²S) leaves a residual sulphate pool enriched in ³⁴S (cf. Torres et al., 2003; Canfield, 2001). Atmospheric oxidation in the distal flow path produces dissolved sulphate with $\delta^{34}\text{S}_{\text{sulphate}}$ values much lower than those measured proximal to the vents (14.3-15.5 ‰ vs. 17.3-19 ‰), indicating that sulphate in the distal flow path is derived by oxidation of bacterially reduced sulphur. Sulphate reducing bacteria (SRB) counteract atmospheric oxidation of the spring water, prolonging dysoxic conditions in the Flybye Springs flow path, and thus limit the inorganic barite precipitation window to the proximal flow paths. Prolonged dysoxia also extends the environmental niche favoured by redox boundary sulphur oxidizing bacteria.

Biologically-mediated barite precipitation takes place throughout the Flybye Springs flow paths but is most important outside of the inorganic barite precipitation window. Microbial mats and biofilms are generally enriched in divalent cations due to the adsorptive capacity of microbial cells and extracellular polysaccharides (EPS) (Arp et al., 1999; Schultze-Lam et al., 1993). Barium-enrichment in microbial mats and biofilms growing in barium-rich solutions is well documented (Douglas and Douglas, 2001; Tazaki and Watannabe, 2004), and secondary exposure to dissolved sulphate may induce precipitation of sub-euhedral barite microcrystals in microbial biomass (Tazaki et al., 1997; Sanchez-Moral et al., 2004; Glamoclija et al., 2004). Direct nucleation of barite on microbial surfaces has not been documented from a natural setting, however, nor have microbial mats with discretely baritised lamina.

The development of barite laminae at Flybye Springs is attributable to redox stratification in floating mats which prevents homogeneous exposure to dissolved sulphate. In vent-fed ponds, the barite laminae form between *Beggiatoa* and *Oscillatoria*

layers - a transition that usually spans an oxic/anoxic boundary (Larkin and Strohl, 1983; Jorgensen and Des Marais, 1986). Barite precipitation may also be limited in the lower levels of floating mats by SRB-established anoxia amongst degrading filaments. The thickness of the baritised laminae probably corresponds to the thickness of the redox boundaries in the floating microbial mats, with barite undersaturated on the lower side due to a lack of sulphate, and supersaturated in barium-enriched EPS above.

The top layers of floating mats may escape baritisation because of a directional barium source. Evaporative wicking at the mat surface (Arp et al., 1999), and directional barium delivery from a vent source below the mats, would favour upward diffusion of barium. Fixation of this barium by precipitation at the redox boundary (Torres et al., 2003) might prevent mineralisation of the upper mat layers, allowing upwards microbial growth. The sub- and anhedral granular barite microcrystals found in the barite laminae are similar to laboratory barite precipitated from highly supersaturated solutions (Bala et al., 2005), which supports the idea that the redox boundary is an efficient barium immobilizer. As mat growth proceeds upwards, vertical migration of the redox boundary might generate the stacked barite laminae found in some mats.

The arrangement of barite spherulites in 'leafy mats' may, likewise be determined by a local redox boundary between anoxia in degrading leaf tissue and oxygenated fluids across the outer, waxy cuticle. The leaf-associated spherulites are similar in size and morphology to barite spherulites experimentally precipitated in solutions rich in fulvic acid by Smith et al. (2004). Humic acids, including fulvic acid, inhibit barite nucleation and crystal growth (Smith et al., 2004), and may be responsible for the morphological distinction between the leaf-associated and other mat-bound barite laminae at Flybye Springs. Ultimately, the barite laminae formed as a result of barium enrichment in biomass. In this regard, the laminae may be considered biologically mediated (cf. Braithwaite and Whitton, 1987), but degrading leaves are equally able to induce barite precipitation as microbes. True microbial biomineralisation at the Flybye Springs occurs in direct contact with microbial cells.

Microbial surfaces are generally negatively charged due to the presence of carboxyl and phosphoryl groups in the outer cell membrane (gram-negative bacteria), peptidoglycan layer (gram-positive bacteria), or ESP sheaths (Schultze-Lam et al., 1993;

Fortin et al., 1998). Binding of cations to these sites promotes the binding of counterions and can, thus, facilitate mineral precipitation. In this scenario, biomineralisation takes place passively, as a result of the chemical properties of the external cell surface (Leadbeater and Riding, 1986). Passive biomineralisation has been invoked to explain the formation of microbial molds, or tubes, in silica (Konhauser et al., 2003), calcite (Merz-Preiß, 2000), zinc and arsenic sulphides (Douglas and Douglas, 2001; Jackson et al., 2001), and iron oxides (Fortin et al., 1998), but has never before been reported in barite.

At Flybye Springs, primary barite coatings and secondary encrustations are common on and around various microbial genera. Concentration of barium on cell and sheath surfaces would lower the activation energy for barite in close proximity to microbial cells exposed to sulphate. In dysoxic Flybye spring water, sulphate sourced from atmospheric and microbial sulphur oxidation could react with adsorbed barium to precipitate barite globules on microbial cells. Barium adsorbed to the EPS sheaths of *Thioploca* would have less opportunity to interact with dissolved sulphate because of the anoxia that prevails in the methane-rich, vent-fed bottom waters of the ponds that *Thioploca* inhabits. Hydrated methane has been reported to decrease barite solubility (Tomson et al., 2003), however, so vent sourced methane may actually promote barite precipitation on *Thioploca* sheaths exposed to even trace amounts of sulphate.

Localization of barite globules around hyphal tips suggests that distinct processes control barite solubility around fungi. Fungi have a subcrystalline protein latticework, called chitin, imbedded among polysaccharides in their outer cell wall. Chitin contains a variety of anionic subgroups, including phosphate, carboxyl, and sulphhydryl groups, but does not readily bind divalent cations, and resists mineralisation (Gadd, 1993). Mineral precipitation on fungal hyphae, thus, takes place either around degrading cells, or as a by-product of energy-dependent cellular processes related to detoxification (Gadd, 1993).

Fungi growing in barium-rich solutions employ several mechanisms to avoid barium toxicity, including sequestering barium ions into inert precipitates, preventing barium uptake by secreting chelating enzymes, and actively 'flushing' barium ions out of the cell after accumulating them in cytoplasmic vacuoles (Aruguete et al., 1998; Mukherjee et al., 2001; Weber, 2002; Steiman et al., 2004). Both secretion of chelating enzymes and flushing of metal-enriched vacuoles take place at the apex of fungal hyphae

(Gadd, 1993; Weber, 2002) and could produce a barium-enriched microenvironment around hyphal tips that would favour barite precipitation in sulphate-bearing solutions.

Fungi growing in sulphide-rich solutions also battle sulphide toxicity, and many detoxify by carrying out non-metabolic sulphur-oxidation (Natorff et al., 2003). In this process, sulphur is oxidized intracellularly, and sulphate ions are complexed with the enzyme sinigrin, which is expelled to release sulphate extracellularly (Sakorn et al., 2002). When hyphae are grown on barium-enriched agar, this process induces rapid precipitation of barite around sulphur-oxidizing cells (Sakorn et al., 2002). Reaction of barium dissolved in spring water with fungally sourced sulphate could also drive precipitation of barite globules around fungal tips in the Flybye Springs flow path.

Irrespective of the detoxification process involved, *Penicillium* can be considered to be actively biomineralising at the Flybye Springs, precipitating barite as a by product of physiological processes (Leadbeater and Riding, 1986). Precipitates nucleated against microbial substrates are generally small, hydrated, and amorphous (Douglas and Douglas, 2001), but can act as substrates for the growth of secondary crystalline phases. Gonzalez-Munoz et al. (2003) induced barite precipitation around bacteria (*Myxococcus xanthus*) growing in barium-enriched agar and documented a progression from spherical to rhombic barite precipitation, similar to the crystallographic change from globular coatings to crystalline barite encrustations. It can be suggested that, once the nucleation threshold is crossed by formation of barite globules on microbial surfaces at Flybye Springs, barium and sulphate are able to diffuse towards the globule surface from the springwater, allowing growth of secondary barite encrustations.

Barite permineralisation of cell walls requires that barium and sulphate ions diffuse through the outer cell surface. Permineralisation was observed only in filaments of *Thiothrix*, *Beggiatoa*, and *Oscillatoria*. These are all redox interface organisms (Jorgensen and Des Marais, 1986; Nelson, 1987; Garcia-Pichel and Castenholz, 1990) found near oxic/anoxic interfaces where sulphate is not expected to limit barite saturation; once again, barite precipitation requires concentration of barium, this time within the outer cell layer. The fact that these genera are permineralised, rather than simply coated, may arise from the distinct properties of their outer cellular surfaces.

Neither *Oscillatoria* nor *Beggiatoa* form EPS sheaths, and sheath formation in *Thiothrix* is inconsistent, and probably environmentally determined (Reichenback, 1981). No sheathed *Thiothrix* filaments were found in samples from the Flybye Springs.

This lack of an EPS sheath may be important to facilitating permineralisation as it allows barium ions to diffuse unimpeded towards the external cell surface (Oehler and Schopf, 1971). Binding of barium in EPS may, in fact, prevent permineralisation of *Thioploca* sheathed filaments, despite their morphological similarity to *Beggiatoa* and *Oscillatoria*.

Beggiatoa, *Thioploca* and *Oscillatoria* have similar multilayered cell walls, in which only the inner layers (cytoplasmic membrane and murein layers) participate in septation, and outer layers are continuous along the length of the filaments (Larkin and Strohl, 1983; Teske and Nelson, 2005). The outer layers of all three gram negative genera include an outer membrane, a peptidoglycan wall, a cell envelope, and, in some species, a subcrystalline fibrillar arrays of proteins, which may facilitate cation adsorption to the outer cell surface (Larkin and Strohl, 1983; Adams et al., 1999). *Beggiatoa* and *Oscillatoria* also have similar perforations through their peptidoglycan walls, which are arranged near septal cross-walls in both microbial groups (Palinska and Krumbein, 2000; Teske and Nelson, 2005). The cellular structure of *Thiothrix* is not as well documented but is generally considered to be simpler, composed of an inner cytoplasmic membrane, a peptidoglycan cell wall, and an outer cellular envelope (Larkin and Strohl, 1983; Teske and Nelson, 2005).

Silica permineralised microfossils are common in the geologic record, and are thought to form by nucleation of silicic acid on reactive carboxyl, hydroxyl, and phosphoryl groups within the permineralising 'organic template' (Westall, 1999; Konhauser et al., 2003). Subsequent polymerization of silica then preserves the organic structure. A similar mechanism is proposed here for permineralisation by barite wherein barium cations are adsorbed to reactive groups in the organic template, and subsequently complex with dissolved sulphate to form barite globules that preserve the organic structure. In thick-walled filaments of *Beggiatoa* and *Oscillatoria*, the peptidoglycan layer perforations may be important to the permineralisation process. These structures are thought to function as transport pathways between the cytoplasm and external solutions

(Palinska and Krumbein, 2000) and may facilitate barium-diffusion into thick, multi-layered cell walls at Flybye Springs.

Barite precipitation inside cellular cavities requires transport of barium through the cell walls. Intracellular barite precipitation at Flybye Springs takes place in *Beggiatoa* and *Thiothrix* filaments that are commonly surrounded by completely non-mineralised cells of the same and other genera. Clearly, intracellular barite precipitation takes place when barite supersaturation is achieved inside, rather than around, microbial cells.

Barium enrichment in cytoplasmic fluids has been reported for various microbial groups including fungi (Cormack et al., 1975; Grupe and Herrmann, 1988), green algae (Mann and Fyfe, 1984; Ganeshram et al., 2003), and diatoms (Vinogradova and Koval'skiy, 1962). Above a certain concentration, however, barium bioaccumulators approach a toxicity threshold (Baldi et al., 1996) and must actively rid themselves of barium, sequester barium in an inert form, block further transport of barium into their cells, or face death (Arguete et al., 1998).

In the Flybye spring waters microbes are exposed to barium concentrations up to 12 ppm (Table 2-1), which are well above seawater and continental freshwater norms of 5 and 54 ppb (Bolze et al., 1974). Barium toxicity may be a plausible explanation for intracellular barite precipitation in *Beggiatoa* and *Thiothrix* at the Flybye Springs, as a cellular mechanism to combat metal toxicity has not been documented for either genera.

If cytoplasmic barium concentrations achieved toxic levels and induced the death of single cells, or groups of cells along a filament, they would cease osmoregulation and dissolved sulphate might be able to diffuse across the cellular membranes, producing barite supersaturated conditions inside the cell. If there were ambient sulphate and high barium concentrations in fluids surrounding the microbes, however, it is a mystery as to why their cell walls were not permineralised, coated, or encrusted. One explanation may be that barium is bound in EPS, inhibiting extracellular barite precipitation in this part of the flow path (cf. Arp et al., 1999). Alternately, if sulphate is limiting in the ambient environment, it might be sourced within the boundary of the cell wall – perhaps from oxidizing sulphur globules. An intracellular sulphate source would also explain why *Oscillatoria*, which is morphologically similar to *Thiothrix* and *Beggiatoa* but does not

accumulate intracellular sulphur granules, does not experience intracellular barite precipitation at Flybye Springs.

Filaments of *Beggiatoa*, *Thiothrix*, and *Chromatium* throughout the Flybye spring flow paths and ponds contain numerous intracellular sulphur globules. The composition of bacteriogenic sulphur globules varies between microbial genera and within single genera growing in distinct physiochemical environments. Pasteris et al. (2001) found inclusions in marine *Beggiatoa* strains that are composed of relatively pure fine-grained, microcrystalline sulphur in a protein envelope; but in most cases, sulphur inclusions have lower density than crystalline elemental sulphur (Mas and van Gemerden, 1987). In filamentous sulphur oxidizing bacteria, sulphur globules are commonly composed of metastable fluid polythionates (Steudel et al., 1987; Pattargulwanit et al., 1998), whereas sulphur globules in anoxygenic phototrophs are dominated by sulphur chains (Prange et al., 2002).

Oxidation of any composition of sulphur globules to sulphate in a barium-enriched cytoplasmic chamber could initiate rapid precipitation of barite in the cellular cavity. Oxidation of intracellular sulphur globules has been reported to occur spontaneously upon cell death (Brigmon et al., 1994). It is more common, however, for sulphur globules to crystallize as elemental sulphur (Steudel, 1987). Cells with densely packed sulphur inclusions may, in fact, be 'permineralised' by elemental sulphur crystals that breach globule-restraining membranes soon after cell death (Ohno and Tazaki, 2000). Oxidation of permineralising sulphur in a barium-enriched cytoplasmic chamber exposed to oxygen-rich fluids by degradation of the cell wall could provide a means to baritise the intracellular cavity wholesale, as is found in many of the *Beggiatoa* and *Thiothrix* filaments at Flybye Springs (Fig. 2-10).

Apparent baritisation of sulphur globules (Fig. 2-11) is more difficult to explain. Sulphur globules in *Thiothrix* and *Beggiatoa* are located inside the outer cell wall, but are restricted to invaginations of the cytoplasmic membrane and further surrounded by a 'sulphur-inclusion envelope'; they do not come into contact with cytoplasmic fluids (Larkin and Strohl, 1983; Nelson, 1987; Larkin and Henk, 1996). Sulphur globules in *Chromatium* are dispersed in the cytoplasm but surrounded by extracytoplasmic vesicular membranes that prevent contact between the contents of the sulphur globule and the

cytoplasm (Pattaragulwanit et al., 1998; Reinartz et al., 1998). Precipitation of barite within the globule-restraining membrane, thus, necessitates barium diffusion from the cytoplasm into the sulphur globule. This might take place if the cell was approaching a barium-toxicity threshold and lost its ability to regulate transport of ions across the cytoplasmic membrane. Alternately, the sulphur globules themselves may have become barium enriched.

Some sulphur globules have been found to incorporate organic molecules (Mas and van Gernerden, 1987) and up to 5% iron, calcium, silica, aluminum, and magnesium (Douglas and Douglas, 2000). Anionic groups in the sulphur globules or their restraining membranes render them hydrophilic (Stuédel, 1987), and trace element enrichments may be explained by adsorption of cations to these charged sites. Barium could potentially be adsorbed likewise, and oxidation of barium-enriched sulphur globules might initiate barite precipitation in the sulphur globule restraining membrane without supplying sulphate to the cytoplasm. This process could take place upon cell death and desiccation, but the barium-enriched inclusions found in *Chromatium* (Fig. 2-11F) suggest that sulphur globules may become barium enriched (or baritised) in viable cells.

Metabolic oxidation of sulphur globules to sulphate is carried out by *Chromatium*, as well as select species of freshwater *Thiothrix* and *Beggiatoa* (Nelson, 1987; Patriskaya et al., 2001). Complete oxidation to sulphate generally only takes place, however, in stressed environmental conditions; for example, in light-restricted *Chromatium* colonies (Overmann and Pfennig, 1992) or among bundles of sulphur oxidizing bacteria stranded in low-sulphide waters (Nelson, 1987). In *Chromatium*, sulphur oxidation sites are located inside the extracytoplasmic membranes that surround sulphur globules (Pattaragulwanit et al., 1998), and could produce sulphate for barite precipitation *in situ*. Sulphur oxidation in *Beggiatoa* and *Thiothrix* is also thought to be mediated by membrane bound-enzymes, though the process is not well understood (Reinartz et al., 1998; Patriskaya et al., 2001). It is interesting to speculate that, in addition to low sulphide concentrations in desiccating tributaries and in aerated splash zones, stresses associated with barium-toxicity might prompt microbes to oxidize their sulphur globules – with unexpected results. Both cellular cavity-filling barite precipitation and baritisation of sulphur globules are ultimately thought to arise as a result of intracellular sulphur

storage and/or barium bioaccumulation and can, thus, be considered end-products of 'active' biomineralisation (Leadbeater and Riding, 1986).

Though both passive and active biomineralisation have been reported from diverse mineralogies (Westall, 1999; Riding and Awramik, 2000; Jackson et al., 2001), microfossil-generating biomineralisation in barite has not been documented prior to this study. Passive barite biomineralisation at the Flybye Springs is dependent upon microbial barium concentration via adsorption to cell surfaces and exudates. Active biomineralisation proceeds by physiological mediation of barite saturation gradients around and inside of microbial cells. Microbial taphonomy in carbonate, silica, and iron oxides has been found to be texturally sensitive to differences in cellular structure, metabolism, and ambient chemistry (e.g. Walter and DesMarais, 1993; Arp et al., 1999), which has important implications for their interpretative potential in the geologic record. Generally, microfossils have more textural variability in minerals that can precipitate by both active and passive biomineralisation (e.g. calcium carbonate precipitated actively via photosynthetic CO₂ withdrawal, or passively by calcium adsorption to cell surfaces and exudates); thus, they provide the most insight into the physiochemical conditions of their environment of formation (Arp et al., 2001; Kaufman and Xiao, 2003, Shen et al., 2001).

Active and passive biomineralisation processes are associated with distinct microbial genera at the Flybye Springs (with some overlap) and generate texturally specific detrital barite microfossils. Barite laminae, tunnels, multi-layered cylinders, intracellular casts, and sulphur-globule mimicking grains all bear textural details that are determined in part by the ecology, morphology, cellular structure and metabolism of the microbes involved in their formation. Such microfossils would have high interpretative potential if preserved in the geologic record.

Barite is highly insoluble and stable through diagenesis if it is sequestered from anoxic solutions (Karnachuk et al., 2002) and commonly forms in microbially colonized environments (Carroue, 1996; Burhan et al., 2002; Torres et al., 2003). Indeed, some of the Earth's earliest putative stromatolites formed in barite precipitating environments (Buick et al., 1981; Shen et al., 2001; Kiyokawa et al., 2006). The biomineralisation processes taking place at the Flybye Springs offer a rare glimpse into how some of

Earth's earliest organisms may have interacted with their geochemical environment, and the kinds of microfossil evidence they might have left behind.

Microfossil-generating biomineralisation at Flybye Springs takes place where spontaneous inorganic barite precipitation is no longer favoured by spring water physiochemistry. Practically speaking, these microfossils represent fixation of barium from spring water that is ultimately destined for dispersal in the watershed surrounding the Flybye Springs. Barium is highly toxic to many plants and animals and creates environmental problems when it leaches into groundwater (Baldi et al., 1996). Barium bioaccumulating fungi have been applied in bioremediation of barium-rich petroleum waste products (Dominguez-Rosado et al., 2004), and barite biomineralising bacteria might be equally suited to bioremediation technologies. Radioactive barite scale and sludge generated by the hydrocarbon industry are relatively inert under oxic conditions but can be remobilized if they are exposed to anoxic solutions or sulphate reducing bacteria after disposal (Desideri et al., 2006). Dysoxic niche-occupying barite biomineralising microbes, like those found at the Flybye Springs, may be well suited to controlling barium leachates generated at redox boundaries.

Conclusions

The Flybye spring water emerges rich in sulphide and barium, precipitates elemental sulphur and barite, and supports a rich community of sulphur-tolerant and sulphur-metabolizing microbes. Proximal to the spring vents, barite microcrystals precipitate inorganically from barite supersaturated spring water. In distal tributaries and vent- and stream-fed ponds, barite precipitates in direct association with microbes.

Adsorption of barium to negatively charged molecules in microbial cell walls, sheaths, and EPS, is considered important to establishing localized barite supersaturation, and produces the following passively bio-mediated and biomineralised precipitates:

- Microcrystalline barite laminae at microbially mediated oxic/anoxic boundaries in floating microbial mats.
- Nanometric coatings and micrometric encrustations of barite on diverse microbial cells, which generate tunnel-shaped microfossils.

- Barite permineralised outer cell layers in *Beggiatoa*, *Thiothrix* and *Oscillatoria*, which can be encrusted and filled by secondary precipitates to form three-layered microfossils.

Intracellular barium-enrichment and/or physiologic sulphur oxidation may be important to the formation of actively biomineralised precipitates, including:

- Nanometric barite globules near the tips of fungal hyphae.
- Barite impregnated cellular cavities in non-permineralised *Beggiatoa* and *Thiothrix* filaments.
- Baritised sulphur globules produced in and released from *Chromatium*, *Beggiatoa*, and *Thiothrix*.

The variability in biomineralisation at Flybye Springs stems from differences in the chemical microenvironment where barite precipitation takes place, and differences in cellular structure and metabolic strategy between microbial genera.

References

- Adams, D.G., Ashworth, D., and Nelmes, B. 1999. Fibrillar array in the cell wall of a gliding filamentous cyanobacterium. *Journal of Bacteriology*, 181: 884-892.
- Al-Jundi, J. 2001. Comparison of neutron activation analysis and inductively coupled plasma-atomic emission spectroscopy for the determination of elements in environmental samples. *Dirasat – University of Jordan, Engineering Sciences*. 28: 49-55.
- Allen, C.C., Grasby, S.E, Longazo, T.G., Lisle, J.T., and B. Beauchamp. 2002. Life beneath the ice – Earth (!), Mars (?), Europa (?). 33rd Lunar and Planetary Science Abstracts, March 11-15, Houston, Texas, Online: <http://www.lpi.usra.edu/publications/abstracts.shtml#1psc>, 1134.pdf.
- Arp, G. Theil, V., Reimer, A. Michaelis, W., and Reitner, J. 1999. Biofilm exopolymers control microbialite formation at thermal springs discharging into the alkaline Pyramid Lake, Nevada, USA. *Sedimentary Geology*, 126: 159-176.
- Arp, G., Reimer, A., and Reitner, J. 2001. Photosynthesis-induced biofilms calcification and calcium concentrations in Phanerozoic oceans. *Sciences*, 292: 1701-1704.
- Arguete, D.M., Aldstadt, J.H. III, and Mueller, G.M. 1998. Accumulation of several heavy metals and lanthanides in mushrooms (Agaricales) from the Chicago region. *The Science of the Total Environment*, 224: 43-56.
- Bala, H., Fu, W., Zhae, J., Ding, X., Jiang, Y., Yu, K., and Wang, X. 2005. Preparation of BaSO₄ nanoparticles with self-dispersing properties. *Colloids and Surfaces A*, 252:129-134.
- Baldi, F., Pepi, M., Burrini, D., Kniewald, G., Scali, D., and Lanciotti, E. 1996. Dissolution of barium from barite in sewage sludges and cultures of *Desulfobibrio desulfuricans*. *Applied and Environmental Microbiology*, 62: 2398-2404.
- Bertram, M.A., and Cowen, J.P. 1997. Morphological and compositional evidence for biotic precipitation of marine barite. *Journal of Marine Research*, 55: 677-693.
- Bolze, C.E., Malone, P.G., and Smith, M.J. 1974. Microbial mobilization of barite. *Chemical Geology*, 13: 141-143.
- Bonny, S., and Jones, B. 2003. Microbes and mineral precipitation, Miette Hot Spring, Jasper National Park, Alberta, Canada. *Canadian Journal of Earth Sciences*, 40:1483-1500.
- Braithwaite, A., and B.A. Whitton. 1987. Gypsum and halite associated with the cyanobacterium *Entophysalis*. *Geomicrobiological Journal*, 5: 43-55.
- Buick, R., Dunlop, J.S.R. and D.I. Grooves. 1981. Stromatolite recognition in ancient rocks: an appraisal of irregularly laminated structures in an Early Archaean chert-barite unit from North Pole, Western Australia. *Alcheringa*, 5: 161-181.
- Brigmon, R.L., Martin, H.W., Morris, T.L., Bitton, G., and S.G. Zam. 1994. Biogeochemical ecology of *Thiothrix* spp. in underwater limestone caves. *Geomicrobiology Journal*, 12:141-159
- Burhan, R.Y.P., Trendel, J.M., Adam, P., Wehrung, P., Albrecht, P., and Nissenbaum, A. 2002. Fossil bacterial ecosystem at methane seeps; origin of organic matter from Be'eri sulfur deposit, Israel. *Geochimica et Cosmochimica Acta*, 66: 4085-4101.

- Cadigan, R.A. and Felmlee, J.K. 1977. Radioactive springs geochemical data related to uranium exploration. *Journal of Geochemical Exploration*, 8: 381-395.
- Canfield, D.E. 2001. Isotope fractionation by natural populations of sulfate-reducing bacteria. *Geochimica et Cosmochimica Acta*, 65: 1117-1124.
- Carroue, J-P. 1996. Une presentation originale de la barytine ou des stromatolithes de poids. *Mineraux et Fossiles*, 246: 21-22.
- Cecile, M.P., Goodfellow, W.D., Jones, L.D., Krouse, H.R., and M.A. Shakur. 1984. Origin of radioactive barite sinter, Flybye springs, Northwest Territories, Canada. *Canadian Journal of Earth Sciences*, 21: 383-395.
- Cecile, M.P. 2000. Geology of the northeastern Nidderly Lake map area, east-central Yukon and adjacent Northwest Territories. *Geological Survey of Canada Bulletin* 553.
- Cormack, K., Todd, R.L., and Mond, C.D. 1975. Patterns of basidiomycete nutrient accumulation in conifer and deciduous forest litter. *Soil Biology and Biochemistry*, 106: 545-554.
- Desideri, D., Feduzi, L., Meli, A.A., and Roselli, C. 2006. Leachability of naturally occurring radioactive materials. *Journal of Radioanalytical and Nuclear Chemistry*, 267: 551-555.
- Dominguez-Rosado, E., Pichtel, J., and Coughlin, M. 2004. Phytoremediation of soil contaminated with used motor oil: I. Enhanced microbial activities from laboratory and growth chamber studies. *Environmental Engineering Sciences*, 21: 157-168.
- Douglas, S., and Douglas, D.D. 2000. Environmental scanning electron microscopy studies of colloidal sulfur deposition in a natural microbial community from a cold sulfide spring near Ancaster, Ontario, Canada. *Geomicrobiology Journal*, 17: 275-289.
- Douglas, S., and Douglas, D.D. 2001. Structural and geomicrobiological characteristics of a microbial community from a cold sulfide spring. *Geomicrobiology Journal*, 18: 201-422.
- Fortin, D., Ferris, F.G., and Scott, S.D. 1998. Formation of Fe-silicates and Fe-oxides on bacterial surfaces in samples collected near hydrothermal vents on the Southern Explorer Ridge in the northeast Pacific Ocean. *American Mineralogist*, 83: 1399- 1408.
- Gadd, G.M. 1993. Interactions of fungi with toxic metals. *New Phytologist*, 124: 25-60.
- Ganeshram, R.S., Francois, R., Commeau, J., and Brown-Leger, L. 2003. An experimental investigation of barite formation in seawater. *Geochimica et Cosmochimica Acta*, 67: 2599-2605.
- Garcia-pichel, F., and Castenholz, R.W. 1990. Comparative anoxygenic photosynthetic capacity in 7 strains of a thermophilic cyanobacterium. *Archives of Microbiology*, 153: 344-355.
- Glamoclija, M., Garrel, L., Berthon, J., and Lopez-Garcia, P. 2004. Biosignatures and bacteria diversity in hydrothermal deposits of Solfatara Crater, Italy. *Geomicrobiology Journal*, 21: 529-541.
- Gonzalez-Munoz, M.T., Fernandez-Luque, B., Martinez-Ruiz, F., Chekroun, K.B., Arias, J.M., Rodriguez-Gallego, M., Martinez-Canamero, M., de Linares, C., and A.Paytan. 2003. Precipitation of Barite by *Myxococcus xanthus*: Possible Implications for the Biogeochemical Cycle of Barium. *Applied and Environmental Microbiology*, Sept. 2003: 5722-5725.

- Greinert, J., Bollwerk, S.M., Derkachev, A., Bohrmann, G., and Suess, E. 2002. Massive barite deposits and carbonate mineralisation in the Derugin Basin, Sea of Okhotsk: Precipitation processes at cold seep sites. *Earth and Planetary Science Letters*, 203: 165-180.
- Grupe, G., and Herrmann, B. 1988. Trace elements in environmental history. New York: Springer-Verlag.
- Jackson, C.R., Langner, H., Danohoe-Christiansen, J., Inskeep, W.P., and McDermott, T.R. 2001. Molecular analysis of microbial community structure in an arsenite-oxidizing acidic thermal spring. *Environmental Microbiology*, 3: 532-542.
- Jewell, P.W. 2000. Bedded barite in the geologic record. Special Publication – Society for Sedimentary Geology, 66: 147-161.
- Jones, B., Renaut, R.W., and Rosen. 2000. Trigonal dendritic calcite crystals forming from hot spring waters at Waikite, North Island, New Zealand. *Journal of Sedimentary Research*, 70: 56-603.
- Jørgensen, B. B., and Des Marais, D.J. 1986. Competition for sulfide among colorless and purple sulfur bacteria in cyanobacterial mats. *FEMS Microbial Ecology*, 38: 179-186.
- Karnachuk, O.V., Kurochkina, S.Y., and Tuovinen, O.H. 2002. Growth of sulfate-reducing bacteria with solid-phase electron acceptors. *Applied Microbiology and Biotechnology*, 58:482-486.
- Kaufman, A.J., and Xiao, S. 2003. High CO₂ levels in the Proterozoic atmosphere estimated from analyses of individual microfossils. *Nature*, 425: 279-281.
- Kiyokawa, S., Ito, T., Ikehara, M., and Kitajima, F. 2006. Middle Achaean volcano-hydrothermal sequence: Bacterial microfossil-bearing 3.2 Ga Dixon Island Formation, coastal Pilbara terrane, Australia. *GSA Bulletin*, 118: 3-22.
- Knoll, A.H. 1985. Exceptional preservation of photosynthetic organisms in silicified carbonates and silicified peats. *Philosophical Transactions of the Royal Society of London*, 311: 111-122.
- Kojima, H., Teske, A., and Fukui, M. 2003. Morphological and phylogenetic characterizations of freshwater *Thioploca* species from Lake Biwa, Japan and Lake Constance, Germany. *Applied and Environmental Microbiology*, 69: 390-398.
- Konhauser, K.O., Jones, B., Reysenbach, A-L., and R.W. Renaut. 2003. Hot spring sinters: keys to understanding Earth's earliest life forms. *Canadian Journal of Earth Sciences*, 40: 1713-1724.
- Larkin, J.M., and Henk, M.C. 1996. Filamentous sulfide-oxidizing bacteria at hydrocarbon seeps of the Gulf of Mexico. *Microscopy Research and Technique*, 33: 23-31.
- Larkin, J.M., and Strohl, W.R. 1983. *Beggiatoa*, *Thiothrix*, and *Thioploca*. *Annual Reviews in Microbiology*, 37: 341-67.
- Leadbeater, B.S.C., and Riding, R. 1986. *Biominalisation in lower plants and animals*. Oxford University Press, New York.
- Lindgren, W., 1933. *Mineral Deposits*, 4th Edition. McGraw-Hill Publishers, New York.

- Lu, Z.C., Liu, C.Q., Liu, J.J. and Wu, F.C. 2004. The bio-barite in witherite deposits from Southern Qinling and its significance. *Progress in Natural Science*, v. 14, no. 10, p. 889-895.
- Mann, H., and W.S. Fyfe. 1984. An experimental study of algal uptake of U, Ba, V, Co and Ni from dilute solutions. *Chemical Geology*, 44: 385-398.
- Mas, J., and van Gernerden, H. 1987. Influence of sulfur accumulation and composition of sulfur globule on cell volume and buoyant density of *Chromatium vinosum*. *Archives of Microbiology*, 146: 362-369.
- Merz-Preiß, M. 2000. Calcification in cyanobacteria. *In* *Microbial Sediments*. Edited by R.E. Riding and S.M. Awramik, Springer-Verlag: Heidelberg Germany, pp. 50-56.
- Mukherjee, P., Ahmad, A., Mandal, D., Senapati, S., Sinkar, S.R., Khan, M.I., Ramani, R., Parischa, R., Ajayakumar, P.V., Alam, M., Sastry, M., and Kumar, R. 2001. Bioreduction of $AuCl_4^-$ ions by the fungus *Verticillium sp.* and surface trapping of the gold nanoparticles formed. *Angew, Chemistry International Edition*, 40: 3585-3588.
- Natorff, R., Sienko, M., Brzywczy, J., and Paszewski, A. 2003. The *Aspergillus nidulans metR* gene encodes a bZIP protein which activates transcription of sulphur metabolism genes. *Molecular Microbiology*, 49: 1081-1094.
- Nelson, D.C. 1987. Physiology and biochemistry of filamentous sulfur bacteria. *In* *Autotrophic Bacteria*. Edited by H.G. Schlegel and B. Bowien, Science Tech Publishers, Madison, Wisconsin, pp. 219-238.
- Oehler, J.J., and Schopf, J.W. 1971. Artificial microfossils - Experimental studies of permineralisation of blue-green algae in silica (Artificial microfossil permineralisation of blue green algae in silica, simulating Precambrian geochemical preservation). *Sciences*, 174: 1229-1231.
- Ohno, M., and K. Tazaki. 2000. Biomineralisation in biomats at Hirayu Hot Springs. *Earth Science*, 54: 298-309.
- Orberger, B., Gallien, J-P., Pinti, D.L., Failin, M., Daudin, L., Grocke, D.R. and Pasava, J. 2005. Nitrogen and carbon partitioning in diagenetic and hydrothermal minerals from Paleozoic Black Shales, (Selwyn Basin, Yukon Territories, Canada). *Chemical Geology*, 218, 249-264.
- Overmann, J., and Pfennig, N. 1992. Continuous chemotropic growth and respiration of *Chromatiaceae* species at low oxygen concentrations. *Archives of Microbiology*, 158: 59-67.
- Palinska, K.A.; and Krumbein, W.E. 2000. Perforation patterns in the peptidoglycan wall of filamentous cyanobacteria. *Journal of Phycology*, 36: 139-145.
- Pasteris, J.D., Freeman, J.J., Goffredi, S.K., and Buck, K.R. 2001. Raman spectroscopic and laser scanning confocal microscopic analysis of sulfur in living sulfur-precipitating marine bacteria. *Chemical Geology*, 180: 3-18.
- Patrinskaya, V., Grabovich, M., Muntyan, M.S., and Dubinina, G.A. 2001. Lithoauto-trophic growth of the freshwater colorless sulfur bacterium *Beggiatoa* 'leptomitiformis' D-402. *Microbiology*, 70: 14-150.

- Pattaragulwanit, K., Brune, D.C., Truper, H.G., and Dahl, C. 1998. Molecular genetic evidence for extracytoplasmic localization of sulfur globules in *Chromatium vinosum*. *Archives of Microbiology*, 169: 434-444.
- Prange, R.C., Chauvistre, R., Modrow, J., Hormes, J., Truper, H.G., and Dahl, C. 2002. Quantitative speciation of sulfur in bacterial sulfur globules: X-ray adsorption spectroscopy reveals at least three different species of sulfur. *Microbiology*, 148: 267-276.
- Radanovic-Guzvica, B., 1999. The average structural density of barite crystals of different habit types. *Geologia Croatica*, 52: 59-65.
- Rajashekhara, M., and Kaveriappa, K.M. 2003. Diversity of aquatic hyphomycetes in the aquatic ecosystem of the Western Ghats of India. *Hydrobiological*, 501: 167-177.
- Reichenback, H. 1981. The taxonomy of the gliding bacteria. *Annual Reviews in Microbiology*, 35: 339-364.
- Reinartz, M., Tschape, J., Bruser, T., Truper, H.B., and Dahl, C. 1998. Sulfide oxidation in the phototrophic sulfur bacterium *Chromatium vinosum*. *Archives of Microbiology*, 170: 59-68.
- Riding, R.E., and Awramik, S.M. 2000. *Microbial Sediments*. Springer: New York.
- Rippka, R., Deruelles, J., Waterbury, J.B., Herdman, M., and Stanier, R.Y. 1979. Generic assignments, strain histories and properties of pure cultures of cyanobacteria. *Journal of General Microbiology*, 111: 1-16.
- Sakorn, P., Rakariyatham, N., Niamsup, H., and Nognkunsarn, P. 2002. Rapid detection of myrosinase-producing fungi: a plate method based on opaque barium sulphate formation. *World Journal of Microbiology and Biotechnology*, 18: 73-74.
- Sanchez-Moral, S., Luque, L., and Canaveras, J.C. 2004. Bioinduced barium precipitation in *St. Callixtus* and *Domitilla* catacombs. *Annals of Microbiology*, 54: 1-12.
- Sasaki, N., and Minato, H. 1982. Relationship between lattice constants and strontium and calcium contents of hokutolite. *Mineralogical Journal*, 11: 62-71.
- Schlegel, H.G. and Bowien, B. 1987. *Autotrophic Bacteria*. Science Tech Publishers, Madison, Wisconsin.
- Schopf, J.W., Kudrayavtsev, A.B., Agresti, D.G., Wdowiak, T.J., and Czaja, A.D. 2002. Laser-Raman imagery of Earth's earliest fossils. *Nature*, 416: 73-76.
- Schultze-Lam, S., Douglas, T., Thompson, J.B., and Beveridge, T.J., 1993. Metal ion immobilization by bacterial surfaces in freshwater environmental: *Water Pollution Research Journal of Canada*, v. 28, p. 51-81.
- Senko, J.M., Campbell, B.S., Henriksen, J.R., Elshahed, M.S., Dewers, T.A., and Krumholz, L.R. 2004. Barite deposition resulting from phototrophic sulfide-oxidizing bacterial activity. *Geochimica et Cosmochimica Acta*, 68: 773-780.
- Sermon, P.A., McLellan, N.M., and Collins, I.R. 2004. Formation of BaSO₄ nanoribbons from a molecular mangle. *Crystal Engineering Communications*, 6: 469-473.
- Shen, Y., Buick, R., and D.E. Canfield. 2001. Isotopic evidence for microbial sulphate reduction in the early Achaean era. *Nature*, 410: 77-81.

- Shikazono, N. 1994. Precipitation mechanisms of barite in sulfate-sulfide deposits in back-arc basins. *Geochimica et Cosmochimica Acta*, 58, 2203-2213.
- Simonsen, R. 1987. Atlas and catalogues of the diatom types of Freidrich Hustedt, Volume 2 - Atlas, Stuttgart/J. Cramer, Berlin, Plates 1-139.
- Smith, E., Hamilton-Taylor, J., Davison, W., Fullwood, N.J., and McGrath, M. 2004. The effect of humic substances on barite precipitation-dissolution behaviour in natural and synthetic lake waters. *Chemical Geology*, 207: 81-89.
- SOLMINEQ88 (1988). A computer program for geochemical modeling of water-rock interactions developed by the United States Geological Survey. Water Investigations Report 88-05.
- Stark, A.I.R., Wogelius, R.A., Collins, I.R., and Vaughan, D.J. 2004. Kinetic and thermodynamic controls on the precipitation and morphology of barite (BaSO₄). Extended abstract, Goldschmidt conference proceedings, Copenhagen. Theme 2: The dynamic interface, p. A148.
- Steiman, R., Ford, L., Ducros, V., Lafond, J.L., and Guiraud, P. 2004. First survey of fungi in hypersaline soil and water of Mono Lake area (California). *Antonie van Leeuwenhoek International Journal of General and Molecular Microbiology*, 85: 69-83.
- Steudel, R. 1987. On the nature of the "elemental sulfur" (S⁰) produced by sulfur-oxidizing bacteria – a model for S⁰ globules. *In Autotrophic Bacteria. Edited by H.G. Schlegel and B. Bowien*, Science Tech Publishers, Madison, Wisconsin, pp. 289-303.
- Su, H-Y., Lee, J-S., and Yu, S-C. 2002. Dopant effect on hokutolite crystals synthesized with hydrothermal process. *Western Pacific Earth Sciences*, 2:301-318.
- Tazaki, K., and Watanabe, H. 2004. Biomineralisation of radioactive sulfide minerals in strong acidic Tamagawa Hot Springs. *Science Reports of the Kanazawa University*, 49:1-24.
- Tazaki, K., Webster, J., and W.S. Fyfe. 1997. Transformation processes of microbial barite to sediments in Antarctica. *Japanese Journal of Geology*, 26: 63-68.
- Teske, A., and Nelson, D.C. 2005. The genera *Beggiatoa* and *Thiothrix*. *in The Prokaryotes – an evolving online resource for the microbiological community. Edited by M. Dworkin*, BETA Release 3.20: http://141.150.157.117:8080/prok_PUB/chaphtm/432/01_00.htm
- Tomson, M.B., Kan, A.T., Fu, G., and Al-Thubaiti, M. 2003. NORM Scale Formation, Control, and Relation to Gas Hydrate Control. Extended abstract. Proceedings of the 10th International Petroleum Environmental Conference (IPEC), Houston, Texas, November 11-14, 2003: 34.
- Torres, M.E., Bohrmann, G., Dube, T.E., and F.G. Poole. 2003. Formation of modern and Paleozoic stratiform barite at cold methane seeps on continental margins. *Geology*, 31: 897-900.
- Van Everdingen, R.O. 1972. Thermal and Mineral Spring in the Southern Rocky Mountains of Canada. Water Management Service, Department of the Environment, Environment Canada.
- Vinogradova, Z.A., and Koval'skiy, V.V. 1962. Elemental composition of Black Sea plankton. *Doklady Rossiskoj Akademii Nauk. SSSR*, 147: 217-219.

- Wagner, T., Kirnbauer, T., Boyce, A.J., and Fallick, A.E. 2005. Barite-pyrite mineralisation of the Wiesbaden thermal spring system, Germany: a 500-kyr record of geochemical evolution. *Geofluids*, 5:124-139.
- Walter, W.R., and DesMarais, D.J. 1993. Preservation of biological information in thermal spring deposits; developing a strategy for the search for fossil life on Mars. *Icarus*, 101: 129-143.
- Weber, R.W.S. 2002. Vacuoles and the fungal lifestyle. *Mycologist*, 16: 10-20.
- Westall, F. 1999. The nature of fossil bacteria: A guide to the search for extraterrestrial life. *Journal of Geophysical Research*, 104: 16437-16451.
- Wher, J.D., and Sheath, G. 2003. *Freshwater Algae of North America: Ecology and Classification*. Academic Press, San Diego, CA.
- Younger, P. 1986. Barite travertine from southwestern Oklahoma and west-central Colorado. Unpublished M.Sc.Thesis, Oklahoma State University, Stillwater, OK, USA.

Chapter 3 **Petrography and textural development of inorganic and biogenic lithotypes in relict barite (BaSO₄) tufa at Flybye Springs***

Introduction

Barite (BaSO₄)-precipitating subaerial springs are rare, with less than ten sites known worldwide (Cadigan and Felmlee, 1977; Sasaki and Minato, 1982; Cecile et al., 1984). Barium is highly insoluble in oxygenated solutions, so it is carried to the earth's surface exclusively by anoxic aquifers; once exposed to the atmosphere, oxidation of dissolved sulphide to sulphate incites barite precipitation (Hanor, 2000; Senko et al., 2004). Reported products of subaerial barite precipitation include 'inorganic' layered crystalline crusts (Suganuma, 1928; Sasaki and Minato, 1982) and isopachous coatings on submerged and splashed substrates (Clowes, 1889; Craig and Bloch, 1981; Younger, 1986; Sanders, 1998). More commonly, barite is co-precipitated with volumetrically dominant calcite (Bove and Felmlee, 1982; Younger, 1986; Arenas et al., 2000; Canet et al., 2005; Bonny and Jones, 2007b).

This paper describes a unique occurrence of subaerial barite formed at a cold sulphur spring system in the Sahtu Region of Canada's Northwest Territories (Fig. 3-1A). The Flybye Springs currently issue ≤ 20 L/min, and precipitate small quantities of substrate-encrusting barite (≤ 250 $\mu\text{m}/\text{year}$) (Bonny and Jones, 2007a). They are underlain, however, by a mound of Holocene barite tufa, whose extent indicates that it probably formed during a time when the springs were larger and had higher rates of flow, than are presently observed. In stark contrast to crystalline deposits at other barite-precipitating springs (Suganuma, 1928; Sasaki and Minato, 1982; Criag and Bloch, 1981; Younger, 1986), the Flybye barite tufa is texturally complex, with six distinct lithotypes: coated bubble, coated grain, raft, undulatory sheet, microfossil-bearing stromatolite tufa and a barite-cemented detrital conglomerate.

Though unprecedented in barite, these lithotypes are readily accommodated by carbonate spring deposit classification systems (Chafetz and Folk, 1984; Ford and Pedley, 1996; Kano and Fuji, 2000; Guo and Riding, 2002; Pentecost, 2005). Indeed,

* *A version of this chapter has been accepted for publication.*
Bonny, S. and Jones, B. xxxx. Petrography and textural development of inorganic and biogenic lithotypes in a relict barite (BaSO₄) tufa deposit at Flybye Springs, Northwest Territories, Canada. Sedimentology.

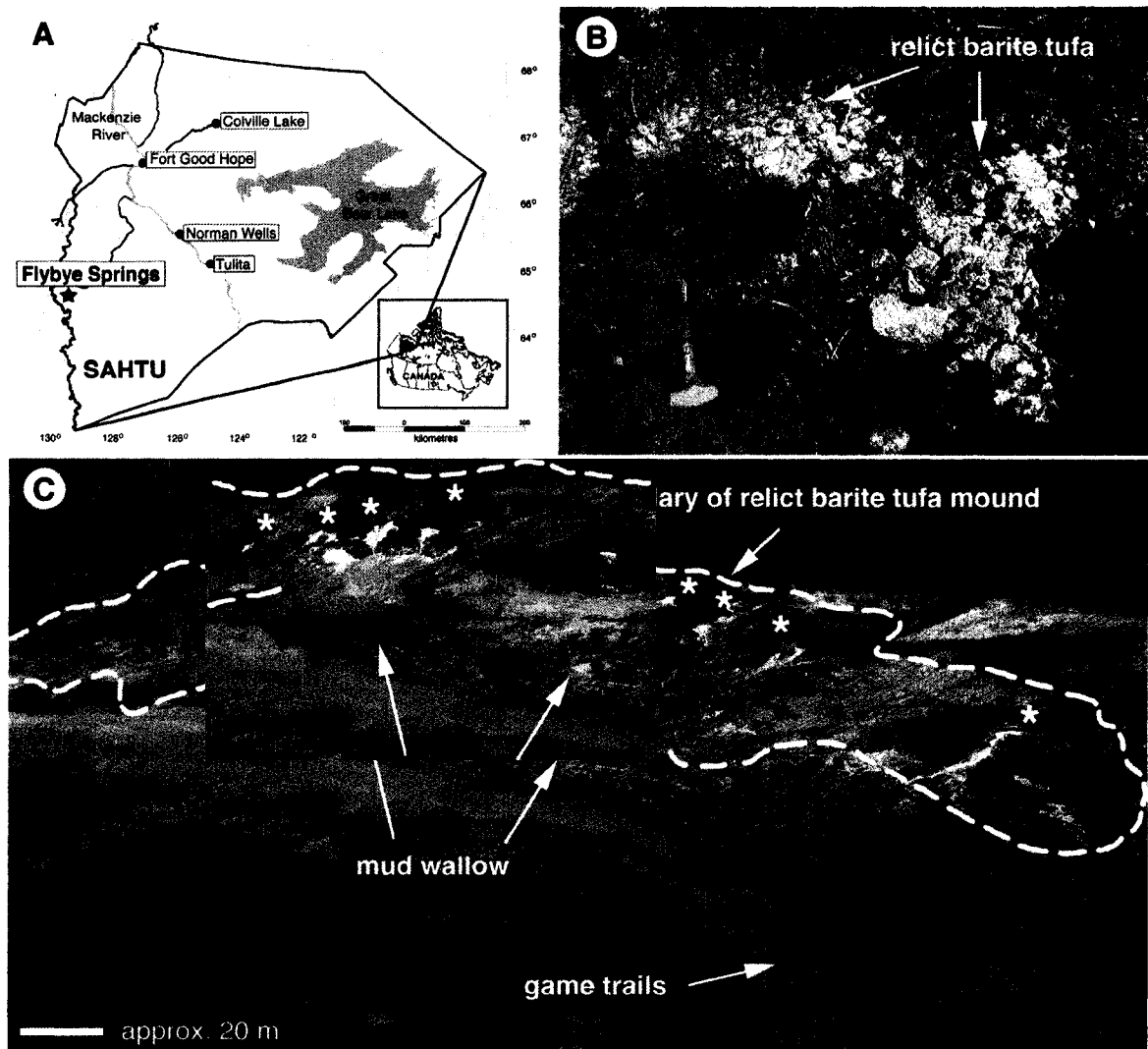


Figure 3-1. Flybye Springs field site. (A) Geographic setting. (B) Vegetated surface of relict barite tufa mound (hammer is 25 cm long). (C) Aerial photograph showing modern Flybye Springs (most active vents marked by asterisks) and extent of relict barite tufa mound

many of these lithotypes (rafts, coated grains, coated bubbles) have previously been considered unique to carbonate-precipitating systems, as they form under the constraints of calcite and aragonite's inverse ($p\text{CO}_2$ controlled) solubility (Andrews et al., 1997; Takashima and Kano, 2005; Pentecost, 2005). Barite's solubility is directly controlled by the redox state of the precipitating solution, which controls the concentration of dissolved SO_4^{2-} available for reaction with Ba^{2+} (Hanor, 2000). Both barite and carbonate mineral precipitation can also be mediated by microbes (e.g. Senko et al., 2004; Bonny and Jones, 2007b), but different taxa inhabit carbonate-rich and sulphur-rich spring waters (Castenholz, 1976). The similarity of the Flybye tufa to carbonate spring deposits, thus illustrates that texturally convergent lithotypes can form in depositional systems with divergent chemistry, mineralogy and resident biology.

Barite is precipitated in numerous microbially-colonised marine and continental habitats (e.g. marine cold seeps, white smokers, upper water column of lakes and oceans) but the influence of microbes in barite precipitation is neither well constrained, nor widely recognized (Aharon, 2000; Aloisi et al., 2004; Riedinger et al., 2006). This has inhibited interpretation of putatively 'biogenic' sedimentary barite, including Archean barite-bearing stromatolites from Australia (Buick et al., 1981) and Paleozoic barite stromatolites in Senegal (Carroue, 1996). Biogenic textures and microfossils preserved in barite tufa at Flybye Springs provide an exciting opportunity to examine microbial influences on the development of barite at ambient temperature.

This paper uses a combined microscopic and analytic approach to describe the Flybye Springs barite tufa lithotypes. The physiochemical and biological conditions that combined to produce each lithotype are interpreted by analogy to processes operating in the modern Flybye Springs flow paths and at carbonate springs. The Flybye Springs barite tufa deposit is rare, quite possibly globally unique, but yields insight into the textural development of barite precipitated in the presence of microbes, which may facilitate recognition of biomarkers in barite precipitated in microbially-colonised marine systems and preserved in the Earth's geologic record.

Methods

The geometry and extent of the Flybye barite tufa mound were documented by ground mapping and aerial photography. Relict tufa samples were collected in situ from non-vegetated areas of the mound, fractures on the eastern edge of the mound and excavations along the borders of active spring water tributaries, and from a detrital tufa fan.

The mineralogy of the tufa samples was determined by optical petrography and X-ray diffraction (XRD) of powdered samples on a Rigaku Geigerflex Cobalt Tube Power Diffractometer with a graphite monochromator and JCPDS online mineral identification database. The radioactivity of the samples was measured using a Ludlum Model 3:44-9 radiometric survey meter held 5 cm above the samples. Textural and elemental variations in the tufa were examined by scanning electron microscopy (SEM) and electron microprobe (EMP). Specimens were fractured, mounted on steel stubs, and sputter coated with gold for 1 to 2 minutes (depending on sample porosity) for analysis on a JEOL 6301 field emission SEM at an average working distance of 12 mm, and an accelerating voltage of 5-10 kV for imaging, and 20 kV for elemental analyses. Both secondary electron and backscattered electron images were collected, and elemental analyses were accomplished using an energy dispersive X-ray analyzer (EDX) coupled to the SEM. Cut, polished and carbon-coated thin sections were prepared for elemental analysis (as weight %) on a JEOL 8900R electron microprobe at an accelerating voltage of 15 kV with a 10nA beam current and 1 μ m beam diameter. Backscattered electron images were also generated on the EMP at an accelerating voltage of 20 kV with a 30nA beam current. Gray levels in these images reflect relative, image specific variations in average atomic weight, with darker areas corresponding to relatively lower average atomic weight, and bright areas to relatively higher average atomic weight. Adobe Photoshop CS 2 © was used to crop and adjust the brightness and contrast of digital field and SEM images. Animal hair found in some tufa samples was identified by SEM comparison with specimens from the University of Alberta Museum of Zoology's mammal collection.

Terminology

Mineral deposits formed in spring flow paths are variously referred to as *tufas*, *travertines*, *sinters* or *geyserites*. These terms carry mineralogical, environmental and textural implications, but are applied with little consistency between studies. In this paper, the barite that forms a relict mound around the Flybye Springs is described as *tufa* following common usage of tufa as a ‘generic name for porous stones’ (Oxford English Dictionary), and embracing the qualifications of Ford and Pedley (1996) that tufa forms by precipitation from cool or ambient temperature water and contains microfossil remains of micro- and macrophytes, bacteria and invertebrates. The mineralogy of tufa is commonly indicated by a qualifying prefix, for example *calcareous tufa* (Ford and Pedley, 1996; Kano and Fuji, 2000) or *calc tufa* (Gaoudie and Viles, 1990) for tufa composed of calcite, or *barite tufa* for tufa composed of barite (herein). The term *lithotype* refers to macroscopically distinguishable varieties of tufa.

Geological Setting

The Flybye Springs are located on the north side of a terraced, northeast trending valley between the Selwyn and Mackenzie mountain ranges in the Sahtu Region of Canada’s Northwest Territories (Fig. 3-1A). There are numerous cold and warm carbonate and sulphur springs within a 30 km radius of the Flybye Springs site, but the Flybye Springs are unique in precipitating barite as a dominant mineral phase (Cecile, 2000). The Flybye Springs aquifer is shallow and runs along a southwesterly dipping, anticlinal contact between massive Devonian limestone and Devonian black, pyritic shale (Cecile, 2000). Barium in the spring water is most likely sourced from microcrystalline barite and barium-enriched feldspars sequestered in the Devonian shale (Cecile *et al.*, 1984; Orberger *et al.*, 2005). Modern spring activity is restricted to ten small vents with combined discharge ≤ 20 L/min (Cecile *et al.*, 1984). Spring water is anoxic at the vents, cool (8.5 °C), circumneutral, and rich in sulphur (≤ 54 ppm), bicarbonate (≤ 245 ppm), calcium (≤ 47 ppm) and barium (≤ 12 ppm) (Bonny and Jones, 2007a). Sulphur-tolerant microbes (including *Beggiatoa*, *Thiothrix*, *Thioploca*, *Oscillatoria*, *Chromatium* and diatoms) inhabit all inundated parts of the flow path (Bonny and Jones, 2007a). Unconsolidated precipitates of barite and elemental sulphur are found among microbial

colonies and as coatings on submerged substrates. The Flybye Springs drain into a mud wallow that is frequented by caribou, and the surface of the spring mound is locally eroded and marked by hoof prints.

An extensive relict deposit of indurated barite tufa underlies the modern springs, indicating that the rate of tufa deposition previously exceeded erosion. This area of the Mackenzie Mountains was deglaciated by 10 ka (Cecile, 2000), which provides a maximum age for tufa at Flybye Springs, since spring deposits rarely survive glaciations. The relict tufa is sparsely vegetated (Fig. 3-1B), crescent shaped, $\sim 200 \text{ m}^2$ in aerial extent, and rises up to 5 m above the surrounding terrace slope (Fig. 3-1C). Shallow vent pools at the crown of the mound expose convex to subhorizontal tufa beds that trail down slope into a fluted detrital tufa fan. Relict tufa is locally exposed along fractures and above modern spring vents and seeps.

Relict Barite Tufa Composition

EMP and EDX analyses indicate that relict barite tufa from the Flybye Springs is relatively pure, with little substitution of foreign divalent cations ($\leq 0.34 \text{ wt.}\% \text{ Ca}^{2+}$; $\leq 0.77 \text{ wt.}\% \text{ Sr}^{2+}$). Elevated radioactivity ($\leq 8 \text{ }\mu\text{Sv/hr}$) is presumed to indicate co-precipitation of small amounts of radium (Cecile *et al.*, 1984). Rare inclusions of framboidal pyrite and elemental sulphur were also observed in SEM.

Minor variations in trace element abundance along crystal growth axes produce fine scale compositional banding that is reflected by varying grey-levels in backscattered electron EMP images (Fig. 3-2A, B, C). Traverses across these bands show that dark bands are enriched in Sr, Ca and K relative to the lighter bands (Figs. 3-2 and 3-3). Fine scale bands, $\leq 5 \text{ }\mu\text{m}$ wide, are not represented in Figure 3-3 because they exceed the combined precision of the microprobe beam spot size ($1 \text{ }\mu\text{m}$) and automated stage positioner ($\pm 1.5 \text{ }\mu\text{m}$).

Light bands have euhedral crystal terminations (Fig. 3-2C). In contrast, dark bands commonly have rounded edges (Fig. 3-2C), which may represent dissolution surfaces (cf. Younger, 1986), or episodic barite lattice poisoning. It was not possible to assess wt. % C, because samples were carbon coated prior to EMP analysis, but brown and orange stains visible in thin section indicate incorporation of organic compounds.



Figure 3-2. Backscattered electron EMP images of relict barite tufa. (A) Overview of barite tufa with fine scale compositional banding; note progression from microcrystalline barite plates to bladed barite. Solid line shows microprobe traverse, square brackets correspond to annotations in Figure 3. (B) Detail of platy barite microcrystals from A. (C) Bladed barite showing dark bands with rounded boundaries (arrows) and light bands with angular terminations.

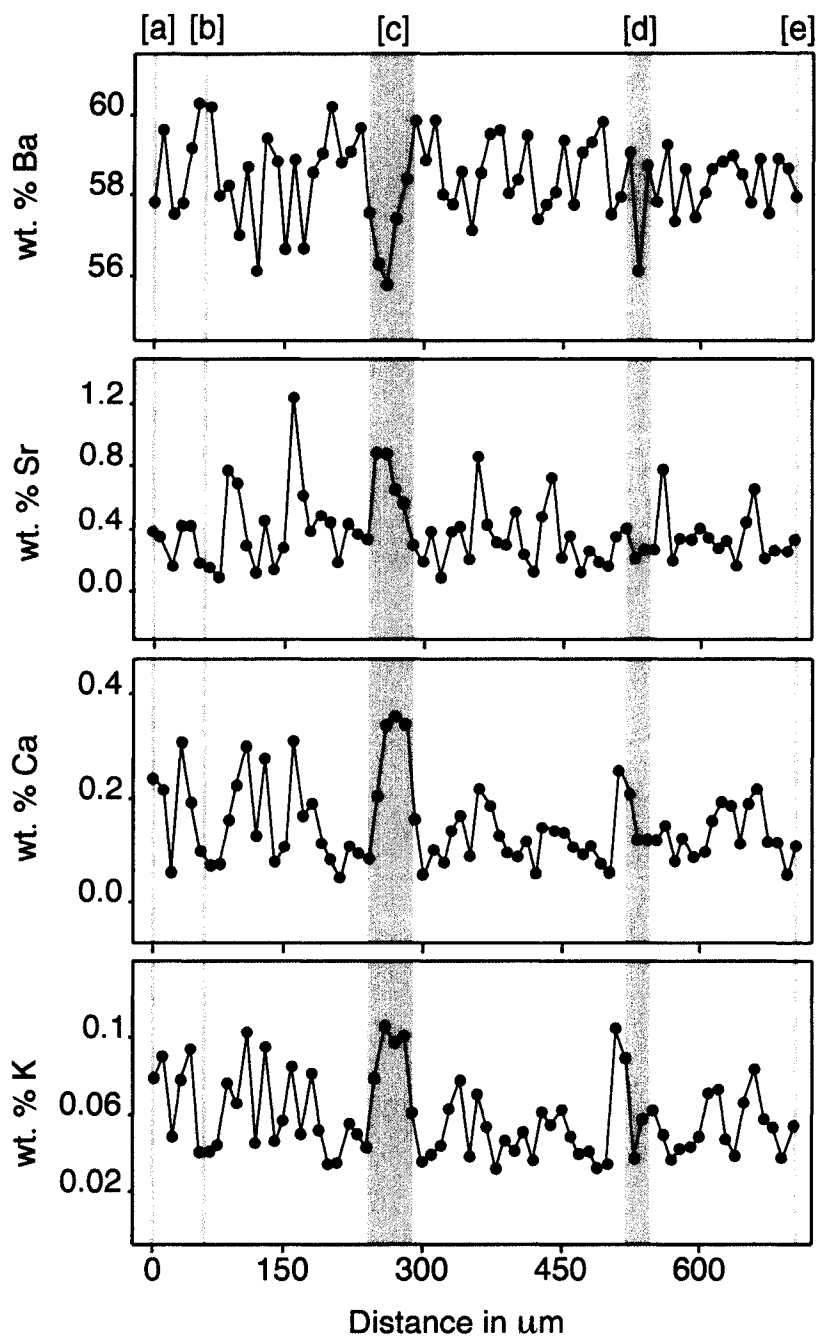


Figure 3-3. Variations in weight % barium, strontium, calcium and potassium in Flybye barite, measured along traverse [a]-[e] from Figure 2. Highest weight percent barium was measured in a light band at point [b], whereas highest weight percent percentages of co-precipitated cations were measured in dark bands around points [c] and [d].

Humic acids inhibit barite precipitation (Smith et al., 2004), and may be responsible for rounded barite crystal terminations in dark bands. Dark bands also contain higher abundances of co-precipitated Ca, Sr and K (Fig. 3-3 [c]). Divalent cations are incorporated into the barite crystal lattice as a result of ionic attraction, and strontium ≤ 5 mol % is common in sedimentary barite (Malinin and Urusov, 1984). Significant amounts of calcium can also be accommodated (Fu et al., 1994, Sanders, 1998). Co-variance with calcium and strontium at points [b], [c] and [d] (Fig. 3-3) indicates that potassium is also substituting into the barite crystal lattice despite its monovalency, likely as a result of its similar ionic radius to barium ($K = 1.38\text{\AA}$, $Ba = 1.35\text{\AA}$).

Compositional bands in Flybye barite alternate rhythmically along crystal growth axes and do not show the systematic increases or decreases in atomic weight typical of closed system and diagenetic barite (Hannington and Scott, 1988; Hanor, 2000; Tekin et al., 2002). Barite at Flybye Springs precipitated from circulating spring water, so compositional banding probably developed in response to variations in the degree of barite supersaturation (cf. Fu et al., 1994) and the dissolved organic carbon content of the spring water (cf. Smith et al., 2004).

The compositional bands in the Flybye barite tufa provide a temporal record of crystal growth boundaries, and commonly reveal unidirectional shifts in barite crystal habit. Randomly arranged, ellipsoid primary barite plates with cores $< 20\ \mu\text{m}$ long are surrounded by compositionally layered cements (Fig. 3-2B) that precede radially arranged bladed barite crystals in many samples (Fig. 3-2C). Small ($5\text{-}20\ \mu\text{m}$) disordered barite crystals are typical of precipitation from highly supersaturated solutions, whereas larger ($\geq 15\ \mu\text{m}$) euhedral crystals are more typical of barite precipitation from solutions with low degrees of supersaturation (Shikazono, 1994; Fu et al., 1994). Two phases of barite precipitation are, thus, inferred for most relict barite tufa samples. Textural development of the barite tufa proceeded by precipitation of a primary 'framework' of microcrystalline barite from strongly supersaturated solutions, which was basal to coarser barite precipitated from less supersaturated solutions.

Relict Barite Tufa Lithotypes

Relict barite tufa at Flybye Spring is texturally diverse, with six readily distinguishable lithotypes: coated bubble, raft, undulatory sheet, stromatolitic, coated grain and detrital conglomerate.

Coated bubble tufa

Description

Tufa composed of irregularly stacked, thin walled coated bubbles 0.3-1.3 cm in diameter, is locally abundant on the relict tufa mound, occurring in lenses visible in cross section for up to 25 x 60 cm. The hollow interiors of most coated bubbles imbue this lithotype with porosity up to 75 % (Fig. 3-4A). Strings and drapes of nanometric-barite (< 500 nm) are commonly found attached to inner coated bubble walls and span gaps between adjacent coated bubbles (Fig. 3-4B, C). Coated bubble walls are layered, with an inner microcrystalline barite core and an outer (and, in fractured specimens, inner) layer of isopachous barite cement (Fig. 3-4D, E). Pyrite framboids, 4-8 μm in diameter (with pyritohedral microcrystals 0.3-0.8 μm wide) are present in many coated bubble walls (Fig. 3-4E, F). Ductile deformations of some bubble walls indicates that they were elastic during early mineralisation. Lithified coated bubbles are brittle, and punctured coated bubbles are commonly filled by microcrystalline barite, detrital clays and organics, and/or allochthonous grains (Fig. 3-4D).

Interpretation

Although previously unreported from barite, coated bubble tufa or 'foam rock' is abundant in carbonate spring deposits. In carbonate travertines, coated bubbles form by rapid mineralisation of bubbles of oxygen, methane and/or carbon dioxide (Chafetz and Folk, 1984; Guo and Riding, 1998). Although coated bubbles have been described mainly from thermal springs, they are also known to occur in cold spring tufas and speleothem deposits (Pentecost, 2005). Carbonate bubble mineralisation requires ambient saturation of the spring water with respect to calcium carbonate, and that the gas bubble be trapped subaqueously by surface tension or an overlying object (Guo and Riding, 1998). Stagnant conditions are most favourable for coated bubble formation (Folk et al, 1985; Kam and

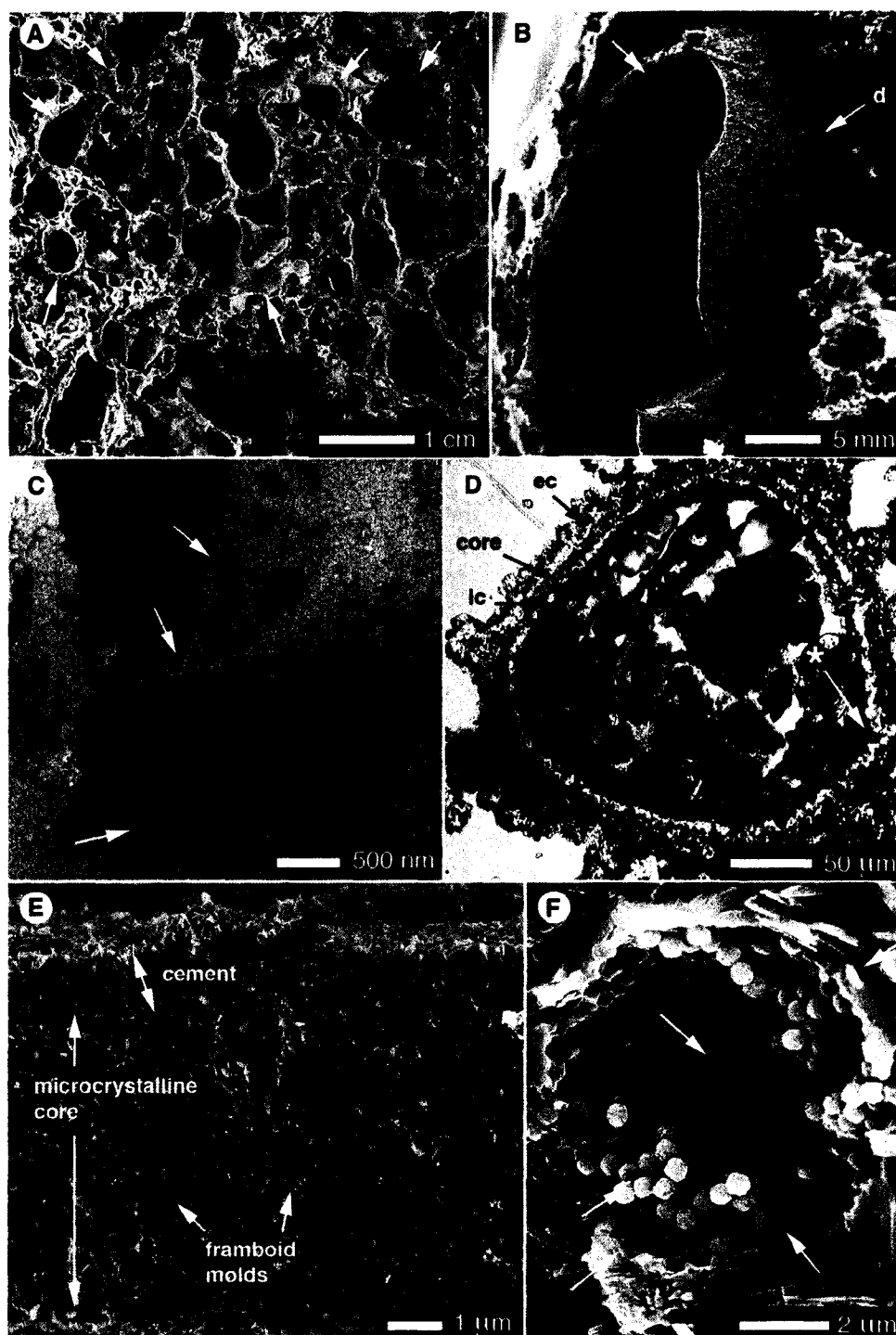


Figure 3-4. Coated bubble barite tufa. (A) Coated bubbles (arrows) in hand sample. (B) SEM image of punctured bubble with external 'drapes' of barite (d-arrow). (C) SEM detail of barite drapes found inside a coated bubble. (D) Thin section photograph, cross-section of a tri-layered bubble with an inner microcrystalline core (core-arrow), external hyaline barite cement (ec-arrow) and fine inner cement layer (ic-arrow). This bubble was punctured, contains detrital grains, and shows evidence of brittle deformation (*). (E) SEM image cross-section of a bi-layered bubble wall. (F) SEM image of partially preserved pyrite framboid embedded in bubble wall.

Rosen, 1999; Ozkul et al., 2002), but they may also be preserved in flowing water, particularly if the gas bubble is protected by a ductile medium like microbial EPS (Takashima and Kano, 2005). Remnants of microbial EPS can be preserved as 'fine drapes' of micrite that envelop or span coated bubbles in carbonate tufa (Folk et al., 1985).

The presence of framboidal pyrite in Flybye barite coated bubble walls indicates that early mineralisation proceeded along a redox boundary (Sawlowicz, 2000). The solution surrounding the bubble must have been barite-saturated, hence partially oxidized, to permit barite precipitation. Thus, the coated gas bubbles probably contained reduced gaseous phases. Hydrogen sulphide, methane, and carbon dioxide exsolve from the modern Flybye Spring vent waters, and are generated by degradation of organic detritus in spring water ponds (Bonny and Jones, 2007a). These gases most likely formed the bubbles that were coated by barite in the flow path of the relict spring system. Nanometric barite drapes found between and inside barite coated bubbles in the relict tufa probably represent mineralised EPS, which restrained the gas prior to mineralisation (cf. Folk et al., 1985).

Initial precipitation of microcrystalline barite (and framboidal pyrite) probably took place along an EPS-restrained redox interface. EPS readily adsorbs divalent cations (Arp et al., 1999; Schultze-Lam and Beveridge, 1993) and may become barium-enriched in the presence of barium-bearing solutions (Douglas and Douglas, 2001; Tazaki and Watanabe, 2004). In the presence of sulphate, barium-enriched EPS is an efficient substrate for nucleation of barite microcrystals (Tazaki et al., 1997; Sanchez-Moral et al., 2004; Glamoclija et al., 2004). Adsorption of barium to thin sheets of gas-restraining EPS may, thus, have facilitated bubble mineralisation at the Flybye Springs. Once the microcrystalline barite layer overcame the barite nucleation threshold, diffusion of barium and sulphate from surrounding barite-saturated solutions would permit precipitation of the outer layer of barite cement. Similar layering has been described in calcified bubbles which have an inner micritic layer bordered externally by radial cements of calcite or aragonite (Chafetz and Folk, 1984; Chafetz et al., 1991; Ozkul et al., 2002). The innermost isopachous layer of barite cement found in some fractured Flybye barite coated bubbles (Fig. 3-4D) likely formed secondarily, by deposition from spring

water percolating through lithified coated bubbles.

Raft tufa

Description

Tufa composed of thin rafts of barite was collected from the upper Flybye tufa mound and from the detrital fan. Subhorizontal rafts, 1-12 cm², show brittle deformations and are cemented non-conformably, preserving elongate porosity (Fig. 3-5A, B). In friable tufa samples, barite rafts are 100-500 µm thick, and consist of an inner layer of tightly packed microcrystalline barite, 5-50 µm thick, that is bordered by fringes of bladed barite crystals 5-300 µm long (Fig. 3-5C, D, E). The bladed barite fringes are asymmetric in many samples, with crystals two to three times larger on one side of the microcrystalline barite raft (Fig. 3-5D). The thicker barite fringe is found on the lower side of most rafts, but locally rafts were found with thicker barite fringes on their upper sides. Precipitation of secondary cements increased the apparent thickness of the rafts up to 0.4 cm in indurated barite tufa. In some indurated tufa samples, rafts are cored by coarse, crystalline barite, which is separated from upper and lower fringes of bladed barite by crystal discontinuities and/or bands of microporosity (Fig. 3-5F).

Interpretation

The Flybye Spring raft tufa lithotype has textural analogues in carbonate 'paper-thin sheet' travertine (Folk et al., 1985), 'paper-thin raft' travertine (Guo and Riding, 1998), 'calcite raft' tufa (Carthew et al., 2006), and 'calcite floe' that accumulates in cave pools (Jones, 1989; Drysdale et al., 2003). Calcite rafts form in low-turbulence settings where CO₂ degassing at the air-water interface initiates nucleation of calcite crystals on particulate matter suspended by surface tension (Jones, 1989) and/or floating biofilms (Carthew et al., 2006). Coalescence of growing crystals produces rafts of variable size (Renaut et al., 1999), which sink if they attain a critical mass or are disturbed and fragmented. Cementation or burial at the sediment-water interface promotes their preservation in tufa and travertine (Folk et al., 1985; Carthew et al., 2006).

Rafts of barite at the Flybye Springs probably also formed at the air-water interface, with initial barite nucleation driven by degassing of carbon dioxide (Lindgren,

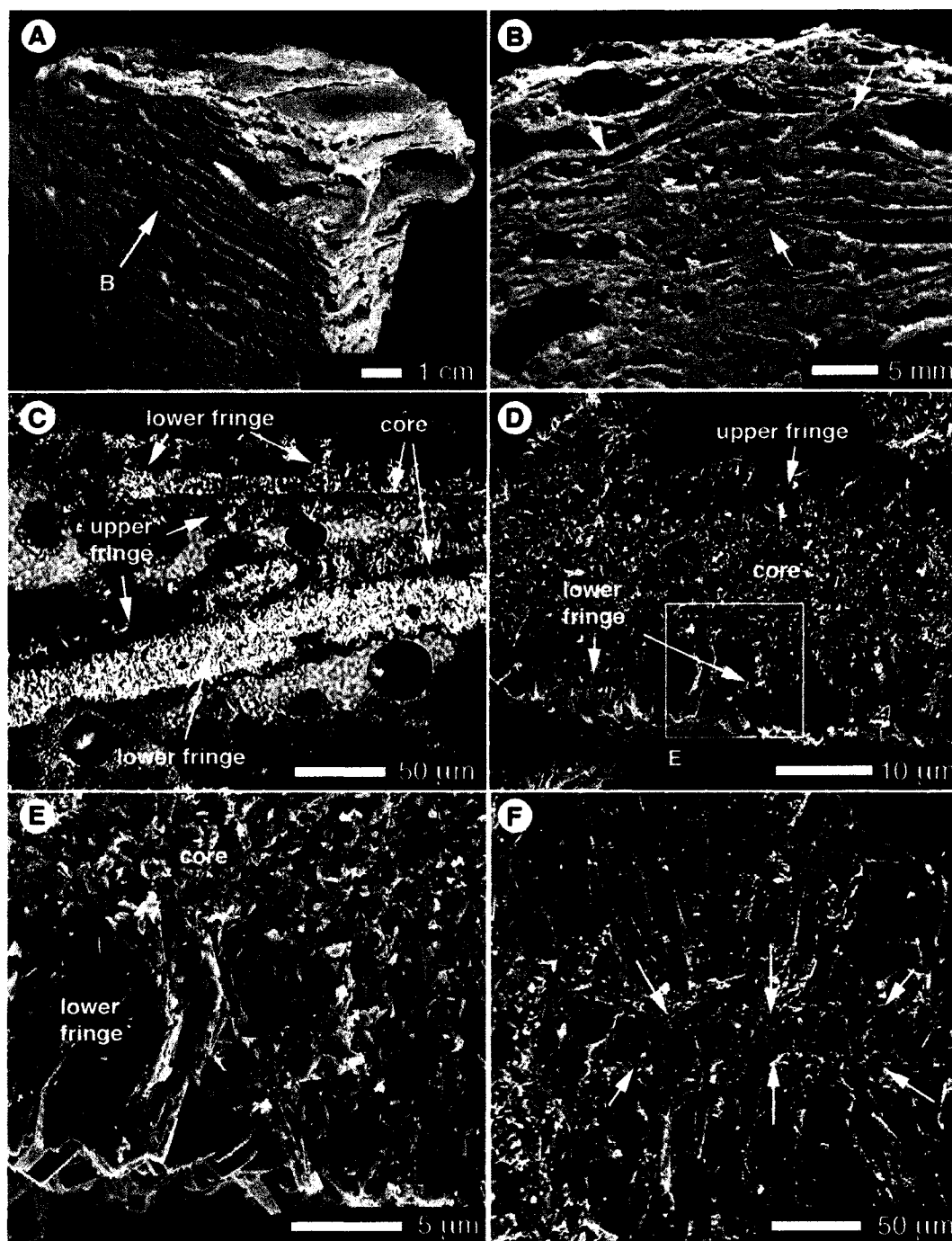


Figure 3-5. Raft barite tufa. (A) Rafts in hand sample. (B) Cut section of raft tufa showing brittle deformation of rafts (arrows). (C) Thin section photograph, rafts with asymmetric fringes of bladed barite cement. (D) SEM image showing cross-section of raft with microcrystalline barite core and asymmetric fringes of bladed barite cement. (E) Detail of core/lower cement fringe boundary from D. (F) SEM image cross-section of raft from indurated tufa with coarsely crystalline core defined by bounding crystal discontinuities (arrows).

1933) and atmospheric oxidation of dissolved sulphide to sulphate. These conditions might be met at the surface of ponds fed by anoxic springs, but no barite rafts were seen on the surfaces of ponds at the modern Flybye Springs springs. It may be that rafts no longer form at the Flybye Springs, or that they form in fall or winter (all field work was conducted in July and August).

The tri-layered structure of the barite rafts is evident in many carbonate rafts. In travertine deposits of central Italy, calcite rafts have a dark micritic core that is bordered by asymmetric fringes of coarser calcite crystals (Folk et al., 1985). Layering develops as a result of the decreasing buoyancy of growing rafts. Initial precipitation of micrite takes place at the air-water interface and is followed by growth of small calcite spar crystals downwards. Growth of the spar layer causes the raft to sink slightly, allowing fluid to come into contact with the topside of the raft, permitting growth of upwards trending calcite spar. Asymmetry of sparry cements can be preserved and/or enhanced by continued crystal growth after rafts settle to the sediment-water interface (Pentecost, 2005).

In barite tufa from Flybye Springs, initial barite precipitation is represented by disordered platy barite microcrystals. Asymmetric bladed barite fringes may then have developed analogously to the asymmetric spar layers in calcite rafts. Barite rafts with thicker upper barite fringes may have flipped over during deposition, or been deposited against substrates that prevented continued cement growth on the lower side. The high density of barite (4.48 g cm^{-3}) would limit the thickness attainable by suspended barite rafts, and if they sank into underlying anoxic, barite-undersaturated spring water, they would have low preservation potential. Preservation of rafts in Flybye barite tufa likely required that they be entrained and deposited under dysoxic or fully oxygenated conditions which would allow precipitation of indurating barite cements. Transformation of microcrystalline raft cores to crystalline barite is likely diagenetic.

Undulatory sheet tufa

Description

Tufa composed of non-conformably stacked sheets, 0.05-0.1 cm thick and $\leq 10 \text{ cm}^2$, was found throughout the relict barite tufa mound (Fig. 3-6). The sheets are

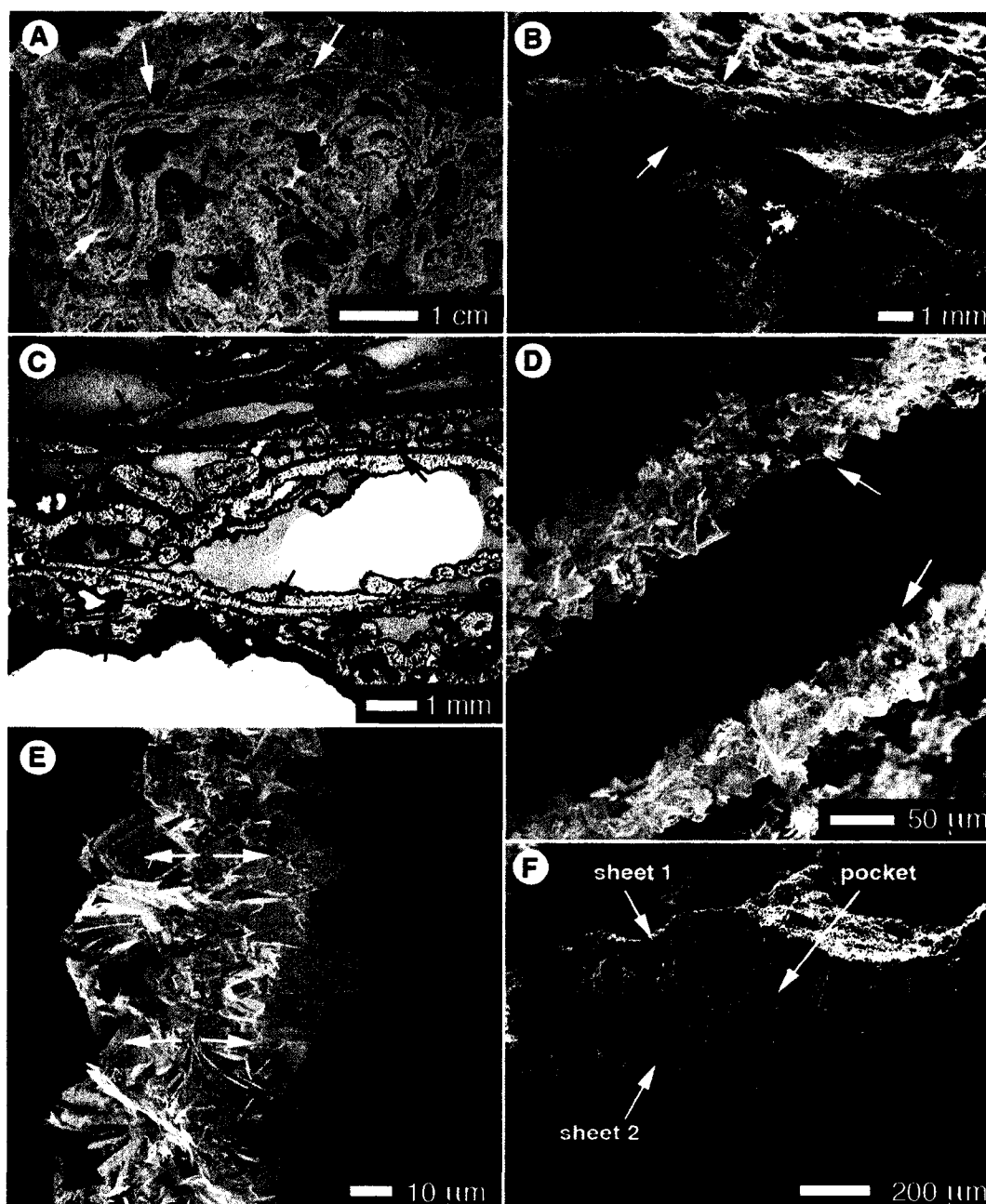


Figure 3-6. Undulatory sheet barite tufa. (A) Undulatory sheets with imbricated concave-up structures (arrows) in hand sample. (B) SEM image of undulatory sheets in indurated barite tufa. (C) Thin section photograph, undulatory sheets with 'false' layering (arrows). (D) SEM image of sub parallel undulatory sheets in young barite tufa. (E) Detail of lower sheet from image D showing bi-directional growth of bladed barite (arrows) away from sheet mid-line. (F) SEM image of subparallel sheets abutting one another in indurated barite tufa; note trapped pocket of microcrystalline barite.

undulatory due to local concave distortions, which shelter vacuous porosity (Fig. 3-6A, B, C). Unlike the barite rafts, the undulatory sheets show little evidence of brittle deformation and may have been ductile during early mineralisation. Rafts and undulatory sheets are not found together in relict barite tufa and are not considered to be genetically related.

Undulatory sheets appear similar to rafts in thin section, where organic inclusions give the impression of an inner core fringed by coarser barite (Fig. 3-6C). At higher magnification, the structure of the undulatory sheets is distinct from that of the rafts; the 'core' of undulatory sheets consists of bi-directional bladed barite crystals that grow outwards from a texturally non-descript midline (Fig. 3-6D, E). Thickening of closely spaced sheets by growth of the bladed barite crystals, and/or deposition of secondary cements, causes them to abut one another and form composite structures. Pockets of microcrystalline barite, organics and/or detrital clays trapped between abutting sheets generates the 'false layering' observed in thin section (Fig. 3-6F).

Interpretation

The undulatory surfaces of these barite sheets indicates that they formed by mineralization of a thin, ductile medium. Calcite precipitation in desiccating microbial mats has produced similar sheet-like lithotypes in calcareous tufas (Chafetz and Folk, 1984; Das and Mohanti, 1997; Bonny and Jones, 2003), but undulatory sheets in Flybye barite tufa are texturally distinct from their carbonate counterparts. Sheets formed by calcification of biofilms are typically composed of non-oriented crystals, and contain clotted organic material or bacterial 'clumps'. Undulatory sheets from Flybye Springs are composed of bidirectional euhedral bladed barite crystals that lack organic inclusions.

EPS-rich films of bacteriogenic sulphur globules found floating in tributary fed spring water ponds at the modern Flybye Springs are very thin (< 0.5 mm), semi-resistant to disturbance, and commonly undulatory due to the presence of trapped gas bubbles. It is possible that the undulatory sheet lithotype formed by barite precipitation around colloidal sulphur films, which caused them to increase in mass, sink, and accumulate at the sediment-water interface. This scenario fails, however, to explain the lack of an apparent core in the sheets; if the barite crystals did nucleate on sulphur films, it is

difficult to explain the lack of elemental sulphur inclusions. An alternate explanation is that the undulatory barite sheets formed at the expense of colloidal sulphur films, by reaction of barium with sulphate derived from the oxidation of elemental sulphur. Spontaneous oxidation of bacteriogenic elemental sulphur can occur in oxygenated solutions (Brigmon *et al.*, 1994), and *in situ* reaction of newly oxidized sulphate with barium adsorbed to EPS in the floating films might cause them to sink, while still semi-cohesive and ductile. Preservation of large undulatory sheets implies formation and settling in quiescent pools, but discontinuous thin barite sheets are also found in stromatolitic barite tufa.

Stromatolitic tufa

Description

Barite tufa with dark and light banding is found on the upper relict tufa mound and as cobble- to gravel-sized grains in the detrital fan (Fig. 3-7A). Bands, 0.5-3 cm thick, have sharp contacts defined by variations in colour, porosity and micro texture (Fig. 3-7B), but no regular chemical variations were identified between stromatolitic bands. Although transitional textures exist, two main 'band types' are readily identifiable. Porous bands (porosity > 60%) are generally light gray to pale brown in colour and contain vertical and sub vertical strings of barite, as well as isolated coated bubbles, ≤ 0.5 cm in diameter, and discontinuous undulatory sheets, ≤ 3 cm² in size (Fig. 3-7B, C). Dense bands (porosity 30-60%) are pale to dark gray or reddish-brown and are composed almost entirely of horizontal, sub-aligned strings of barite (Fig. 3-7B, D-F).

Other than their orientation, strings of barite in the dense and porous stromatolitic bands are structurally analogous, and can be divided into three groups on the basis of petrographic texture and external diameter (Fig. 3-7F):

(1) Thin strings of barite, 10-30 μm in diameter, are composed of microcrystalline barite, which is surrounded by a smooth outer envelope in friable tufa samples (Fig. 3-8A, B). Indurated tufa commonly contains thin barite strings that lack an outer envelope and are composed of radially arranged bladed or tabular barite microcrystals, ≤ 8 μm long (Fig. 3-8C, D).

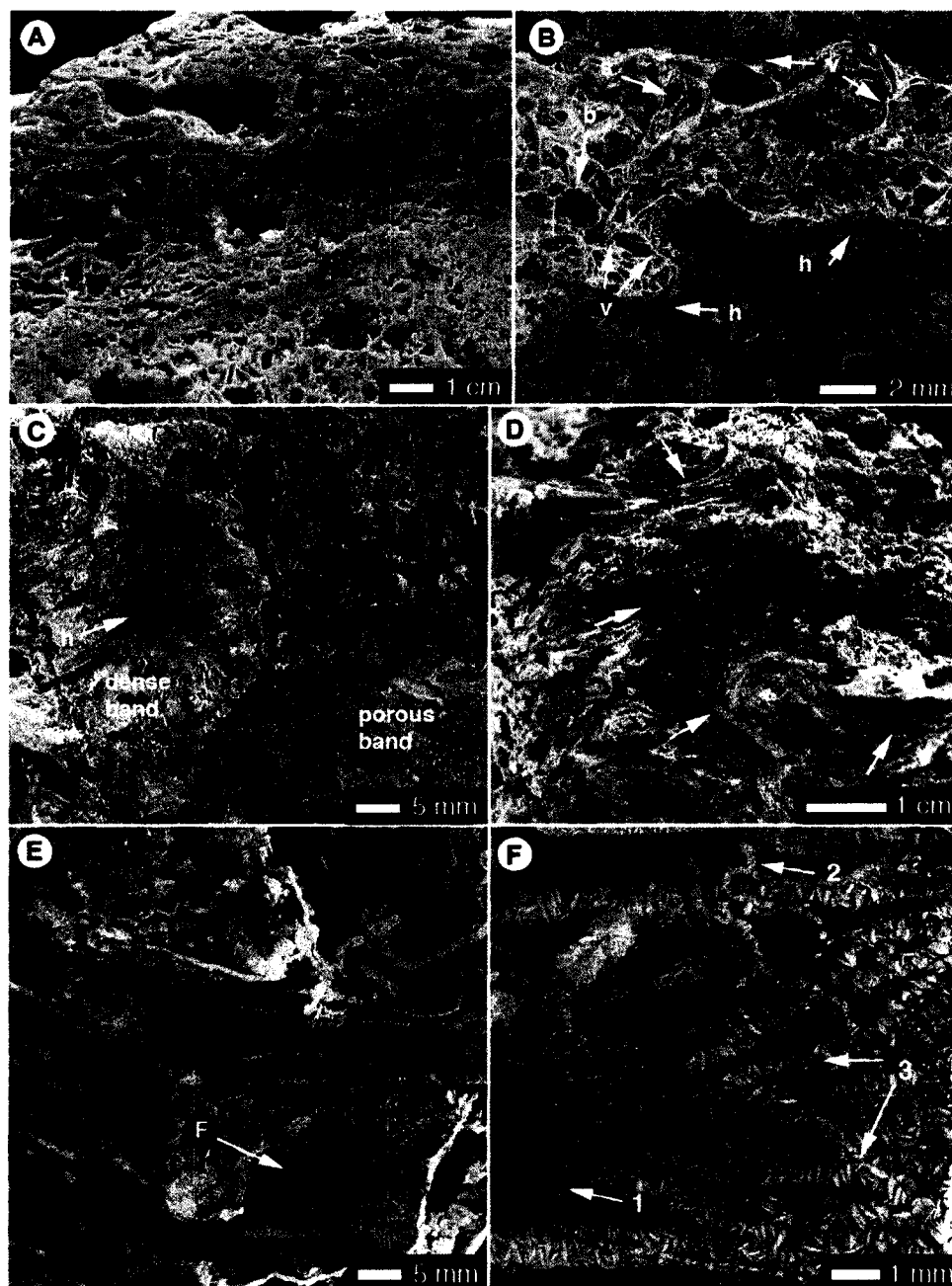


Figure 3-7. Stromatolitic barite tufa. (A) Cut hand sample with chromatic banding. (B) Cross-section of contact between lower, dense band, with horizontal barite strings (h-arrow) and upper, porous band, with coated bubbles (b-arrow), discontinuous undulatory sheets (s-arrow), and sub vertical barite strings (v-arrow). (C) Lateral contact between dense band with horizontal columns (h-arrow) and lower, porous band with abundant coated bubbles. (D) Sub-aligned barite strings on top surface of dense band (arrows). (E) SEM image of sub-horizontal barite strings in friable tufa. (F) Detail of image E showing co-occurrence of three sizes of barite string.

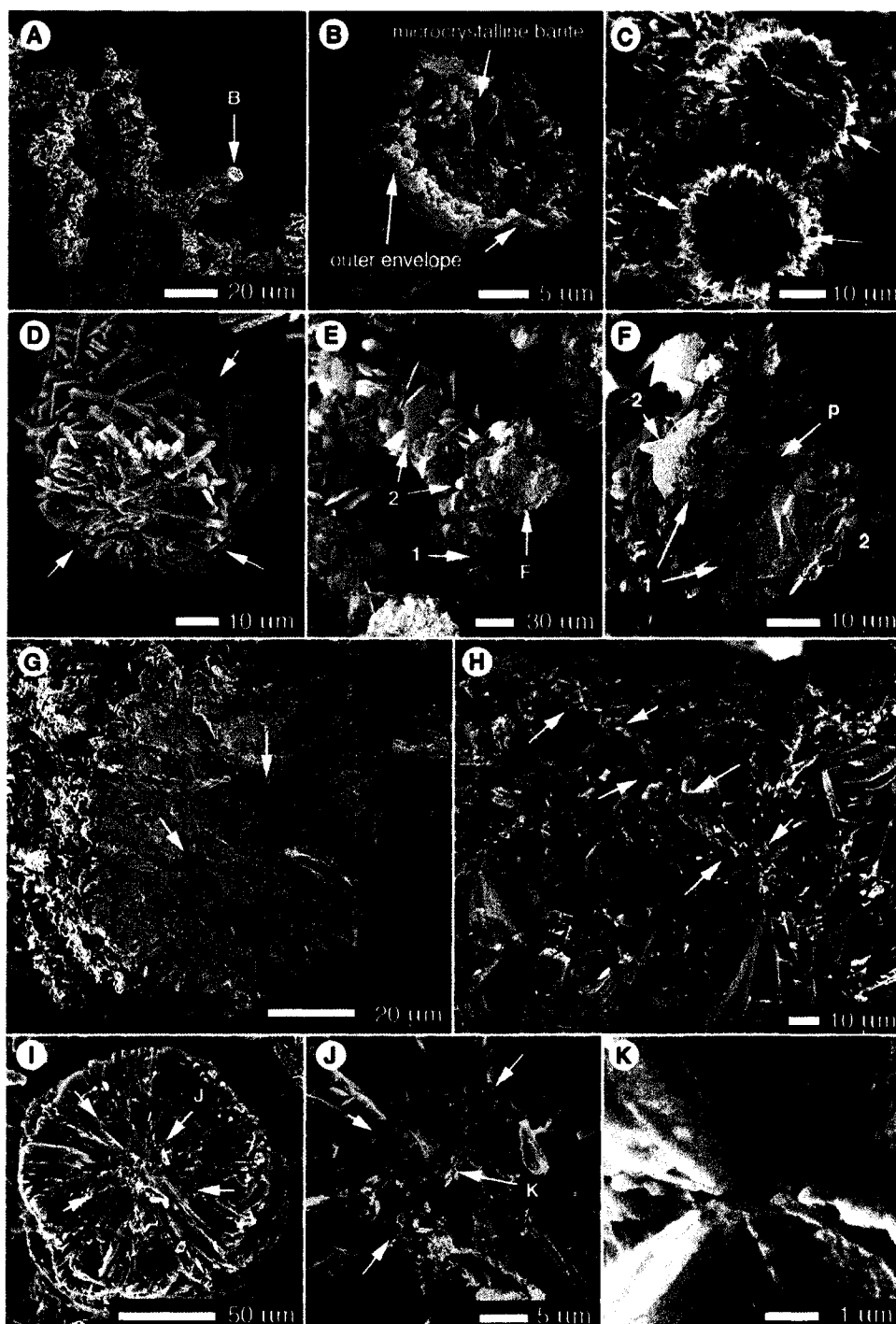


Figure 3-8. SEM images of barite strings. (A) Thin strings in barite tufa. (B) Detail of string from A with microcrystalline barite inside smooth outer envelope. (C) Thin barite string composed of radially arranged microcrystalline barite. (D) Thin barite string composed of platy barite. (E) Medium-sized barite string composed of microcrystalline barite plates (1) and coarse bladed barite (2). (F) Cross-section detail of E showing internal porosity (p-arrow), and coarse bladed barite (2) nucleated on microcrystalline platy barite (1). (G) Composite barite string with two high-porosity cores (arrows). (H) Long-section view of a barite string with high porosity core (arrows). (I) Cross-section of wide barite string with concentric layers of bladed barite (arrows). (J) Detail of I showing former column diameter defined by crystal discontinuities (arrows). (K) Detail of J showing extension of bladed barite crystals to core of barite string.

(2) Medium-sized strings of barite, 30-50 μm in diameter, are composed of sub radial bladed barite crystals that are nucleated upon, and commonly engulf, microcrystalline barite (Fig. 3-8E, F). The cores of these barite strings are commonly porous (Fig. 3-8F, G, H). Closely spaced medium-sized barite strings form irregularly shaped composite strings by intergrowth of radial bladed barite (Fig. 3-8G).

(3) Wide strings of barite, $\leq 300 \mu\text{m}$ in diameter, consist of one or more smaller strings of barite that have been coarsened by concentric, radially arranged bladed barite cements. Former growth diameters are preserved as concentric crystal discontinuities, but interior porosity is commonly occluded (Fig. 3-8I, J, K).

In thin section, aligned micro-porosity and remnant traces of organic matter define a core, 5-10 μm in diameter, in most barite strings. Approximately 20% of the strings from dense stromatolitic bands and 5% of strings from porous stromatolitic bands also contain a distinct organic trace of one or more filamentous microbe. Most filaments are 10-15 μm in diameter and have apically rounded, non-tapering terminations (Fig. 3-9). These are filled by crypto or micro-crystalline barite, contain microporosity, and/or contain irregularly arranged opaque granules (Fig. 3-9A, B, C, D). They are commonly surrounded by an aureole of micro-porosity (Fig. 3-9E). Spot electron microprobe analyses indicate that cryptocrystalline barite inside filamentous microfossils has low average atomic weight and is mildly enriched in sulphur (103% avg.), nitrogen (111% avg.) and sodium (134% avg.), and strongly enriched in potassium (380% avg.) and iron (521% avg.), relative to average weight % values in surrounding barite (Fig. 3-9F). Ovoid bodies, $\sim 5 \times 8 \mu\text{m}$, are located beside the filamentous microfossils in some samples (Fig. 3-9C). Microfossils commonly form the core of the barite strings in which they are found. In some medium and wide barite strings, radial bladed barite crystals are syntaxial with barite inside the microfossils, and display simultaneous extinction in crossed-polars (Fig. 3-9D).

Interpretation

Stromatolites (laminated organo-sedimentary structures produced by trapping, binding or precipitation of minerals in microbial mats; Awramik et al., 1976) are a common feature of many carbonate tufas and travertines (Andrews and Brasier, 2005;



Figure 3-9. Microfossils in stromatolitic barite tufa and microbes from the modern Flyby Springs. (A-D) Thin section photographs of longitudinal sections through filamentous microfossils in barite strings in indurated barite tufa. Arrows in A and B indicate granular inclusions in microfossils. Arrows in C indicate ovoid body external to the filamentous microfossil. D shows two filamentous microfossils in crossed polarized light; note barite inside microfossils has simultaneous extinction with surrounding barite. (E, F) Backscattered electron EMP images of microfossils: (E) Longitudinal view of microfossil with high internal porosity, surrounded by a porous aureole (arrows); (F) Cross-section of filamentous microfossil filled cryptocrystalline barite with fine variations in average atomic weight (arrows). (G) Light microscope photographs of *Oscillatoria* filaments with intracellular storage granules, and *Chromatium* with intracellular sulphur beads. (H) SEM image of *Beggiatoa* filaments with numerous intracellular sulphur beads.

Pentecost, 2005), and are abundant in the carbonate sedimentary record (Seong-Joo et al., 2000). Putative barite stromatolites are rare (Buick et al., 1981; Carroue, 1996) and have not previously been identified in a barite spring deposit.

Stromatolitic tufa at Flybye Springs formed by barite precipitation around microbes growing in spring flow paths. The sub aligned horizontal barite strings in dense stromatolitic bands are similar to 'streamers' in carbonate and silica spring deposits, which form by rapid mineral encrustation of current-aligned filamentous bacteria, cyanobacteria or EPS strands (e.g. Weed, 1889; Irion and Muller, 1968; Jones et al., 2001). Sub vertical barite strings in porous stromatolitic bands probably formed by barite precipitation among upright or floating microbial filaments and/or EPS strands (Chafetz et al., 1991). The preservation of coated bubbles and discontinuous undulatory sheets among upright barite springs indicates that the porous stromatolitic bands formed in ponded water. At the modern Flybye Springs, bubbly microbial mats are found in quiet, surface oxygenated ponds, whereas prostrate, current-aligned filaments proliferate in turbulent, dysoxic tributaries (Bonny and Jones, 2007a). Alternation of dense and porous bands in stromatolitic barite tufa may, thus, reflect local changes in water depth, turbulence and oxygenation.

Stromatolitic banding is commonly cyclic, developed in response to regular diurnal or seasonal changes in microbial growth and/or physiochemical variables (Irion and Muller, 1968; Pentecost and Riding, 1986; Jones et al., 1998; Kano et al., 2004; Andrews and Brasier, 2005). Located just south of the Arctic Circle, the Flybye Springs experience wide seasonal variation in temperature and incident light, which almost certainly influence rates of microbial growth and assert control over the development of stromatolitic textures. Introduction of snowmelt to the shallow Flybye aquifer may also produce episodic (spring-summer) increases in spring water discharge (van Everdingen, 1972), prompting reorganization of spring flow paths with local changes in water depth and turbulence. Precipitation of barite amongst microbes growing under these variable conditions produced stromatolitic bands of irregular thickness, which are not easily correlated to specific seasonal conditions.

Chromatic variations between stromatolitic layers in carbonate tufas are commonly attributable to differential rates of mineral precipitation (Andrews, 2006) with

darker bands forming at peak precipitation rates (Matsuoka et al., 2001). At Flybye Springs, barite precipitation rate is determined by the rate of spring water oxidation, which would be maximized in turbulent tributaries, and minimized in quiescent pools. Higher precipitation rates may, thus, explain the generally darker colour of dense bands and paler colour of porous bands. Barite may also be darkened by inclusion of organic material and microbial pigments (Suganuma, 1928), indicating more incorporation of microbial remains in dense stromatolitic tufa bands.

The barite strings clearly formed in association with filamentous microbes. This is demonstrated by their similarity to biogenic 'streamers', and by the presence of microfossils in the cores of some strings. The smooth envelopes that surround thin barite strings in friable barite tufa probably represent remnants of original EPS associated with the string-forming microbial filaments. The multiple barite string sizes indicates either that barite strings formed around filaments of multiple sizes, or that they are genetically related.

Thin barite strings are presumed to form by precipitation of microcrystalline barite upon and/or within microbial filaments. Bladed barite crystals in medium-sized barite string may have formed by recrystallization of this primary microcrystalline barite. Early recrystallization of microcrystalline barite to coarser, euhedral forms is a poorly understood but common component of ambient-temperature barite diagenesis, which has been reported from cave deposits (Radanovic-Guzvica, 1999), diagenetic marine barite (Shikazono, 1994) and marine cold seep barite (Fu et al., 1994). Medium-sized barite strings that contain both microcrystalline and euhedral barite may represent recrystallization 'in progress' (Fig. 3-8E, F). Composite and wide barite strings seem to form by continued outwards growth of bladed barite. Co-occurrence of multiple barite string sizes in stromatolitic barite tufa implies multiple generations of barite string formation, arising by growth of new microbial filaments over and through tufa pore space.

Many microorganisms have been implicated in the formation of stromatolites, including bacteria, cyanobacteria, fungi and diatoms (Riding and Awramik, 2000). Comparison of the morphology and diameter of microfossils in Flybye stromatolitic barite tufa with genera known to inhabit the modern Flybye Springs suggests that most

represent either the cyanobacterium *Oscillatoria* (Fig. 3-9G) or the morphologically similar sulphur-oxidising bacterium *Beggiatoa* (Fig. 3-9H). Ovoid microfossils found external to some filamentous microfossils have similar size and shape to the purple sulphur bacterium *Chromatium* (Fig. 3-9G), which also proliferates at the modern springs (Bonny and Jones, 2007a). Granular inclusions in the microfossils (Fig. 3-9A, B, C) may represent degraded primary organic material, or intracellular storage vacuoles for elemental sulphur in *Beggiatoa* and *Chromatium* (Nelson, 1987). Trace element enrichments in iron, nitrogen and potassium are common in microfossils and microbial trace fossils (Konhauser, 1997; Banerjee and Muehlenbachs, 2003) and enrichments of sulphur in the Flybye stromatolite microfossils may be a residual artifact of intracellular sulphur globules. Microporosity inside Flybye Springs microfossils is probably primary, representing the former position of cellular tissues that have since been removed. Aureoles of microporosity around microfossils may be secondary, produced by partial dissolution of barite by pore fluids rendered anoxic by degradation of trapped microbial cells.

Barite strings that do not contain microfossils probably also formed around microbial filaments, or EPS strands, which were not preserved. Fungi and other filamentous microbes are present at the modern Flybye Springs (Bonny and Jones, 2007a) and may have acted as substrates for barite string formation without being preserved as microfossils. Preservation of microfossils in chemical sediments is the exception, rather than the rule; a biological presence during mineral precipitation does not guarantee microfossil preservation (Walter and Des Marais, 1993; Jones et al., 2001). Microfossil preservation is most likely, however, where rates of mineral precipitation outpace microbial decay (Walter and Des Marais, 1993; Konhauser et al., 2003). Faster rates of barite precipitation in turbulent spring water tributaries compared to ponds may explain both the selective preservation of *Beggiatoa* (a streamer-forming microbe), and the relatively higher abundance of microfossils in dense vs. porous bands in the Flybye stromatolitic tufa.

Coated grain tufa

Description

Poorly sorted spherical to sub spherical coated grains are found in loosely packed grainstones that are locally exposed in beds up to 10 cm thick and 50 cm long (Fig. 3-10A, B). This coated grain tufa has sharp contacts with stromatolitic and sheet lithotypes, but locally intergrades with coated bubble tufa (Fig. 3-10B). Most coated grains are radial ooids (Pentecost, 2005), 50 μm to 0.8 cm in diameter, that consist of a nucleus surrounded by concentric layers of radially arranged bladed barite (Fig. 3-10C, D). Nuclei, $\leq 40 \mu\text{m}$ wide, include organic material, microdetrital tufa clasts and allochthonous lithoclasts. Laminae bladed cements display a gradual coarsening of crystal size towards the outer surface of the ooids, giving a saw toothed texture to the exterior of the ooids (Fig. 3-10C, D). Several coated grain tufa samples also contain similar-sized oncoids (Pentecost, 2005) with irregular concentric laminae formed by tiny bladed barite crystals deposited over the undulatory surfaces of bacterial colonies, organic carbon and detrital clay (Fig. 3-10E, F). Locally, oncoids are surrounded by smooth, laminar cements, indicating that the two coated grain types are transitional. Coalescence of both types of coated grains is common, producing multilobate or 'popcorn-shaped' composite grains (Fig. 3-10D, E).

Interpretation

Coated grains have been found in spring deposits of various mineralogies, including pyrite (Ozerova et al., 1971), silica (Jones et al., 2001), and calcite (Ozkul et al., 2002; Sant'Anna et al., 2004). They form in flowing or agitated ponded water where rolling and saltation allow concentric precipitation around a nucleus (Pentecost, 1981; Guo and Riding, 1998; Sant'Anna et al., 2004).

The symmetrical laminations in the Flybye ooids and oncoids is congruent with formation in turbulent spring water (Folk and Chafetz, 1983); however, coalescence of coated grains generally requires that grains settle beside each other, and be cemented together in situ by precipitation of enveloping laminae (Chafetz and Meredith, 1983). The Flybye coated grains probably formed in a dynamic setting, with periods of agitation punctuated by relatively stagnant conditions.

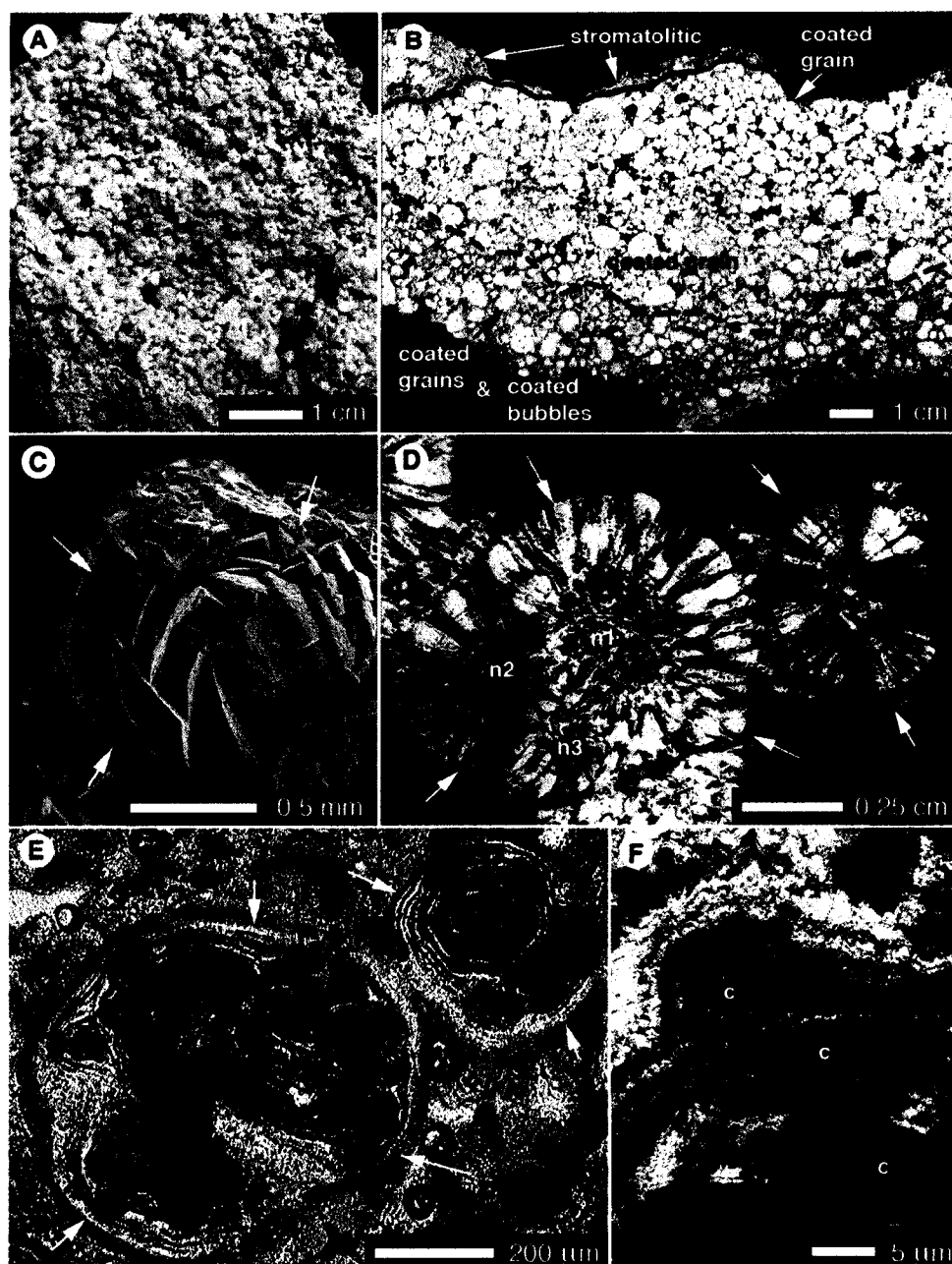


Figure 3-10. Coated grain barite tufa. (A) Coated grains in hand sample. (B) Cut section of coated grain tufa showing sharp upper boundary with stromatolitic tufa (solid line) and gradual lower boundary with bubble tufa (dashed line). (C) SEM image of radial ooid extracted from coated grain tufa. (D) Thin section photograph in crossed polarized light, two radial ooids; left hand ooid is composite, with three primary nuclei (n1, n2, n3). (E) Thin section photograph of oncoids from coated grain tufa; note irregularity of laminations compared to radial ooids in D. (F) Detail of laminations in an oncoid showing envelopment of carbon rich granules (c) by laminar cements.

Radial ooids are generally considered ‘inorganic’ products of rapid, physiochemically

controlled mineral precipitation (Folk et al., 1985). Conversely, oncoids form through organic agency (e.g. by adsorption of reactive ions to an enveloping biofilm) and have irregular laminae and contain organic inclusions (Chafetz and Meredith, 1983; Folk and Lynch, 2001). The Flybye barite ooids probably formed under conditions of high barite supersaturation, at rates that exceeded the ability of biofilms to colonize the outer surface of the grains. These conditions might be met in rapidly oxidizing dysoxic spring water. The oncoids, in contrast, were colonized repeatedly during growth, indicating a slower rate of barite precipitation. Adsorption of barium to grain colonizing biofilms may have been important in inducing precipitation of barite laminae in oncoids formed in spring water that was mostly oxygenated and no longer strongly barite supersaturated (Tazaki and Watanabe, 2004; Glamoclija et al., 2004). The co-occurrence of ooids, oncoids and oncoids with 'ooid-type' outer laminae in some coated grain tufa samples indicates that the conditions for the formation of the two types of grains were met in the same parts of the relict Flybye springs flow path at different times.

Detrital conglomerate tufa

Description

Micro-detrital barite tufa clasts and allochthonous lithoclasts, ≤ 4 cm long, clots of soil, and plant and animal artifacts are cemented together in a grain-supported detrital conglomerate that is common in the Flybye relict tufa mound (Fig 11A, B). Locally, incorporation of clumped animal hair produces a 'spaghetti' texture, which superficially mimics 'streamer' textures observed in the stromatolitic tufa (Fig. 3-11C). This animal hair conglomerate forms by precipitation of tabular barite microcrystals on the outer hair cuticle (Fig. 3-11D), followed by precipitation of engulfing isopachous and/or pendant cements. Most of the animal hair found in detrital conglomerate barite tufa was shed by caribou.

Interpretation

Microdetrital barite tufa is abundant at the modern Flybye Springs, forming a broad fan in the distal flow path. It is generated by erosion of older tufa via animal

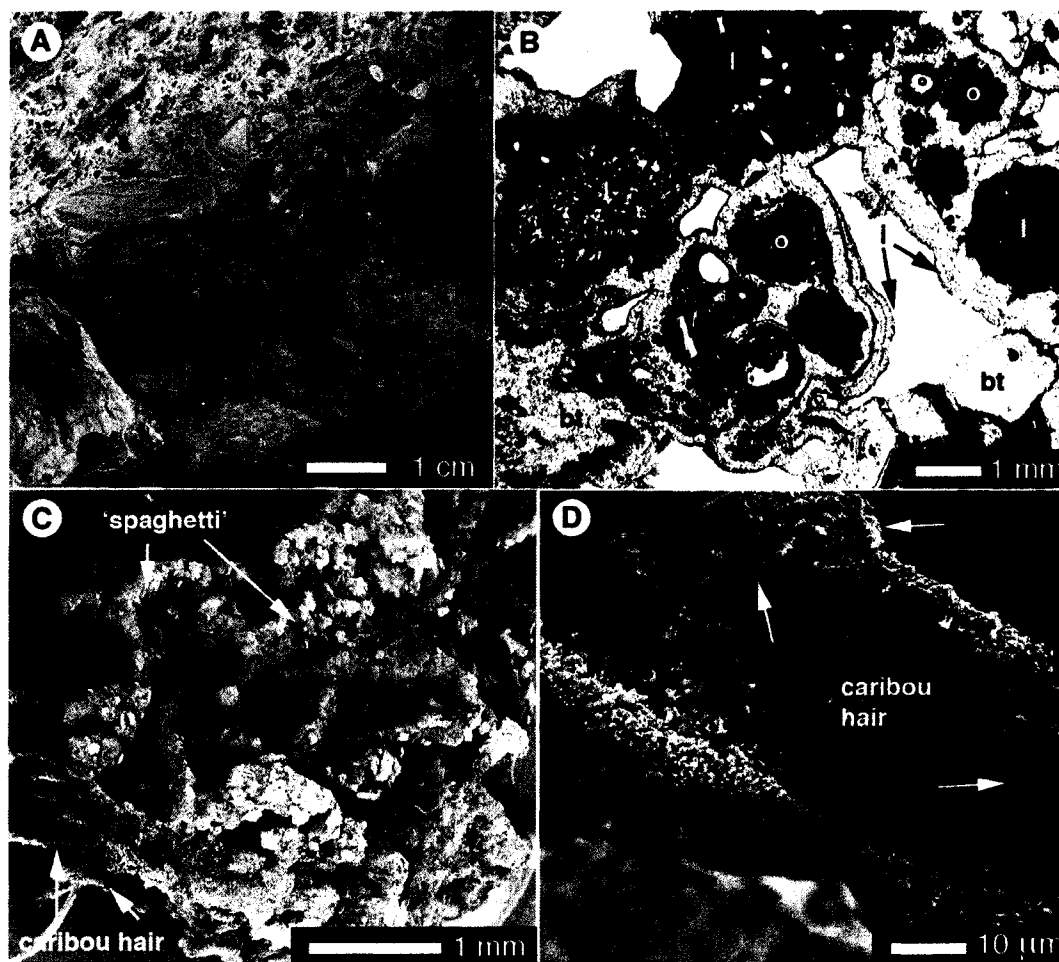


Figure 3-11. Detrital lithoclast barite tufa. (A) Lithotype in hand sample. (B) Thin section photograph of lithotype showing detrital organics (o), allochthonous lithoclasts (l) and microdetrital barite tufa (bt) surrounded by isopachous cements (i). (C) SEM image of 'spaghetti' textured barite formed around caribou hair. (D) Detail of caribou hair extracted from friable barite tufa with partial coating of tabular microcrystalline barite (arrows).

trampling, frost wedging and root wedging. Allochthonous lithic and organic materials are transported into spring flow paths by meteoric run off from a talus cone upslope, and are generated *in situ* by mound colonizing vegetation, visiting animals and erosion of Devonian limestone that crops out at the eastern boundary of the relict tufa mound. Precipitation of isopachous and pendant barite cements by spring water percolating through detrital alluvium consolidated the detrital conglomerate barite tufa lithotype.

Detrital conglomerates are a common component of many spring deposits (e.g. Ozkul et al., 2002; Bonny and Jones, 2003), but the amounts of caribou hair incorporated into the Flybye detrital lithoclast tufa is unusual. Caribou shed their winter hair in clumps that fall into and generate turbulence in shallow tributaries at the modern Flybye Springs, thus accelerating spring water oxidation and inducing barite precipitation (Bonny and Jones, 2007a). Caribou hair tufa records the impact of megafaunal participation in the development of the Flybye relict tufa mound.

Barite Tufa Diagenesis

Young barite tufa is friable and easily weathered; thus, secondary cements are essential for the preservation of textural details in relict barite tufa. Cements occlude permeability, limiting possibilities for dissolution and recrystallization, and transform friable barite tufa to erosion-resistant indurated barite tufa. Isopachous cements composed of bladed barite crystals, 20-130 μm long (Fig. 3-12A), were found in all of the barite tufa samples. Bladed barite is composite in many samples, formed by aggradation of crystallographically uniform, microcrystalline barite plates (Fig. 3-12B). Composite cements, which appear fan-like in side view and chevron-shaped in plan view (Fig. 3-12A, B), commonly have euhedral crystal terminations indicative of phreatic precipitation (Younger, 1986). Growth lines, delineated by inclusions of organic matter and dissolution boundaries, combine with compositional zoning to produce strong banding in isopachous cements (Fig. 3-12A). These bands record a history of episodic cement growth, permitted by percolation of barite supersaturated spring water through tufa pore space.

Isopachous cements are nucleated on 'primary' textural elements, which are constructed, in whole or in part, by platy barite crystals in most tufa lithotypes.

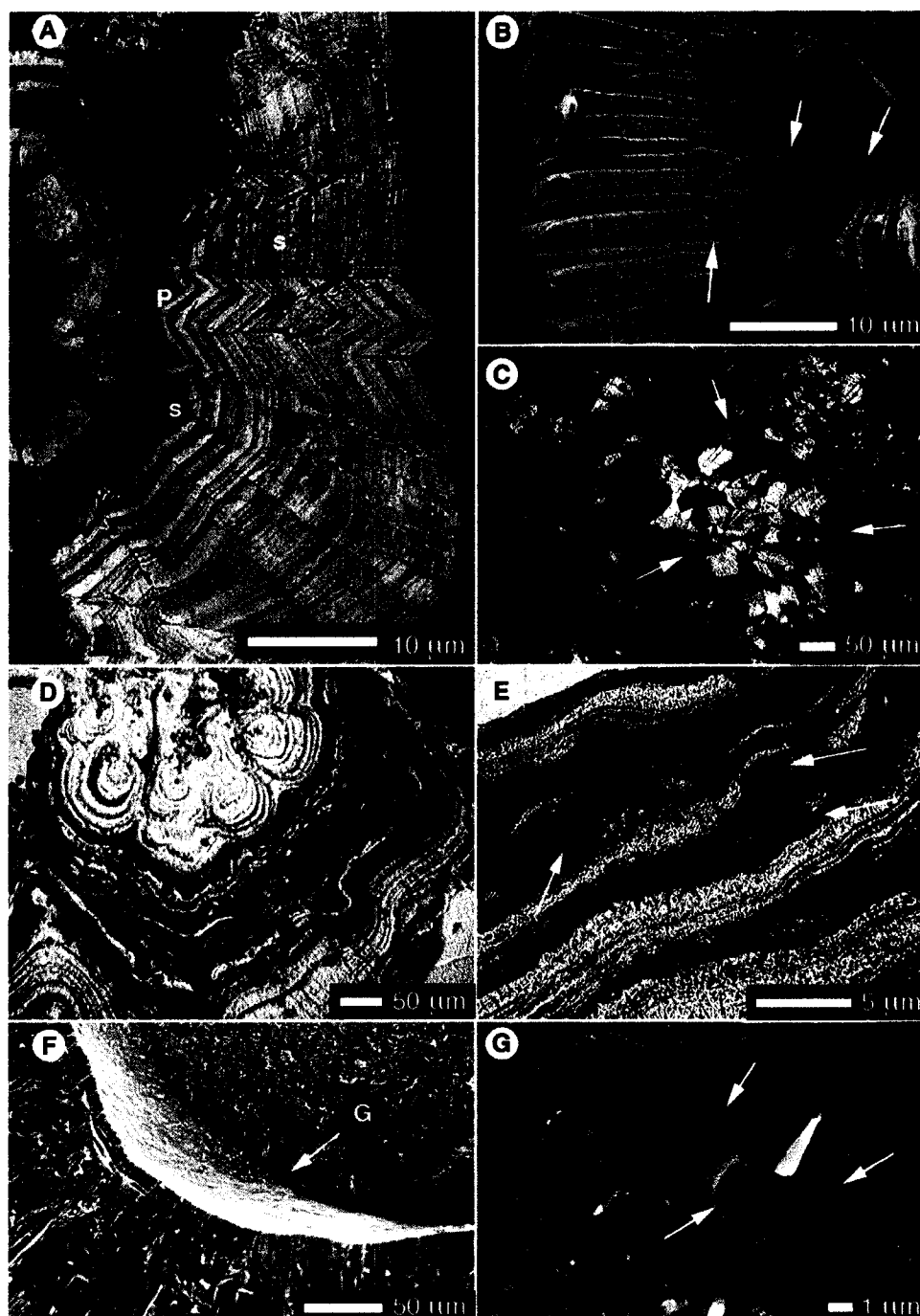


Figure 3-12. Barite tufa cements. (A) Backscattered electron EMP image of bladed isopachous barite crystals in (s) side and (p) plan view. (B) SEM image of composite bladed barite crystals in side view, arrows indicate platy sub crystals. (C) Thin section photograph, crossed polarized light, pore filling mosaic barite cement. (D) Thin section photograph, irregularly layered pendant barite cements. (E) Detail of D showing organic-rich laminae with bacterioform inclusions (arrows). (F) SEM image of pendant cements cleaved along organic-rich lamina. (G) Detail of cleavage surface from F showing casts of unicellular and filamentous microbes (arrows).

Recrystallization of platy barite to coarser, bladed barite crystals is indicated by microtextural distinctions between friable and indurated samples of the raft and stromatolitic tufa lithotypes (Figs. 3-5 and 3-8). It is difficult to distinguish potentially recrystallized primary barite (Figs. 3-5F and 3-8J) from surrounding cements (Figs. 3-5F and 3-8H), as they are crystallographically syntaxial in many samples. This indicates that isopachous cements may develop by extension of recrystallized barite crystal lattices, which would require recrystallization during very early diagenesis. Diagenetic recrystallization of barite is well documented, but poorly constrained (Shikazono, 1994; Radanovic-Guzvica, 1999; Hanor, 2000). In calcite tufas, recrystallization of micrite to sparite (aggrading neomorphism) is commonly accompanied by a reduction in porosity facilitated by delivery of additional carbonate from circulating pore fluids (Love and Chafetz, 1988; Janssen et al., 1999; Freydet and Verrecchia, 1999). The processes of recrystallization and cement deposition are probably contemporaneous.

In addition to isopachous cements, many barite tufa samples contain pore-occluding mosaic cements (Fig. 3-12C) and/or pendant cements with rounded crystal terminations (Fig. 3-12D). Pendant cements have irregular growth banding defined by organic rich laminae that commonly contain bacterioform bodies (Fig. 3-12D, E). Samples cleave readily along these bands, exposing casts of unicellular and filamentous microbes (Fig. 3-12F, G). These organic-rich laminae clearly represent hiatuses in cement precipitation when growth surfaces were colonized by microbial biofilms. Adsorption of barium to biofilms can facilitate barite precipitation (Fagel et al., 1997; Glamoclija et al., 2004), so colonizing microbes may have been important to re-instigating pendant cement growth.

Cements envelop and preserve diverse detrital artifacts in the Flybye barite tufa, including pockets of soil, clay, elemental sulphur, volcanic ash, plant pollen, insect skin and setae, and casts and molds of diatom frustules (Fig. 3-13). This indicates that they precipitate from aerially-exposed spring or meteoric water, which has opportunity to entrain surficial and wind-blown detritus before percolating through pre-deposited tufa.

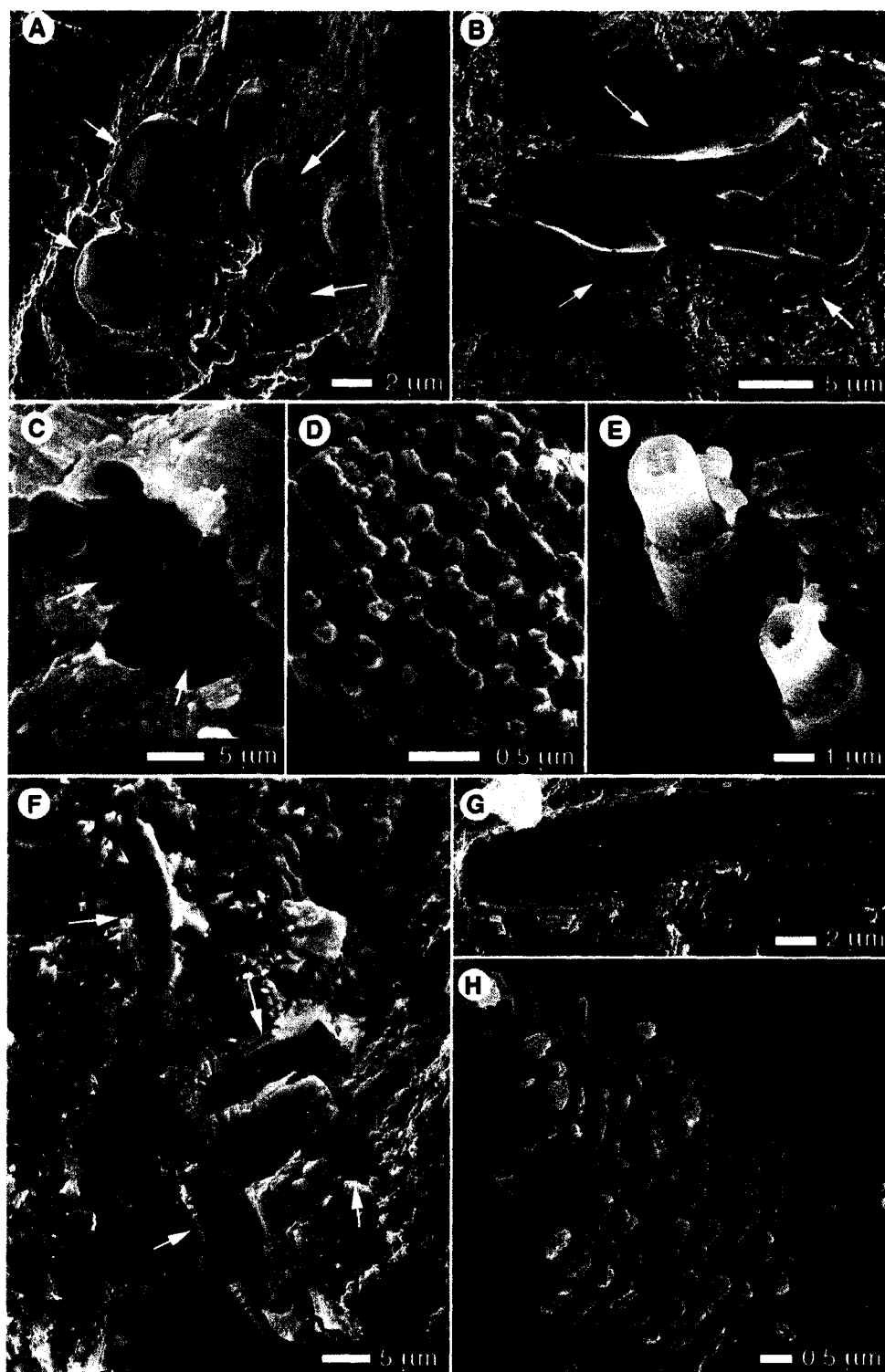


Figure 3-13. SEM images of artifacts preserved in barite tufa cements. (A) Elemental sulphur globules. (B) Volcanic ash. (C) Plant pollen. (D) Cast of snow mite skin and (E) preserved setae. (F) Diatom molds with partially preserved silica (arrows). (G) External and (H) internal casts of diatom frustules that preserve silica biopatterns.

Discussion

The spring system that formed the relict barite tufa mound at Flybye Springs was physiochemically and biologically complex. Distinct depositional niches defined by physiochemical and biologic parameters were arranged in close proximity and yielded six distinct barite tufa lithotypes (Fig. 3-14A). Reorganization of these niches by animal trampling, surges in spring water volume during spring snowmelt, and auto-cyclic rerouting of spring flow paths produced the rapid lithotype alternations observed in the relict barite tufa mound (van Everdingen, 1972; Guo and Riding, 2002).

In gross morphology, the Flybye relict tufa mound conforms to the morphology of Ford and Pedley's (1996) and Pentecost's (2005) 'perched spring line' carbonate tufa model, with the notable exception that it lacks prograding terraces. The maximum height attainable for perched tufa mounds is determined by the hydrostatic head of the aquifer, and low relief mounds like that at Flybye Springs typically form around low pressure artesian spring systems (Pentecost, 2005). In carbonate spring systems, mound morphology is also correlated to spring water temperature: hot springs degas CO₂ rapidly, resulting in rapid 'inorganic' carbonate precipitation localized proximal to the vent, whereas warm and cool spring waters degas more slowly, and typically precipitate carbonate in mid to distal spring flow paths colonized by microbial mats and/or macrophytes (Ford and Pedley, 1996; Guo and Riding, 1998). Carbonate spring mounds also develop rim-pools, and smaller scale terraces, as a result of rapid inorganic calcite precipitation at points of turbulence that promote CO₂ degassing (Pentecost, 2005). Spring mound morphology and the presence or absence of specific biogenic textures are commonly used to infer the physiochemical conditions under which relict carbonate tufa and travertine formed (e.g. Andrews et al., 1997; Bonny and Jones, 2003).

By direct comparison to carbonate systems, relict barite tufa at Flybye Springs, localized close to spring orifices and lacking macrophytic textures, might be interpreted as a thermal spring deposit. The modern Flybye Springs emerge at only 8.5°C in the summer, however, and are likely cooler in winter and spring when snowmelt is introduced into the shallow aquifer (van Everdingen, 1972). Barite saturation is also inversely related to the partial pressure of CO₂ in solution (due to low pH in CO₂-saturated solutions, which places limits the concentration of deprotonated SO₄²⁻ available

| # | Tufa lithotypes | XXX | Spring Biology |
|---|-------------------------------|-----|---|
| | Barite & carbonate | | |
| 1 | raft | SOB | filamentous sulphur oxidising bacteria |
| 2 | coated bubble | OSC | <i>Oscillatoria</i> (sulphur-tolerant filamentous cyanobacteria) |
| 3 | oid | FM | filamentous microbes |
| 4 | oncoïd | MM | mat-forming microbes |
| 5 | stromatolite | SRB | sulphate reducing bacteria |
| 6 | lithoclast | BRY | bryophytes |
| | Barite | MAC | macrophytes |
| | 7 sheet | | |
| | Carbonate | | |
| | 8 crystalline crust | | |
| | 9 bryophyte | | |
| | 10 plant fossils | | |

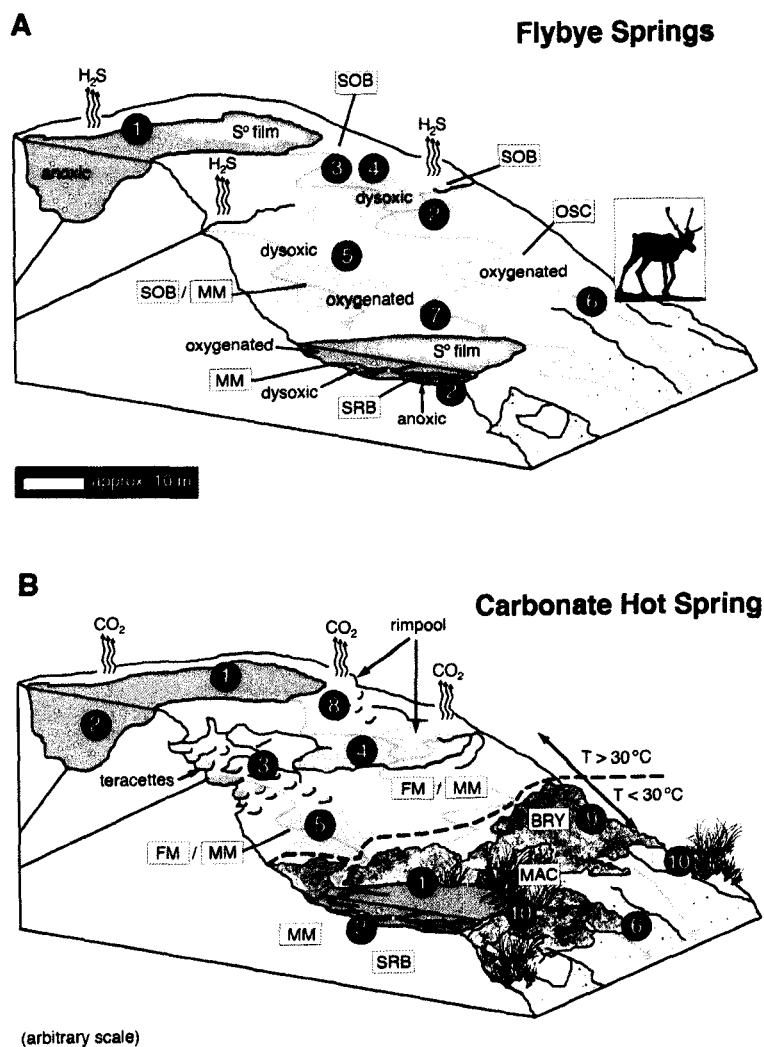


Figure 3-14. Comparison of barite and carbonate spring systems. (A) Idealized schematic diagram showing **depositional niches** in the Flybye Springs flow path and associated barite tufa lithotypes. (B) Depositional niches and associated carbonate tufa lithotypes on a carbonate spring mound (compiled after Pentecost, 2005).

for reaction with barium - Lindgren, 1933; Arenas, 2000). This effect, however, is greatly overshadowed by the influence of sulphur redox chemistry. In anoxic waters, barium is highly soluble; in oxygenated, sulphate-bearing waters, barite is the least soluble sulphate salt (Hanor, 2000). At the modern Flybye Spring vents, partial oxidation of anoxic spring water results in spontaneous precipitation of microcrystalline barite in proximal flow paths. 8 m downstream, Flybye spring waters are fully oxygenated and barite precipitation is achieved by bioaccumulation of barium in microbial cells and EPS. Beyond 20 m, barite is not precipitated (Bonny and Jones, 2007a). Oxidation control of barite saturation, thus, readily explains the restricted extent of the Flybye relict tufa. Rapid oxidation of spring water at points of turbulence can initiate barite precipitation (Sanders, 1998; Bonny and Jones, 2007a), so rimpool-type structures could, hypothetically, develop on a barite spring mound. Mechanical stress imposed by caribou hooves may have precluded their development at Flybye Springs (Emig, 1917).

The Flybye tufa lithotypes are also most compatible with those formed by thermal carbonate spring systems (Fig. 3-14A, B). Cold carbonate spring deposits generally contain bryophyte tufas and abundant plant fossils (Ford and Pedley, 1996). The absence of these typical cold water tufa lithotypes in the Flybye relict tufa mound is attributable to the sulphur-rich chemistry of the Flybye springs. High levels of dissolved sulphur inhibit the growth of macrophytes and photosynthetic microbes and promote the growth of sulphur-tolerant microbes (Castenholz, 1976; Douglas and Douglas, 2001; Elshahed et al., 2003). In carbonate spring systems, stromatolites are generally restricted to temperatures $\geq 30^{\circ}\text{C}$, where growth of macrophytes is inhibited. At the Flybye Springs, high levels of dissolved sulphide permitted development of stromatolitic fabrics in spring water emerging at ambient temperature. Coated bubble, undulatory sheet, raft and radial ooid coated grain lithotypes are also more typical of thermal carbonate spring deposits (Pentecost, 2005).

The remarkable similarity of Flybye relict barite tufa to carbonate spring deposits demonstrates that similar facies can form in systems with divergent chemistry, precipitate mineralogy, and resident biology. However, the different controls on carbonate and sulphate solubility produce interpretive discrepancies that must be considered when comparing textures across mineralogy. Coated bubbles and rafts, for example, are

commonly found together in carbonate tufa and travertine, and provide joint evidence for low turbulence conditions in CO₂-rich spring water (Ozkul et al., 2002; Taylor et al., 2004). In carbonate systems, rafts and bubbles are found in vent pools, but are also found in tributary fed pools and flow path eddies (Carthew et al., 2006). At Flybye Springs, barite rafts probably formed in anoxic spring fed ponds, whereas coated bubbles formed in ambiently barite-saturated, dysoxic or oxygenated water (Fig. 3-14). The two lithotypes were not found together in the relict barite tufa. A second example is found in coated grains. In carbonate systems, radial ooids form where rates of degassing, and hence calcite precipitation, are high, whereas oncoids form where slower rates of precipitation permit the growth of biofilms on cortical laminae (Pentecost, 2005). Thus, ooids are commonly taken to indicate high turbulence depositional environments, and oncoids more stagnant conditions (Folk and Chafetz, 1983). At Flybye Springs, ooid and oncoid formation were probably similarly controlled by rates of barite precipitation, but this would not be determined by CO₂ degassing. Barite precipitation rates are directly related to the oxygenation state of the precipitating solution (Shikazono, 1994), thus the co-occurrence of ooids and oncoids in the Flybye relict barite tufa suggests that they formed in a common depositional niche that experienced variations in dissolved oxygen concentrations.

Percolation of cement-precipitating spring water through detrital tufa and allochthonous grains generates conglomerate lithotypes in many carbonate spring mounds. Branches, leaves and plant stems are also cemented by calcite or aragonite, and preserved as fossil molds and casts in carbonate tufa and travertine mounds (Pentecost, 2005). At the barite-precipitating warm Zodletone Springs in Oklahoma, rapid atmospheric and bacterial oxidation of barium and sulphur-rich water produces isopachous barite coatings on plants, branches and insects that fall into the spring flow path (Younger, 1986; Senko et al., 2004). The Flybye Spring mound is vegetated, but plant and leaf fossils were not found in the relict barite tufa. This may indicate that the relict spring mound was inundated by sulphur-rich water, and therefore not vegetated during its development, or that macrophytic detritus introduced to the flow path failed to be preserved.

At the modern Flybye Springs, plant detritus remains largely unmineralised in spring water tributaries and pools. This may be explained by the limited window of spontaneous barite precipitation and colonization of organic detritus by sulphate reducing bacteria (SRB). At Zodletone Springs, rapid barite precipitation engulfs organic detritus before it reaches an advanced state of decay (Younger, 1986). Slow rates of barite precipitation in dysoxic spring water tributaries at the modern Flybye Springs permit colonization of organic detritus by *Chromatium* and SRB (Bonny and Jones, 2007a). In carbonate spring systems, calcite precipitation can proceed under anoxic conditions around degrading organics and may, in fact, be promoted by bacterial sulphate reduction (Castanier et al., 2000). SRB-established anoxia inhibits barite precipitation, and likely precludes preservation of leaves and branches in barite tufa if precipitation rates are low. Early barite precipitates may also be subject to preservation biases. The low solubility of barite might protect early precipitates from dissolution if they were transported into anoxic ponds, but they would be unlikely to experience further cementation. Lithotypes generated in or transported into the path of dysoxic or oxygenated spring water would have the highest potential of being indurated by secondary cements and preserved in barite tufa. By default, the coated bubble, raft, undulatory sheet, stromatolitic and coated grain tufa lithotypes may be understood as the lithotypes most likely to persist through lithification.

One of the most important findings from the Flybye Springs barite tufa deposit is that biogenic textures can be preserved in sedimentary barite. At most barite-precipitating hot springs, the combined effects of spring water oxidation and cooling drive rapid precipitation of crystalline barite travertine (Suganuma, 1928; Sasaki and Minato, 1982; Younger, 1986). At Flybye Springs, ambient temperature spring water underwent less rapid physiochemical change, permitting the development of texturally complex precipitates. Proximal to spring vents, barite supersaturation achieved by oxidation of dissolved sulphide produced 'inorganic' thin barite rafts and radial ooids. In dysoxic and oxygenated spring water, barite precipitates were localized around gas bubbles trapped in EPS, EPS-rich colloidal sulphur films and microbial cells. Thus, the coated bubble, oncoid, undulatory sheet and stromatolitic barite lithotypes record textural microbial-

mediation of barite precipitation. Microfossils provide conclusive evidence for the involvement of microbes in the formation of the stromatolitic lithotype.

Preservation of microbial casts, moulds and permineralised extracellular sheaths is common in cool and warm carbonate spring deposits, but rare in the crystalline deposits that form in water $> 70\text{ }^{\circ}\text{C}$ (Bonny and Jones, 2003 vs. Jones and Renaut, 1996).

Crystalline hot spring barites also lack fossils (Suganuma, 1928; Sasaki and Minato, 1982), but the Flybye Springs preserved microfossils in tufa that most likely precipitated at $< 10\text{ }^{\circ}\text{C}$. In the modern flow paths, microbes mediate barite saturation gradients by adsorbing barium to their external surfaces and EPS and/or accumulating barium intracellularly (Bonny and Jones, 2007a). Reaction of this bioaccumulated barium with spring water sulphate produces encrustations around diverse microbial cells and drives intracellular barite precipitation in filaments of *Beggiatoa* and *Thiothrix*. Due to slow rates of precipitation at the modern springs, this biomineralised barite is released from degrading biomass as 'detrital microfossils' that are entrained in the modern spring flow paths (Bonny and Jones, 2007a). Detrital microfossils were not identified in the Flybye relict barite tufa, which indicates that microfossils in the relict spring system were not as easily dispersed. Higher volumes of spring water flow in the relict system probably allowed sequestration of microbial cells by more rapid barite precipitation, ultimately generating the stromatolitic tufa lithotype.

Preservation of biogenic textures and microfossils through early diagenetic recrystallization in the Flybye barite tufa yields the possibility that similar biomarkers may survive in the geologic record. Biogenic textures persist in Quaternary carbonate tufas and travertines (Andrews, 2006), and are identifiable in carbonate travertines from the Paleocene (Sant'Anna et al., 2004) through to the Jurassic (Richardson et al., 2004). Barite is highly insoluble and stable during diagenesis if sequestered from anoxic solutions (Karnachuk et al., 2002), but microcrystalline barite is prone to early aggradational recrystallization (Shikazono, 1994), and recrystallization to equigranular textures can follow at burial pressures (Hanor, 2000). As a result, barite is generally not considered a likely host for evidence of life through geologic time. Gross depositional textures can be preserved through barite diagenesis, however, as demonstrated by

putative barite stromatolites in Archaean and Paleozoic sequences (Buick *et al.*, 1981; Carroue, 1996).

Barite forms in diverse microbially colonized environments (Palinkas *et al.*, 1993; Aharon, 2000; Burhan *et al.*, 2002; Torres *et al.*, 2003; Canet *et al.*, 2005; Riedinger *et al.*, 2006), and is abundant through Earth's chemical sedimentary record, first appearing in bedded stratiform deposits in the Archean (Jewell, 2000; Huston and Logan, 2004) and interbedded with Neoproterozoic carbonates (Jiang *et al.*, 2006), and becoming increasingly important in the Paleozoic when the basin-scale stratiform barites of the Yukon Territory, Alaska, Nevada, Arkansas, Mexico, and South China were formed (Cecile, 2000; Hanor, 2000; Torres *et al.*, 2003). Smaller, metre-scale lenses of barite deposited around localized hydrothermal and gas hydrate seeps are also common in Paleozoic-Recent marine siliclastics (Maynard and Okita, 1991; Hanor, 2000; Jewell, 2000; Torres *et al.*, 2003). It seems likely that the barite sedimentary record contains biomarkers that have yet to be recognized.

For example, Fu *et al.* (1994) described string-like structures in a Holocene barite chimney that formed around a cold marine hydrocarbon seep. Composed of radially arranged barite microcrystals with distinct cores delineated by traces of organic carbon, barite-replaced coccolith tests, cryptocrystalline barite and bands of microporosity, these structures are described as 'dendritic' because they abut one another and coalesce to form wider diameter structures with dendrite-like composite textures (Fu *et al.*, 1994). Their structural similarity to microfossil-cored barite strings in stromatolitic Flybye barite tufa suggests that these 'dendrites' may also have formed by barite precipitation around microbial filaments. Similar radial barite strings have also been described from Late Cretaceous bedded marine barites in Israel (Bogoch and Shirav, 1978).

Many large stratiform barite deposits that were initially interpreted as having high-temperature exhalative origins have been reassessed as cold methane seep deposits (Jewell, 2000; Torres *et al.*, 2003; Huston and Logan, 2004), and some contain organic carbon of biogenic origin (Sanders, 1998; Burhan *et al.*, 2002). Barite solubility at modern submarine cold seeps is commonly mediated by methanogenic and/or sulphur metabolizing bacterial communities (Larkin and Henk, 1996; Riedinger *et al.*, 2006), which raises the exciting possibility that cold seep Paleozoic and Precambrian barite may

contain an untapped palaeoecological record (Sanders, 1998). The kinetics of sulphate mineral formation and sequestration in sediments are pivotal in determining ocean chemistry (Bottrell and Raiswell, 2000), thus, a potential role of microbes in the formation of large-scale sulphate deposits may call for reassessment of current models of barium cycling, which are based on the thermodynamics of abiotic chemical systems (Hanor, 2000).

Conclusions

Relict barite tufa at Flybye Springs formed from a spring system with higher volumes of flow and rates of barite precipitation than exist at the site today. The relict tufa contains six lithotypes formed in distinct physiochemical and biological niches on the relict spring mound:

- Raft tufa and ooids in coated grain barite tufa formed via 'inorganic' barite precipitation where rapid oxidation of sulphide to sulphate established high levels of barite supersaturation.
- Undulatory sheet tufa may have formed by reaction of dissolved barium with sulphate derived from spontaneous oxidation of EPS-rich colloidal sulphur films floating in quiescent pools.
- Coated bubble tufa, stromatolitic barite tufa with filamentous microfossils, and oncoids in coated grain tufa formed in close association with microbes inhabiting dysoxic to oxygenated spring water tributaries and ponds and are considered 'biogenic' lithotypes.
- Detrital conglomerate tufa formed by cementation of microdetrital barite tufa, allochthonous lithoclasts and organic detritus, including caribou hair.

Although unprecedented in barite, these lithotypes are common in carbonate tufas and travertines; this similarity emphasizes the importance of physical and hydrological parameters, rather than specific biological or chemical/mineralogical processes, in determining the texture of chemical sediments. Nonetheless, microbes growing in the Flybye Springs flow path acted as substrates for, and may have locally catalyzed, barite precipitation. Inorganic and biogenic lithotypes, microfossils and organic artifacts in the Flybye relict barite have survived early diagenetic aggradational recrystallization and

deposition of secondary isopachous, mosaic and pendant cements. They are considered to have long-term preservation potential.

References

- Aharon, P. 2000. Microbial processes and products fueled by hydrocarbons at submarine seeps. In: Riding, R., Awramik, S.M. (Eds.), *Microbial Sediments*, Springer-Verlag: Heidelberg Germany, pp. 270-281.
- Aloisi, G., Wallmann, K., Bollwerk, S.M., Derkachev, A., Bohrmann, G. and Suess, E. 2004. The effect of dissolved barium on biogeochemical processes at cold seeps. *Geochimica et Cosmochimica Acta*, 63: 1735-1748.
- Andrews, J.E. 2006. Palaeoclimatic records from stable isotopes in riverine tufas: synthesis and review. *Earth-Science Reviews*, 75: 85-104.
- Andrews, J.E., and Brasier, A.T. 2005. Seasonal records of climatic change in annually laminated tufas: short review and future prospects. *Journal of Quaternary Science*, 20: 411-421.
- Andrews, J.E., Riding, R. and Dennis, P.F. 1997. The stable isotope record of environmental and climatic signals in modern terrestrial microbial carbonates from Europe. *Palaeogeography, Palaeoclimatology, Palaeoecology*, 129: 171-189.
- Arenas, C., Gutierrez, F., Osacar, C. and Sancho, C. 2000. Sedimentology and geochemistry of fluvio-lacustrine tufa deposits controlled by evaporite solution subsidence in the central Ebro Depression, NE Spain. *Sedimentology*, 47: 883-909.
- Arp, G. Theil, V., Reimer, A. Michaelis, W. and Reitner, J. 1999. Biofilm exopolymers control microbialite formation at thermal springs discharging into the alkaline Pyramid Lake, Nevada, USA. *Sedimentary Geology*, 126: 159-176.
- Awramik, S.M., Margulis, L. and Barghoorn, E.S. 1976. Evolutionary processes in the formation of stromatolites. In: Walter, M.R. (Ed.), *Stromatolites*, *Developments in Sedimentology*, 20: 149-162.
- Banerjee, N.R. and Muehlenbachs, K. 2003. Tuff life: Bioalteration in volcanoclastic rocks from the Ontong Java Plateau. *Geochemistry, Geophysics, Geosystems*, 4: 1037, doi:10.1029/2002GC000470.
- Bogoch, R. and Shirav, M. 1978. Petrogenesis of a Senonian barite deposit, Jean Desert, Israel. *Mineralium Deposita*, 13: 383-390.
- Bonny, S. and Jones, B. 2003. Relict tufa at Miette Hot Springs, Jasper National Park, Alberta, Canada. *Canadian Journal of Earth Sciences*, 40: 1459-1481.
- Bonny, S. and Jones, B. 2007a. Barite (BaSO₄) biomineralisation at Flybye Springs, a cold sulphur spring system in Canada's Northwest Territories. *Canadian Journal of Earth Sciences*, 44: 835-856.
- Bonny, S. and Jones, B. 2007b. Diatom-mediated barite precipitation in microbial mats calcifying at Stinking Springs, a warm sulphur spring system in Northwester Utah, USA. *Sedimentary Geology*, 194: 223-244.
- Bottrell, S.H. and Raiswell, R. 2000. Sulphur isotopes and microbial sulphur cycling in sediments. In: Riding, R., Awramik, S.M. (Eds.), *Microbial Sediments*, Springer-Verlag: Heidelberg Germany, pp. 96-104.

- Bove, D. and Felmlee, J.K. 1982. Mineralogy and autoradiography of selected mineral-spring precipitates in the western United States. US Geological Survey, Open-file Report 82-792, 74 pp.
- Brigmon, R.L., Martin, H.W., Morris, T.L., Bitton, G. and Zam, S.G. 1994. Biogeochemical ecology of *Thiothrix* spp. in underwater limestone caves. *Geomicrobiology Journal*, 12: 141-159.
- Buick, R., Dunlop, J.S.R. and Grooves, D.I. 1981. Stromatolite recognition in ancient rocks: an appraisal of irregularly laminated structures in an Early Archaean chert-barite unit from North Pole, Western Australia. *Alcheringa*, 5: 161-181.
- Burhan, R.Y.P., Trendel, J.M., Adam, P., Wehrung, P., Albrecht, P. and Nissenbaum, A. 2002. Fossil bacterial ecosystem at methane seeps; origin of organic matter from Be'eri sulfur deposit, Israel. *Geochimica et Cosmochimica Acta*, 66: 4085-4101.
- Canet, C., Prol-Ledesma, R.M., Torres-Alvarado, I., Gilg, H.A., Villanueva, R.E. and Cruz, R. L-S. 2005. Silica-carbonate stromatolites related to coastal hydrothermal venting in Baia Concepcion, Baja California Sur, Mexico. *Sedimentary Geology*, 174: 97-113.
- Cadigan, R.A. and Felmlee, J.K. 1977. Radioactive springs geochemical data related to uranium exploration. *Journal of Geochemical Exploration*, 8: 381-395.
- Carroue, J-P. 1996. Une presentation originale de la barytine ou des stromatolithes de poids. *Minereaux et Fossiles*, 246: 21-22.
- Carthew, K.D., Taylor, M.P. and Drysdale, R.N. 2006. An environmental model of fluvial tufas in the monsoonal tropics, Barkly karst, northern Australia. *Geomorphology*, 73: 78-100.
- Castanier, S. Le Metayer-Levrel, G. and Perthuisot, J-P. 2000. Bacterial roles in the precipitation of carbonate minerals. In: Riding, R., Awramik, S.M. (Eds.), *Microbial Sediments*, Springer-Verlag: Heidelberg Germany, pp. 32-39.
- Castenholz, R.W. 1976. The effect of sulfide on the blue green algae of hot springs. I. New Zealand and Iceland. *Journal of Phycology*, 12: 54-68.
- Cecile, M.P., Goodfellow, W.D., Jones, L.D., Krouse, H.R. and Shakur, M.A. 1984. Origin of radioactive barite sinter, Flyby Springs, Northwest Territories, Canada. *Canadian Journal of Earth Sciences*, 21: 383-395.
- Cecile, M.P. 2000. Geology of the Northeastern Nidderly Lake Map Area, East-central Yukon and adjacent Northwest Territories. *Geological Survey of Canada Bulletin 553*, 120 pp.
- Chafetz, H.S. and Meredith, J.C. 1983. Recent travertine pisoliths (pisoids) from Southeastern Idaho, USA. In: Peryt, T.M. (Ed.) *Coated Grains*, Springer-Verlag, Heidelberg, pp. 450-455.
- Chafetz, H.S. and Folk, R.L. 1984. Travertines: Depositional morphology and the bacterially constructed constituents. *Journal of Sedimentary Petrology*, 54: 289-316.
- Chafetz, H.S., Rush, P.F. and Utech, N.M. 1991. Microenvironmental controls on mineralogy and habit of CaCO_3 precipitates: an example from an active travertine system. *Sedimentology*, 38: 107-126.
- Clowes, F. 1889. Deposits of barium sulphate from mine-water. *Proceedings of the Royal Society of London*, 46: 368-369.

- Craig, S. and Bloch, R.L. 1981. Radioactive springs in the watershed of a proposed reservoir in Sequoyah County, Oklahoma; origin and environmental effect. *Geology*, 9: 195-199.
- Das, S. and Mohanti, M. 1997. Holocene microbial tufas: Orissa state, India. *Carbonates and Evaporites*, 12: 204-219.
- Douglas, S. and Douglas, D.D. 2001. Structural and geomicrobiological characteristics of a microbial community from a cold sulfide spring. *Geomicrobiology Journal*, 18: 201-422.
- Drysdale, R.N., Taylor, M.O. and Ihlenfeld, C. 2003. Factors controlling the chemical evolution of travertine-depositing rivers of the Barkly karst, northern Australia. *Hydrological Processes*, 16: 2941-2962.
- Elshahed, M.S., Senko, J.M., Dewers, T.A., Spear, J.R., Najjar, F.Z., Kenton, S.M., Roe, B.A. and Krumholz, L.R. 2003. Bacterial diversity and sulfur cycling in a mesophilic sulfide-rich spring. *Applied Environmental Microbiology*, 69: 5609-5621.
- Emig, W.H. 1917. Travertine deposits of Oklahoma. *Oklahoma Geol. Surv. Bull.*, 76 pp.
- Fagel, N., Andre, L. and Debrabant, P. 1997. Multiple seawater-derived geochemical signatures in Indian oceanic pelagic clays. *Geochimica et Cosmochimica Acta*, 61: 989-1008.
- Folk, R.L. and Chafetz, H.S. 1983. Pisoliths (pisoids) in Quaternary travertines of Tivoli, Italy. In: Peryt, T.M. (Ed.) *Coated Grains*. Springer-Verlag, Heidelberg, pp. 474-487.
- Folk, R.L., Chafetz, H.S. and Tiezzi, P.A. 1985. Bizarre Forms of depositional and diagenetic calcite in Hot-spring travertines, central Italy. In: Schneidermann, N. and Harris, P.M. (Eds.) *Carbonate Cements*, SEPM Special Publication, 36: 349-369.
- Folk, R.L. and Lynch, F.L. 2001. Organic matter, putative nannobacteria and the formation of ooids and hardgrounds. *Sedimentology*, 48: 215-229
- Ford, T.D. and Pedley, H.M. 1996. A review of tufa and travertine deposits of the world. *Earth-Science Reviews*, 41: 117-175.
- Fu, B., Aharon, P., Byerly, G.R. and Roberts, H.H. 1994. Barite chimneys on the Gulf of Mexico slope; initial report of their petrography and geochemistry. *Geo-Marine Letters*, 14: 81-87.
- Freytet, P. and Verrecchia, E.P. 1999. Calcitic radial palisadic fabric in freshwater stromatolites: diagenetic and recrystallized feature or physicochemical sinter crust? *Sedimentary Geology*, 126: 97-102.
- Gaoudie, A.S. and Viles, H.A. 1990. Tufas, travertines, and allied carbonate deposits. *Progress in Physical Geography*, 14: 19-41.
- Glamoclija, M., Garrel, L., Berthon, J. and Lopez-Garcia, P. 2004. Biosignatures and bacteria diversity in hydrothermal deposits of Solfatara Crater, Italy. *Geomicrobiology Journal*, 21: 529-541.
- Guo, L. and Riding, R. 1998. Hot-spring travertine facies and sequences, Late Pleistocene, Rapolan Terme, Italy. *Sedimentology*, 45: 163-180.
- Guo, L. and Riding, R. 2002. Rapid facies changes in Holocene fissure ridge hot spring travertines, Rapolano Terme, Italy. *Sedimentology*, 46: 1145-1158.

- Hannington, M.S. and Scott, S.D. 1988. Mineralogy and geochemistry of a hydrothermal silica sulfide sulfate spire in the Caldera of axial seamount, Juan-de-Fuca Ridge. *Canadian Mineralogist*, 26: 603-625.
- Hanor, J.S. 2000. Barite-celestine geochemistry and environments of formation. *Reviews in Mineralogy and Geochemistry*, 40: 193-275.
- Huston, D.L. and Logan, G.A. 2004/ Barite, BIFs and bugs: evidence for the evolution of the Earth's early hydrosphere. *Earth and Planetary Science Letters*, 220: 41-55.
- Irion, G. and Muller, G. 1968. Mineralogy, petrology and chemical composition of some calcareous tufa from Schwabische Alb, Germany. In: Muller, G. and Friedman, G.M. (Eds.) *Recent Developments in Carbonate Sedimentology in Central Europe*, Springer-Verlag, New York, pp. 157-171.
- Janssen, A., Swennen, R., Podoor, N. and Keppens, E. 1999. Biological and diagenetic influence in recent and fossil tufa deposits from Belgium. *Sedimentary Geology*, 126: 75-95.
- Jewell, P.W. 2000. Bedded barite in the geologic record. *SEPM Special Publication*, 66: 147-161.
- Jiang, G.Q., Kennedy, M.J., Christie-Blick, N., Wu, H.C. and Zhang, S.H. 2006. Stratigraphy, sedimentary structures, and textures of the late neoproterozoic doushantuo cap carbonate in south Chian. *Journal of Sedimentary Research*, 76: 978-995.
- Jones, B. 1989. Calcite rafts, peloids, and micrite in cave deposits from Cayman Brac, British West Indies. *Canadian Journal of Earth Sciences*, 26: 654-664.
- Jones, B. and Renaut, R.W. 1996. Morphology and growth of aragonite crystals in hot spring travertines at Lake Bogoria, Kenya Rift Valley. *Sedimentology*, 43: 323-340.
- Jones, B., Renaut, R.W. and Rosen, M.R. 1998. Microbial biofacies in hot-spring sinters: a model based on Ohaaki Pool, North Island, New Zealand. *Journal of Sedimentary Research*, 68: 413-434.
- Jones, B., Renaut, R.W. and Rosen, M.R. 2001. Microbial construction of siliceous stalactites at geysers and hot springs: examples from the Whakarewarewa Geothermal area, North Island, New Zealand. *Palaios*, 14: 73-94.
- Kam, S.I. and Rosen, W.R. 1999. Anomalous capillary pressure, stress, and stability of solids-coated bubbles. *Journal of Colloid Interface Sciences*, 213: 329-339.
- Kano, A. and Fugii, H. 2000. Origin of the gross morphology and internal texture of tufas of Shirokawa Town, Ehime Prefecture, southwest Japan. *Journal of the Geological Society of Japan*, 106: 397-412.
- Kano, A., Matsuoka, J., Kojo, T. and Fujii, H. 2004. Origin of annual laminations in tufa deposits, southwest Japan. *Palaeogeography Palaeoclimatology Palaeoecology*, 91: 243-262.
- Karnachuk, O.V., Kurochkina, S.Y. and Tuovinen, O.H. 2002. Growth of sulfate-reducing bacteria with solid-phase electron acceptors. *Applied Microbiology and Biotechnology*, 58: 482-486.
- Konhauser, K.O. 1997. Bacterial iron biomineralisation in nature. *FEMS Microbiology Reviews*., 20: 315-326.

- Konhauser, K.O., Jones, B., Reysenbach, A-L., and Renaut, R.W. 2003 Hot spring sinters; keys to understanding Earth's earliest life forms. *Canadian Journal of Earth Sciences*, 40: 1713-1724.
- Larkin, J.M. and Henk, M.C. 1996. Filamentous sulfide-oxidizing bacteria at hydrocarbon seeps of the Gulf of Mexico. *Microsc. Res. Tech.*, 33, 23-31.
- Lindgren, W. 1933. *Mineral deposits*, 4th edition. McGraw-Hill Publishers, New York, 930 pp.
- Love, K.M. and Chafetz, H.S. 1988. Diagenesis of laminated travertine crusts, Arbuckle Mountains, Oklahoma. *Journal of Sedimentary Petrology*, 58: 441-445.
- Malinin, S.D. and Urusov, V.S. 1984. The experimental and theoretical data on isomorphism in the (Ba, Sr) SO₄ system in relation to barite formation. *Geochemistry International*, 20: 70-80.
- Matsuoka, J., Kano, A., Oba, T., Watanabe, T., Sakai, S. and Seto, K. 2001. Seasonal variation of stable isotopic compositions recorded in a laminated tufa, SW Japan. *Earth and Planetary Science Letters*, 192: 31-44.
- Maynard, J.B., and Okita, P.M. 1991. Bedded barite deposits of the U.S., Canada, Germany, and China: Two major types based on tectonic setting. *Economic Geology*, 86: 364-376.
- Nelson, D.C. 1987. Physiology and biochemistry of filamentous sulfur bacteria. In: Schlegel, H.G. and Bowein, B. (Eds.) *Autotrophic Bacteria*, Science Tech Publishers, Madison, pp. 219-238.
- Orberger, B., Gallien, J-P., Pinti, D.L., Fialin, M., Daudin, L., Grocke, D.R. and Pasava, J. 2005. Nitrogen and carbon partitioning in diagenetic and hydrothermal minerals from Paleozoic Black Shales, (Selwyn Basin, Yukon Territories, Canada). *Chemical Geology*, 218: 249-264.
- Ozkul, M., Varol, B. and Alcicek, M.C. 2002. Depositional environments and petrography of Denizli travertines. *Bulletin of the Mineral Resources and Exploration Institute of Turkey*, 125: 13-29.
- Ozerova, N.A., Naboko, S.I. and Vinogradov, V.I. 1971. Sulphides of mercury, antimony, and arsenic, forming from the active thermal spring of Kamchatka and Kuril Islands. *Journal of the Mineralogy and Geology Society of Japan*, Special Issue 2: 164-171.
- Palinkas, L.A., Pezdeic, J. and Sinkovec, B. 1993. The Lokve Barite Deposit, Croatia: an example of early diagenetic sedimentary ore deposits. *Geologica Croatia*, 46: 97-106.
- Pentecost, A. 1981. The tufa deposits of the Malham District, North Yorkshire. *Field Studies*, 5: 365-387.
- Pentecost, A. and Riding, R. 1986. Calcification in cyanobacteria. In: Leadbeater, B.S.C. and Riding, R. (Eds.) *Biominalisation in Lower Plants and Animals*, Systematics Association Special Publication, 20: 73-90.
- Pentecost, A. 2005. *Travertine*. Springer-Verlag, Heidelberg, 429 pp.
- Radanovic-Guzvica, B. 1999. The average structural density of barite crystals of different habit types. *Geologica Croatia*, 52: 59-65.

- Riedinger, N., Kasten, S., Groger, J., Franke, C. and Pfeifer, K. 2006. Active and buried authigenic barite fronts in sediments from the Eastern Cape Basin. *Earth and Planetary Science Letters*, 241: 876-887.
- Renaut, R.W., Jones, B. and Le Turdu, C. 1999. Calcite lily pads and ledges at Lorusio Hot Springs, Kenya Rift Valley: travertine precipitation at the air-water interface. *Canadian Journal of Earth Sciences*, 36: 649-666.
- Riding, R.E. and Awramik, S.M. 2000. *Microbial Sediments*, Springer-Verlag, Berlin, 331 pp.
- Richardson, J.R., Evans, J.E. and Yacobucci, M.M. 2004. Assessing the preservation potential of biogenic features in pre-Quaternary tufas and travertines - applications to exobiology. *Geological Society of America, Abstracts with Programs*, 36, p. 474.
- Sanchez-Moral, S., Luque, L. and Canaveras, J.C. 2004. Bioinduced barium precipitation in St. Callixtus and Domitilla catacombs. *Annals of Microbiology*, 54: 1-12.
- Sanders, W.E. 1998. Rate and Mechanism of Barite Mineralisation at Zodletone Mountain, Southwestern Oklahoma. Unpublished M.Sc. Thesis, University of Oklahoma, Norman, 150 pp.
- Sant'Anna, L.G., Riccomini, C., Rodrigues-Francisco, B.H., Sial, A.N., Carvalho, M.D. and Moura, C.A.V. 2004. The Paleocene travertine system of the Itaborai basin, Southeastern Brazil. *Journal of American Earth Sciences*, 18: 11-25.
- Sasaki, N. and Minato, H. 1982. Relationship between lattice constants and strontium and calcium contents of hokutolite. *Mineralogical Journal*, 11: 62-71.
- Sawlowicz, Z. 2000. Framboids: from their origin to application. *Prace Mineralogica*, 88: 1-80.
- Schultze-lam, S. and Beveridge, T.J. 1993. Nucleation of celestite and strontianite on a cyanobacterial S-layer. *Applied and Environmental Microbiology*, February 1993, 447-453.
- Senko, J.M., Campbell, B.S., Henriksen, J.R., Elshahed, M.S., Dewers, T.A. and Krumholz, L.R. 2004. Barite deposition resulting from phototrophic sulfide-oxidizing bacterial activity. *Geochimica et Cosmochimica Acta*, 68: 773-780.
- Seong-Joo, L., Browne, K.M. and Golubic, S. 2000. On stromatolite lamination. In: Riding, R.E. and Awramik, S.M. (Eds.) *Microbial Sediments*, Springer-Verlag, Heidelberg, pp. 16-24.
- Shikazono, N. 1994. Precipitation mechanisms of barite in sulfate-sulfide deposits in back-arc basins. *Geochimica et Cosmochimica Acta*, 58: 2203-2213.
- Smith, E., Hamilton-Taylor, J., Davison, W., Fullwood, N.J. and McGrath, M. 2004. The effect of humic substances on barite precipitation-dissolution behaviour in natural and synthetic lake waters. *Chemical Geology*, 207: 81-89.
- Suganuma, I. 1928. On the constituents and genesis of a few minerals produced from hot springs and their vicinities in Japan. I. The Akita Hokutolite. *Journal of the Chemical Society of Japan*, 3: 69-73.
- Takashima, C. and Kano, A. 2005. Depositional processes of travertine developed Shionoha hot spring, Nara Prefecture, *Journal of the Geological Society of Japan*, 111: 751-764.

- Taylor, M.O., Drysdale, R.N. and Carthew, K.D. 2004. The formation and environmental significance of calcite rafts in tropical tufa-depositing rivers of northern Australia. *Sedimentology*, 51: 1089-1101.
- Tazaki, K., Webster, J. and Fyfe, W.S. 1997. Transformation processes of microbial barite to sediments in Antarctica. *Japanese Journal of Geology*, 26: 63-68.
- Tazaki, K. and Watanabe, H. 2004. Biomineralisation of radioactive sulfide minerals in strong acidic Tamagawa Hot Springs. *Science Reports of Kanazawa University*, 49: 1-24.
- Tekin, E., Varol, B. and Sayili, I.S. 2002. Indications of intermediate compositions in the BaSO₄-SrSO₄ solid-solution series from the Bahaceciktepe Celestine deposit, Sivas, east-central Anatolia, Turkey. *Canadian Mineralogist*, 40: 895-908.
- Torres, M.E., Bohrmann, G., Dube, T.E. and Poole, F.G. 2003. Formation of modern and Paleozoic stratiform barite at cold methane seeps on continental margins. *Geology*, 31: 897-900.
- van Everdingen, R.O. 1972. Thermal and Mineral Springs in the Southern Rocky Mountains of Canada. Water Management Service, Department of the Environment, Environment Canada, 151 pp.
- Walter, W.R., Des Marais, D.J. 1993. Preservation of biological information in thermal spring deposits; developing a strategy for the search for fossil life on Mars, *Icarus*, 101: 129-143.
- Weed, W.H. 1889. Formation of travertine and siliceous sinter by the vegetation of hot springs. *US Geological Survey Annual Report*, 9: 613-676.
- Younger, P. 1986. Barite travertine from southwestern Oklahoma and west-central Colorado. M.Sc. Thesis, Oklahoma State University, Stillwater, 163 pp.

Chapter 4 **Diatom-mediated barite precipitation in microbial mats calcifying at Stinking Springs***

Introduction

Diatoms are eukaryotic algae that produce ornamented opal-A shells, or frustules, whose formation, dissolution and/or sequestration in sediments dominates both the marine silica and carbon cycles (Treguer et al., 1995). Preserved diatom frustules are important index fossils in marine sediments, and are widely applied as proxies for palaeoproductivity, palaeoclimate and palaeobathymetry (e.g. Thomson et al., 2000; van Eetvelde et al., 2004). The solubility, surface reactivity and trace element chemistry of diatom frustules differs from abiogenic silica (Dixit and Van Cappellen, 2002), and varies with sample age, size, and species (Darley, 1977). There is no simple correlation between diatom frustule preservation and pore water silica saturation (Dixit et al., 2001); the fate of diatom silica is determined by poorly-constrained interactions between dissolved ions, organic molecules and exposed silanol sites on the frustule, which variously inhibit or catalyze silica dissolution (Dixit and Van Cappellen, 2002). Adsorption of dissolved and bioaccumulated cations to silanol sites can also facilitate precipitation of certain mineral phases, suggesting a role for diatoms in the formation of microcrystalline barite (BaSO_4) in the marine water column (Bishop, 1988).

The Stinking Springs, Utah, provide a unique opportunity to investigate the relationship between diatom silica and barite precipitation. Diatoms proliferate in the warm ($\sim 48^\circ\text{C}$), saline, bicarbonate and sulphur-rich spring water, and form thick microbial mats in association with cyanobacteria and sulphate reducing bacteria. These mats are lithified by minerals precipitating from the spring water, and diatoms are trapped and preserved *in situ* in porous calcite deposits (tufas). Relict tufa deposits underlie the modern spring flow path, allowing examination of diatom frustule preservation through early diagenesis.

Cells of cyanobacteria and sulphate reducing bacteria are encrusted or impregnated with calcite as the microbial mats lithify. Diatom frustules, however, are

* A version of this chapter has been published.

Bonny, S. and Jones, B. 2007. Diatom-mediated barite precipitation in microbial mats calcifying at Stinking Springs, a warm sulphur spring system in Northwestern Utah, USA, *Sedimentary Geology*, 194, 223-244.

commonly associated with microcrystalline barite: barite precipitates in haloes around diatom bundles, lines and fills diatom frustules, and even replaces diatom silica. Some relict tufas also contain pore-filling 'diagenetic' barite cements.

Barite precipitation at subaerial springs is rare, occurring at only a handful of springs worldwide (Cecile et al., 1984; Younger, 1986; Su et al., 2002; Senko et al., 2004), and bio-induced barite precipitation is equally uncommon (Sanchez-Moral et al., 2004; Senko et al., 2004; Bonny and Jones, 2007). The selective association of primary barite with diatoms at Stinking Springs, as opposed to soft-bodied microbes, dramatically exhibits the importance of diatom barium bioaccumulation and frustule delineated microniches in promoting localized barite precipitation. This paper describes the diatom-associated and diagenetic barite at the Stinking Springs, and discusses implications for the interpretation of microcrystalline barite preserved in marine sediments.

Study Site

The Stinking Springs are located in Boxelder County, Utah, USA (Fig. 4-1A). They emerge through normal faulted Mississippian Lodgepole Limestone Formation, which crops out as cliffs and ledges north of Great Salt Lake on the south side of Little Mountain in the Wasatch Mountain Range (Blackett and Wakefield, 2004). The Stinking Springs aquifer emerges near the base of Little Mountain at ~ 48°C, with TDS (total dissolved solids) averaging 15,500 ppm, and a discharge rate that has varied historically between 19 and 170 L/min (Klauk and Budding, 1984; Blackett and Wakefield, 2004).

The spring orifices are capped and piped south under Highway 83 to two sheltered bathing tubs. After flowing through the tubs, the water is diverted into a culvert that flows through a gravel levee that marks the southern boundary of a small parking lot. South of the levee, the spring water disperses and flows down three stepped, fan-shaped terraces (Fig. 4-1B, C). Submerged areas of the flow path are carpeted by colourful microbial mats and surrounded by yellow, white and gray mineral precipitates (Fig. 4-1B).

Bedded tufas underlie the modern spring and extend ~ 700 m westwards along the highway (Fig. 4-1C). Four cold seeps with an average temperature of 7°C emerge through the tufa along the highway, forming small erosion channels. The marshlands

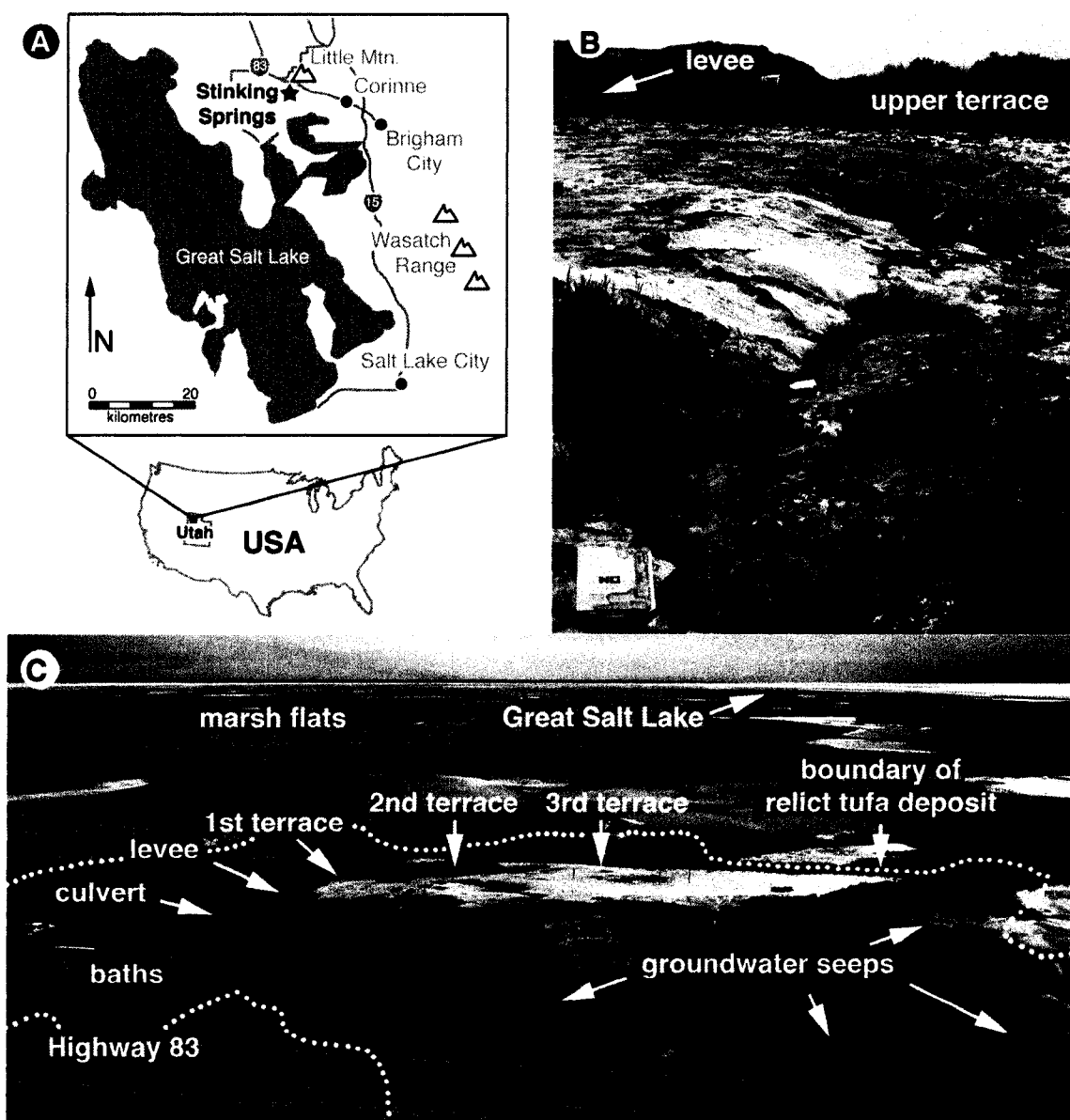


Figure 4-1. Overview of Stinking Springs, Utah. (A) Location map. (B) Photograph of the upper spring flow path (notebook is 10 cm wide). (C) Aerial photograph of the spring site showing locations referred to in the text.

south of Little Mountain have a shallow water table, consistently < 3 m, and these cold seeps likely represent localized ground water discharge (Jensen, 1994).

Methods

Fieldwork was conducted in October 2004. Water temperature, pH and conductivity were measured along the spring flow path with a portable Accumet AP62 pH/mV meter. Microbial communities, fresh mineral precipitates and relict tufa underlying the spring and extending westwards along Highway 83 were described *in situ*, and representative samples were collected. Ten glass slides were inserted vertically in the proximal spring flow path and collected 24 hours later.

Microbial samples were dissected and examined by light and scanning electron microscopy (SEM). SEM samples were rinsed in distilled water, desiccated, mounted on steel stubs, sputter coated with gold, and imaged at accelerating voltages of 5 to 20 kV, in both secondary electron and backscattered electron mode, on a JEOL 6301F field emission scanning electron microscope (SEM). Soft-bodied microbes were assigned to morphologically defined genera following Rippka et al. (1979) and Wehr and Sheath (2003) and diatoms were identified following Guttinger (1986a-f) and Simonsen (1987). Microbial mats at Stinking Springs are volumetrically and texturally dominated by cyanobacteria, sulphate reducing bacteria (SRB) and diatoms; other microbial groups (unicellular and filamentous bacteria, fungi, etc.) were observed during SEM analysis, but are not a focus of this study.

Minerals were examined by thin section petrography, X-ray diffraction of powdered sample on a Rigaku Geigerflex Cobalt Tube Power Diffractometer with a graphite monochromator and online data processor for mineral identification (using the JCPDS database), SEM and energy dispersive X-ray analysis of fractured samples. Cut, polished and carbon-coated samples were also examined on a JEOL 8900 electron microprobe at 30 kv. Selected samples were coarsely crushed, digested in 10% hydrochloric acid, rinsed in distilled water and soaked overnight in consumer grade bleach. This removed both the volumetrically dominant carbonate minerals and entrapped organic matter, allowing examination of minor mineralogical constituents (silica and barite) by dissecting microscope and SEM.

Results and interpretation

Spring water physiochemistry

In October 2004, the Stinking Springs waters were 41.6°C where they emerge beneath the bathhouses, with pH of 6.26. The water cools and becomes increasingly basic as it disperses and flows over the terraces, reaching a minimum temperature of 9.8°C, with pH 7.85, where it flows into marshlands south of the spring (Fig. 4-2A).

The water is anoxic to dysoxic within 10 m of the bathhouses, and has a strong sulphurous odour. It is rich in bicarbonate, sulphur, sodium and chloride and notably enriched in dissolved silica and barium relative to other springs in the area (Table 4-1: Felmlee and Cadigan, 1982; Blackett and Wakefield, 2002). Barium concentrations (~ 5 ppm) are well above the average content of seawater (5 ppb) and continental fresh water streams (54 ppb)(Bolze et al., 1974).

| | Min. | Max. | Avg. |
|--------------------------------|-------|-------|-------|
| Concentration (ppm): | | | |
| Na ⁺ | 6300 | 15000 | 10530 |
| K ⁺ | 490 | 870 | 574 |
| Ca ²⁺ | 660 | 920 | 825 |
| Mg ²⁺ | 250 | 440 | 310 |
| Sr ²⁺ | 24 | 38 | 31 |
| Ba ²⁺ | 0.4 | 7.8 | 2.9 |
| Al ³⁺ | 0.03 | 1.2 | 0.46 |
| Fe ³⁺ | 0.02 | 0.4 | 0.16 |
| SiO ₂ | 27 | 54 | 42.7 |
| H ₂ CO ₃ | 170 | 528 | 405 |
| Cl ⁻ | 12000 | 26000 | 19750 |
| F ⁻ | 0.9 | 3.7 | 1.75 |
| SO ₄ ²⁻ | 59 | 470 | 154 |
| TDS (ppm) | 20400 | 34600 | 30540 |
| T (°C) | 42.5 | - 56 | 48.2 |
| pH | 6.3 | 7.4 | 6.7 |
| Eh (mV) | -580 | -150 | -360 |

Table 4-1. Chemistry of the Stinking Springs water compiled from multiple data sets collected between 1977 and 2002; from Felmlee and Cadigan (1982:analyses by atomic absorption mass spectrometry) and Blackett and Wakefield (2004:analyses by ICP-MS).

Spring biology

Brightly coloured microbial assemblages are found in all inundated parts of the Stinking Springs flow path. Nearest the bathing tubs, bright green, gelatinous, substrate attached colonies of *Oscillatoria* sp. flourish in dysoxic water. Past the levees, layered

orange and olive green microbial mats carpet the terraced flow path. These mats, 0.5-4 cm thick, contain an assemblage of cyanobacteria, diatoms, and sulphate reducing bacteria, whose relative abundance varies across the three terraces (Fig. 4-2B).

On the upper terrace, microbial mats are locally textured by evenly spaced projections, or nodes, ≤ 4 mm high, that are formed by upwards trending bundles of *Oscillatoria* sp. and *Phormidium* sp. filaments (Fig. 4-2C, D). Diatoms proliferate on the lee side of these structures, and are commonly enveloped by cyanobacterial filaments (Fig. 4-2E).

Diatoms become increasingly abundant in the surface layer of the mats on the middle terrace and outnumber cyanobacteria by volume on the lower terrace. The switch from cyanobacteria- to diatom-dominated mats probably reflects oxidation of the spring water and reducing H₂S toxicity, which inhibits diatom growth and photosynthesis (Eppley, 1977). The mats contain a diverse diatom assemblage that includes *Achnantheidium minutissima*, *Amphora lineolata*, *Nitzschia filiformis*, *Navicula menisculus*, *Brachysira aponina* and four unidentified species of *Amphora*, *Navicula*, and *Nitzschia* (Fig. 4-3). Locally, *Achnanthes miutissima* and *Nitzschia* sp-a. proliferate to the exclusion of other species (Fig. 4-3A, B).

Microbial mats on all three terraces have a red layer, 0.1-0.4 cm thick, immediately beneath the cyanobacteria/diatom surface layer, which is composed of decaying cyanobacterial filaments, diatom frustules, and unicellular purple sulphur bacteria. The red layer is underlain by semi-cohesive organic-rich black sediment that contains abundant rod-shaped unicellular SRB .

Dry areas of the terraces contain desiccated microbial mats, shrunk into polygons with curled edges that form tepee structures (Fig. 4-4A). These desiccating mats commonly have surficial mineral crusts and/or are impregnated by granular precipitates (Fig. 4-4B).

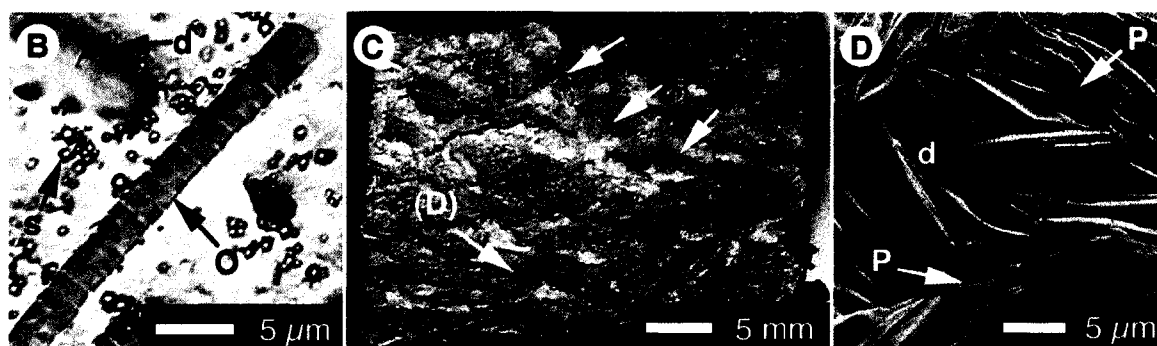
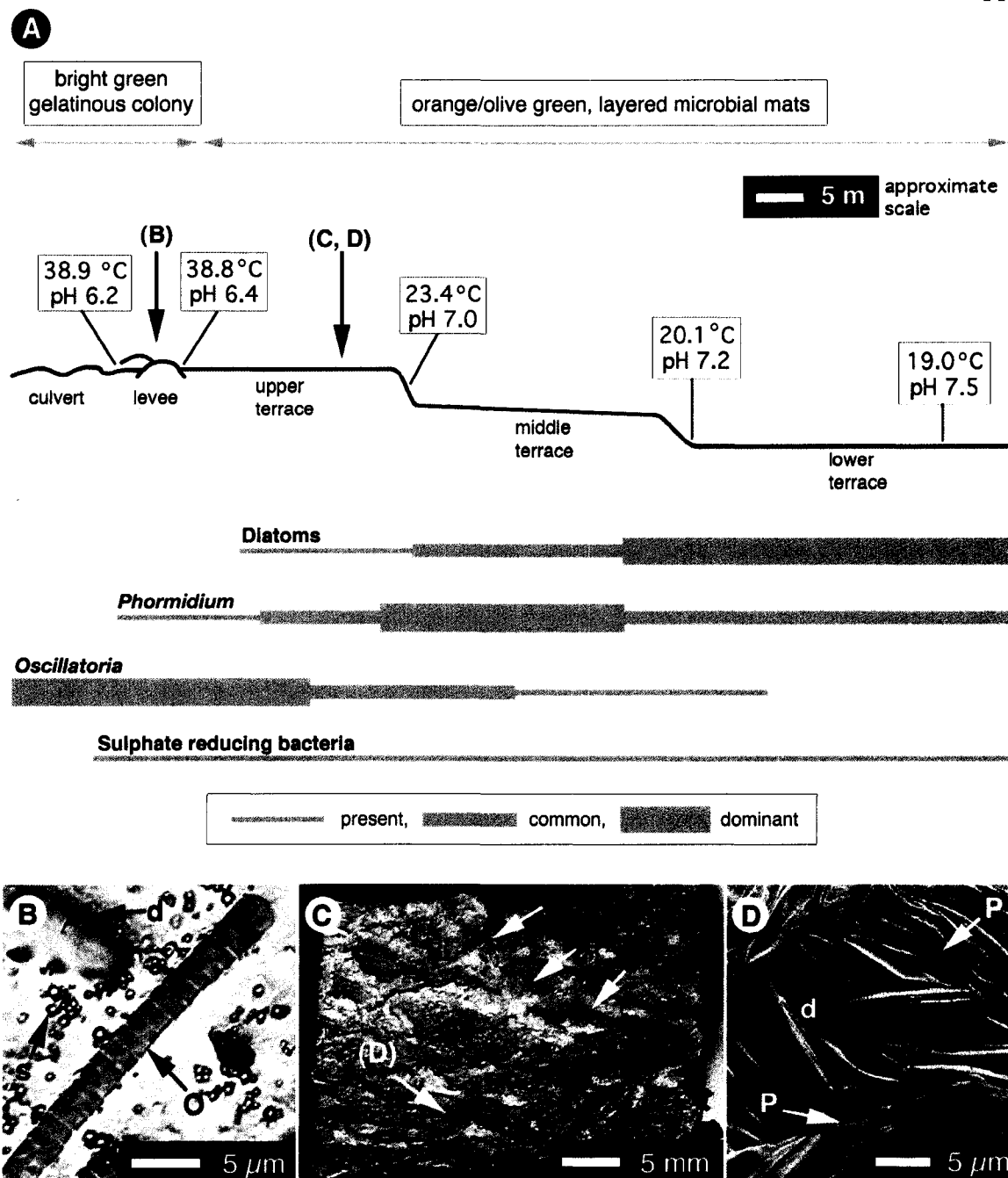


Figure 4-2. Details of the Stinking Springs flow path. (A) Schematic drawing showing physiochemical measurements, collection sites for samples shown in images B-D, and compositional variations in the microbial assemblage. (B) Light microscope photograph of an *Oscillatoria* sp. filament (O-arrow), sulphur globules (s-arrow) and a diatom (d-arrow) on a slide collected from the levee channel. (C) Photograph of a microbial mat collected from the upper terrace with well-developed surface nodes (arrows). (D) Detail of diatoms (d) and *Phormidium* sp. filaments (P) in the lee side of a node from image C.

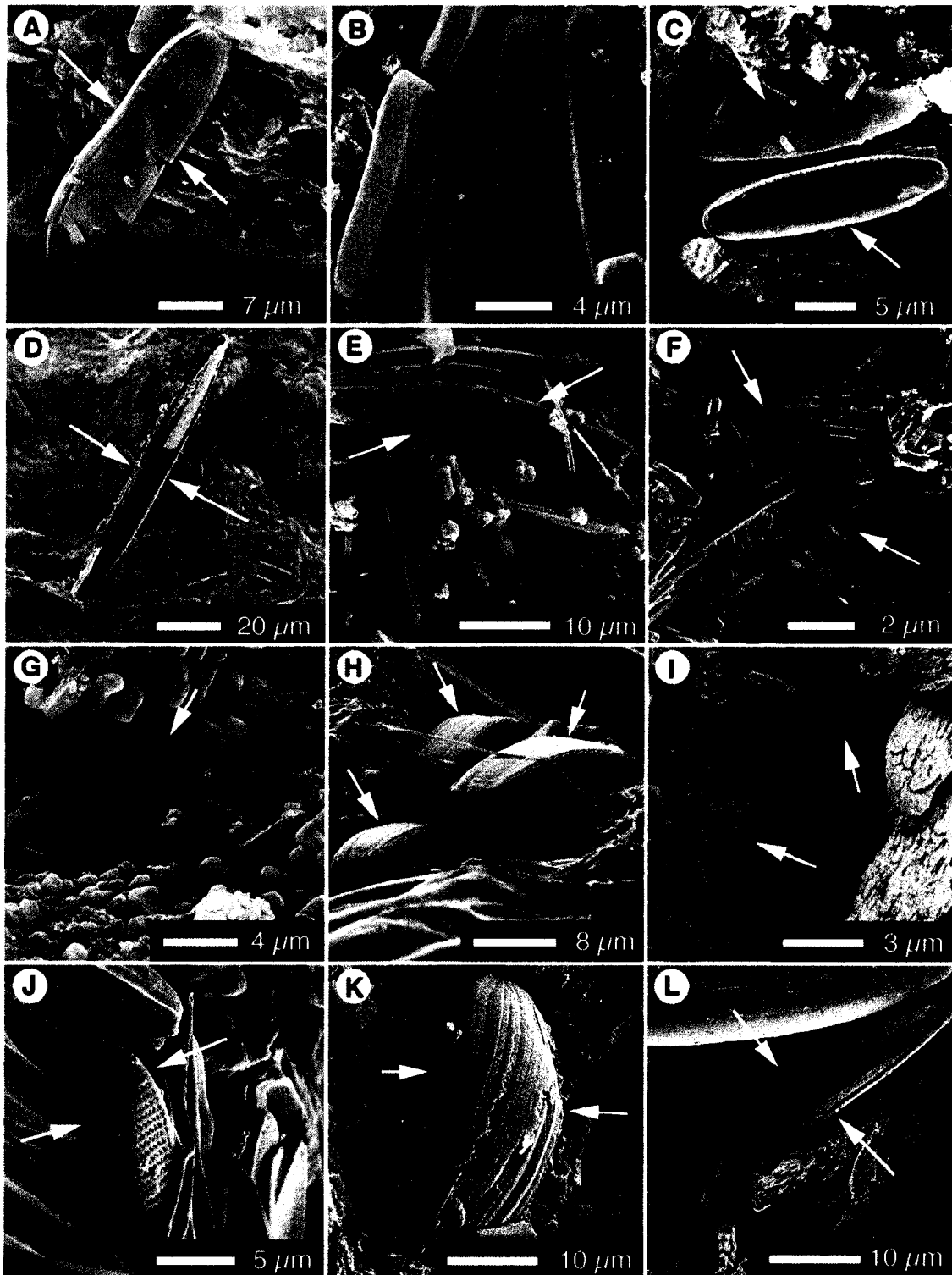


Figure 4-3. SEM images of diatoms from Stinking Springs: (A) *Nitzschia sp-a.*, (B) *Achnanthidium minutissima*, (C) *Achnanthes sp.*, (D) *Nitzschia filiformis*, (E) *Amphora lineolata*, (F) *Brachysira aponina*, (G) *Navicula menisculus*, (H) *Navicula sp.*, (I, J) *Nitzschia sp-b, -c.*, (K, L) *Amphora sp-a, -b.*

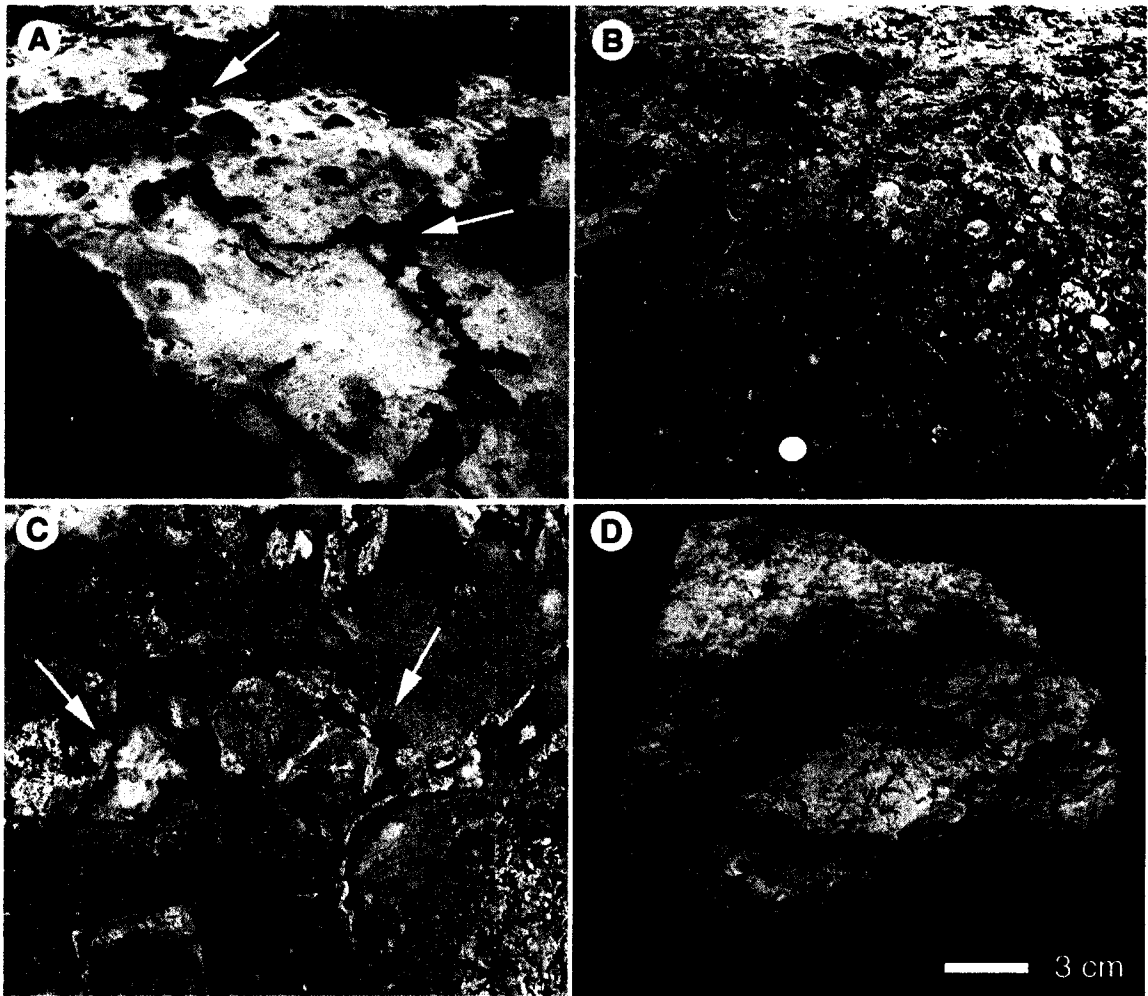


Figure 4-4. Photographs of mineralizing microbial mats and tufa. (A) Desiccating mats from the middle terrace, arrows indicate tepee structures (rock hammer is 30 cm long). (B) Mineral crusts formed on mats on the upper terrace (coin is 2.25 cm in diameter). (C) Surface of fully lithified tufa, arrows indicate fossil tepee structures (rock hammer head is 18 cm long). (D) Hand sample of layered relict tufa.

Mineral precipitates

Due to the ubiquity of microbes in the Stinking Springs flow path, virtually all mineral precipitation takes place on or inside microbial mats. Early precipitates of calcite and sulphur are found in live, hydrated mats, and desiccating mats are rapidly coated by evaporative salts and impregnated by calcite to produce lithified tufas (Fig. 4-4C, D).

XRD analyses of hydrated mats shows that they contain elemental sulphur, calcite, high-magnesium calcite, and opal. Sulphur is found as crystalline rhombs and as amorphous spheres and globules (Fig. 4-5A). Subhedral microcrystalline calcite precipitates in the proximal flow path coating and lining gas bubbles (Fig. 4-5B) and encrusting cyanobacterial filaments (Fig. 4-5C). It probably forms in response to alkalinity gradients in cyanobacterial sheaths and extracellular polysaccharides (EPS) produced by photosynthesis and/or anaerobic sulphide oxidation (cf. Arp et al., 1999; Castanier et al., 2000). Diatom frustules account for the opaline silica content of the hydrated microbial mats.

Tiny stellate barite crystals were found in some hydrated mats, and on one of the glass slides inserted on the upper terrace (Fig. 4-5D). Stellate crystals are typical of barite precipitated at an air-liquid interface where surfactants are adsorbed (Sermon et al., 2004), and these tiny precipitates probably formed as atmospheric oxidation of H_2S to SO_4^{2-} provided an anionic reactant for dissolved barium. They are the only evidence for spontaneous barite precipitation from the spring water whose high salinity precludes ambient barite supersaturation through electrostatic interactions that reduce free ionic activity (cf. Hennessey and Graham, 2002).

Older mats, and those abandoned by the flow path, are increasingly lithified. Mineralisation proceeds by through flow of calcite-supersaturated waters that precipitate isopachous euhedral microcrystalline calcite (and locally high-Mg calcite) cements in pore spaces (Fig. 4-5E) and around cyanobacterial filaments (Fig. 4-5F). Calcification is also facilitated by desiccation, which concentrates ions adsorbed in EPS (Arp et al., 1999), and by wicking of fluids to the surface of the mats where evaporation drives precipitation of halite, sylvite and calcite.

Barium is measurable by dispersive X-ray analysis in desiccating mats, and is enriched in pockets of microbial EPS localized under surface nodes in the upper mat

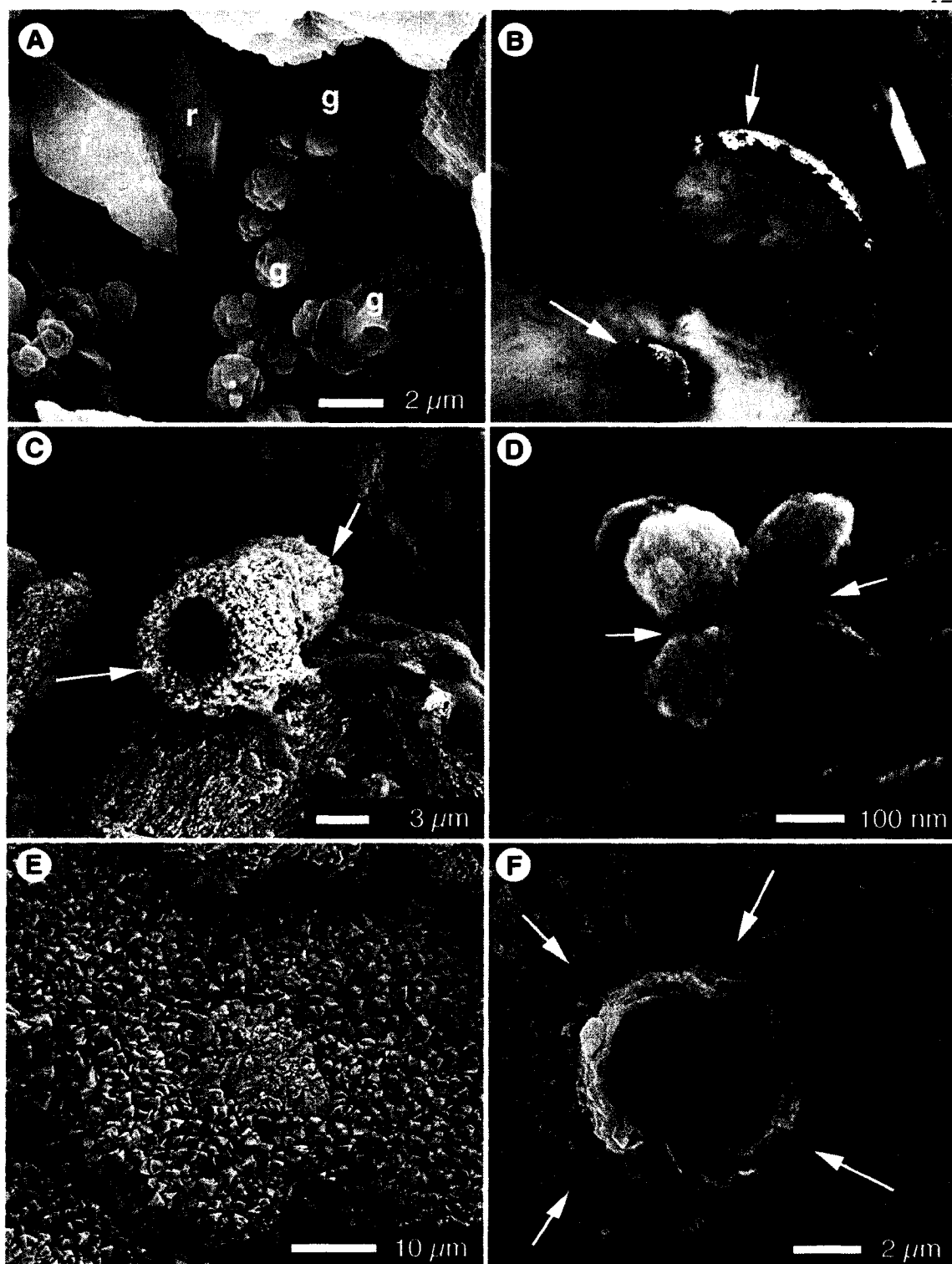


Figure 4-5. Mineral precipitates. (A) SEM image of rhombs (r) and globules (g) of elemental sulphur. (B) Photograph of microcrystalline calcite lining bubbles in microbial colonies in the culvert (pen is 1.5 cm wide). (C) Subhedral microcrystalline calcite tube formed around a cyanobacterial filament (arrows). (D) Stellate barite microcrystal (arrows). (E) Euhedral microcrystalline calcite crust on a microbial mat surface. (F) Cross-section of a calcite encrusted microbial filament from a partially mineralized mat.

layer, apparently associated with diatoms that accumulate there. Partially mineralized mats are deformable, making it difficult to examine barite precipitates *in situ*. As lithification proceeds mineral and microbial components of the mat are gradually sequestered from the spring water, made rigid, and preserved in place.

Fully lithified tufas are composed of 80-98% calcite, which is locally enriched in magnesium. Evaporative salts and elemental sulphur, typical of early mat mineralisation, are scarce in fully lithified mats as a result of their high solubility. The opal content of the tufas (2-10%) is almost entirely attributable to the presence of incorporated diatom frustules. Diatoms are found throughout the mineralized mats, and commonly exhibit irregular surface textures as a result of partial dissolution. This indicates that pore fluids in lithifying tufa are undersaturated with respect to opal-A silica, however, some tufa samples contain thin ($\leq 1 \mu\text{m}$) sheets of colloidal silica, which are sandwiched between layers of calcite cements, and apparently precipitated from solution. Dissolution of diatom-derived silica in the upper flow path may facilitate localized silica supersaturation downstream.

Two types of barite are found in fully lithified tufas: primary 'diatom-associated' barite, and pore-filling 'diagenetic' barite.

Primary 'diatom-associated' barite

Primary barite in the relict tufa is exclusively associated with (mostly articulated) diatom frustules. Barite is found (1) surrounding diatoms, (2) lining diatoms, (3) forming casts of diatoms, and (4) replacing diatom silica.

(1) Barite surrounding diatoms

The barium-enriched EPS pockets observed beneath and in the lee side of surface nodes in partially mineralized mats have a direct counterpart in barite haloes that surround diatom frustules trapped in fully mineralized mats and relict tufa. The haloes are lens shaped with cross-sectional areas of 200 to 7500 μm^2 . They are easy to pick out in electron microprobe and backscattered SEM images where density contrasts between mineral phases are represented by varied brightness (Fig. 4-6A). The haloes are most commonly composed of stubby prismatic barite crystals, 1-5 μm long, that typically have

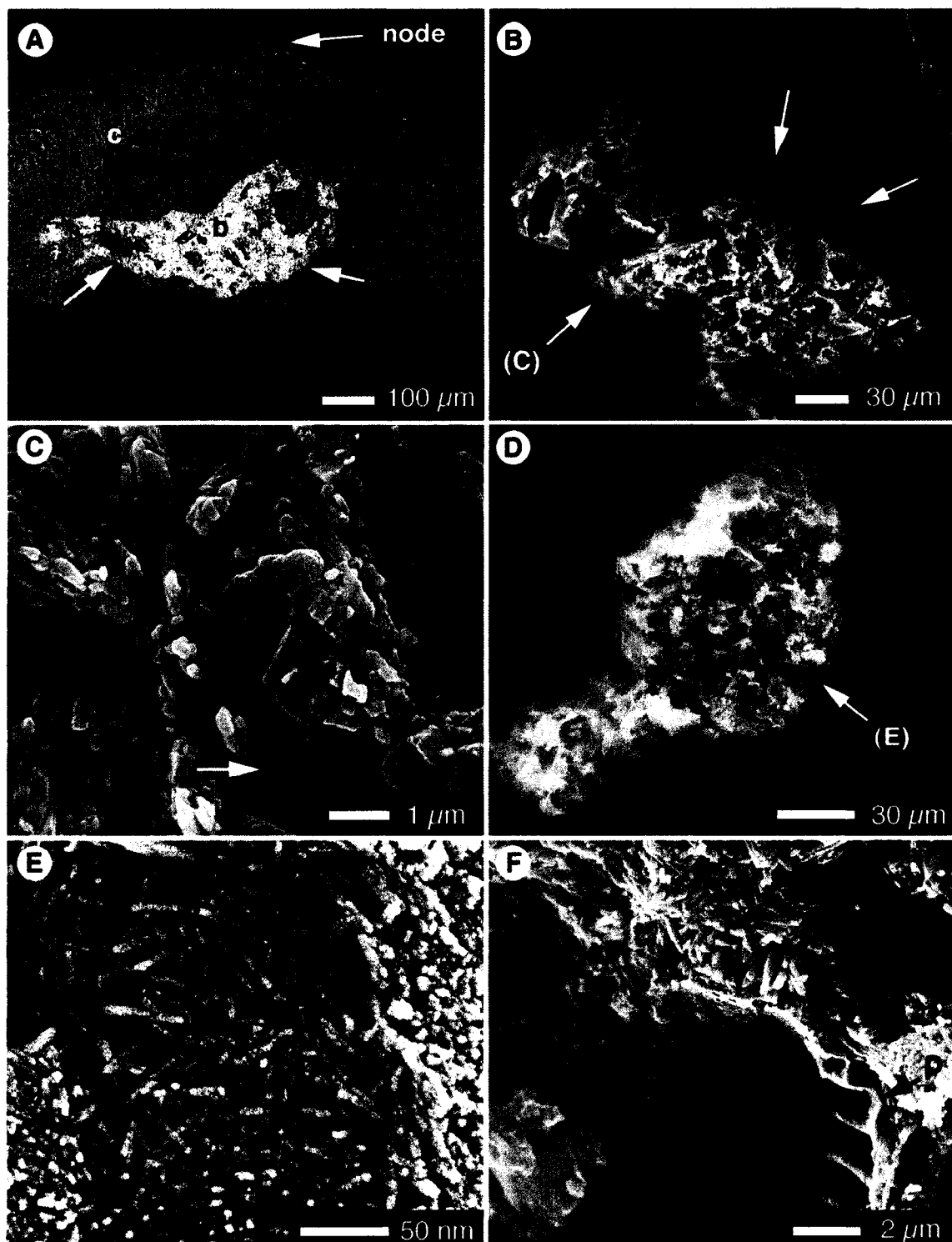


Figure 4-6. Barite surrounding diatom frustules. (A) Backscattered SEM image of a barite halo (b-arrow) beneath a mat surface node. (B) SEM image of a barite halo removed from tufa by acid digestion, note abundant frustules (arrows). (C) Detail of stubby prismatic barite from halo shown in B. (D) Fluffy barite halo removed from tufa by acid digestion. (E) Detail of nanometric barite rods from fluffy halo shown in D. (F) Partially dissolved diatom frustule; at p-arrow, silica is preserved, at pd-arrow, silica is etched, and by d-arrow, silica is completely removed, frustule form is preserved in surrounding barite microcrystals.

rounded ends (Fig. 4-6B, C). Less commonly, diatoms are surrounded by porous 'fluffy' precipitates (Fig. 4-6D) composed of subhedral barite rods ≤ 100 nm long (Fig. 4-6E). Diatoms trapped in the barite haloes show varying degrees of preservation; those completely surrounded by barite tend to be well preserved, whereas those exposed to porosity are badly etched (Fig. 4-6F).

The capacity for microbial mats to adsorb divalent cations, both in EPS and on cell walls, is well established (Alldredge et al., 1993; Schultze-Lam et al., 1993). Microbial mats and biofilms are commonly enriched in calcium and magnesium, compared to surrounding waters (e.g. Arp et al., 1999) and barium enrichment has been described in microbial biomass from acid thermal spring in Japan (Tazaki and Watanabe, 2004), mat pore waters at cold sulphur springs in Ontario (Douglas and Douglas, 2001), and in marine plankton (Ganeshram et al., 2003).

Barite precipitation can result when barium-enriched biomass is exposed to a source of sulphate, and microcrystalline barite precipitation has been reported from microbial mats in Antarctic Lakes (Tazaki et al., 1997), hypogean cyanobacterial biofilms in the Roman Catacombs (Sanchez-Moral et al., 2004), and in bacterial EPS at fumaroles in Solfatara Crater, Italy (Glamoclija et al., 2004). These EPS bound barite microcrystals share sub- to euhedral prismatic habits (Tazaki et al., 1997; Sanchez-Moral et al., 2004; Glamoclija et al., 2004) similar to the 'stubby' prismatic barite found in haloes from the Stinking Springs. Crystal growth can be inhibited by retarded ionic diffusion to growth faces in viscous media, including microbial EPS (Buczinsky and Chafetz, 1991; Arp et al., 1999), and this may explain the small crystal size of EPS-bound barite.

The sub- and anhedral microcrystals found in 'fluffy' barite haloes are more typical of barite precipitated rapidly in highly supersaturated solutions (cf. Bala et al., 2005). The 'fluffy' barite is, thus, thought to represent EPS mineralized under rapidly established conditions of barite supersaturation; perhaps by exposure of barium-enriched EPS to a sudden influx of SO_4 -bearing water.

If barite is formed by spring water sourced barium accumulating in microbial EPS, it is curious that barite was not precipitated pervasively through the Stinking Springs microbial mats. Sanchez-Moral et al. (2004) showed that cyanobacterial EPS can host barite precipitation equally well as EPS generated by diatoms. At the Stinking

Springs, however, cyanobacteria are commonly encased in calcite precipitates. It may be that EPS throughout the mats adsorbs barium, but that calcite supersaturation is so high amongst photosynthesizing microbes that barium is incorporated into calcite phases.

The diatoms bundled beneath surface nodes in the mats are shaded by cyanobacterial overburden and exposed to high sulphur concentrations, which may necessitate facultative heterotrophy (cf. Darley, 1977). If photosynthetic CO₂ withdrawal was not able to drive calcite precipitation in these protected niches, EPS could become significantly barium-enriched. Barite precipitation would be inhibited, however, by SRB-established anoxia beneath the surface layer of living mats. Calcite precipitation can occur under reduced conditions, and can be catalysed by SRB metabolism (Riding, 2000), but barite precipitation requires a source of oxidized sulphate and would be inhibited so long as SRB were extant.

In desiccating mats, sulphate derived from degrading organics, or delivered by spring or meteoric waters, likely facilitates barite precipitation within barium-enriched EPS haloes. Additional barium may also have been supplied to the EPS by dead and decaying diatoms.

Several studies have identified barium-enrichment (up to 100 times seawater concentrations) in the frustules (Vinogradova and Koval'skiy, 1962; Brongersma-Sanders, 1967) and soft tissues (Bishop, 1988; Ganeshram et al., 2003) of marine diatoms. Comparable barium enrichments have been identified in non-siliceous plankton, so diatoms may not be more adept at barium bioaccumulation than other microbial groups (Ganeshram et al., 2003). Their siliceous frustules, however, may have unique importance in establishing barite-supersaturated microniches in the marine water column during release of bioaccumulated barium from decaying algal tissues (Bishop, 1988). The presence of barite precipitates inside well-preserved diatom frustules in the Stinking Springs tufa supports the idea that barium released by decay of diatom tissues can precipitate *in situ*.

(2) Barite lining diatom frustules

Away from barite haloes, individual diatom frustules are commonly encased in calcite cements and show little evidence of dissolution (Fig. 4-7A). Many are unaltered,

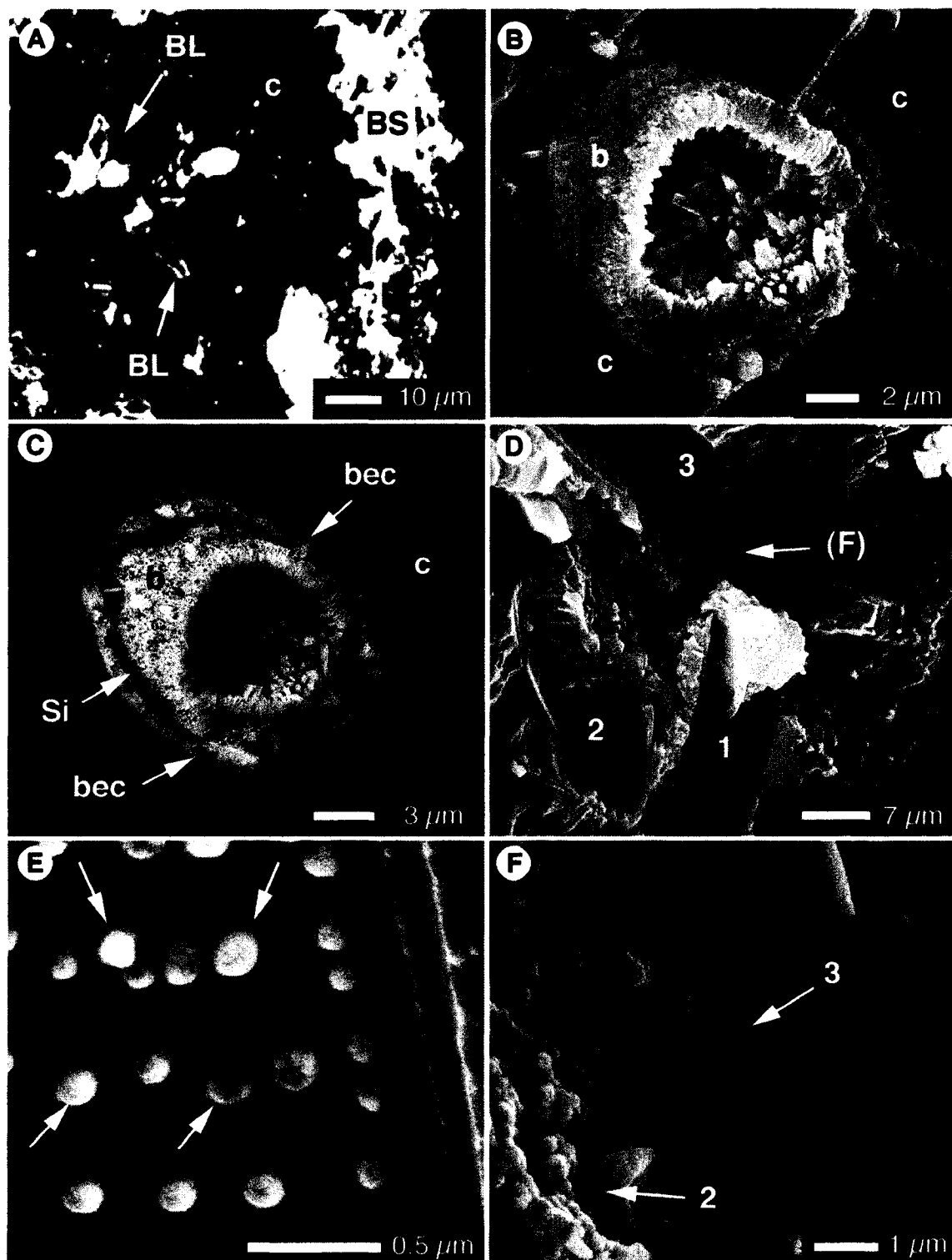


Figure 4-7. Barite lining diatom frustules. (A) Electron microprobe image of barite surrounding (BS) and lining (BL) frustules trapped in calcite (c). (B) SEM image of fractured barite-lined frustule (b) in calcite (c). (C) Backscattered SEM image of the frustule in B, note bright barium-enriched calcite (bec-arrow) external todiatom silica (Si-arrow). (D) Frustules in calcite cement with 1-no lining, 2-spherical barite at areolae, and 3-rhombic barite. (E) Detail of spherical barite in frustule areolae (arrows). (F) Detail of frustule in D with areole aligned anhedral barite (2-arrow) overgrown by rhombic barite (3-arrow).

maintaining void porosity, but others are lined by barite crystals, forming spectacular 'mini-geodes' (Fig. 4-7B). In backscattered electron images, calcite cements surrounding barite-lined diatoms are brighter than the ambient cement matrix, indicating that they may be enriched in barium (Fig. 4-7C). In some diatoms, barite is present as small spheres that project inwards from frustule areolea (Fig. 4-7D, E, F). In several fractured samples, silica was displaced, revealing contact between the barite spheres and calcite cement through the areolae (Fig. 4-7E). In other specimens, anhedral areole-aligned barite is overgrown by cubic and/or stubby prismatic barite crystals found both at pore sites, and growing inwards from diatom silica on the frustule wall (Fig. 4-7F).

Barite microcrystals have been described forming inside the frustules of dead planktonic marine diatoms. Bishop (1988) postulated that barite formed by reaction of sulphur released from decaying tissues with labile barium adsorbed to exposed silanol sites on fresh diatom silica surfaces. Ganeshram et al. (2003) proved experimentally that barite precipitation could also be facilitated by reaction of bioaccumulated barium with externally sourced sulphate during diatom decay. In their experiments only 2-4% of bioaccumulated barium was precipitated, while the remainder was dispersed extracellularly, and barite precipitates incorporated both bioaccumulated barium and barium dissolved in the growth medium (Ganeshram et al., 2003). Neither study examined the spatial arrangement of barite in the diatom frustule to assess the importance of the bioaccumulated barium source.

The Stinking Springs barite diatom linings seem to have been initiated in areolae, at the interface between mat pore fluids and frustule restricted fluids. Living diatoms are surrounded by a tightly bound proteinaceous cuticle of gelatinous glucuronic acid and polyglucuronic acid within which diatoms are able to maintain homeostasis (Duke and Reimann, 1977; Coradin and Lopez, 2003). If diatom soft tissues were barium-enriched due to intracellular barium bioaccumulation, death and decay would establish a reducing, barium-enriched microenvironment within the frustule walls. As the diatom's exterior cuticle began to decay surrounding pore fluids would be able to seep in through frustule areolae, and purge fluids (organic tissues liquefied by putrefaction) could seep out. Infiltration of dissolved sulphate would drive precipitation of barite inside the frustule. Exudation of barium-enriched purge fluids from floating diatoms would result in barium

dispersion (Ganeshram et al., 2003), but caused barium-enrichment of diatom enveloping calcite cements in the Stinking Springs microbial mats.

The spherical barites located at frustule areolae represent the initiation of barite precipitation in the decaying frustules. Gonzalez-Munoz et al. (2003) reported similar spherical barites forming in laboratory cultures at the interface between barium-enriched bacterial cell walls and surrounding sulphate-enriched fluids. Based on a lack of barite precipitation in dead cultures, they concluded that barite precipitation had been initiated by bacterial production of metabolites and local pH heterogeneities. Once the barrier to crystal nucleation was passed, these spherical barite precipitates began to grow abiotically, and took on rhombic and cubic crystal habits (Gonzalez-Munoz et al., 2003).

Crystal development follows a similar pattern inside the diatom frustules. Early precipitates are spherical, whereas thicker barite linings are composed of rhombic and prismatic crystal forms. By analogy to Gonzalez-Munoz et al.'s (2003) study, this shift in crystal habit may reflect a change from localized to general barite supersaturation within the diatom frustule – in effect, a shift from supersaturation at meniscus interfaces within areolae, to ambient supersaturation in the frustule cavity as it is infiltrated by sulphate bearing waters. The linings clearly grow inwards from the frustule wall, indicating that barium adsorption to fresh silica surfaces may indeed provide nucleation sites for barite precipitating from solution as Bishop (1988) hypothesized.

The preservation of diatom silica in lined frustules may be an indication that the infiltrating waters were not silica-undersaturated, or that surrounding calcite cements and internal barite linings limited direct contact between diatom silica and the fluids that wrought dissolution on frustules elsewhere in the mineralizing mats. Dissolution has completely removed silica from much of the Stinking Springs tufa, sometimes leaving enigmatic barite casts that attest to the former presence of diatoms.

(3) Barite diatom casts

Internal casts of diatoms are preserved in barite haloes and dispersed throughout calcite cements (Fig. 4-8). The casts are composed of randomly arranged, intergrown microcrystalline barite rods averaging $1 \times 0.2 \times 0.2 \mu\text{m}$ (Fig. 4-8C, D). The casts record details of the diatom frustules with varying fidelity; the topography of the girdle band is

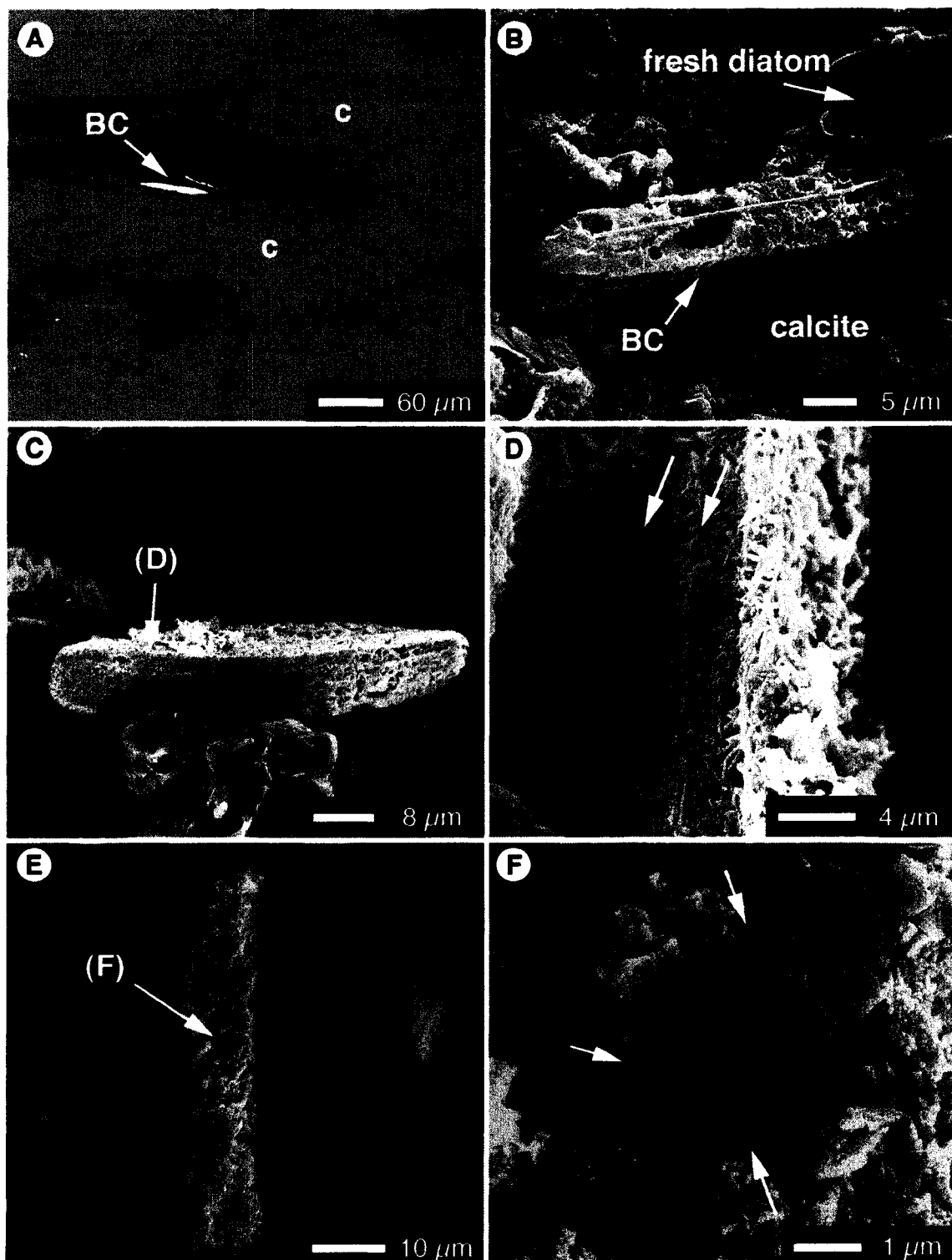


Figure 4-8. Barite diatom casts. (A) Electron microprobe image of a barite diatom cast (BC-arrow) in calcite (c). (B) SEM image of a diatom cast (BC-arrow) resting on calcite cement (c), note unaltered diatom nearby. (C) Diatom cast removed from tufa by acid digestion. (D) Detail of diatom cast from C showing rod-shaped barite microcrystals that preserve the topography of the girdle band (arrows). (E) Diatom cast with a remnant of its siliceous frustule. (F) Detail of etched raphe attached to the diatom cast shown in E (arrows).

clear in many specimens (Fig. 4-8D), but details of the raphe valve are rarely discernable. The frustules that molded the barite are usually absent, but heavily etched raphe structures remain attached to some casts (Fig. 4-8E, F).

Like the barite linings, the barite casts clearly formed in a barite supersaturated microenvironment delineated by the frustule walls. These casts are distinct from the frustule linings, however, in that the composite crystals show no evidence for nucleating against, or growing inwards from, the frustule walls. Barite supersaturation seems to have been achieved throughout the diatom's interior, rather than at menisci in areolae. The small size and subhedral habit of the barite microcrystals making up the diatom casts is more reminiscent of 'fluffy' haloes of baritised EPS, than of barite crystals precipitated in free space. It may be that the diatom casts also formed by rapid mineralisation of a viscous medium, perhaps barium-enriched soft tissues that had not reached a liquefied state of putrefaction.

Though precipitation of authigenic minerals within diatom frustules is not uncommon in sedimentary diagenesis, casts are usually composed of reduced mineral phases, like pyrite, griegite or glauconite (e.g. Dellwig et al., 2001; van Eetvelde et al., 2004). Only one other discovery of barite-filled diatoms has been reported by van Eetvelde et al. (2005) who found casts composed of 3 to 4 μm long prisms of strontium- and silica-enriched barite within concretions in lower Eocene marine sediments from Denmark. These casts preserved details of the diatoms' internal morphology with enough fidelity to allow taxonomic identification, and yet are thought to be silica enriched by virtue of incorporation of silica from dissolving diatom frustules (van Eetvelde et al., 2005). The etched raphe structures found attached to some diatom casts suggests that moldic silica was also removed by dissolution at the Stinking Springs, as the central raphe is the most electron-dense (hence least soluble) part of raphe-bearing diatom frustules (Almqvist et al., 2001).

This poses a conceptual conundrum – how can a cast be formed from a mold that is in the process of dissolving? There are two plausible answers. The first is that dissolution of diatom silica was not truly contemporaneous with barite precipitation. A second possibility is that the frustule silica was replaced by barite, which then acted as a mold for precipitates of like mineralogy.

(4) Barite replacing diatom silica

In barite haloes, some diatom frustules are partially or completely replaced by barite (Fig. 4-9). The mineralogy of the replacing phase was determined by backscattered SEM (Fig. 4-9A) and electron microprobe imagery, and by dispersive X-ray analysis, which showed strong barium and sulphur peaks, rarely accompanied by a weak silica peak. Replacive-barite preserves imperfect, but specifically recognizable, copies of diatom biopatterning (Fig. 4-9B, C, D, E, F). Original diatom silica in partially replaced frustules is heavily etched, such that the constituent silica spheres are visible (Fig. 4-9G, H). Replacing barite microcrystals are irregularly shaped, and slightly larger than the silica spheres (Fig. 4-9G, H). Barite replacement is most common along the girdle edge of diatom frustules, and proceeds upwards along striae towards the valve face. Though the valve faces of rapheless diatoms are replaced (Fig. 4-9E), frustules with raphes rarely show replacement of the raphe itself (Fig. 4-9I), suggesting that its electron density is inhibitory to both silica dissolution and barite precipitation.

Some replaced diatom frustules are filled by microcrystalline barite rods (Fig. 4-9I). If a complete barite cast were to form in a barite-replaced frustule, it would be very difficult to distinguish the cast-forming barite from the replaced silica. The outer surface of some casts may in fact be a nanometric layer of barite-replaced diatom silica (Fig. 4-9J, K).

Conversion of diatom silica by epigenesis is rare, though molecule-by-molecule replacement of silica by sheet-like microcrystalline pyrite can take place during sedimentary diagenesis (e.g. van Eetvelde et al., 2004). Nanomaterials engineers have also experimentally 'replaced' silica by magnesium-oxide (Sandhage et al., 2002), anatase (Unocic et al., 2004), and BaTiO_3 (Weatherspoon et al., 2005) using labour intensive methods united by requirements for high temperatures (up to 900°C) and extreme chemistries. To the best of our knowledge, this is the first discovery of diatom silica replacement by barite, and it took place, rather remarkably, at ambient temperature in chemical conditions similar to those that supported the diatoms' growth.

Nanometric, microcrystalline barite layers have also been produced by 'dip-coating' fused silica surfaces in colloidal barite solutions (Sermon et al., 2004); and free-standing nanocrystalline zirconia sheets have been engineered by precipitation on

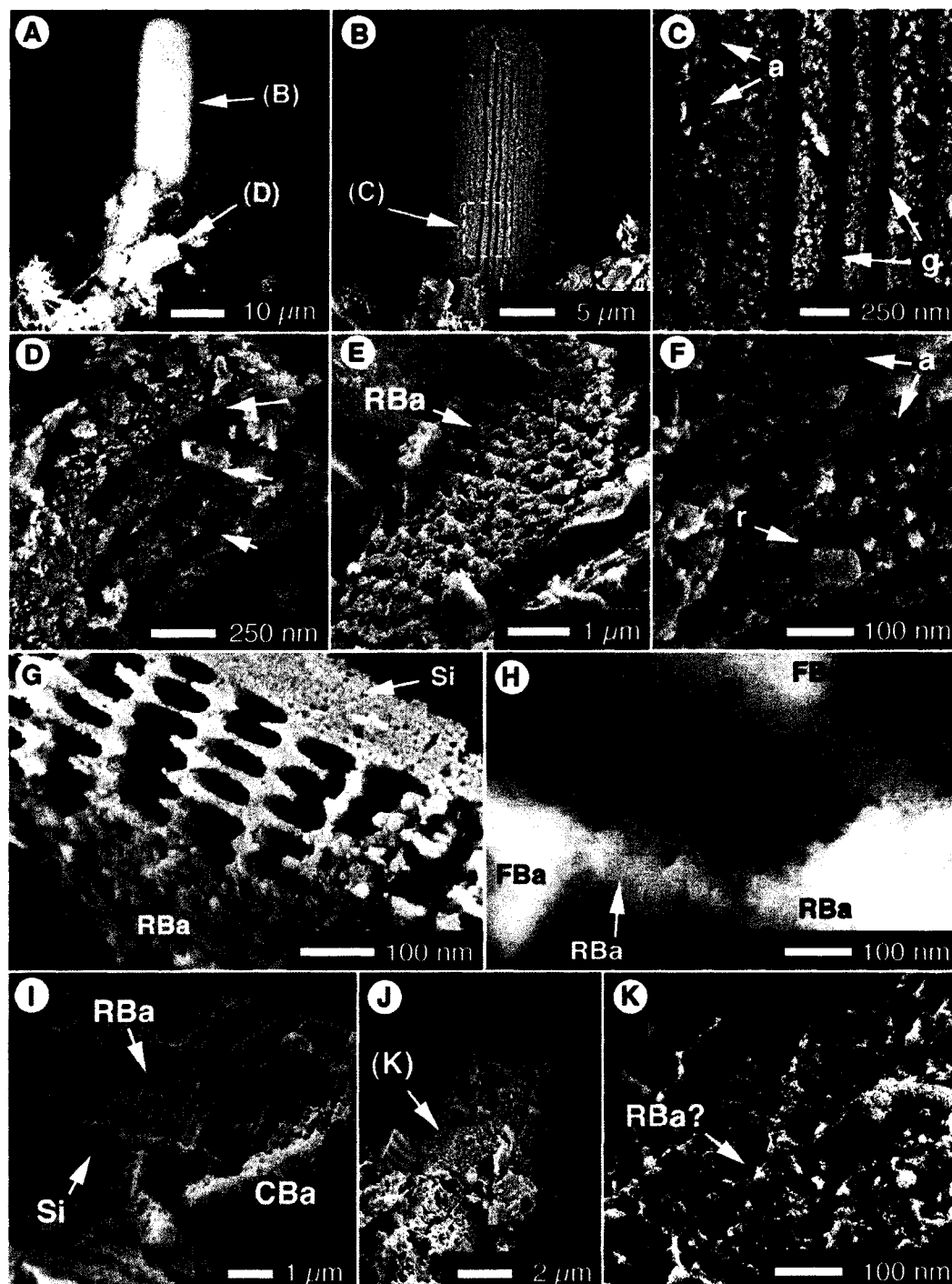


Figure 4-9. Barite replaced diatom silica. (A) Backscatter SEM image of barite-replaced diatom silica (B) SEM image of an intact barite-replaced frustule from A. (C) Detail of B showing preservation of areolae (a) and grooves (g). (D) Detail of ribs (arrows) in broken barite-replaced frustule from A. (E) Valve face biopatterning in replacive barite (RBa-arrows). (F) Detail of areoles (a) and central raphe (r) in replacive barite. (G) Detail of a partially replaced frustule; silica (Si) is etched, replacive barite is anhedral (RBa). (H) Backscatter SEM image of the frustule from G showing original silica (Si), replacive barite (RBa) and surrounding 'fluffy' barite (FBa). (I) Frustule with a barite-replaced valve (RBa-arrow) and silica raphe (Si-arrow). (J) Diatom cast surrounded by fragmented frustules. (K) Surface detail of the diatom cast from E showing a textured outer layer that may represent barite-replaced silica (RBa?).

templates of diatom silica that were subsequently dissolved (Zhao et al., 2005). With these precedents, the possibility that the frustule-shaped barite structures in the Stinking Springs crusts formed as a coating on diatoms silica, rather than by true replacement, must be considered. Adsorption of barium to diatom silica freshly exposed by degradation of the cuticle could have provided nucleation sites for nanocrystalline barite laminae. Considering, however, that no examples were found in which a nanocrystalline layer of barite clearly overlay diatom silica, that baritisation affected more soluble parts of the frustule first, and that some replacive barite contains trace amount of silica, it seems more likely that barite precipitation occurred along silica dissolution fronts.

Barite-replaced diatom frustules are commonly surrounded or filled by barite, indicating that silica conversion took place in a microenvironment that favoured barite precipitation; and etched non-replaced silica surfaces attest to the fact that barite precipitation was paired with silica dissolution. Site-specific replacement may have been facilitated by adsorption of barium onto freshly exposed silanol sites on dissolving frustules, and penecontemporaneous reaction of adsorbed barium with dissolved SO_4^{2-} . Silanol groups on biogenic silica have demonstrated affinity to adsorb metals (including aluminum, cadmium, zinc and iron; Criscenti and Sverjensky, 1999), and do so most efficiently at higher pH values, which also promote silica dissolution (Dixit and Capellen, 2002). Elevation of pore water pH by photosynthetic CO_2 withdrawal, may, thus, indirectly catalyze silica-replacement in the Stinking Springs microbial mats.

Diatoms cannot incorporate more than ~ 0.02 wt% of foreign ions or mineral phases into their siliceous frustules without compromising structural integrity (Mehard et al., 1974; Ragueneau et al., 2000), so it is unlikely that barium accumulated in the diatom silica prior to replacement. The silica spheres that make up diatom frustules are, however, embedded in an organic matrix composed of glycoproteins, carbohydrates, and silaffins, all of which may be phosphorylated, glycosylated, or sulphated (Mehard et al., 1974). It is possible that barium is also adsorbed to some of these negatively charged organic molecules. In fact, incomplete removal of the organic matrix might explain the barium-enriched diatom silica described by Vinogradova and Koval'skiy (1962) and Brongersma-Sanders (1967), which current researchers have largely discounted (Bishop, 1988). When calcite shells are replaced by pyrite, early pyritisation is commonly

localized in the shell's organic matrix, rather than within carbonate, partly as a result of adsorption of iron to negatively charged organic molecules (Gaffey, 1993). Likewise, adsorption of barium to charged elements in the diatom's organic matrix may facilitate barite precipitation when embedded organics are exposed by silica dissolution. Once barite was nucleated, additional sulphate and barium might be supplied to the seed crystal by diffusion from nearby pore waters.

The silica-replacing barite is poorly formed, and consistently $\leq 100\text{nm}$ in size, so diffusion cannot be terribly efficient at supporting continued crystal growth. This may be an effect of the high ionic strength of the spring water, which would only be enhanced in desiccating mats. Barite solubility increases dramatically with ionic strength (Hanor, 2000) and ionic interference likely prevents precipitation of barite away from reactive surfaces (diatom silica, EPS and soft tissues) able to adsorb and localize barium. Cation interactions also enhance the solubility of silica, especially in basic solutions (Dove and Elston, 1992), and evaporative salinity increases likely promote frustule dissolution in the desiccating mats.

'Diagenetic' barite

In addition to primary barite, some Stinking Springs tufa samples contain pore-filling barite cements. Relict tufa samples collected downstream of ground water seeps along Highway 83 are particularly barite-rich, and contain up to 20% barite, by volume. Most of this barite is found either as isopachous pore-filling cements, or as subspheroidal clumps, 50-400 μm in diameter that 'float' in tufa chambers (Fig. 4-10A). The barite forms bundles and fringes of radially arranged euhedral prisms, 100-150 μm long (Fig. 4-10B, C); and intergrown tabular crystals 10-100 μm long, and 2-50 μm thick (Fig. 4-10D). Some tufas have anomalous radioactivity, which is correlated to the volume of barite they contain - fresh mineral crusts register at background levels, whereas emissions up to 0.3 $\mu\text{Sv/hr}$ were measured from relict tufas containing 5-20% barite.

The radioactivity of tufa surrounding the Stinking Springs first drew the attention of Cadigan and Felmlee (1977) during a radiometric survey. They determined that it arose by co-precipitation of uranium-derived radium with barium in barite (Cadigan and Felmlee, 1977). Bove and Felmlee (1982) later examined several thin sections of Stinking

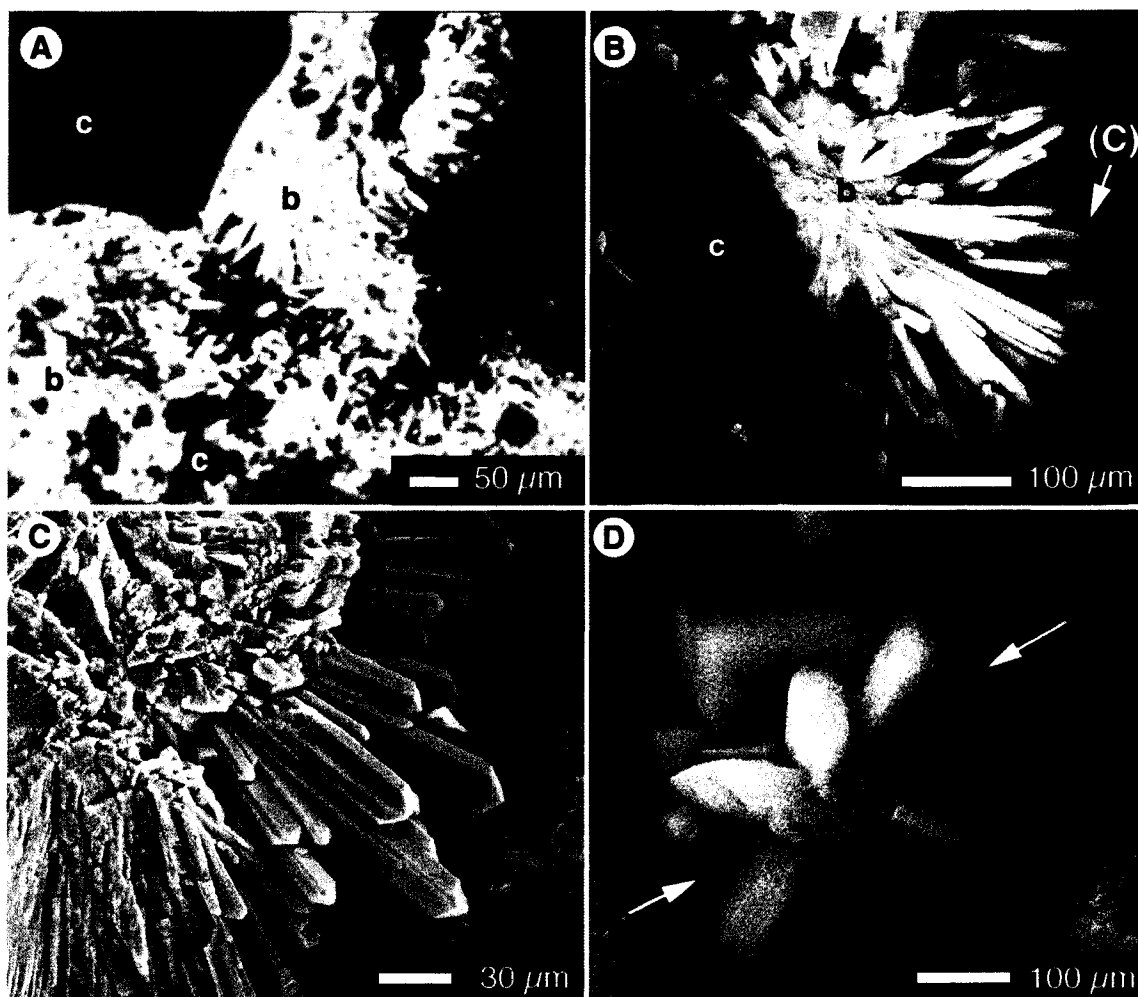


Figure 4-10. Diagenetic barite crystals. (A) Electron microprobe image of isopachous barite cements (b) filling porosity in calcite (c). (B) Backscattered SEM image of prismatic barite crystals (b) forming an isopachous fringe on calcite (c). (C) SEM image of prismatic barite in B. (D) SEM image of intergrown tabular barite crystals (arrows).

Springs tufa, noted the localisation of barite as a pore-filling precipitate, and concluded that it formed diagenetically in tufa pore space, not by direct precipitation from the spring water. Interpretation of this barite as 'diagenetic' is supported by its increasing abundance in older tufa, its spatial correlation with ground water seeps, its crystallographic distinction from stellate barite precipitated directly from the spring water, and its isopachous arrangement in pore space.

Barite forms as a product of fluid mixing in diverse sedimentary environments, including spring water and fluvio-lacustrine mixing zones (Arenas et al., 2000), and spring water/seawater mixing zones (Sugitani et al., 2003; Canet et al., 2005). In the Stinking Springs tufa, diagenetic barite probably forms by mixing between spring-derived dysoxic, saline, barium-rich pore waters and dilute, oxygenated ground waters issuing from seeps along Highway 83. The amount of barite deposited in the tufa varies as a function of tufa porosity, permeability, and proximity to the spring vents and ground water seeps.

Barite crystal habit is influenced by the physical and chemical environment in which it forms (Radanovic-Guzvica, 1999). Euhedral platy crystals are typical of barite precipitated at liquid/liquid interfaces (Sermon et al., 2004); but high ionic strength solutions, and the presence of divalent cations other than barium (e.g. Ca^{2+} and Mg^{2+}), promote growth along the b axis at the expense of the a and c axes, generating prismatic rather than tabular crystal forms (Hennessey and Graham, 2002). Polyhedral and rhombic barites are also more common with increasing supersaturation (Su et al., 2002; Wagner et al., 2005). The two forms of diagenetic barite in the Stinking Springs tufa are, thus, thought to represent precipitation from pore fluids whose chemistry varies with fluctuating mixing ratios of meteoric, ground, and pore waters.

Discussion

Barite microcrystals (commonly referred to as particulate marine barite, PMB) are ubiquitous in marine surface waters around the globe (Dehairs et al., 1980), and are usually found amongst decaying planktonic matter. The barium and carbon content of ocean sediments are positively correlated (Dehairs et al., 1980), which suggests that PMB can be used as a palaeoproductivity proxy (Cardinal et al., 2000). Application of the

proxy has been limited, however, by discrepancies with other records (McManus et al., 1998), and a lack of consensus over the importance of different microbial groups to PMB formation.

Current consensus is that PMB forms by reaction of free and bioaccumulated barium with sulphur released from planktonic material degrading in concentrated microenvironments, such as fecal pellets and marine snow clots (Dehairs et al., 1980; Paytan et al., 2002; Ganeshram et al., 2003; Paytan et al., 2004). Laboratory experiments have produced barite microcrystals in both siliceous and non-siliceous algal cultures (Ganeshram et al., 2003); but barite in grab samples of marine plankton is commonly localized inside diatom frustules (Bishop, 1988). It is unclear if the diatom frustules simply house barite supersaturated microniches, or if diatom silica actually catalyzes or mediates barite precipitation (Bishop, 1988).

Early studies indicated that some diatoms were more efficient barium bioaccumulators than other planktonic groups (Vinogradova and Koval'skiy, 1962; Brongersma-Sanders, 1967), but follow up laboratory work demonstrating barium accumulation and barite precipitation in non-siliceous plankton (e.g. Ganeshram et al., 2003) seemed to indicate that diatoms were not uniquely important.

At the Stinking Springs, however, barite precipitation is specifically diatom-associated, and cyanobacteria and SRB showed no evidence for significant barium accumulation. It may be that barium bioaccumulation is not specific to microbial groups, but varies between genera, or even species (cf. Neff, 2002). Ion transport of dissolved silica and iron occurs through distinct mechanisms, and at different periods of growth, in different diatom species (Ragueneau et al., 2000), and bioaccumulation mechanisms may vary likewise. Barium is highly toxic to many bacteria, fungi, mosses and algae, and some common soil organisms, like *Nitrobacter* sp., have toxicity thresholds as low as 10-100 $\mu\text{mol/L}$ (Baldi et al., 1996). Toxicity effects are enhanced by bioaccumulation (Neff, 2002), so one might even expect certain organism to avoid high barium concentrations, or actively block transport of barium into their cells. That said, some organisms have evolved extremely high thresholds for toxic metals (such as arsenic) that allow them to thrive at concentrations that are inhibitory to most organisms (e.g. Jackson et al., 2001).

The Stinking Springs diatoms obviously tolerate elevated barium levels, and barium bioaccumulation and adsorption to diatom EPS is essential to primary barite precipitation in the mineralizing microbial mats. No spatial dependency on diatom frustules or EPS has been described in spring flow paths where barite is ambiently supersaturated (Cecile et al., 1984; Senko et al., 2004). The importance of diatom bioaccumulation to barite precipitation at the Stinking Springs arises because the spring water is not supersaturated with barite except in microniches around and inside of barium-enriched diatoms.

Seawater is also undersaturated with barite (Dehairs et al., 1980), but dead and degrading marine diatoms are commonly enriched in barium, perhaps because they have become 'accidental' microenvironments or substrates for PMB precipitation (cf. Bishop, 1988). Barium enrichments have also been noted in organisms that selectively exploit diatoms as a food source, however (Lea, 1989), indicating that diatoms become barium enriched while alive, presumably through bioaccumulation (cf. Neff, 2002). Diatoms are abundant in surface layer planktonic assemblies around the globe, and are dominant above nutrient upwelling zones, where they make up as much as 70% of the biomass (Ragueneau et al., 2000). These high productivity zones are associated with the highest PMB 'rain' to ocean sediments (Thomson et al., 2000; Paytan et al., 2004). The possibility that, in some instances, PMB may better represent diatom productivity than total productivity must be examined if it is to be used as an accurate palaeoproductivity proxy.

Diatom productivity can be limited by low silicic acid concentrations (Egge and Aksnes, 1992), which do not affect the productivity of soft-bodied algae. If diatom silica is indeed a requirement, or even an important catalyst, for barite precipitation, blooms of non-siliceous algae will not be accurately recorded in the PMB record. This might explain some of the anomalies between PMB and other palaeoproductivity proxies noted by McManus et al (1998).

Diatoms come in many shapes and sizes, which may not be equally suited to housing barite precipitation. Indeed, the abundant *Nitzschia* sp-a. at the Stinking Springs was rarely represented amongst the barite casts and linings. Perhaps its large, thin frustule is too fragile, or dissolves too readily to support the growth of large barite crystals. Alternately, its high porosity may result in loss of bioaccumulated barium before barite

supersaturation can be established. Marine diatom species assemblages vary geographically (Ragueneau et al., 2000), and the thickness of the diatom frustules varies with dissolved silica concentrations (Brzezinski et al., 1990). As a result, diatom silica will not be equally preserved, or equally efficient at catalyzing barite precipitation across all parts of the world's ocean.

Laboratory experiments have shown that only 2-4 % of diatom bioaccumulated barium is precipitated as barite, while the remainder is dispersed into solution (Ganeshram et al., 2003). In the marine water column, however, planktonic diatoms commonly produce discrete EPS particles and streamers that have lower solubility than EPS produced by other phytoplankton (Alldredge et al., 1993). By analogy to the barium-enriched EPS haloes at the Stinking Springs, these diatom EPS particles may be capable of facilitating PMB formation by adsorbing and concentrating of barium released from decaying diatoms.

The true importance of diatoms to PMB formation will be difficult to ascertain, because barite microcrystals are not preserved *in situ*, as they are in the Stinking Springs tufas, but settle to the sediment-water interface through a water column undersaturated with respect to both barite and silica (Dehairs et al., 1980). Dissolution is the norm for marine diatoms, with an average of 60% dissolution in the upper 50-100 m of the water column (Dixit et al., 2001) and further 95% dissolution at the sediment-water interface (Treguer et al., 1995; Ragueneau et al., 2000). Barite is much more refractory (Viollier et al., 2002; Paytan et al., 2004), at least during oxic diagenesis (Neff, 2002; Lu et al., 2004), so diatom-associated PMB will almost always be found without accompanying silica.

PMB takes on a variety of crystal habits, from stubby prismatic to ovoid and rounded anhedral forms (Paytan et al., 2004). These crystal habits are considered to be distinct from hexagonal prismatic barite crystals formed within benthic foraminifera, blocky euhedral diagenetic barite, and submicron-sized anhedral barite aggregates that are abundant in marine sediments (Bertram and Cowen, 1997). Paytan et al. (1993) found that the Sr-isotope composition of ovoid barite crystals 1-5 μm in size had the best match with the Sr-isotope composition of contemporaneous marine carbonates. Others have taken this as an indication that only ovoid crystals in this size range are truly

representative of barite precipitated within phytoplankton blooms (e.g. Bains et al., 2000).

The stubby, rounded prismatic crystals found lining diatom frustules and impregnating diatom EPS at the Stinking Springs are similar in size and morphology to the ovoid and prismatic marine barite crystals. Smaller precipitates also formed in direct association with the diatoms, however, including EPS impregnating nanometric barite rods, spherical and anhedral barite in frustule pores, and nano-particulate barite that replaced diatom silica. Clearly bio-associated barite crystals can take on a variety of sizes and forms; the submicron-sized barite aggregates, and stubby prismatic barite crystals found in marine sediments may also represent biological productivity.

The Eocene barite diatom casts described by van Eetvelde et al. (2004) prove that baritisation can be a diagenetically-persistent mode of taphocoenosis in diatoms. At Stinking Springs, diatoms seem to have been baritised as a direct result of barium bioaccumulation and/or adsorption of barium to diatom EPS. These bio-mediated processes, operating under weakly basic pH conditions, resulted not only in the formation of frustule casts and linings, but also in conversion of diatom silica to barite at ambient temperature - a feat not-yet accomplished by nano-materials researchers. Current diatom silica conversion methods are preceded by removal of the silica bound organics (Zhao et al., 2005) but 'natural' barite replacement at the Stinking Springs took place in the presence of organic molecules. Indeed, the frustule's organic matrix may have facilitated conversion by adsorbing barium or incorporating barium from surrounding fluids. This suggests that chemical conversion might be facilitated by use of diatoms with intact organic matrices, perhaps cultured in media of tailored chemistry. This method might be especially promising for conversion of diatom silica to BaTiO_3 , a compound with dielectric, ferroelectric, piezoelectric, and electro-optical properties (Weatherspoon et al., 2005), as the Stinking Springs diatoms demonstrate the propensity for diatom silica patterned in barium-rich media to convert to barium bearing mineral phases.

Conclusions

Analysis of the microbial mats and relict tufas associated with Stinking Springs, Utah has produced the following important conclusions.

(1) Thick microbial mats in the discharge path of the Stinking Springs, Utah, are volumetrically dominated by diatoms, cyanobacteria and SRB.

(2) The spring water precipitates calcite in and on the mats, producing layered tufa deposits that contain calcified microbial cells.

(3) Relict tufa underlying the modern spring is composed of 80-98% calcite, but locally contains weakly radioactive pore-filling prismatic and tabular diagenetic barite cements.

(4) Primary barite is found in and around diatom frustules trapped in partially mineralized mats and preserved in relict tufa. There are four types of diatom-associated barite: (a) microcrystalline barite haloes that surround trapped diatom frustules, which formed by mineralisation of barium-enriched diatom EPS; (b) microcrystalline barite spheres, rhombs, and stubby prisms found lining diatom frustules, which formed as barium released from putrefying diatom tissues came into contact with sulphate-bearing mat pore waters through frustule areolae; (c) nanometric barite rods delineating internal casts of diatom frustules, which formed by rapid establishment of barite supersaturation in the interior of actively dissolving diatom frustules; and (d) barite-replaced diatom frustules, which formed by precipitation of nanometric barite particles along a silica dissolution front.

(5) At the Stinking Springs, bioaccumulation of barium by diatoms is directly responsible for barite precipitation in and around degrading diatom frustules.

References

- Allredge, A.L., Passow, U., and Logan, B.E. 1993. The abundance and significance of a class of large, transparent organic particles in the ocean. *Deep-Sea Research. Part I: Oceanographic Research Papers*, 40: 1131-1140.
- Almqvist, N., Delammo, Y., Smith, B.L., Thomson, N.H., Bartholdson, A., Lal, R., Brzezinski, M., and Hansma, P.K. 2001. Micromechanical and structural properties of a pennate diatom investigated by atomic force microscopy. *Journal of Microscopy*, 202: 518-532.
- Arenas, C., Gutierrez, F., Osacar, C., and Sancho, C. 2000. Sedimentology and geochemistry of flucio-lacustrine tufa deposits controlled by evaporite solution subsidence in the central Ebro Depression, NE Spain. *Sedimentology*, 47: 883-909.
- Arp, G. Theil, V., Reimer, A. Michaelis, W., and Reitner, J. 1999. Biofilm exopolymers control microbialite formation at thermal springs discharging into the alkaline Pyramid Lake, Nevada, USA. *Sedimentary Geology*, 126: 159-176.
- Bains, S., Norris, R.D., Cornfield, R.M., and Faul, K.L. 2000. Termination of global warmth at the Palaeocene/Eocene boundary through productivity feedback. *Nature*, 407: 171-174.
- Bala, H., Fu, W., Zhae, J., Ding, X., Jiang, Y., Yu, K., and Wang, X. 2005. Preparation of BaSO₄ nanoparticles with self-dispersing properties. *Colloids and Surfaces A*, 252: 129-134.
- Baldi, F., Pepi, M., Burrini, D., Kniewald, G., Scali, D., and Lanciotti, E. 1996. Dissolution of barium from barite in sewage sludges and cultures of *Desulfobibrio desulfuricans*. *Applied and Environmental Microbiology*, 62: 2398-2404.
- Bertram, M.A. and Cowen, J.P. 1997. Morphological and compositional evidence for biotic precipitation of marine barite. *Journal of Marine Research*, 55: 677-693.
- Bishop, J.K.B. 1988. The barite-opal-organic carbon association in oceanic particulate matter. *Nature*, 332: 341-343.
- Blacket, R.E. and Wakefield, S. 2004. Geothermal resources of Utah: A digital atlas of Utah's geothermal resources. Utah Geological Survey Open-File Report 431.
- Bolze, C.E., Malone, P.G., and Smith, M.J. 1974. Microbial mobilization of barite. *Chemical Geology*, 13: 141-143.
- Bonny, S. and Jones, B. 2007. Barite (BaSO₄) biomineralisation at Flybye Springs, a cold sulphur spring system in Canada's Northwest Territories, *Canadian Journal of Earth Sciences*, 44: 835-856.
- Bove, D. and Felmlee, J.K. 1982. Mineralogy and autoradiography of selected mineral-spring precipitates in the western United States. United States Geological Survey, Open-file Report 82-792, 74 p.
- Brongersma-Sanders, M. 1967. Barium in pelagic sediments and in diatoms. *Proceedings of the Koninklijke Nederlandse Akademie van Wetenschappen. Series B: Paleontology, Geology, Physics, Chemistry, Anthropology*, 70: 93-99.
- Brzezinski, M.A., Olson, R.J., and Chisholm, S.W. 1990. Silicon availability and cell-cycle progression in marine diatoms. *Marine Ecology Progress Series*, 67: 83-96.

- Buczynski, C. and Chafetz, H.S. 1991. Habit of bacterially induced precipitates of calcium carbonate and the influence of medium viscosity on mineralogy. *Journal of Sedimentary Petrology*, 61: 226-233.
- Cadigan, R.A. and Felmlee, J.K. 1977. Radioactive springs geochemical data related to uranium exploration. *Journal of Geochemical Exploration*, 8: 381-395.
- Canet, C., Prol-Ledesma, R.M., Torres-Alvarado, I., Gilg, H.A., Villanueva, R.E., and Cruz, R. L-S. 2005. Silica-carbonate stromatolites related to coastal hydrothermal venting in Baia Concepcion, Baja California Sur, Mexico. *Sedimentary Geology*, 174: 97-113.
- Castanier, S. Le Metayer-Levrel, G., and Perthuisot, J-P. 2000. Bacterial roles in the precipitation of carbonate minerals. In: Riding, R., Awramik, S.M. (Eds.), *Microbial Sediments*, Springer-Verlag: Heidelberg Germany, pp. 32-39.
- Cardinal, D., Savoye, N., Trull, T.W., Luc, A., Kopcynska, E.E., and Dehairs, F. 2000. Variations of carbon remineralisation in the Southern Ocean illustrated by the Baxs proxy. *Deep Sea Research Part I: Oceanographic Research Papers*, 52: 355-370.
- Cecile, M.P., Goodfellow, W.D., Jones, L.D., Krouse, H.R., and Shakur, M.A. 1984. Origin of radioactive barite sinter, Flybye Springs, Northwest Territories, Canada. *Canadian Journal of Earth Sciences*, 21: 383-395.
- Coradin, T. and Lopez, P.J. 2003. Biogenic silica patterning: simple chemistry of subtle biology? *ChemBioChem*, 3: 1-9.
- Criscenti, L.J. and Sverjensky, D.A. 1999. The role of electrolyte anions (ClO_4^- , NO_3^- , and Cl^- in divalent metal (M^{2+}) adsorption on oxide and hydroxide surfaces in salt solutions. *American Journal of Sciences*, 299: 828-899.
- Darley, W.M. 1977. Biochemical Composition. In: Werner, D. (Ed.), *The Biology of Diatoms*. Botanical Monographs: Blackwell Scientific Publications, London, England, pp. 198-224.
- Defarge, C., Trichet, J., Jaunet, A-M., Robert, M., Tribble, J., and Sansone, F.J. 1996. Texture of microbial sediments revealed by cryo-scanning electron microscopy. *Journal of Sedimentary Research*, 66: 935-947.
- Dehairs, F., Chesselet, R., and Jedwab, J. 1980. Discrete suspended particles of barite and the barium cycle in the open ocean. *Earth and Planetary Science Letters*, 49: 528-550.
- Dellwig, O., Watermann, F., Brumsack, H-J., Gerdes, G., and Krumbein, W.E. 2001. Sulphur and iron geochemistry of Holocene coastal peats (NW Germany): a tool for palaeoenvironmental reconstruction. *Palaeogeography, Palaeoclimatology, Palaeoecology*, 167: 359-379.
- Dixit, S. and van Cappellen, P. 2002. Surface chemistry and reactivity of biogenic silica. *Geochimica et Cosmochimica Acta*, 66: 2559-2568.
- Dixit, S., Van Cappellen, P., and Van Bennekom, A.J. 2001. Processes controlling solubility of biogenic silica and pore water build-up of silicic acid in marine sediments. *Marine Chemistry*, 73: 333-352.
- Douglas, S. and Douglas, D.D. 2001. Structural and geomicrobiological characteristics of a microbial community from a cold sulfide spring. *Geomicrobiology Journal*, 18: 201-422.

- Dove, P.M. and Elston, S.F. 1992. Dissolution kinetics of quartz in sodium chloride solutions: Analysis of existing data and a rate model for 25°C. *Geochimica et Cosmochimica Acta*, 56: 4147-4156.
- Duke, E.L. and Reimann, B.E.F. 1977. The ultrastructure of the diatom cell. In: Werner, D., ed., *The Biology of Diatoms*, Blackwell Scientific Publications, London, England, pp. 65-76.
- Egge, J.K. and Aksnes, D.L. 1992. Silicate as regulating nutrient in phytoplankton competition. *Marine Ecology Progress Series*, 83: 281-289.
- Emeis, K.C., Richnow, H.H., and Kempe, S. 1987. Travertine formation in Plitvice National Park, Yugoslavia: chemical versus biological control. *Sedimentology*, 34: 595-609.
- Eppley, R.W. 1977. The growth and culture of diatoms. In: Werner, D. (Ed.), *The Biology of Diatoms*, Blackwell Scientific Publications, London, England, pp. 24-64.
- Felmlee, J.K. and Cadigan, R.A. 1982. Radioactivity and geochemistry of selected mineral-spring waters in the Western United States; basic data and multivariate statistical analysis. Open-File Report – US Geological Survey, Report: OF 82-0324, 107 pp.
- Gaffey, S.J. 1993. Susceptibility of carbonate skeletons to early diagenetic alteration; role of organic matrices. *Abstracts with Programs – Geological Society of America*, 25: 227.
- Ganeshram, R.S., Francois, R., Commeau, J. and Brown-Leger, L. 2003. An experimental investigation of barite formation in seawater. *Geochimica et Cosmochimica Acta*, 67: 2599-2605.
- Glamoclija, M., Garrel, L., Berthon, J., and Lopez-Garcia, P. 2004. Biosignatures and bacteria diversity in hydrothermal deposits of Solfatara Crater, Italy. *Geomicrobiology Journal*, 21: 529-541.
- Gonzalez-Munoz, M.T., Fernandez-Luque, B., Martinez-Ruiz, F., Chekroun, K.B., Arias, J.M., Rodriguez-Gallego, M., Martinez-Canamero, M., de Linares, C. and Paytan, A. 2003. Precipitation of Barite by *Myxococcus xanthus*: Possible Implications for the Biogeochemical Cycle of Barium. *Applied and Environmental Microbiology*, 69: 5722-5725.
- Guttinger, W. 1986a, Collection of SEM Micrographs of Diatoms, CH-6984 Pura, 1.
- Guttinger, W. 1986b, Collection of SEM Micrographs of Diatoms, CH-6984 Pura, 2.
- Guttinger, W. 1986c, Collection of SEM Micrographs of Diatoms, CH-6984 Pura, 3.
- Guttinger, W. 1986d, Collection of SEM Micrographs of Diatoms, CH-6984 Pura, 4.
- Guttinger, W. 1986e, Collection of SEM Micrographs of Diatoms, CH-6984 Pura, 5.
- Guttinger, W. 1986f, Collection of SEM Micrographs of Diatoms, CH-6984 Pura, 6.
- Hanor, J.S. 2000. Barite-celestine geochemistry and environments of formation. *Reviews in Mineralogy and Geochemistry*, 40: 193-275.
- Hennessy, A.J.B. and Graham, G.M. 2002. The effect of additives on the co-crystallisation of calcium with barium sulphate. *Journal of Crystal Growth*, 239: 2153-2159.

- Jackson, C.R., Langner, H., Danohoe-Christiansen, J., Inskip, W.P. and McDermott, T.R. 2001. Molecular analysis of microbial community structure in an arsenite-oxidizing acidic thermal spring. *Environmental Microbiology*, 3: 532-542.
- Jensen, M.E. 1994. Geologic map of the Bear River City Quadrangle, Box Elder County, Utah. Utah Geological Survey Map 151, 12 pp.
- Klauck, R.H. and Budding, K.E. 1984. Geothermal assessment of the lower Bear River drainage and northern east shore groundwater areas, Box Elder County, Utah. Utah Geological and Mineral Survey Report of Investigation 186, 64 pp.
- Lea, D.W. 1989. Foraminiferal and coralline barium as paleoceanographic tracers. Ph.D. Thesis, Massachusetts Institute of Technology, Cambridge, MA, USA, 173 pp.
- Lu, Z.C., Liu, C.Q., Liu, J.J. and Wu, F.C. 2004. The bio-barite in witherite deposits from Southern Qinling and its significance. *Progress in Natural Science*, 14: 889-895.
- McManus, J., Bareelson, W.M., Klinkhammer, G.P., Johnson, K.S., Coale, K.H., Anderson, R.F., Kumar, N., Burdige, D.J., Hammond, D.E., Brumsack, H.J., McCorkle, D.V. and Rushdi, A. 1998. Geochemistry of barium in marine sediments: implications for its use as paleoproxy. *Geochimica et Cosmochimica Acta*, 62: 3454-3473.
- Mehard, C.W., Sullivan, C.W., Azam, F. and Volcani, B.E. 1974. Role of silicon in diatom metabolism. I.V. Subcellular localization of silicon and germanium in *Nitzschia alba* and *Cylindrotheca fusiformis*. *Physiology of Plants*, 30, 265 pp.
- Merz-Preiß, M. 2000. Calcification in cyanobacteria. In: Riding, R., Awramik, S.M. (Eds.), *Microbial Sediments*, Springer-Verlag: Heidelberg Germany, p. 50-56.
- Neff, J.M. 2002. Bioaccumulation in marine organisms. Elsevier, Amsterdam, The Netherlands, 452 pp.
- Paytan, A., Kastner, M., Martin, E.E., Macdougall, J.D., and Herbert, T. 1993. Marine barite as a monitor of seawater strontium isotope composition. *Nature*, 366: 445-449.
- Paytan, A., Mearon, S., Cobb, K., and Kastner, M. 2002. Origin of marine barite deposits: Sr and S isotope characterization. *Geology*, 30: 747-750.
- Paytan, A., Martinex-Ruix, F., Eagle, M., Ivy, A. and Wankel, S.D. 2004. Using sulfur isotopes to elucidate the origin of barite associated with high organic matter accumulation events in marine sediments. In: Amend, J.P., Edwards, K. J., Lyons, T.W. (Eds.), *Sulphur Geochemistry, Past and Present*. Geological Society of America Special Paper 379, p. 151-159.
- Radanovic-Guzvica, B. 1999. The average structural density of barite crystals of different habit types. *Geologia Croatia*, 52: 59-65.
- Ragueneau, O., Treguer, P., Leynaert, A., Anderson, R.F., Brzezinski, M.A., DeMaster, D.J., Dugdale, R.C., Dymond, J., Fischer, G., Rancois, R., Heinze, C., Maier-Reimer, E., Martin-Jezequel, V., Nelson, D.M. and Queguiner, B. 2000. A review of the Si cycle in the modern ocean: recent progress and missing gaps in the application of biogenic opal as a paleoproductivity proxy. *Global and Planetary Change*, 26: 317-365.
- Riding, R. 2000. Microbial carbonates: the geological record of calcified bacterial-algal mats and biofilms. *Sedimentology*, 47 (supp. 1): 179-214

- Rippka, R., Deruelles, J., Waterbury, J.B., Herdman, M. and Stanier, R.Y. 1979. Generic assignments, strain histories and properties of pure cultures of cyanobacteria. *Journal of General Microbiology*, 111: 1-16.
- Sanchez-Moral, S., Luque, L., and Canaveras, J.C., 2004. Bioinduced barium precipitation in *St. Callixtus* and *domitilla* catacombs. *Annals of Microbiology*, 54: 1-12.
- Sandhage, K.H., Dickerson, M.B., Huseman, P.M., Caranna, M.A., Clifton, J.D., Bull, T.A., Heibel, T.J., Overton, W.R., and Schoenwaelder, M.E.A. 2002. Novel, bioclastic route to self-assembled, 3D, chemically tailored meso/nanostructure: shape-preserving reactive conversion of biosilica (diatom) microshells. *Advanced Materials*, 14: 429-433.
- Schultze-Lam, S., Douglas, T., Thompson, J.B., and Beveridge, T.J. 1993. Metal ion immobilization by bacterial surfaces in freshwater environmental. *Water Pollution Research Journal of Canada*, 28: 51-81.
- Senko, J.M., Campbell, B.S., Henriksen, J.R., Elshahed, M.S., Dewers, T.A., and Krumholz, L.R. 2004. Barite deposition resulting from phototrophic sulfide-oxidizing bacterial activity. *Geochimica et Cosmochimica Acta*, 64: 773-780.
- Sermon, P.A., McLellan, N.M., and Collins, I.R. 2004. Formation of BaSO₄ nanoribbons from a molecular mangle. *Crystal Engineering Communications*, 6: 469-473.
- Simonsen, R. 1987. Atlas and catalogues of the diatom types of Freidrich Hustedt, Volume 2-Atlas, Stuttgart/J. Cramer, Berlin, Germany, Plates 1-139.
- Su, H-Y., Lee, J-S., and Yu, S-C. 2002. Dopant effect on hokutolite crystals synthesized with hydrothermal process. *Western Pacific Earth Sciences*, 2: 301-318.
- Sugitani, K., Mimura, K., Suzuki, K., Nagamine, K. and Sugisaki, R. 2003. Stratigraphy and sedimentary petrology of an Achaean volcanic-sedimentary succession at Mt. Goldsworthy in the Pilbara Block, Western Australia; implications of evaporite (nahcolite) and barite deposition. *Precambrian Research*, 120: 55-79.
- Tazaki, K., Webster, J., and Fyfe, W.S. 1997. Transformation processes of microbial barite to sediments in Antarctica. *Japanese Journal of Geology*, 26: 63-68.
- Tazaki, K. and Watanabe, H. 2004. Biomineralization of radioactive sulfide minerals in strong acidic Tamagawa Hot Springs. *Science Reports of the Kanazawa University*, 49: 1-24.
- Thomson, J., Nixon, S. Summerhayes, C.P., Rholing, E.J., Schoenfield, J., Xahn, R., Grootes, P., Abrantes, F. Gaspar, L. and Vaqueiro, S. 2000. Enhanced productivity on the Iberian margin during glacial/interglacial transitions revealed by *barium* and diatoms. *Journal of the Geological Society of London*, 157: 667-677.
- Treguer, P., Nelson, D.M., van Bennekom, A.J., DeMaster, D.J., Leynaert, A., and Queguiner, B. 1995. The silica balance in the world ocean: A re-estimate. *Science*, 268: 375-379.
- Unocic, R.R., Zalar, F.M., Sarosi, P.M., Cai, Y. and Sandhage, K.H. 2004. Anatase assemblies from algae: coupling biological self-assembly of 3-D nanoparticle structures with synthetic reaction chemistry. *Chemical Communications*, 4: 796-797.
- van Eetvelde, Y., Dupuis, C., and Cornet, C. 2004. Pyritized diatoms; a good fossil marker in the upper Paleocene-lower Eocene sediments from the Belgian and Dieppe-Hampshire Basins. *Netherlands Journal of Geosciences*, 83: 173-178.

- van Eetvelde, Y., Heilmann-Clausen, C., Dupuis, C., and Cornet, C. 2005. The presence of (celesto-) barite molds in Paleogene deposits from Olst and Albaekhoved (Denmark). *Diatom Research*, 20: 201-210.
- Viollier, E., Voitel, L., and Rabouille, C., 2002. Kinetic study of bio-barite preservation in deep-sea sediments. *Geochimica et Cosmochimica Acta*, 66: A808.
- Vinogradova, Z.A. and Koval'skiy, V.V. 1962. Elemental composition of Black Sea plankton. *Doklady Rossijskoj Akademii Nauk, SSSR*, 147: 217-219.
- Wagner, T., Kirnbauer, T., Boyce, A.J., and Fallick, A.E. 2005. Barite-pyrite mineralization of the Wiesbaden thermal spring system, Germany: a 500-kyr record of geochemical evolution. *Geofluids*, 5: 124-139.
- Weatherspoon, M.R., Allan, S.M., Hunt, E., Cai, Y., and Sandhage, K.H., 2005. Sol-gel synthesis on self-replicating single-cell scaffolds: applying complex chemistries to nature's 3-D nanostructured templates. *Chemical Communications*, 5: 651-653.
- Wehr, J.D. and Sheath, G. 2003. *Freshwater Algae of North America: Ecology and Classification*. Academic Press, San Diego, CA, 950 pp.
- Younger, P. 1986. Barite travertine from southwestern Oklahoma and west-central Colorado. Unpublished M.S. Thesis, Oklahoma State University, Stillwater, OK, USA, 163 pp.
- Zhao, J., Gaddis, C.S., Cai, Y., and Sandhage, K.H. 2005. Free-standing microscale structures of nanocrystalline zirconia with biologically replicable 3-D shapes. *Journal of Materials Research*, 20: 282-287.

Chapter 5 **Controls on the precipitation of barite crystals in calcite travertine at Twitya Spring***

Introduction

Sedimentary barite has high utility for paleoenvironmental reconstruction because of its link with marine (Bishop, 1988; Paytan et al., 1993; Bains et al., 2000; Greinert et al., 2002; Lu et al., 2004) and lacustrine productivity (Smith et al., 2004) and its geochemical sensitivity to changes in redox chemistry and to local and global perturbations in the sulphur cycle (Miller et al., 1977; Kastner, 1999; Hanor, 2000; Bottrell and Newton, 2006). Barite hosted in carbonate sediments can be especially useful for palaeoenvironmental geochemistry, as carbonates are prone to recrystallization and chemical and isotopic readjustment during diagenesis (Martin et al., 1995; Kastner, 1999). In highly altered carbonates, diagenetically refractory barite microcrystals may provide the only accurate access to palaeo-geochemical signals (Martin et al., 1995; Newton et al., 2004; Kipli et al., 2004).

In clastic marine sediments, barites formed through different mechanisms (i.e. biogenic vs. diagenetic) commonly preserve distinct geochemical signals, and are distinguishable on the basis of crystal size and habit (Paytan et al., 1993). Barite precipitated among plankton in the upper marine water column, for example, is morphologically distinct from barite precipitated at the sediment water interface, allowing separation of sediment core samples for environmentally-specific $\delta^{34}\text{S}$ analyses (Paradis and Lavoie, 1996; Bains et al., 2000; Paytan et al., 2002). Morphologically-based separation methods have limited usefulness in the geologic record, however, because environmental influences on barite crystal size and habit are unconstrained in many depositional environments, such as dysoxic marine bottom waters, and hydrothermal and methane seeps (Fu et al., 1994; Martin et al., 1995; Alfonso et al., 2005; Riedinger et al., 2006). The potential utility of barite microcrystals hosted in limestones and dolostones is further limited by a lack of data pertaining to the influence

* A version of this chapter has been submitted for publication.

Bonny, S. and Jones, B. Controls on the precipitation of barite (BaSO_4) crystals in calcite travertine at Twitya Spring, a warm sulphur spring in Canada's Northwest Territories. *Sedimentary Geology*.

of co-deposited carbonate on barite precipitation and preservation (Aharon, 2000; Alfonso et al., 2005).

Twitya Spring in Canada's Northwest Territories (Fig. 5-1) provides a rare opportunity for examining controls on the distribution and morphology of barite crystals hosted in carbonate. At Twitya Spring, warm (24 °C), sulphur- and bicarbonate-rich spring water precipitates laminated carbonate travertine that contains up to 5% barite by volume. During the course of this study, detailed petrographic analysis revealed that barite crystal morphology corresponds to precipitation substrate at Twitya Spring: type 1 (T1) detrital intergrown tabular crystals are deposited from solution; type 2 (T2) tabular and rhombic crystals are nucleated against calcite; and type 3 (T3) subhedral and anhedral crystals are nucleated on microbial cell surfaces and in microbial extracellular polymeric substances (EPS). This paper describes the physiochemistry, biology and mineralogy of the Twitya Spring flow path, discusses the controls on the formation and distribution of T1, T2 and T3 barite in the Twitya travertine, and explores potential implications for the interpretation of barite microcrystals in the geologic record.

Study Site

The Twitya Spring aquifer emerges from one main spring vent and two smaller seeps through surficial deposits of fractured shale approximately ~15 m above the level of the Twitya River in the Sahtu Region of Canada's Mackenzie Mountains (Fig. 5-1A). It is underlain by limestone and dolostone of the middle Devonian Arnica Formation, and calcareous shale, limestone, and chert from the upper Ordovician to Silurian Road River Formation (Blusson, 1971). Structural faults and folds allow deep penetration of ground water throughout the Mackenzie Mountains and there are numerous cold and geothermal mineral springs in the Sahtu Region (Blusson, 1971; Cecile et al., 1984). Many springs have developed extensive deposits of porous carbonate tufa, and the Flybye Springs ~35 km to the north have produced a deposit of rare barite tufa (Cecile et al., 1984; Bonny and Jones, 2007a). The Twitya Spring site is regionally unique in that it contains barite hosted in macrocrystalline calcite travertine.

The Twitya travertine reaches maximum thickness in a mound, ~10 m long and 2 m high, beneath the main spring vent (Fig. 5-1B, C, D). The mound is composed of

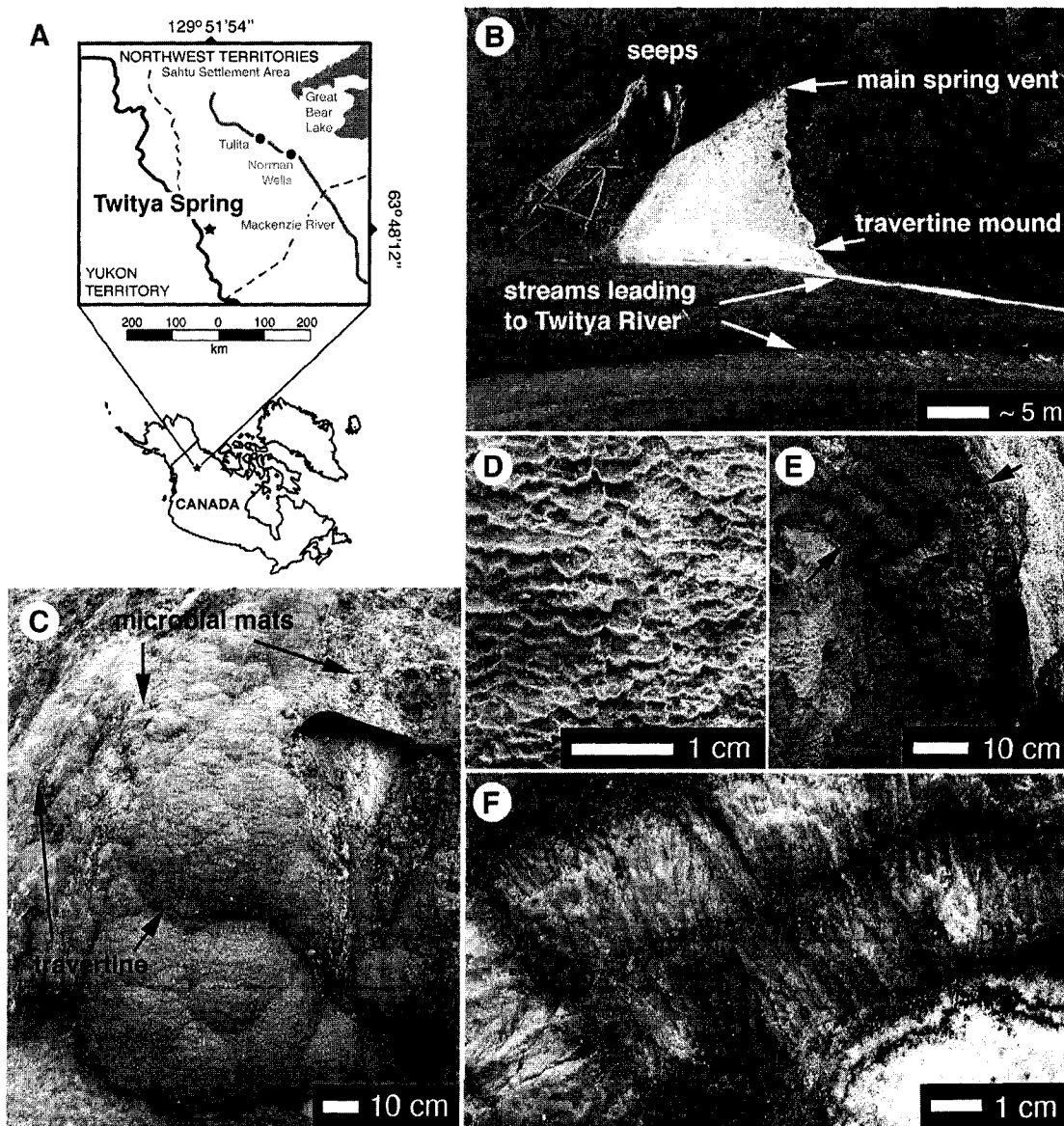


Figure 5-1. (A) Location map for Twitya Spring. (B-F) Photographs of Twitya Spring showing (B) overview; (C) surface of travertine mound; (D) detail of microgours on surface of travertine mound; (E) side view of bedding in travertine mound; (F) Detail of calcite dendrites in bedded travertine from image E.

parallel, undulatory beds of 'feather' dendrite calcite crystals, 1-5 cm long. Individual beds contain numerous internal growth laminations (Fig. 5-1E), and grey and green chromatic banding (Fig. 5-1F). The bright white travertine, skirted by a green microbially-colonised drainage stream, provides a striking contrast to surrounding gray and brown limestone and shale, and is considered a sacred heritage site by the Sahtu Dene people.

Methods

Field Work

The geometry and extent of the Twitya Spring travertine deposit were documented by ground survey and aerial photography. The pH, conductivity, and dissolved oxygen (D.O.) content of the Twitya Spring water were measured in August, 2005, using a portable Accumet AP62 pH/mV meter and an Orion Model 1230 D.O./pH/mV probe. Two water samples were collected at the spring vent and 10 m downstream through a 0.45 μm pore size FisherBrand water-testing membrane and stored in sterile 250 ml Nalgene containers. Ten microbial samples were collected from the spring flow path that encompassed the textural and chromatic variability of the communities. One half of each microbial sample was stored in spring water and the other half was preserved in a 6:3:1 solution of water, 95% alcohol and formalin with 5 ml of glycerol added per 100 ml. Thirty samples of fresh precipitates and calcite travertine were collected at intervals of ~ 1 m across the flow path (four from zone 1, six from zone 2, eight from zone 3, and twelve from zone 4; see Fig. 2).

Laboratory Work

Spring water composition was determined by inductively coupled mass spectrometry (ICP-MS) at the University of Saskatchewan, and SOLMINEQ88 was used to evaluate the saturation indices (S.I. = \log [ion activity product/solubility constant]) of relevant mineral phases (see Appendix 2). The mineralogy of solid samples was determined by optical petrography and powder X-ray diffraction (XRD) on a Rigaku Geigerflex Cobalt Tube Power Diffractometer with a graphite monochromator and JCPDS online mineral identification database.

Whole and acid etched (10% HCl) travertine samples were fractured, mounted on steel stubs, and sputter coated with gold, and analyzed on a JEOL 6301 field emission scanning electron microscope (SEM). Both secondary electron and backscattered electron SEM images were collected at accelerating voltages of 5 and 20 kV, respectively. Backscattered electron SEM images reflect variations in atomic weight through image brightness – barium (atomic mass of 137.3) is very bright in contrast to increasingly dark strontium (87.6), calcium (40.1), sulphur (32.1), silicon (28.1), and organic matter (~12.0). Qualitative elemental analyses were conducted using an energy dispersive X-ray analyzer coupled to the SEM.

Cut, polished, and carbon-coated thin sections of travertine were prepared for quantitative elemental analysis (as wt. %) on a JEOL 8900R electron microprobe (EMP) at an accelerating voltage of 15 kV with a 10 nA beam current and 1 μm beam diameter. Backscattered electron images generated on the EMP (at an accelerating voltage of 20 kV with a 30 nA beam current) have gray levels that reflect image specific variations in average atomic weight - darker areas correspond to relatively lower average atomic weights, and bright areas to relatively higher average atomic weights.

Microbe samples were examined by light microscopy and soft-bodied microbes were identified to genus level by morphological criteria (Table 5-1) following Rippka et al. (1979), Larkin and Strohl (1983), Schlegel and Bowien (1987), Wher and Sheath (2003) and Teske and Nelson (2005). Microbes viewed by SEM analyses were given tentative taxonomic assignments based on their similarity to fresh and preserved microbial samples. No attempt was made to identify submicron-sized Actinomycetes or unicellular microbes revealed by scanning electron microscopy.

Results

Spring water physiochemistry

Twitya Spring emerges at ~ 24 °C, indicating a minimum circulation depth of 600 m for the aquifer (cf. van Everdingen, 1972). The spring water is rich in sodium, calcium, bicarbonate and sulphate, and anomalously rich in strontium, barium, and soluble silica (Table 5-2) relative to regional stream and ground waters (Cecile et al., 1984; Day et al., 2005). At the vent, the spring water contains < 0.61 mgL⁻¹ dissolved oxygen and is

Table 5-1. Morphological characteristics and environmental preferences of microbial genera from Tuitye Springs. ISD = ‘intracellular sulphur deposition’; ESD = ‘extracellular sulphur deposition’; ST = ‘sulphide tolerant’ (after Rippka et al. 1979; Reichenback 1981; Larkin and Strohl 1983; Schlegel and Bowien 1987; Pentecost, 1995; Wher and Sheath 2003; Teske and Nelson 2005).

| <i>Group / Genus</i> | <i>Morphology</i> | <i>ISD</i> | <i>ESD</i> | <i>ST</i> | <i>Habitat</i> | <i>Tuitye Field Appearance</i> |
|---|--|------------|------------|-----------|--|--|
| <i>Sulphur Oxidising Bacteria</i> | | | | | | |
| <i>Thiothrix</i> | Colourless cylindrical filaments; 2-3 μm wide; septa every 4-5 μm ; unsheathed; occur in rosettes | Yes | No | Yes | Flowing dysoxic water | White fringes; streamers, pervasive from the vent to the top boundary of the travertine mound |
| <i>Beggiatoa</i> | Colourless cylindrical filaments; 5 μm wide; septae every 3-5 μm ; unsheathed; occur singly; form hormogonia | Yes | No | Yes | Oxic/anoxic interface, low turbulence | Basal layers of floating mats in shallow ponds, long white streamers near spillover from ponds to travertine mound |
| <i>Purple Sulphur Bacteria</i> | | | | | | |
| <i>Chromatium</i> | Motile; oval to bean shaped cells 1-3 μm long; pink in light microscope | Yes | No | Yes | Dysoxic to anoxic photic zone | Red non-cohesive films in ponded water behind travertine mound |
| <i>Cyanobacteria</i> | | | | | | |
| <i>Oscillatoria</i> | Olive-green filaments; 3 μm wide; septa every 1 μm (or less); unsheathed; non refractory internal granules; form hormogonia by necrotic cell development; gliding movement; some have sulphur globules attached to outer surface | No | Yes | Yes | Flowing or stagnant oxygenated to dysoxic water, wide chemical and thermal tolerance | Abundant in orange-green mats and films behind travertine mound |
| <i>Spirulina</i> | Green unsheathed filaments; 1 μm wide forming tight coils ~ 10 μm wide | No | No | No | Cool to warm oxygenated freshwater | Bright green non-cohesive films in ponded water; scarce above travertine mound, abundant below |
| <i>Diatoms</i> | | | | | | |
| | Siliceous frustules; pennate, most < 10 μm long <i>Naviculoid</i> , <i>Achnantheid</i> and <i>Nitzschoid</i> types | No | No | Yes | Flowing or ponded oxic to dysoxic water | Abundant in ponded water above and below the travertine mound |
| <i>Rod Shaped (likely sulphur reducing) Bacteria</i> | | | | | | |
| | Straight or arcuate rods, 5 μm long and 0.5 μm wide, some have sulphur globules attached to outer surfaces | No | Yes? | Yes | Flowing and ponded dysoxic water | Throughout the flow path, most abundant amongst <i>Thiothrix</i> filaments in upper flow path |

thermodynamically saturated (S.I. ≥ 0) with respect to calcite (0.06) and barite (1.33) and undersaturated with respect to more soluble celestite (-1.75), gypsum (-1.57), witherite (-2.26), and strontianite (-1.16) (SOLEMINEQ88 – see Appendix 2). Turbulence facilitates atmospheric oxidation in the spring flow path and oxygen concentrations increase to $> 2.44 \text{ mgL}^{-1}$ in the stream at the base of the travertine mound (Fig. 5-2).

| Constituent | Concentration (ppm) |
|-------------------------------|---------------------|
| Na ⁺ | 104 |
| K ⁺ | 12 |
| Ca ²⁺ | 65 |
| Mg ²⁺ | 23 |
| Sr ²⁺ | 1.38 |
| Ba ²⁺ | 0.78 |
| Al ³⁺ | <0.005 |
| Fe ³⁺ | <0.001 |
| Cl ⁻ | 46 |
| HCO ₃ ⁻ | 356 |
| NO ₃ ²⁻ | 0.13 |
| SO ₄ ²⁻ | 140 |
| SiO ₂ | 10.6 |
| Total Alkalinity (mM) | 292 |

Table 5-2. Chemistry of Twitya Spring water measured by ICP-MS (see Appendix 2).

CO₂-degassing is also indicated by an increase in pH from 7.26 at the spring vent to 8.55 at the base of the spring flow path (cf. Chafetz et al., 1991). The dissolved oxygen concentration and pH of the spring water are inversely related to its dissolved sulphide and CO₂ content and, together with hydrologic parameters, these physiochemical variables define four gradational zones in the Twitya flow path, which are characterized by distinct microbial assemblages and mineral precipitates (Fig. 5-2).

Microbes

Thiothrix (Fig. 5-3A) forms white microbial streamers on submerged substrates in zone 1. The streamers also contain rod-shaped bacteria (RSB), elemental sulphur, and EPS. The RSB are probably sulphate-reducing bacteria (Douglas and Douglas, 2001), but this cannot be confirmed by morphological criteria alone. In zone 2, *Thiothrix* streamers

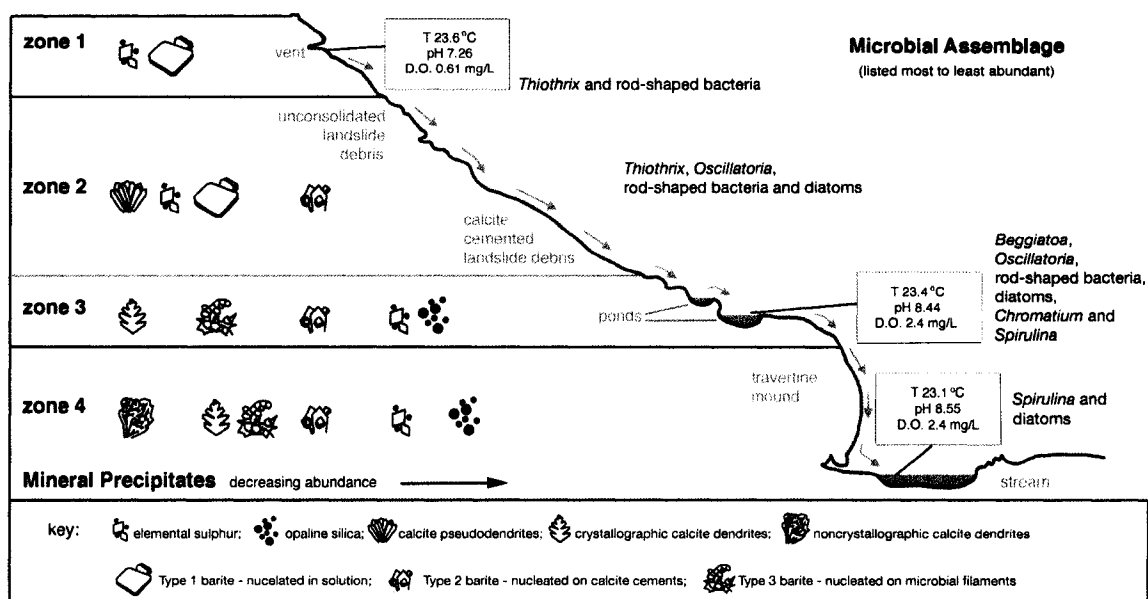


Figure 5-2. Schematic cross-section of the Twitya Spring flow path showing zones defined by spring water physiochemistry (boxed data), microbiology (right hand side), and mineral precipitates (left hand side).

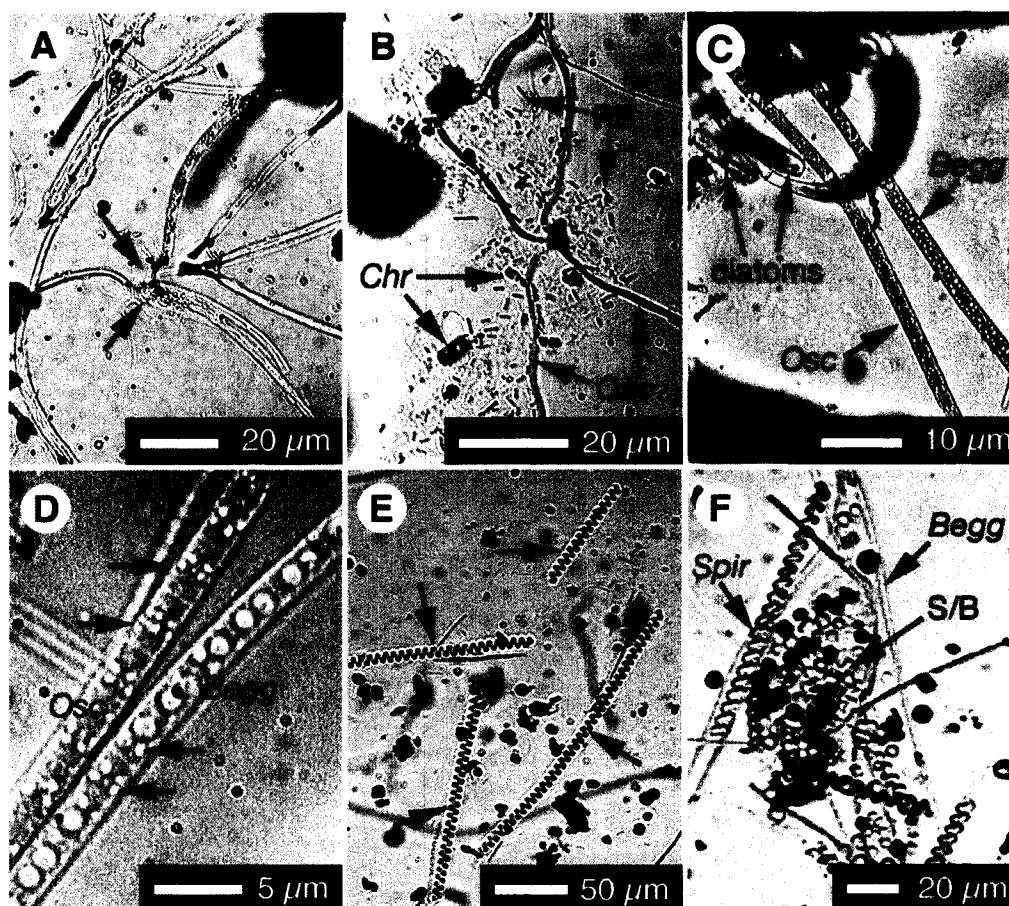


Figure 5-3. Light microscope photographs of microbes from Twitya Spring. (A) *Thiothrix* filaments joined in a rosette (arrows). (B) *Oscillatoria* (Osc-arrows), rod-shaped bacteria (RB-arrows) and *Chromatium* (Chr-arrows). (C) Diatoms and filaments of *Oscillatoria* and *Beggiatoa* (Begg-arrow). (D) Detail of *Oscillatoria* with external elemental sulphur (arrows) and *Beggiatoa* with internal elemental sulphur (arrows). (E) Elemental sulphur and *Spirulina* (arrows). (F) Detail of *Spirulina* (Spir-arrow) with *Beggiatoa* and clumped elemental sulphur and unicellular bacteria (S/B-arrow).

and RSB are joined in dysoxic tributaries by *Oscillatoria* and diatoms, locally forming green/orange films ≤ 5 mm thick (Fig. 5-3B, C, D). In zone 3, spring water forms pools, ≤ 5 cm deep, which contain loose, floating green-white mats of *Beggiatoa* and *Oscillatoria* (Fig. 5-3C, D), diatoms, and RSB. Localized pink patches in these mats also contain *Chromatium* (Fig. 5-3B), and bright green patches contain *Spirulina* and clusters of spherical unicellular bacteria and elemental sulphur beads (Fig. 5-3E, F). Desiccated mats are colonized by unidentified hyaline fungal hyphae. In August 2005, the surface of the travertine mound (zone 4) was locally colonized by orange/green mats dominated by *Oscillatoria* (Fig. 5-1C), and pools and drainage streams beneath the travertine mound were bright green, due to dense colonisation by *Spirulina*.

Mineral Precipitates

Themodynamical modeling predicts that the Twitya spring water is saturated with respect to calcite (0.06) and barite (1.33). Elemental sulphur and silica are also found among precipitates formed from the spring water, however, highlighting the limitation of steady state modeling to natural waters that are in chemical disequilibrium. The distribution, abundance, and habit of precipitates in the Twitya Spring flow path vary downstream with changing physiochemical conditions (Fig. 5-2).

Elemental sulphur is found as single and chained rhombic crystals up to 10 μm long, as spherical beads 0.5-10 μm in diameter (Fig. 5-4A), as crystalline sulphur rhombs that surround elemental sulphur beads (Fig. 5-4B), and locally as chains of sulphur rhombs (Fig. 5-4C). Elemental sulphur is present in decreasing abundance in zones 1 through 4. In zones 1 and 2 it is found among *Thiothrix* streamers and forms a thin coating on rocks and branches. In zones 3 and 4, it is deposited among microbial mats, and incorporated in calcite travertine.

Calcite precipitates in zones 2 and 3, forming laminated rinds on the downstream side of submerged branches and rocks. In zone 2, laminae ≤ 1 cm thick are composed of splaying trigonal calcite crystal bundles with shrub-like pseudo-dendritic habit (cf. Jones et al., 2000) (Fig. 5-4D). The bundles are up to 20 μm high, and are commonly interlaminated with thin layers of micrite and organic detritus (Fig. 5-4E, F). In zone 3, laminae 0.5-2 cm thick are composed of symmetric and subsymmetric crystallographic

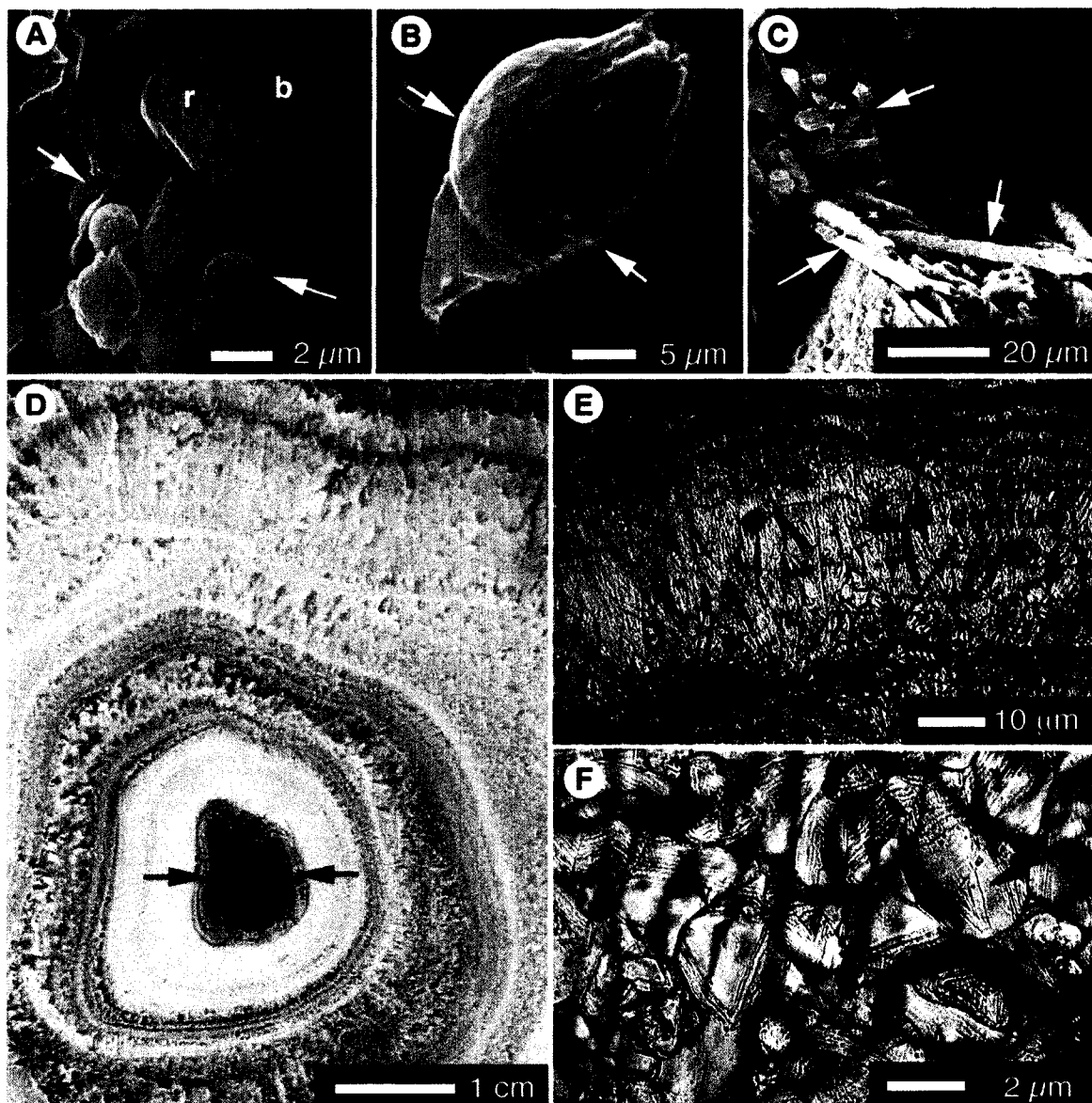


Figure 5-4. Mineral precipitates. (A) Rhombs (r) and beads (b) of elemental sulphur. Rhombs surrounding beads are indicated by arrows. (B) Detail of rhomb surrounding bead. (C) Chains of elemental sulphur rhombs (arrows). (D) Cross-section of laminated calcite rind surrounding twig (arrows). (E) Thin section photograph of splaying calcite pseudo-dendrites from zone 2, arrows indicate growth bands demarcated by detrital organics. (F) Splaying calcite pseudo-dendrites with trigonal cross-section.

calcite dendrites (cf. Jones and Renaut, 1995) with width to height ratios of 0.5-0.1, 2-3 orders of branching, and distinct chevron growth bands (Fig. 5-5A- E). In the travertine mound (zone 4) convex and sub-vertical laminae, 1-5 cm thick, are composed of asymmetric, non-crystallographic dendrites (cf. Jones and Renaut, 1995), with isolated discontinuous laminae of crystallographic dendrites. The non-crystallographic dendrites have a macroscopic 'feathery' appearance (Fig. 5-1F), exhibit up to 4 levels of branching (Fig. 5-5F, G), and gain asymmetry by preferential growth of downstream branches.

Calcite dendrites are backfilled by compositionally distinct secondary calcite cements (Fig. 5-6). Cements and primary dendritic calcite boundaries are reflected by sharp grey-level shifts in backscattered EMP images, which are attributable to variations in the trace abundance of barium, strontium, and magnesium co-precipitated with the calcite (Fig. 5-6). Primary dendrite calcite contains up to 0.58 and 0.53 wt. % Ba^{2+} and Sr^{2+} , respectively, whereas cements have maximum concentrations of 0.12 and 0.04 wt. % Ba^{2+} and Sr^{2+} . Mg^{2+} has a reversed distribution, with enrichment up to 1.26 wt. % compared to 0.26 wt. % in dendritic calcite. Traverses across compositional boundaries show covariation of Ba^{2+} and Sr^{2+} , which vary inversely with Mg^{2+} (Figs. 5-6C, 5-7). Compositional variations at scales $\leq 5 \mu\text{m}$, are not represented in Figure 7 because they approach the combined precision limit of the microprobe beam spot size ($1 \mu\text{m}$) and the automated stage positioner ($\pm 1.5 \mu\text{m}$).

Calcite dendrites are crystallographically continuous across many laminae in the Twitya travertine (Fig. 5-8A) but are locally interrupted by detrital laminae (Fig. 5-8B), and irregular dissolution bands (Fig. 5-8C). Despite the presence of diatoms in microbial samples, no preserved diatom frutules were found in the Twitya travertine, indicate that they experience rapid dissolution. Growth bands between and within calcite dendrite beds do, however, locally contain secondary calcite cement, micritic grains, detrital clay and organics, elemental sulphur (Fig. 5-8D), opaline silica (Fig. 5-8E), and barite (Fig. 5-8A).

Barite crystals are distributed throughout the Twitya travertine, approaching up to 5% by volume along growth bands and in pockets of trapped organics. The Twitya barite is relatively pure (containing 0.9-7.6 wt. % Ca^{2+} , 0.2-3.9 wt. % Sr^{2+} , and < 0.1 wt. % Mg^{2+}) and can be divided into type groups T1, T2, and T3 based on crystal habit and nucleation substrate.

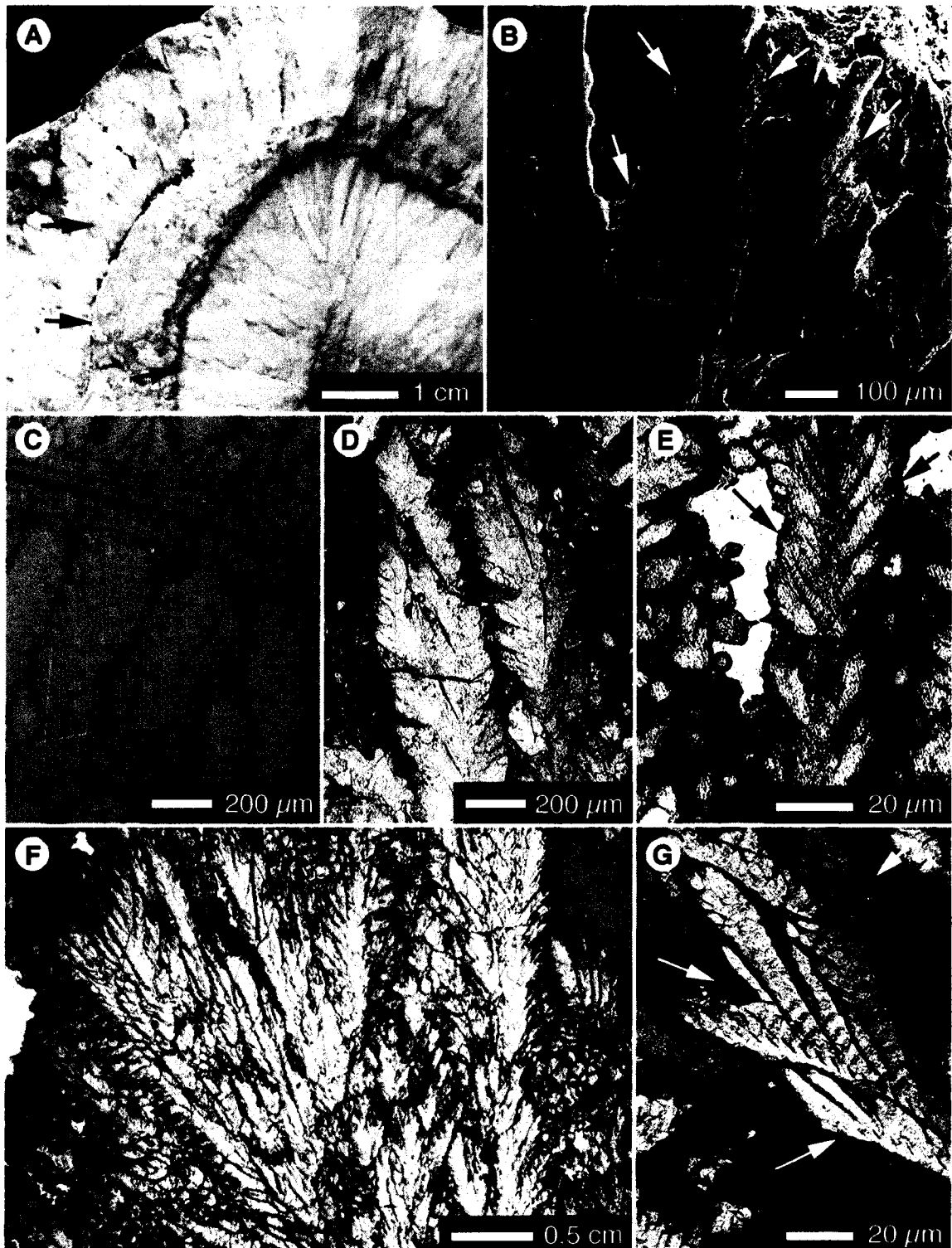


Figure 5-5. Dendritic calcite. (A) Cut sample of calcite dendrites from zone 3 with growth laminations (arrows). (B) SEM image of etched sample, arrows indicate individual dendrite crystals. (C) EMP image of crystallographic dendrites from zone 3. (D) Crossed polar thinsection photograph showing unit extinction of crystallographic dendrites. (E) Elongate crystallographic dendrite with chevron growth bands (arrows). (F) Non-crystallographic calcite dendrites from zone 4. (G) Crossed polar image showing sweeping extinction of non-crystallographic dendrites.

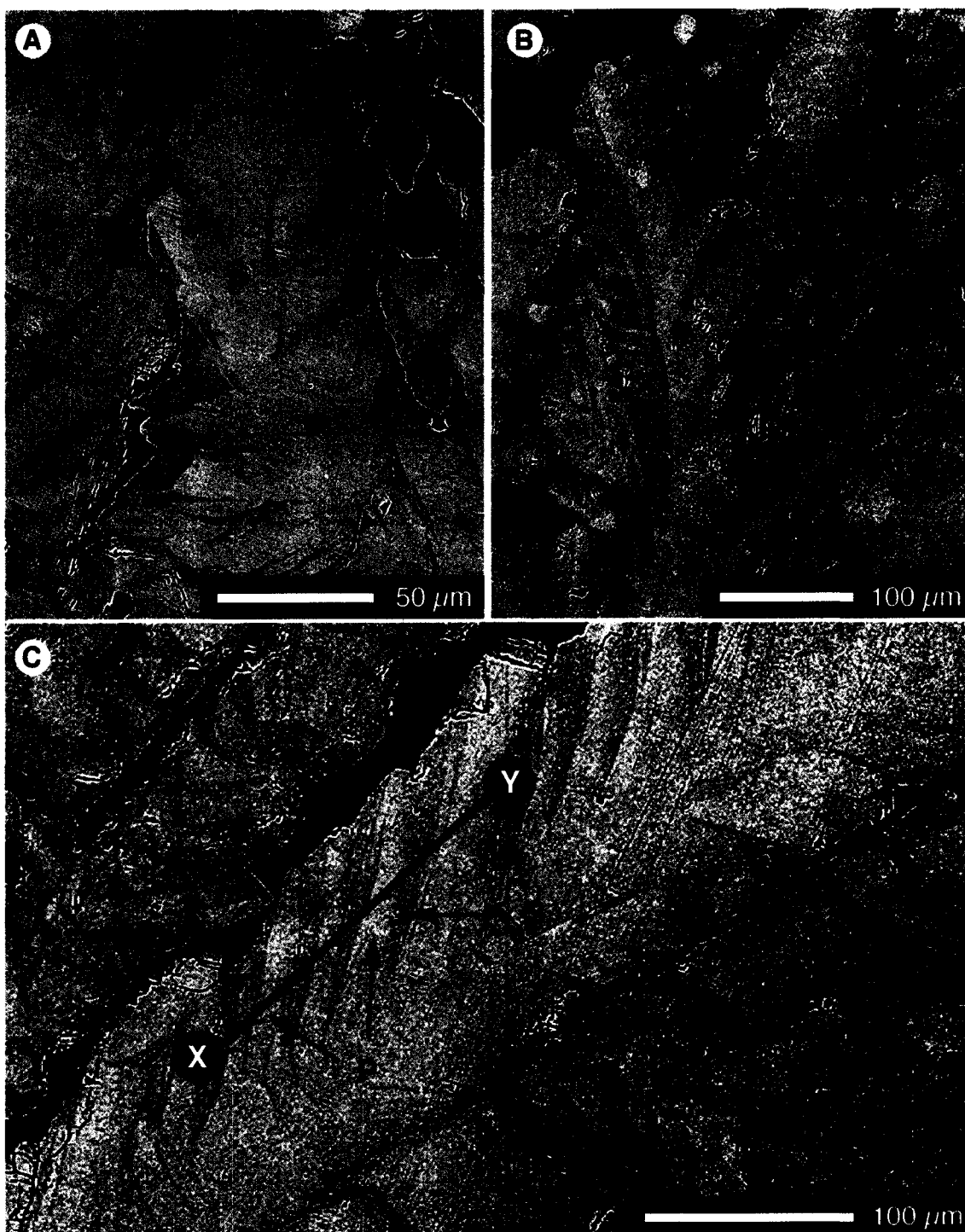


Figure 5-6. Backscattered EMP images showing variation in average atomic weight between primary calcite dendrites (P) and secondary calcite cements (S). (A) Crystallographic dendrite. (B) Non-crystallographic dendrite. (C) Detail of non-crystallographic dendrite with heavy (bright) primary branches (P) infilled by lighter (dark) secondary cements (S). Transect line X-Y corresponds to figure 5-7.

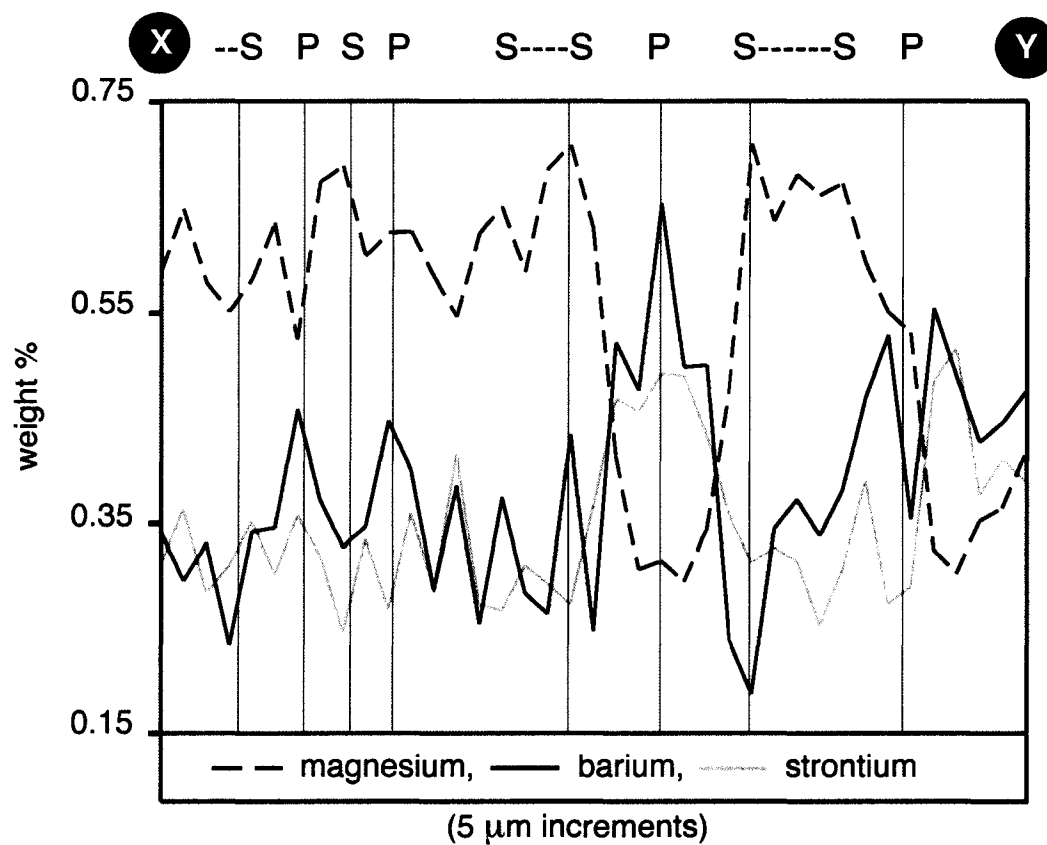


Figure 5-7. Variation in average weight % magnesium, barium and strontium along transect X-Y (Fig. 5-6). Vertical lines correspond to data points collected from primary dendritic calcite (P) and secondary infilling calcite cement (S).

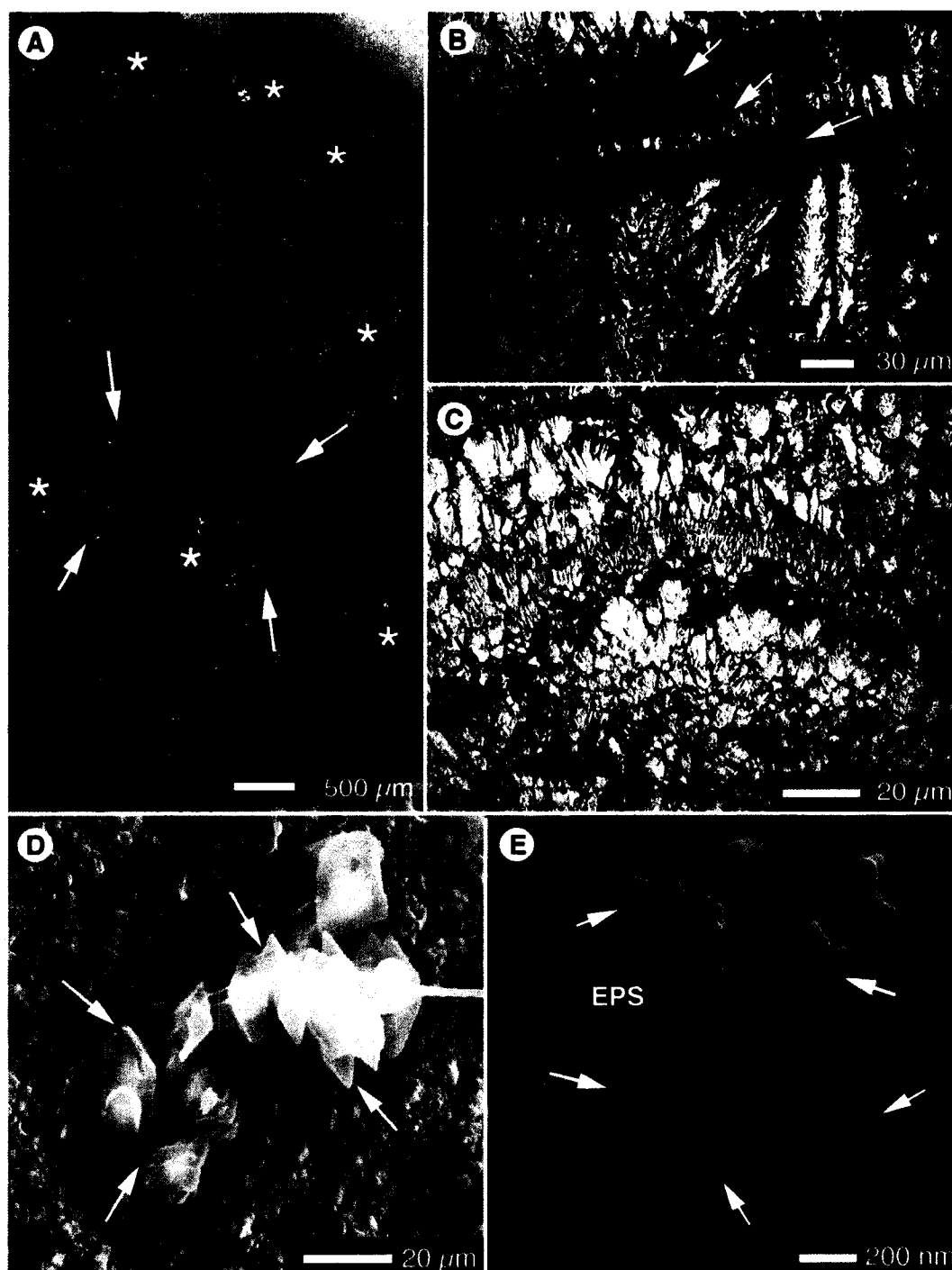


Figure 5-8. Dendrite growth bands. (A) Backscattered SEM image of etched calcite dendrites, arrow indicate growth bands, * indicates area rich in barite crystals (bright speckles). (B) Fine scale laminations composed of clay and organic detritus (arrows). (C) Irregular dissolution boundaries marked by organic detritus (arrows). (D) Detrital elemental sulphur (arrows), and microbial filaments from a dendrite growth band. (E) Beads of opaline silica (arrows) nucleated on EPS along a dendrite growth band.

T1—Single or more commonly intergrown euhedral barite plates, 5-10 μm long and < 1 μm wide, are found suspended in solution and trapped in microbial biomass and calcite rinds in zones 1 and 2 (Fig. 5-9A, B). T1 barite is present in zone 3 calcite rinds, but a rare detrital component in the zone 4 travertine mound.

T2—Single and rarely intergrown tabular barite crystals, up to 50 μm long and 10 μm wide, and blocky barite rhombohedra, ≤ 20 μm wide, nucleate on calcite in zones 2, 3, and 4 (Fig. 5-9C, D). T2 barite crystals have sharp compositional boundaries with calcite substrates (Fig. 5-9E) and rhombohedral T2 crystals are commonly associated with etched elemental sulphur (Fig. 5-7F). T2 barite crystals are most abundant in the travertine mound, where they are localized between calcite dendrites, and commonly nucleated on secondary calcite cements.

T3—Consistently < 5 μm in their longest dimension, T3 barite crystals are found exclusively in association with microbial biomass (Fig. 5-10). They are generally anhedral on and within EPS (Fig. 5-10D), but subhedral-tabular on microbial filaments with little associated EPS (Fig. 5-10E). T3 barite is localized in microbial biomass found along laminar boundaries and in pocket porosity between calcite dendrites. The microbes that host T3 barite are most commonly long nonbranching filaments with collapsed width of 2-3 μm (most likely desiccated filaments of *Thiothrix* and *Oscillatoria*), as well as branching fungal hyphae. T3 barite crystals nucleated on filaments and hyphae commonly grow around them, producing barite crystals with a central cavity (Fig. 5-10F).

Interpretation

Mineral precipitation in the Twitya Spring flow path takes place along dynamic physiochemical gradients established by equilibration of the spring water to atmospheric conditions, precipitated phases, and the metabolism of resident microbes. Elemental sulphur beads are a byproduct of sulphur redox metabolism for diverse microbial genera, including *Thiothrix*, *Beggiatoa*, and *Chromatium* at Twitya Spring (Steudel, 1987). In contrast, crystalline elemental sulphur is usually produced by inorganic redox reactions, and probably formed by spontaneous oxidation of dissolved sulphide and by recrystallization of metastable biogenic sulphur beads at Twitya Spring (Douglas and

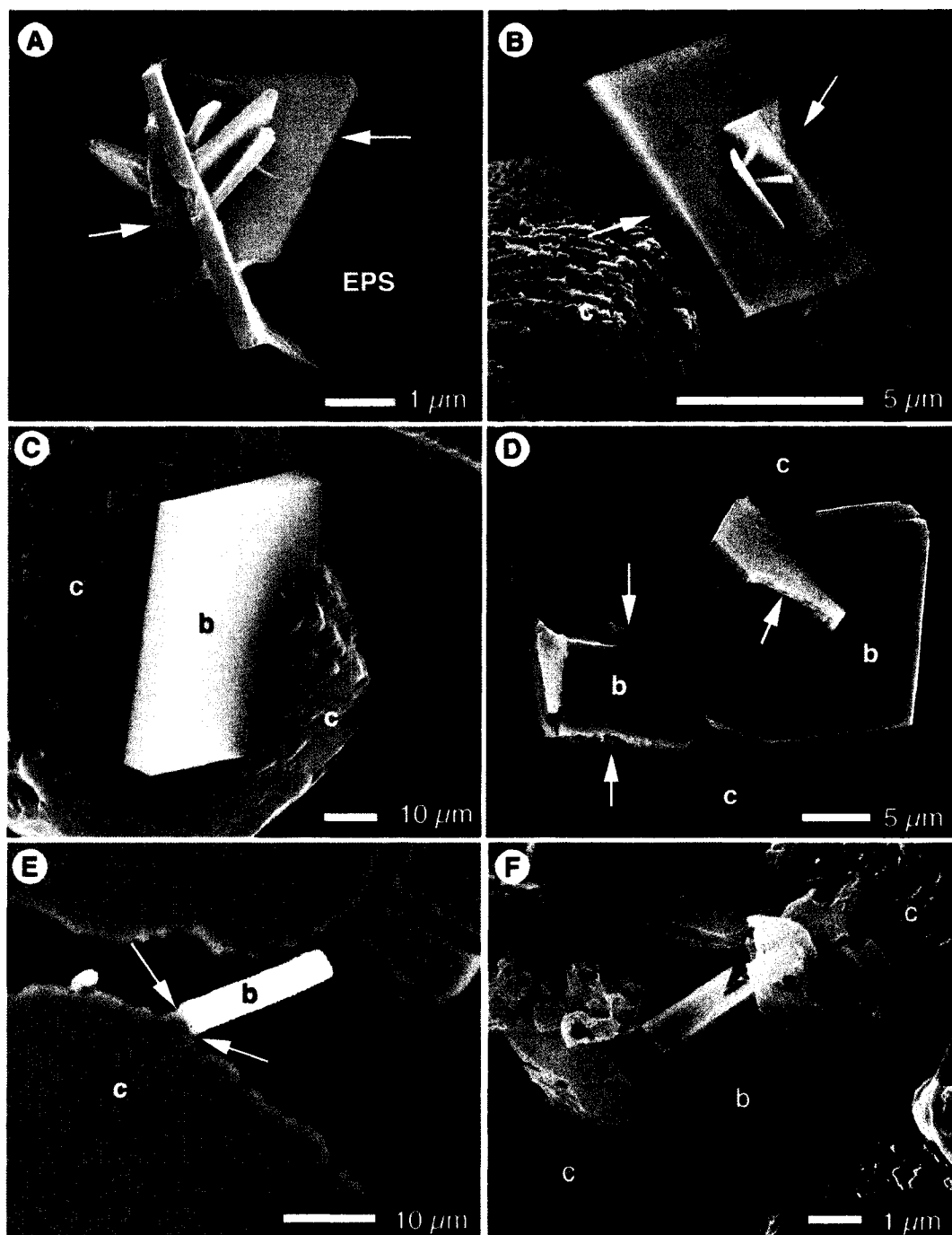


Figure 5-9. SEM images of travertine-hosted barite. (A) T1 barite crystals trapped in EPS. (B) T1 barite crystals (b) deposited on calcite (c). (C) T2 barite crystal (b) nucleated on calcite cement (c). (D) T2 barite crystals (B) surrounded in an etched travertine sample, arrows indicate irregular faces on T2 crystals where they abutted calcite (c) that has been dissolved. (E) EMP image of T2 barite showing sharp compositional boundary between barite (b) and calcite (c). (F) Rhombohedral T2 barite (b) nucleated on calcite (c) and associated with oxidizing elemental sulphur (s).

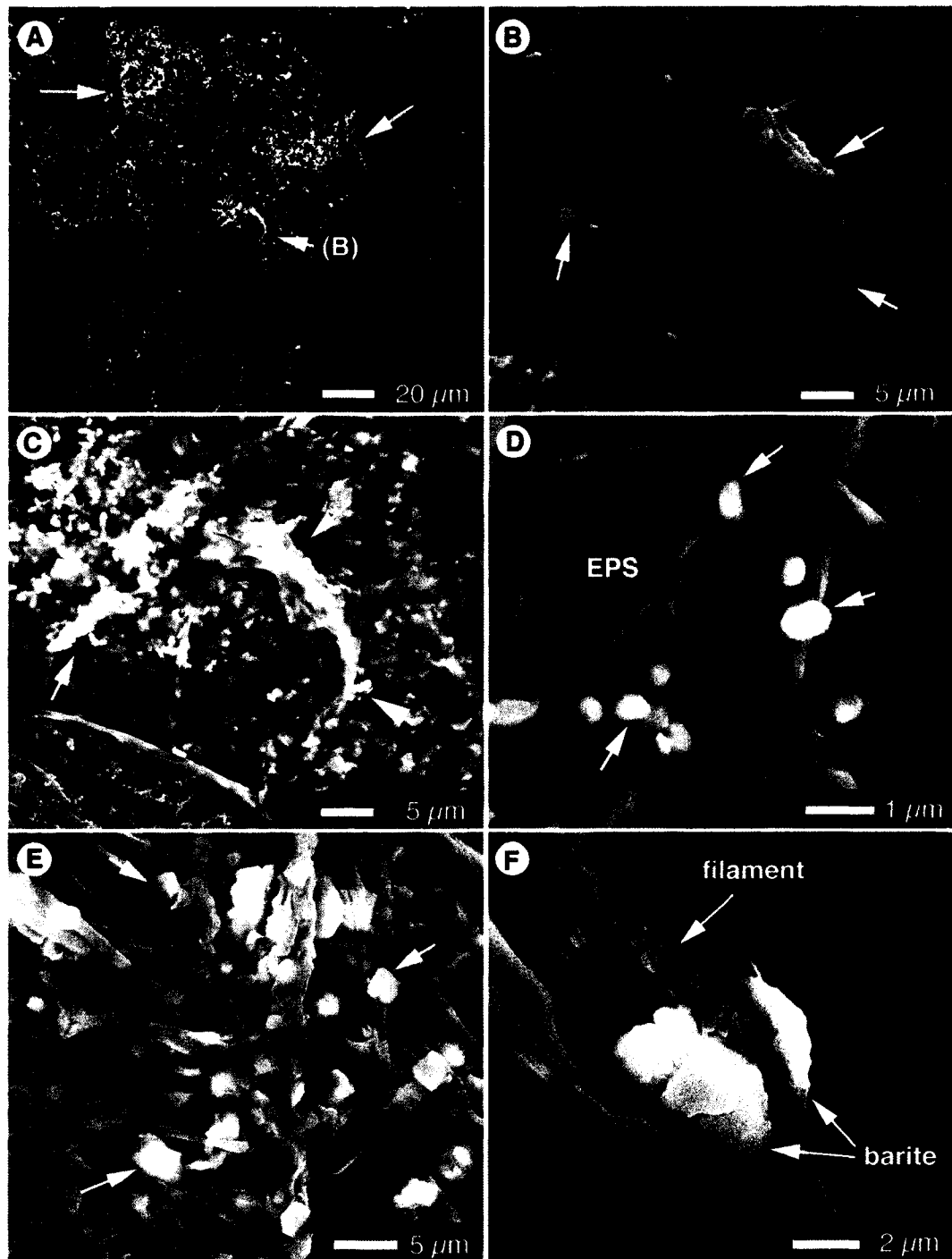


Figure 5-10. SEM images of T3 barite. (A) Backscattered SEM image of calcite dendrites with pockets and drapes or barium-enriched biomass (arrows). (B) Detail SEM image of barium-enriched drape from image A. (C) Backscattered image of the same drape, showing barite mineralisation along microbial filaments and scattered through EPS. (D) Detail backscatter image of anhedral barite (arrows) nucleated on microbial filaments surrounded by EPS (eps). (E) Backscattered image of subhedral rhombs of barite on fungal hyphae (arrows). (F) Detail of subhedral barite surrounding an EPS-free fungal hypha.

Douglas, 2001).

Pseudo-crystallographic, crystallographic, and non-crystallographic calcite dendrites are all considered 'inorganic' crystals, which form in carbonate spring flow paths by disequilibrium precipitation from strongly supersaturated solutions (Jones et al., 2000; Pentecost, 2005). Dendritic calcite growth is thought to be favoured by rapid CO₂ degassing (Jones and Renaut, 1995), the presence of organic impurities (Chafetz and Guirdy, 1999; Pentecost, 2005), an excess of bicarbonate to calcium (Jones et al., 2005), and the presence of divalent metal ions larger than calcium (Astilleros et al., 2000; Fernandez-Diaz et al., 2006). At Twitya Springs, a Ca:CO₃ ratio of 0.18, relatively high concentrations of strontium and barium (Table 1), the presence of detrital and microbially-derived organic compounds, and rapid, turbulence-incited CO₂-degassing probably act in combination to promote precipitation of dendritic calcite.

The downstream progression of dendrite crystals at Twitya Spring parallels Jones and Renaut's (1995) correlation of dendrite type to disequilibrium level: pseudo-dendrites precipitate at relatively lower disequilibrium than crystallographic dendrites, whereas non-crystallographic dendrites precipitate at higher levels of disequilibrium. The dominance of non-crystallographic dendrites in zone 4 thus indicates that highest levels of disequilibrium, i.e. rates of CO₂ degassing (Jones et al., 2005), are achieved over the surface of the travertine mound. Elevation in pH by CO₂ degassing in zone 4 would also promote precipitation of dissolved silica (cf. Jones et al., 2005) generated by precipitation of diatom frustules upstream.

In contrast to calcite and silica, the Twitya spring water precipitates barite proximal to the spring vents. In zone 1, T1 barite represents the first precipitation product of dissolved barium with atmospherically oxidized sulphate. Barite crystal habit varies as a function of the degree of oxygenation, ambient chemistry and the viscosity of the precipitating solutions (Sasaki and Minato 1982; Radanovic-Guzvica, 1999; Su et al. 2002; Torres et al. 2003), and T1 barite's intergrown euhedral plates are typical of barite microcrystals precipitated at interfaces between oxidized and reduced solutions (Stark et al., 2004; Wagner et al., 2005). The fact that T1 barite is increasingly scarce beyond zone 2 indicates that spontaneous nucleation of barite in solution is inhibited, probably by the combined effects of decreasing ambient barium concentration (due to upstream

precipitation as T1 barite and co-precipitation in calcite), CO₂-degassing (cf. Lindgren, 1933; Hamm and Merritt, 1944; Bolze et al., 1974), adsorption of barium to microbial biomass (Tazaki and Watanabe, 2004), and the presence of barite nucleation inhibiting humic acids derived from detrital organics (Smith et al., 2004).

The distribution and abundance of T2 (calcite-nucleated) and T3 (microbially-associated) barite in the Twitya travertine depends on competition for dissolved barium between calcite dendrite lattice sites, calcite cement lattice sites, and negatively charged sites hosted by microbial cells and EPS. Barium adsorption is maximized in oxygenated water, with pH > 7, where free, high charge density Ba²⁺ ions are more abundant in solution than weakly adsorptive BaOH⁺ and BaHS⁺ complexes (Langmuir, 1997). Increasing pH and dissolved oxygen levels in zones 3 and 4, thus, promote adsorption of barium to calcite and microbial surfaces. Sequestration of cations to sorptive sites can either promote or inhibit mineral precipitation, depending on ambient chemistry and reactant concentrations (Arp et al., 1999). Predictive models exist that can be used to assess the relative sorptive capacities of microbial surfaces vs. mineral surfaces and the efficacy of each to host new precipitate phases (e.g. Fein et al., 2001). A complication to modeling the fate of barium at Twitya Spring, however, is that many microbes bioaccumulate barium, including *Thiothrix*, *Beggiatoa*, and *Chromatium* (Bonny and Jones, 2007a); *Oscillatoria* (Younger, 1986; Douglas and Douglas, 2001; Bonny and Jones, 2007a); *Spirulina* (Younger, 1986), and fungi (Arguete et al., 1998). Bioaccumulation can have measurable impact on mineral saturation gradients (Ganeshram et al., 2003; Bonny and Jones, 2007b) and thus precludes application of predictive adsorptive models at Twitya Spring. Based on data gathered in this study, barium remaining in solution beyond zone 2 can be (1) incorporated into dendritic calcite and calcite cements; (2) precipitated as T2 barite nucleated on calcite; and (3) precipitated as T3 barite in association with microbial biomass.

Incorporation of cations with larger ionic radius than calcium (1.00 Å) into calcite is positively correlated to crystal growth rate (Tesoiero and Pankow, 1996). This may explain why rapidly precipitated dendritic calcite from Twitya Spring is barium (1.47 Å) enriched relative to secondary calcite cements (Figs. 5-7, 8). Incorporation of barium into calcite dendrites may limit precipitation of barite, whereas slower growing calcite

cements would selectively exclude barium (Tesoiero and Pankow, 1996) leaving it available for barite precipitation.

T2 barite's rhombohedral and tabular crystals are typical of slow precipitation via surface reaction growth mechanisms (Shikazono, 1994; Greinert et al., 2002). Tabular barite forms are also favoured by the presence of Ca^{2+} and Mg^{2+} , whose concentrations are linearly correlated to increased extension of barite's b axis at the expense of the a and c axes (Hennessey and Graham, 2002). The Twitya spring water is rich in calcium and magnesium relative to barium (Ca:Mg:Ba = 83:29:1), and thus favours growth of tabular barite crystals. The association of etched elemental sulphur with rhombohedral T2 barite microcrystals (Figs. 5-9E, F) indicates that it formed as a secondary precipitate. Elemental sulphur is unstable in well-oxygenated solutions (Pentecost, 1995), and will spontaneously oxidize to sulphate upon desiccation (Brigmon et al., 1994). Rhombohedral T2 barite may, thus, form at the expense of detrital elemental sulphur in parts of the Twitya travertine mound that become aerially exposed, or when the spring flow path is flushed by oxygenated meteoric waters.

During summer, microbes flourish in pools of Twitya spring water, form mats on hydrated portions of the travertine mound, and inhabit hydrated pore space in the upper layers of the travertine – clearly, there are abundant substrates for T3 barite precipitation. At pH 7-8, microbial cells and EPS both host deprotonated carboxyl and phosphoryl groups capable of adsorbing divalent metal cations (Phoenix et al., 2002; Yee et al., 2003). At Twitya Springs, microbial surfaces undoubtedly adsorb divalent cations other than Ba^{2+} (e.g. Ca^{2+} , Mg^{2+} , Sr^{2+} - Table 2), but the solubility of barite at ambient temperature ($\log K \text{BaSO}_4 = 9.97$) is so low that barite nuclei form more readily than other, more soluble sulphate and carbonate salts ($\log K \text{CaSO}_4 = 4.85$, $\text{CaCO}_3 = 8.47$, $\text{SrSO}_4 = 6.47$, $\text{SrSO}_4 = 9.25$, $\text{BaCO}_3 = 8.59$). T3 barite at Twitya Spring probably forms by reaction of barium adsorbed to (and/or released from) microbial cells and EPS with sulphate derived by oxidation of sulphide in pore/mat waters, organic sulphur compounds, and biogenic elemental sulphur (cf. Stoner et al., 1994; Glamoclija et al., 2004; Sanchez-Moral et al., 2004). T3 barite crystals nucleated on EPS-free microbes are subhedral, whereas barite crystals formed on and in microbial EPS are anhedral. This suggests that EPS may prevent development of crystalline barite habits by retarding

diffusion of ions to growing crystal faces (cf. Buczynski and Chafetz, 1991; Arp et al., 1999). Organic acids and phosphates present in degrading biomass also inhibit barite crystal growth (Smith et al., 2004) and may be partly responsible for the anhedral and subhedral T3 barite forms.

T3 barite is localized at laminar boundaries in the travertine, suggesting that microbial colonization of the travertine mound takes place when calcite dendrites are not growing. This is somewhat intuitive because dendrites grow very quickly and might outpace the rate at which microbial mats could form over them. And because, as dendritic crystals grow only at nucleation sites on branch tips, the presence of microbial mats may impede their dendritic crystal growth (Jones and Renaut, 1995). Twitya Spring is located just south of the Arctic Circle and experiences wide seasonal variation in temperature and incident light, which are almost certainly translated into variations in microbial growth rate. In summertime, microbes are abundant in the Twitya flow path (Fig. 5-1C). In fall, dropping temperatures and decreased daylight hours likely reduce microbial growth (cf. Sukanuma, 1928; Jones et al., 2005). At northern latitudes, lowest spring water discharge rates and calcite precipitation rates are also commonly measured during fall-winter conditions (van Everdingen, 1972; Kano et al., 2003). In spring, the introduction of snowmelt to aquifer conduits can produce temporary increases in spring water volume that produce increased turbulence in the spring flow path (van Everdingen, 1972). Increased turbulence favours both rapid CO₂ degassing and spring water oxidation, which, at Twitya Springs, would promote precipitation of barium-enriched dendritic calcite in zone 4 (cf. Jones et al., 2005) and T1 barite crystals in zones 1 and 2.

It is tempting to interpret T2 and T3 barite as fall and summer precipitates, respectively - T2 precipitating in fall when both dendrite growth and microbial growth wane, and T3 precipitating in the summer when reduced dendrite growth allows microbes to colonize the travertine mound. Growth laminations within and between calcite dendrite beds indicate, however, that the Twitya flow path is also subject to episodic, subseasonal physiochemical variation. Detrital clay bands, for example, may represent rainfall or snowmelt events during which detrital sediment was washed onto the surface of the travertine mound (cf. Kano et al., 2004). Flushing of the travertine by meteoric water may also be responsible for dissolution growth bands (cf. Pentecost, 2005), and bands rich in

organic carbon may represent brief interludes where microbial growth outpaced calcite dendrite growth during spring/summer transitional periods. Animal trampling, frost wedging, and dissolution of calcite by humic acids are other stresses that affect and complicate interpretation of seasonal precipitation patterns at Twitya Spring.

Discussion

Barite's precipitation behaviour is commonly assumed to be controlled by inorganic physicochemical variables (Hanor, 2000); indeed, its solubility is so low that thermodynamic models predict barite supersaturation when even trace quantities of barium and sulphate come into contact (SOLMINEQ88). In natural solutions, however, barite precipitation is commonly inhibited by the presence of other divalent metal ions, dissolved sulphide, carbonate, phosphate, and/or organic acids (Lindgren, 1933; Hamm and Merritt, 1944; Davis and Collins, 1971; Bolze et al., 1974; Smith et al., 2004). Oxidation of barium-bearing solutions is also commonly paired to other physiochemical changes, such as cooling, degassing, and changes in pressure or hydrodynamics, which may induce precipitation of other mineral phases (Greinert et al., 2002; Canet et al., 2005).

Significant amounts of barium can be accommodated in carbonate, phosphate, and hydroxide minerals by substitution (Younger, 1986; Tesoiero and Pankow, 1996; Kastner, 1999). In barium-limited solutions, therefore, barite precipitation may require not only the presence of sulphate, but also a means to concentrate barium to a level at which it can form as a separate mineral phase (Younger, 1986; Bonny and Jones, 2007b). At Twitya Springs, T1 barite precipitates in solution, but adsorption of barium to calcite surfaces catalyzes precipitation of T2 barite, and T3 barite forms only in association with microbes that are capable of adsorbing and bioaccumulating barium.

Microbially-mediated barite precipitation has only recently come under investigation (Gonzalez-Munoz et al., 2003; Glamoclija et al., 2004; Sanchez-Moral et al., 2004; Senko et al., 2005; Bonny and Jones, 2007b), but the presence of 'thermodynamically unstable' barite in natural environments indicates that it may be more important than thermodynamic models predict (Riedinger et al., 2006). Microbes do not catalyze 'impossible' precipitation, but establish microgradients around their cells,

through surface adsorption reactions, bioaccumulation, and/or metabolic processes, that support thermodynamically-favourable microenvironments for mineral precipitation (Aharon, 2000). Barite is commonly co-deposited with microbially mediated carbonate minerals in marine and lacustrine sediments and at microbially-colonized methane seeps, hydrothermal vents, and subaerial springs (Tazaki et al., 1997; Arenas et al., 2000; Burhan et al. 2000; Torres et al., 2003; Canet et al., 2005; Schwartz, 2005) but microbial influences on barite crystal habit and distribution have received little attention. This is due partly to the traditional assumption that barite precipitation is not microbially mediated, and partly to the logistic difficulties involved in studying diagenetic, methane seep, and hydrothermal vent minerals *in situ* (Kastner, 1999; Aharon, 2000). In contrast, subaerial springs are more accessible venues for the examination of barite precipitation and preservation in carbonate.

Inorganic barites similar to T1 and T2 barite from Twitya Spring have been reported as accessory minerals in many continental and shallow marine spring deposits. They are generally found as tabular or intergrown platy barite microcrystals nucleated on or trapped in volumetrically dominant calcite, and/or silica (Borneuf, 1983; Younger, 1986; Arenas et al., 2000; Canet et al., 2005; Jones and Renaut, 2006). Microbially mediated barites have also been reported from at least two other continental carbonate-precipitating springs, Stinking Springs in Utah and Doughty Spring in Colorado. At Stinking Springs, barite precipitation among volumetrically dominant calcite is mediated by bioaccumulation of barium in diatoms (Bonny and Jones, 2007b). At Doughty Spring, barium is co-precipitated in calcite, locally forming a mixed phase barytocalcite ((Ba, Ca)CO₃), but forms a pure barium sulphate phase around barium-enriched cyanobacterial cells (Younger, 1986). As at Twitya Spring, microbially mediated barite at Stinking Springs and Doughty Springs are preserved in carbonates together with morphologically distinct inorganic barium-phases (Cadigan and Felmlee, 1977; Younger, 1986; Bonny and Jones, 2007b).

Although conditions at subaerial springs are quite different from the marine and lacustrine environments where most sedimentary barite forms, it is nonetheless revealing that multiple precipitation mechanisms operate in the spring flow paths, producing morphologically distinct barite in overlapping physiochemical niches. In dysoxic marine

sediments and around exhalative vents where sulphur and methane-metabolizing microbes buffer both barite and carbonate solubility (Larkin and Henk, 1996; Alfonso et al., 2005), biogenic and inorganic barite microcrystals are also likely to form in spatial proximity. If microbially mediated barite crystals formed in bottom water environments are anhedral to subhedral in the 5 – 10 μm range, like those formed at Twitya Spring, Doughty Springs (Younger, 1986), and Stinking Springs (Bonny and Jones, 2007b), they will be difficult to distinguish from ‘biogenic’ barite crystals formed in ocean surface waters and deposited as particulate barite ‘rain’ (Dehairs et al., 1980; Bishop, 1988; Paytan et al., 2000; Kipli et al., 2004), and from small hydrothermal barite crystals (Bertine and Keene, 1975; Shikazono, 1994). Examination of substrate associations, and petrographic distributions should, however, allow primary, authigenic and diagenetic barite crystals to be distinguished (Arenas et al., 2000), suggesting a potential for microbially-mediated barites to serve as biomarkers in bedded and stromatolitic carbonates of low metamorphic grade.

As an example, Mesozoic carbonates in the Betic Cordillera, Southern Spain, have been found to contain diagenetic barite crystal clusters and veins, as well as dispersed poorly crystalline barites $\leq 5 \mu\text{m}$ long (Martin-Agarra and Sanchez-Navas, 2000). Scanning electron and electron microprobe analysis of the dispersed barite showed a consistent association with desiccated EPS structures, and more rarely with filamentous microfossils, indicating that they formed through ‘bacterial’ authigenesis, and can be considered biomarkers formed during very early diagenesis (Martin-Agarra and Sanchez-Navas, 2000). Barite microcrystals found in Neoproterozoic carbonates are also commonly associated with preserved organics (Buick et al., 1982), and have $\delta^{34}\text{S}$ signatures indicative of precipitation from a microbially fractionated sulphur pool (Shields et al., 2007). Many of the Neoproterozoic ‘cap carbonates’ contain barite-hosting calcite crystal ‘fans’, commonly interpreted as pseudomorphs after primary aragonite fans and/or dendrites precipitated on the seafloor (Grotzinger and James, 2000). Interpretation of inorganic and biological influences on these crystal fans (which is important to assessing the biologic viability of Earth during one of its most intense glacial periods) has relied heavily upon modern analogues formed in microbially colonised hot spring flow paths (e.g. Frasier and Corsetti, 2003). Interpretation of barite

microcrystals hosted in these Neoproterozoic carbonates has not, however, incorporated nonthermodynamic variables found to affect the distribution of barite at subaerial springs (e.g. Walter and Bauld, 1983; Hoffmann and Schragg, 2000).

Limits placed on barite nucleation by the growth rate of co-deposited calcite at Twitya Spring and the importance of barium bioaccumulation at Stinking, Flybye and Doughty Spring (Bonny and Jones, 2007b; Younger, 1986) are not accommodated by thermodynamic or predictive adsorption precipitation models (e.g. SOLEMINEQ88; Langmuir, 1997; Fein et al., 2001), and remain unconstrained for palaeoenvironmental reconstruction in Recent (Finlay et al., 1983; Kiipli et al., 2004; Riedinger et al., 2006) and Ancient (Hoffmann and Schrag, 2002; Huston and Logan, 2004; Shields et al., 2007) depositional environments. It is well established, however, that microbially-mediated precipitates can record distinct isotopic signals (Paytan et al., 2002) and commonly have higher levels of co-precipitated trace elements than 'inorganic' precipitates formed in the same ambient depositional environment (Paytan et al., 2002; Wentworth et al., 2003). Distinguishing between abiotic and microbially mediated barite microcrystals may, thus, be important not only for establishing evidence of a biological presence in ancient rocks, but for ensuring accurate interpretation of geochemical data retrieved from barite (cf. Jewell, 2000; Bottrell and Newton, 2006).

Conclusions

Controls on the distribution and habit of barite crystals precipitated in the flow path of Twitya Springs include:

- (1) Spring water oxidation state: T1 platy barite crystals precipitate in solution in the upper spring flow path as a result of atmospheric oxidation of dissolved sulphide to sulphate.
- (2) Rate of CO₂-degassing and calcite precipitation: CO₂ degassing drives precipitation of calcite in the lower Twitya Spring flow path, producing laminated travertine. The travertine is dominantly composed of rapidly precipitated calcite dendrites that are barium-enriched relative to infilling calcite cements. Incorporation of barium into calcite may inhibit barite precipitation during springtime surges in calcite dendrite growth.

(3) Availability of adsorptive substrates: precipitation of barite in solution is inhibited in the lower Twitya Spring flow path, such that barite precipitation requires adsorption of barium to a substrate that can catalyze barite nucleation. T2 tabular and rhombohedral barite crystals nucleate on calcite crystal faces, whereas T3 barite forms in association with microbial biomass.

(4) Abundance of microbes and EPS: T3 barite crystals formed among EPS-rich microbes are anhedral, whereas subhedral T3 barite crystals form on and around EPS-free filaments.

At Twitya springs, T1, T2 and T3 barite are morphologically distinct, but form and/or are deposited in overlapping physiochemical niches whose boundaries are continually adjusted by seasonal and episodic variations in spring water flow, microbial growth, and calcite precipitation rate. Although this study confirms that specific precipitation mechanisms produce distinct barite morphologies, it also reveals that similarly-sized microbially mediated and inorganic barites can be co-deposited in microbially colonised sediments, indicating that close attention to petrographic textures and precipitation substrates will be required to resolve barite the genesis of microcrystals in the geologic record.

References

- Aharon, P., 2000. Microbial processes and products fueled by hydrocarbons at submarine seeps. In: Riding, R., Awramik, S.M. (Eds.), *Microbial Sediments*, Springer-Verlag: Heidelberg Germany, pp. 270-281.
- Alfonso, P., Prol-Ledesma, R.M., Canet, C., and Melgarejo, J.C., Fallick, A.E., 2005. Isotopic evidence for biogenic precipitation as a principal mineralization process in coastal gasohydrothermal vents, Punta Mita, Mexico. *Chemical Geology*, 22: 113-121.
- Arenas, C., Gutierrez, F., Osacar, C., and Sancho, C., 2000. Sedimentology and geochemistry of fluvio-lacustrine tufa deposits controlled by evaporite solution subsidence in the central Ebro Depression, NE Spain. *Sedimentology*, 47: 883-909.
- Arguete, D.M., Aldstadt, J.H. III, and Mueller, G.M., 1998. Accumulation of several heavy metals and lanthanides in mushrooms (Agaricales) from the Chicago region. *The Science of the Total Environment*, 224: 43-56.
- Arp, G. Theil, V., Reimer, A. Michaelis, W., and Reitner, J., 1999. Biofilm exopolymers control microbialite formation at thermal springs discharging into the alkaline Pyramid Lake, Nevada, USA. *Sedimentary Geology*, 126:159-176.
- Astilleros, J.M., Pina, C.M., Fernandez-Diaz, A., and Putnis, A., 2000. The effect of barium on calcite {1013} surfaces during growth. *Geochimica et Cosmochimica Acta*, 64: 2965-2972.
- Bains, S., Norris, R.D., Cornfield, R.M., and Faul, K.L. 2000. Termination of global warmth at the Palaeocene/Eocene boundary through productivity feedback. *Nature*, 407: 171-174.
- Bishop, J.K.B., 1988. The barite-opal-organic carbon association in oceanic particulate matter. *Nature*, 332: 341-343.
- Bertine, K.K. and Keene, J.B., 1975. Submarine barite-opal rocks of hydrothermal origin. *Science*, 188: 150-152.
- Blusson, S.L. 1971. Sekwi Mountain map-area, Yukon Territory and District of Mackenzie. Geological Survey of Canada, Open File 71-22, map and booklet, 17 pp.
- Bolze, C.E., Malone, P.G., and Smith, M.J., 1974. Microbial mobilization of barite. *Chemical Geology*, 13: 141-143.
- Bonny, S. and Jones, B. 2007a. Barite (BaSO₄) biomineralisation at Flybye Springs, a cold sulphur spring system in Canada's Northwest Territories, *Canadian Journal of Earth Sciences*, 44: 835-856.
- Bonny, S. and Jones, B., 2007b. Diatom-mediated barite precipitation in microbial mats calcifying at Stinking Springs, a warm sulphur spring system in Northwester Utah, USA. *Sedimentary Geology*, 194: 223-244.
- Borneuf, D., 1983. Earth Sciences Report 82-3: Springs of Alberta. Alberta Research Council, National Resources Division, Groundwater Development, 66 pp.
- Bottrell, S.J. and Newton, R.J., 2006. Reconstruction of changes in global sulfur cycling from marine sulfate isotopes. *Earth-Science Reviews*, 75: 59-83.

- Brigmon, R.L., Martin, H.W., Morris, T.L., Bitton, G., and Zam, S.G., 1994. Biogeochemical ecology of *Thiothrix* spp. in underwater limestone caves. *Geomicrobiology Journal*, 12: 141-159.
- Buczynski, C. and Chafetz, H.S., 1991. Habit of bacterially induced precipitates of calcium carbonate and the influence of medium viscosity on mineralogy. *Journal of Sedimentary Petrology*, 61: 226-233.
- Burhan, R.Y.P., Trendel, J.M., Adam, P., Wehrung, P., Albrecht, P., and Nissenbaum, A., 2000. Fossil bacterial ecosystem at methane seeps; origin of organic matter from Be'eri sulfur deposit, Israel. *Geochimica et Cosmochimica Acta*, 66: 4085-4101.
- Cadigan, R.A. and Felmler, J.K., 1977. Radioactive springs geochemical data related to uranium exploration. *Journal of Geochemical Exploration*, 8: 381-395.
- Canet, C., Prol-Ledesma, R.M., Torres-Alvarado, I., Gilg, H.A., Villanueva, R.E., and Cruz, R. L-S., 2005. Silica-carbonate stromatolites related to coastal hydrothermal venting in Baia Concepcion, Baja California Sur, Mexico. *Sedimentary Geology*, 174: 97-113.
- Cecile, M.P., Goodfellow, W.D., Jones, L.D., Krouse, H.R., and Shakur, M.A., 1984. Origin of radioactive barite sinter, Flybye Springs, Northwest Territories, Canada. *Canadian Journal of Earth Science*, 21: 383-395.
- Chafetz, H.S., Rush, P.F., and Utech, N.M., 1991. Microenvironmental controls on mineralogy and habit of CaCO₃ precipitates: an example from an active travertine system. *Sedimentology*, 38: 107-126.
- Chafetz, H.W. and Guirdy, S.A., 1999. Bacterial shrubs, crystal shrubs, and ray-crystal shrubs: bacterial vs. abiotic precipitation. *Sedimentary Geology*, 126: 57-74.
- Davis, J.W. and Collins, A.G., 1971. Solubility of barium and strontium sulfates in strong electrolyte solutions: *Environmental Science and Technology*, 5: 1039-1043.
- Day, S.J.A., Lariviere, J.M., Friske, P.W.B., Gochner, K.M., MacFarlane, K.E., McCurdy, M.W., and McNeil, R.J., 2005. National Geochemical Reconnaissance, Regional Stream Sediment and Water Geochemical data, Macmillan Pass – Sekwi Mountain Northwest Territories (NTS 105O east and 105 P). Geological Survey of Canada Open File 4949/Northwest Territories Geoscience Office Contribution 0014. 1 CD-ROM.
- Dehairs, F., Chesselet, R., and Jedwab, J., 1980. Discrete suspended particles of barite and the barium cycle in the open ocean. *Earth and Planetary Science Letters*, 49: 528-550.
- Douglas, S. and Douglas, D.D., 2001. Structural and geomicrobiological characteristics of a microbial community from a cold sulfide spring. *Geomicrobiology Journal*, 18: 201-422.
- Fein, J.B., Martin, A.M., and Wightman, P.G., 2001. Metal adsorption to bacterial surfaces: Development of a predictive approach. *Geochimica et Cosmochimica Acta*, 65: 4267-4273.
- Fernandez-Diaz, L., Astilleros, J.M., and Pina, C.M., 2006. The morphology of calcite crystals grown in a porous medium doped with divalent cations. *Chemical Geology*, 225: 314-321.
- Finlay, B.J., Hetherington, N.B., Davison, W., 1983. Active biological participation in lacustrine barium chemistry. *Geochimica et Cosmochimica Acta*, 47: 1325-1329.

- Frasier, M.L., Corsetti, F.A., 2003. Neoproterozoic carbonate shrubs: interplay of microbial activity and unusual environmental conditions in post-snowball Earth oceans. *Palaios*, 18: 378-387.
- Fu, B., Aharon, P., Byerly, G.R., and Roberts, H.H., 1994. Barite chimneys on the Gulf of Mexico slope; initial report of their petrography and geochemistry. *Geo-Marine Letters*, 14: 81-87.
- Ganeshram, R.S., Francois, R., Commeau, J., and Brown-Leger, L., 2003. An experimental investigation of barite formation in seawater. *Geochimica et Cosmochimica Acta*, 67: 2599-2605.
- Glamoclija, M., Garrel, L., Berthon, J., and Lopez-Garcia, P., 2004. Biosignatures and bacteria diversity in hydrothermal deposits of Solfatara Crater, Italy. *Geomicrobiology Journal*, 21: 529-541.
- Gonzalez-Munoz, M.T., Fernandez-Luque, B., Martinez-Ruiz, F., Chekroun, K.B., Arias, J.M., Rodriguez-Gallego, M., Martinez-Canamero, M., de Linares, and C., Paytan, A., 2003. Precipitation of Barite by *Myxococcus xanthus*: Possible Implications for the Biogeochemical Cycle of Barium. *Applied and Environmental Microbiology*, 69: 5722-5725
- Greinert, J., Bollwerk, S.M., Derkachev, A., Bohrmann, G., and Suess, E., 2002. Massive barite deposits and carbonate mineralisation in the Derugin Basin, Sea of Okhotsk: Precipitation processes at cold seep sites. *Earth and Planetary Science Letters*, 203: 165-180.
- Hamm, W.E. and Merritt, C.A., 1944. Barite in Oklahoma, Oklahoma Geological Survey Circular 23, 43 pp.
- Hanor, J.S., 2000. Barite-celestine geochemistry and environments of formation. *Reviews in Mineralogy and Geochemistry*, 40: 193-275.
- Hennessy, A.J.B. and Graham, G.M., 2002. The effect of additives on the co-crystallisation of calcium with barium sulphate. *Journal of Crystal Growth*, 239: 2153-2159.
- Hoffmann, P.F., Schrag, D.P. 2002. The snowball Earth hypothesis: testing the limits of global change. *Terra Nova*, 14: 129-155.
- Huston, D.L., Logan, G.A., 2004. Barite, BIFs and bugs: evidence for the evolution of the Earth's early hydrosphere. *Earth and Planetary Science Letters*, 220: 41-55.
- Jewell, P.W., 2000. Bedded barite in the geologic record. In: Glenn, C.R., Lilliane, P.L. and Jaques, L. (Eds), *Marine authigenesis; from global to microbial*, Special Publication of the Society for Sedimentary Geology, 66: 17-161.
- Jones, B. and Renaut, R.W., 1995. Non-crystallographic calcite dendrites from hot-spring deposits at Lake Bogoria, Kenya. *Journal of Sedimentary Research*, A65: 154-169.
- Jones, B., Renaut, R.W., and Rosen. 2000. Trigonal dendritic calcite crystals forming from hot spring waters at Waikite, North Island, New Zealand. *Journal of Sedimentary Research*, 70: 56-603.

- Jones, B., Renaut, R. W., Owen, R.B., and Torfasons, H., 2005. Growth patterns and implications of complex dendrites in calcite travertines from Lysuholl, Snaefellsnes, Iceland. *Sedimentology*, 52: 1277-1301.
- Jones, B. and Renaut, R.W., 2006. Growth of siliceous spicules in acidic hot springs, Waiotapu Geothermal Area, North Island, New Zealand. *Palaios*, 21: 406-423.
- Kano, A., Matsuoka, J., Kojo, T., and Fujii, H., 2003. Origin of annual laminations in tufa deposits, southwest Japan. *Palaeogeography, Palaeoclimatology, Palaeoecology*, 191: 243-262.
- Kano, A., Kawai, T., Matsuoka, J., and Ihara, T., 2004. High-resolution records of rainfall events from clay bands in tufa. *Geology*, 32: 793-796.
- Kastner, M. 1999. Oceanic minerals: Their origin, nature of their environment, and significance. *Proceedings of the National Academy of Science, USA*, 96: 3380-3387.
- Kiipli, E., Kiipli, T., and Kallaste, T., 2004. Bioproductivity rise in the east Baltic epicontinental sea in the Aeronian (Early Silurian). *Palaeogeography, Palaeoclimatology, Palaeoecology*, 205: 255-272.
- Langmuir, D., 1997. *Aqueous Environmental Geochemistry*. Prentice Hall, New Jersey, 600 pp.
- Larkin, J.M. and Strohl, W.R., 1983. *Beggiatoa*, *Thiothrix*, and *Thioploca*. *Annual Reviews in Microbiology*, 37: 341-67.
- Larkin, J.M. and Henk, M.C., 1996. Filamentous sulfide-oxidizing bacteria at hydrocarbon seeps of the Gulf of Mexico. *Microscopy Research and Technique*, 33: 23-31.
- Lindgren, W., 1933. *Mineral deposits*, 4th edition. McGraw-Hill Publishers, New York, 930 pp.
- Lu, Z.C., Liu, C.Q., Liu, J.J., and Wu, F.C., 2004. The bio-barite in witherite deposits from Southern Qinling and its significance. *Progress in Natural Science*, 14: 889-895.
- Martin, E.E., Macdougall, J.D., Herbert, T.D., Paytan, A., and Kastner, M., 1995. Strontium and neodymium isotopic analyses of marine barite separates. *Geochimica et Cosmochimica Acta*, 59: 1353-1361.
- McManus, J., Barelson, W.M., Klinkhammer, G.P., Johnson, K.S., Coale, K.H., Anderson, R.F., Kumar, N., Burdige, D.J., Hammond, D.E., Brumsack, H.J., McCorkle, D.V., and Rusdhi, A., 1998. Geochemistry of barium in marine sediments: implications for its use as paleoproxy. *Geochimica et Cosmochimica Acta*, 62: 3454-3473.
- Miller, R.E., Brobst, D.A., and Beck, P.C., 1977. The organic geochemistry of black sedimentary barite: significance and implications of trapped fatty acids. *Organic Geochemistry*, 1: 11-26.
- Newton, R.J., Pevitt, E.L., Wignall, P.B., and Bottrell, S.H., 2004. Large shifts in the isotopic composition of seawater sulphate across the Permo-Triassic boundary in northern Italy. *Earth and Planetary Science Letters*, 218: 331-345.
- Paradis, S. and Lavoie, D., 1996. Multiple-stage diagenetic alteration and fluid history of Ordovician carbonate-hosted barite mineralization, Southern Quebec Appalachians. *Sedimentary Geology*, 107: 121-139.
- Paytan, A., Kastner, M., Martin, E.E., Macdougall, J.D., and Herbert, T., 1993. Marine barite as a monitor of seawater strontium isotope composition. *Nature*, 366: 445-449.

- Paytan, A. Mearon, S., Cobb, K., and Kastner, M., 2002. Origin of marine barite deposits: Sr and S isotope characterization. *Geology*, 30: 747-750.
- Pentecost, A., 2005. *Travertine*. Springer-Verlag, Heidelberg, 429 pp.
- Phoenix, V.R., Martinez, R.E., Konhauser, K.O., and Ferris, F.G., 2002. Characterization and implications of the cell surface reactivity of *Calothrix* sp. Strain KC97. *Applied and Environmental Microbiology*, 68: 4827-4834.
- Radanovic-Guzvica, B., 1999. The average structural density of barite crystals of different habit types. *Geologia Croatia*, 52: 59-65.
- Riedinger, N., Kasten, S., Groger, J., Franke, C., and Pfeifer, K., 2006. Active and buried authigenic barite fronts in sediments from the Eastern Cape Basin. *Earth and Planetary Sciences Letters*, 241: 876-887.
- Rippka, R., Deruelles, J., Waterbury, J.B., Herdman, M., and Stanier, R.Y., 1979. Generic assignments, strain histories and properties of pure cultures of cyanobacteria. *Journal of General Microbiology*, 111: 1-16.
- Sanchez-Moral, S., Luque, L., Canaveras, J.C., 2004. Bioinduced barium precipitation in *St. Callixtus* and *domitilla* catacombs. *Annals of Microbiology*, 54: 1-12.
- Sasaki, N. and Minato, H., 1982. Relationship between lattice constants and strontium and calcium contents of hokutolite. *Mineralogical Journal*, 11: 62-71.
- Shields, G.A., Deynoux, M., Strauss, H., Paquet, H., Nahon, D. 2007. Barite-bearing cap dolostones of the Taoudeni Basin, northwest Africa: Sedimentary and isotopic evidence for methane seepage after a Neoproterozoic glaciation. *Precambrian Research*, 153: 209-235.
- Schlegel, H.G. and Bowien, B., 1987. *Autotrophic Bacteria*. Science Tech Publishers, Madison, Wisconsin, 531 pp.
- Schwartz, H., 2005. Microbialites in the Moreno Formation paleoseep carbonates, Panoche-Tumey Hills, San Joaquin Valley. *Geological Society of America, Abstracts with Programs*, 37: 77.
- Shikazono, N., 1994. Precipitation mechanisms of barite in sulfate-sulfide deposits in back-arc basins. *Geochimica et Cosmochimica Acta*, 58: 2203-2213.
- Smith, E., Hamilton-Taylor, J., Davison, W., Fullwood, N.J., and McGrath, M., 2004. The effect of humic substances on barite precipitation-dissolution behaviour in natural and synthetic lake waters. *Chemical Geology*, 207: 81-89.
- SOLMINEQ88, 1988. A computer program for geochemical modeling of water-rock interactions developed by the United States Geological Survey. *Water Investigations Report 88-05*
- Stark, A.I.R., Wogelius, R.A., Collins, I.R., and Vaughan, D.J., 2004. Kinetic and thermodynamic controls on the precipitation and morphology of barite (BaSO₄). Extended abstract, Goldschmidt conference proceedings, Copenhagen. Theme 2: The dynamic interface, p. A148.
- Stoner, D.L., Burbank, N.S., and Miller, K.S., 1994. Anaerobic Transformation of Organosulfur Compounds in Microbial Mats from Octopus Springs. *Geomicrobiology Journal*, 12: 195-202.

- Studel, R., 1987. On the nature of the “elemental sulfur” (S^0) produced by sulfur-oxidizing bacteria – a model for S^0 globules. In: Schlegel, H.G., Bowien, B. (Eds.), *Autotrophic Bacteria*, Science Tech Publishers, Madison, Wisconsin, pp. 289-303.
- Su, H-Y., Lee, J-S., and Yu, S-C., 2002. Dopant effect on hokutolite crystals synthesized with hydrothermal process. *Western Pacific Earth Sciences*, 2: 301-318.
- Suganuma, I., 1928. On the constituents and genesis of a few minerals produced from hot springs and their vicinities in Japan. I. The Akita Hokutolite. *Journal of the Chemical Society of Japan*, 3: 69-73.
- Tazaki, K. and Watanabe, H., 2004. Biomineralization of radioactive sulfide minerals in strong acidic Tamagawa Hot Springs. *Science Reports of the Kanazawa University*, 49: 1-24.
- Tazaki, K., Webster, J., and Fyfe, W.S., 1997. Transformation processes of microbial barite to sediments in Antarctica. *Japanese Journal of Geology*, 26: 63-68.
- Teske, A. and Nelson, D.C., 2005. The genera *Beggiatoa* and *Thiothrix*. In: *The Prokaryotes – an evolving online resource for the microbiological community*. Dworkin, M. (Ed.), BETA Release 3.20: http://141.150.157.117:8080/prokPUB/chaphtm/432/01_00.htm
- Tesoiero, A.J. and Pankow, J.F., 1996. Solid solution partitioning of Sr^{2+} , Ba^{2+} , and Cd^{2+} to calcite. *Geochimica et Cosmochimica Acta*, 60: 1053-1063.
- Torres, M.E., Bohrmann, G., Dube, T.E., and Poole, F.G., 2003. Formation of modern and Paleozoic stratiform barite at cold methane seeps on continental margins. *Geology*, 31: 897-900.
- Van Everdingen, R.O., 1972. *Thermal and Mineral Spring in the Southern Rocky Mountains of Canada*. Water Management Service, Department of the Environment, Environment Canada, 151 pp.
- Wagner, T., Kirnbauer, T., Boyce, A.J., and Fallick, A.E., 2005. Barite-pyrite mineralization of the Wiesbaden thermal spring system, Germany: a 500-kyr record of geochemical evolution. *Geofluids*, 5: 124-139.
- Walter, M.R., Bauld, J. 1983. The association of sulphate evaporates, stromatolitic carbonates and glacial sediments: examples from the Proterozoic of Australia and the Cainozoic of Antarctica. *Precambrian Research*, 21: 129-148.
- Wentworth, J., Nelman, M., Byrne, M., Longazo, T., Galindo, C., McKay, D.S., Sams, C. 2003. Modern microbial fossilization processes as signatures for interpreting ancient terrestrial and extraterrestrial microbial forms. *Lunar and Planetary Science XXIV*: 1909.pdf
- Wher, J.D. and Sheath, G., 2003. *Freshwater Algae of North America: Ecology and Classification*. Academic Press, San Diego, CA, 950 pp.
- Yee, N., Phoenix, V.R., Konhauser, K.O., Benning, L.G., and Ferris, F.G., 2003. The effect of cyanobacteria on silica precipitation at neutral pH - implications for bacterial silicification in geothermal hot springs. *Chemical Geology*, 199: 83-90.
- Younger, P., 1986. Barite travertine from southwestern Oklahoma and west-central Colorado. Unpublished M.Sc.Thesis, Oklahoma State University, Stillwater, OK, USA, 163 pp.

Chapter 6 **Experimental precipitation of barite (BaSO₄) among streamers of sulphur oxidizing bacteria***

Introduction

Barite, which is texturally crystallographically and geochemically sensitive to the conditions of its depositional environment, has high potential to preserve palaeoenvironmental indicators over geologic timescales (Graber 1988; Kastner 1999; Paytan et al. 2002; Bains et al. 2000; Hanor, 2000; Lu et al. 2004). Barite forms in numerous microbially-colonised habitats, including marine cold seeps, white smokers, hot springs, and the upper water columns of lakes and oceans. Despite common recognition that sulphur-metabolizing microbes mediate barite saturation, however (e.g. Baldi et al. 1996; Sakorn et al. 2002; Gonzalez-Munoz et al. 2003; Senko et al. 2004), their influence on the textural development of barite is poorly understood (Fu et al., 1994; Aharon, 2000; Paytan et al. 2002; Riedinger et al. 2006; Bonny and Jones, 2007; Bonny and Jones, *in press*). Interpretation of putative biogenic barite in the geologic record, including stromatolitic barite associated with deep and shallow hydrothermal systems (Graber 1988; Fu et al. 1994; Carroue 1996; Aloisi et al. 2004), requires examination of the conditions under which biogenic textures form and are preserved in barite.

This study initiates investigation into microbial influences on barite precipitation by examining barite produced experimentally by mixing barium and sulphate-rich solutions in the presence of bacterial streamers. Four experiments were designed to assess the impact of limiting the availability and changing the order of addition of barium and sulfate on the arrangement of the barite precipitates. In this paper, the habit and arrangement of the experimentally precipitated barite crystals are described and compared to natural barite crystals precipitated in microbially colonised habitats. Despite the simplicity of these experiments, they provide important information regarding the conditions under which barite precipitation will be localised on microbial cells, which should be factored into petrographic interpretations of low-temperature barite deposits in the geologic record.

* A version of this chapter has been submitted for publication.

Bonny, S. and Jones, B. xxxx. *Experimental precipitation of barite (BaSO₄) among streamers of sulphur oxidizing bacteria*, *Journal of Sedimentary Research*.

Methods

Ten ~100 g samples of streamer-forming microbes were collected in July, 2005, from the Jasper Cold Sulphur Springs in Jasper National Park, Alberta (Fig. 6-1A). These springs emerge at 9°C, pH 7.2, and contain H₂S and CO₂ gas up to 9 and 20 ppm, respectively (van Everdingen 1972). Mineral precipitation is limited to bright yellow-white deposits of elemental sulphur that form colloidal films in spring water eddies and are deposited among the microbial streamers sampled for this study (Fig. 6-1B). One half of each microbial sample was stored in spring water and the other preserved in a 6:3:1 solution of water, 95% alcohol and formalin with 5 ml of glycerol added per 100 ml. Preserved microbes were examined by light microscopy and identified to generic level on the basis of morphological criteria following Wher and Sheath (2003), Douglas and Douglas (2001), and Teske and Nelson (2005). Microbial samples stored in spring water were refrigerated overnight and used for barite precipitation experiments the following day.

Barite precipitation experiments were conducted with barium (deionized water with 14.0 mMol/L BaCl₂, pH 6.8) and sulphate (deionized water with 8.8 mMol/L Na₂SO₄, pH 7.1) solutions in 250 ml glass beakers at room temperature (23 °C). The barium and sulphate solutions were prepared in strong concentrations to promote rapid barite precipitation (cf. Blount, 1977) and deionized water was used to minimize uncontrolled sources of reactive ions.

Experiments were initiated in 250 ml glass beakers that each contained 200 ml of barium solution. Experiment A tested barite precipitation in the absence of bacterial streamers, whereas in experiments B, C, and D subsamples of bacterial streamers (containing trapped elemental sulphur) were immersed in the barium solution for 8 hours, suspended from plastic-coated pins held in place by nylon thread taped to the outside of the beakers (Fig. 1C). Barite precipitation was induced in the final step of each experiment:

Experiment A— 2 ml of sulphate solution was added by pipette.

Experiment B— 2 ml of sulphate solution was added by pipette (Fig. 1D).

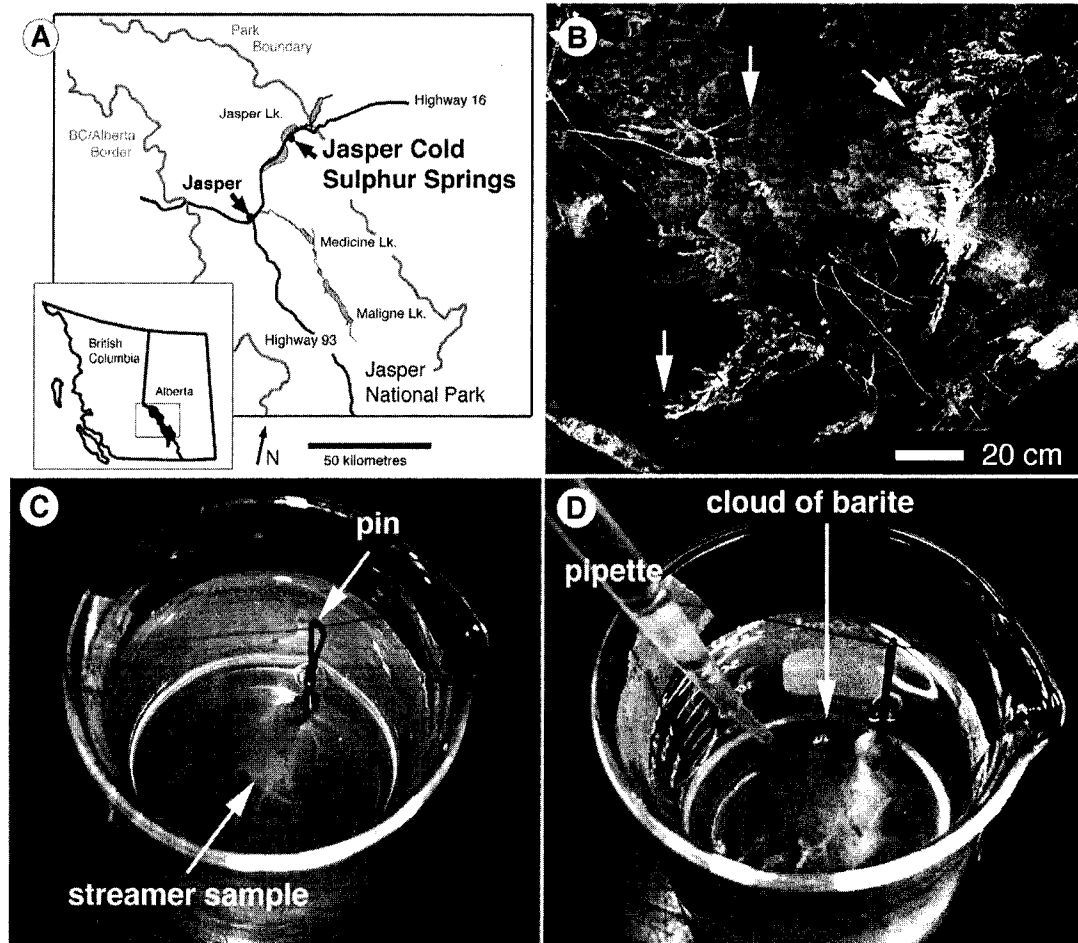


Figure 6-1. (A) Sample location. (B) White microbial fringes (arrows) on branches and grass in the Jasper Cold Sulphur Spring flow path. (C) Experimental set up for barite precipitation experiments. (D) Addition of sulphate solution to barium solution by pipette.

Experiment C—bacterial streamers were removed from the barium solution without addition of sulphate.

Experiment D— the bacterial streamers were removed from the barium solution, rinsed, and immersed in 200 ml sulphate solution.

Fifteen minutes after each final step, the white precipitates collected from the bottom of beakers in experiment A, and bacterial streamers from experiments B, C, and D were rinsed three times in deionized water and placed on glass slides. The slides were examined by petrographic microscope (without cover slips) to determine if mineral precipitates were present, and then desiccated under a lamp (with maximum temperature approaching 40°C).

Samples of un-treated bacterial streamers and subsamples of barite precipitates from each trial of each experiment were mounted on steel stubs with carbon tape, sputter coated with gold (for 1 minute, producing a coating 1 Å thick) and examined on a JEOL 6301 field emission scanning electron microscope (SEM) at accelerating voltages of 5 kV for secondary electron imaging, and 20 kV for backscattered electron imaging. In backscattered electron SEM images, variations in atomic weight are reflected in image brightness – barium (with an atomic mass of 137.3) is very bright in contrast to increasingly dark calcium (40.1), sulphur (32.1), silicon (28.1), calcium and organic material (~12.0). This contrast facilitated recognition of barite crystals in the bacterial streamers. Crystals were then probed by energy dispersive X-ray analysis to determine their elemental composition.

Microbial Samples

The streamer-forming microbes from Jasper Cold Sulphur Spring are colourless with unsheathed, septate filaments and numerous internal sulphur globules (Fig. 6-2A, B). Two sizes of filament are present: small-diameter filaments (3 µm diameter, septa 2-3 µm apart) and less abundant large-diameter filaments (5-6 µm diameter, septa 3-4 µm apart). Both form hormogonia and exhibit gliding motility. These criteria indicate affinity to the sulphur-oxidising bacteria *Beggiatoa*, a dysoxic niche-inhabiting microbe that is

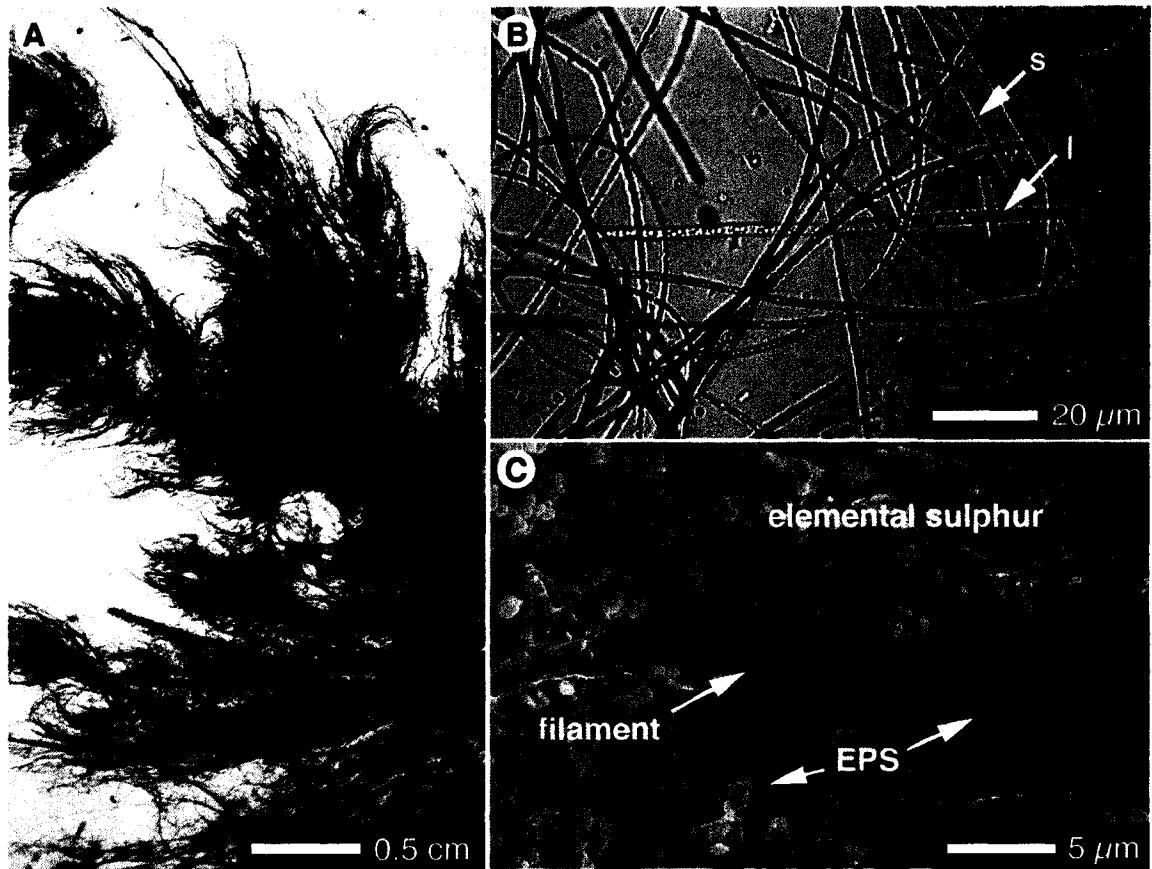


Figure 6-2. (A) Light microscope photograph of a microbial 'streamer'. (B) Filaments of small (s-arrow) and large (l-arrow) diameter *Beggiatoa*. (C) SEM image of collapsed filament surrounded by beads and rhombs of elemental sulphur, and thin strings of desiccated EPS.

common in both marine and continental barite-precipitating environments (Teske and Nelson 2005; Bonny and Jones 2007).

Most of the *Beggiatoa* streamers from Jasper Cold Sulphur Spring contain trapped rhombs and beads of elemental sulphur and extracellular polysaccharides (EPS) (Fig. 6-2C). These were not removed from the samples before the barite precipitation experiments because it would have been difficult to accomplish this without destroying the filaments, and elemental sulphur and EPS are also present in most natural low temperature barite-precipitating environments (Teske and Nelson 2005).

Results

The habit and arrangement of barite precipitates differed greatly between experiments conducted with and without bacterial streamers, and with the relative amount of sulphate provided for barium precipitation.

Experiment A — Introduction of the sulphate to the barium solution produced an instantaneous white ‘cloud’ of microcrystalline barite in all three experimental runs. The precipitated barite formed as stellate rosettes of intergrown microcrystalline plates ≤ 2 μm wide (Fig. 6-3A), microgranules < 300 nm wide (Fig. 6-4B), and scalloped dendritic ‘angel wing’ crystals up to 10 μm wide (Fig. 6-3C).

Experiment B — Introduction of sulphate to the barium solutions produced ‘clouds’ of microcrystalline barite and white frostings on the microbial samples in all three runs. Barite precipitated amid the EPS was euhedral, with ‘bowtie’ and single and intergrown platy to tabular crystal morphologies (Fig. 6-3D, E), whereas barite nucleated on filaments precipitated as tabular and scalloped platy crystals (Fig. 6-3F). Angel wing barite crystals like those formed in Experiment A were also found among the streamers (Fig. 6-3F). The fact that they formed as poly-terminal crystals (without flat edges or other evidence of growth restriction) indicates that they were not nucleated on microbial substrates, but formed in solution and settled onto the streamers.

Experiment C — Immersion of the microbial streamer samples in barium solution for 8 hours, without addition of sulphate did not produce macroscopic evidence (i.e. a cloud or frosting) of barite precipitation. Following rinsing and desiccation, SEM analyses revealed barite crystals localised on bacterial filaments in all three trial beakers.

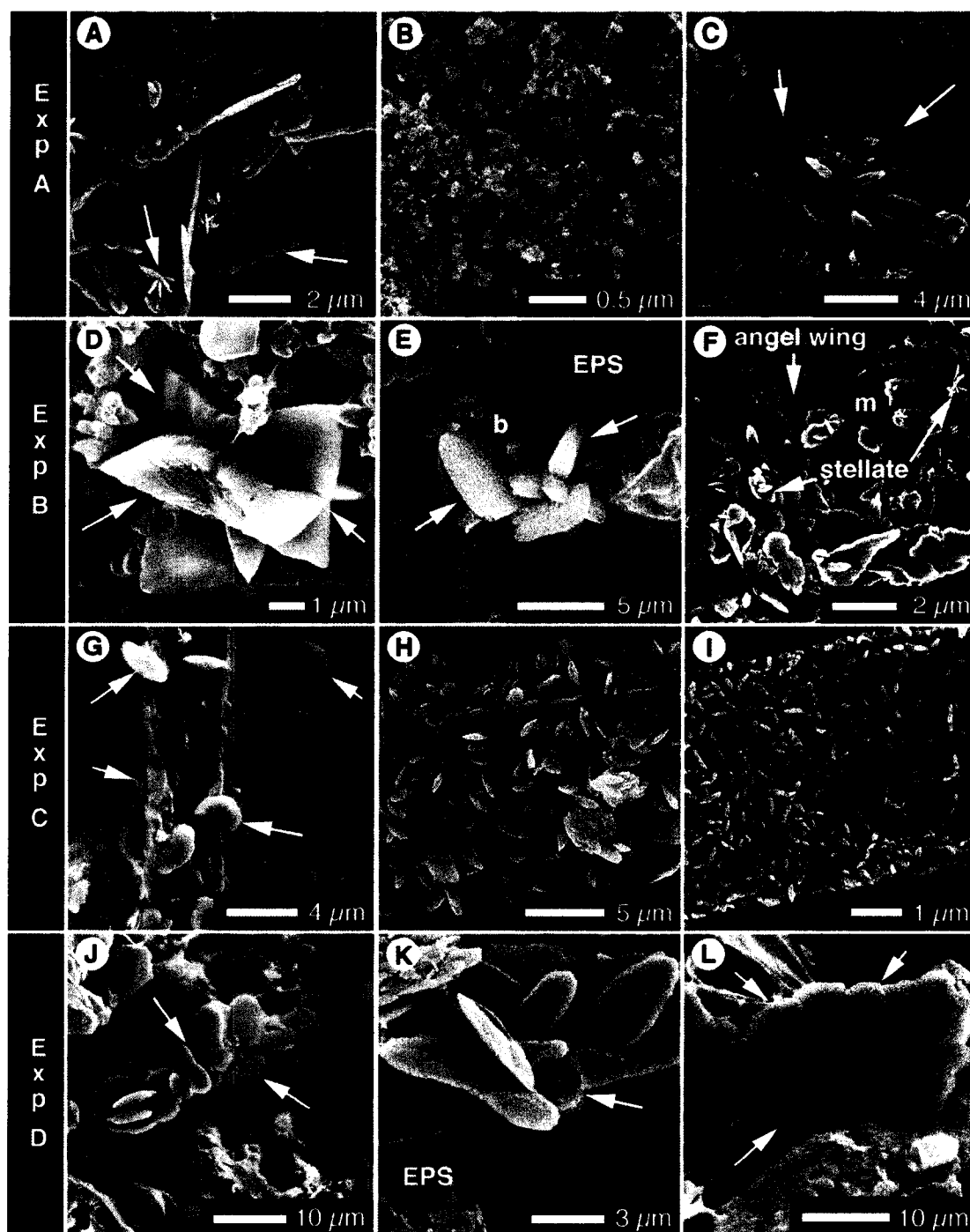


Figure 6-3. SEM images of experimentally precipitated barite. Exp A: (A) 'angel wing' and stellate platy barite (arrows); (B) detail - twinned 'angel wing' barite; (C) anhedral micrometric barite precipitates. Exp B: (D) twinned 'bowtie' barite in EPS; (E) intergrown rounded tabular barite (b) in EPS; (F) angel wing and stellate barite (arrows) on a filament (m) with platy barite microcrystals. Exp C: (G) rounded platy barite crystals (arrows) nucleated on a filament; (H) heavy coat of rounded platy barite on a filament; (I) light coat of submicron-sized anhedral barite plates on a filament. Exp D: (J) 'string' of scalloped platy barite rosettes surrounded by EPS (eps) and elemental sulphur (s); (K) cross-section through a string of platy barite rosettes surrounded by EPS (eps) with a central cylindrical cavity (arrow); (L) detail of scalloped platy barite crystal.

These barite crystals, consistently $\leq 5 \mu\text{m}$, were present as sparse coatings of subhedral rounded barite plates (Fig. 6-3G), as dense coatings of subhedral rounded barite plates (Fig. 6-3H), and as dense coatings of submicron-sized elongate anhedral barite (Fig. 6-3I). Several scalloped platy barite crystals were also found in EPS surrounding barite-hosting microbes.

Experiment D—Immersion of the microbial samples in barium solution for 8 hours followed by rinsing and immersion in sulphate solution immediately produced a white ‘frosting’ around the streamers. Barite precipitated as scalloped plates, up to $10 \mu\text{m}$ wide, that occurred singly, as rosettes nucleated on EPS, and as ‘strings’ (Fig. 6-3J-L). The strings typically have central cavities that contain collapsed microbial filaments (Fig. 6-3J, K).

Iron Oxides and Sulphides—The plastic coating on two of the pins used in the barite precipitation experiments was cracked, allowing reaction between the barium and sulphate solutions and iron in the pins. This interaction was first evident from 1-4 mm diameter rust-coloured aureoles on streamer samples in one trial from experiment B and one from experiment D. The aureole from experiment D contained reticulate coatings of amorphous iron oxides that probably formed by oxidative ‘rusting’ of iron in the pin. The reticulate iron oxides formed indiscriminately on EPS and scalloped platy barite strings (Fig. 6-4A, B). The rusty aureole from experiment B also contained amorphous iron sulphide (FeS) that formed cauliflower shaped clusters $\leq 3 \mu\text{m}$ wide, and was ‘sandwiched’ between platy barite crystals, commonly forming composite rosettes (Fig. 6-4C, D). The barite/FeS sandwiches were surrounded by strings of desiccated EPS, indicating that they were enveloped by hydrated EPS during precipitation.

Interpretation and Discussion

Diffusion membrane controlled barite precipitation experiments generate relatively predictable barite crystal habits that can be correlated to specific chemical and redox conditions (e.g. Sermon et al., 2004; Sanchez-Pastor et al., 2006). In free solutions, however, barite crystal habit can vary widely within a constrained depositional setting (Shikazono, 1994; Radanovic-Guzvica, 1999; Torres et al., 2003). This is well illustrated by the diversity of crystal habits produced within 250 ml beakers in this study. The

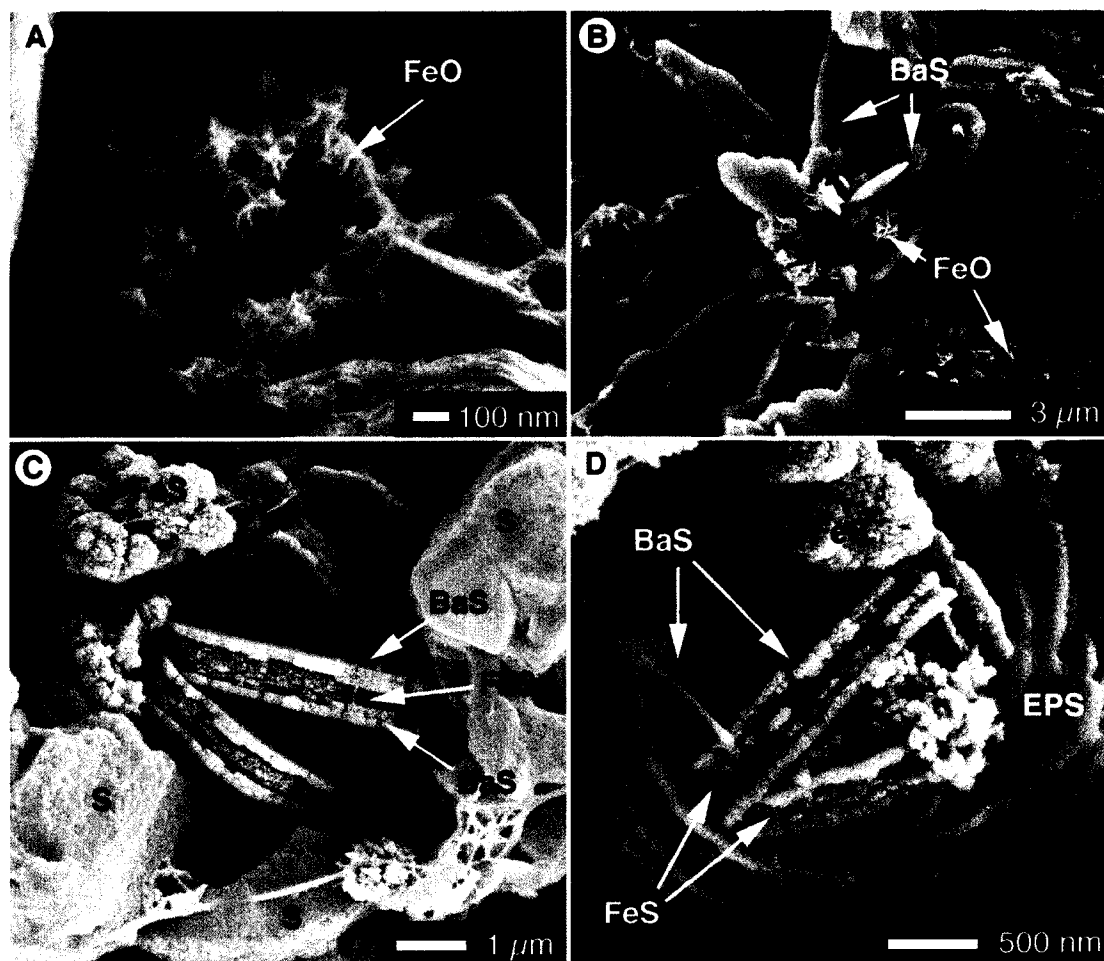


Figure 6-4. SEM images of iron precipitates. (A) Reticulate coating of iron oxide (FeO). (B) Reticulate iron oxides (FeO) on a string of scalloped platy barite (BaS). (C) Amorphous iron sulphide (FeS) occurring as clusters, and 'sandwiched' between platy barite crystals (BaS), surrounded by elemental sulphur (S). (D) Detail of a rosette surrounded by EPS (EPS), which is composed of intergrown barite (BaS)/iron sulphide (FeS) 'sandwiches'.

chemical and redox heterogeneity of natural barite-precipitating solutions and the common presence of adsorptive microbial biomass make it difficult to apply bulk solution thermodynamic models to the petrographic interpretation of low temperature barite. In nature, barite saturation varies along steep (commonly microscale) chemical and redox gradients that, at low temperature, are commonly established or influenced by microbes (Su et al., 2002; Aloisi et al., 2004; Senko et al., 2004; Riedinger et al., 2006). The experimental barite precipitated from oxygenated solutions dissimilar to the dysoxic solutions inhabited by sulphur oxidizing bacteria in nature: the experimental solutions had high levels of Ba^{2+} and SO_4^{2-} , but low concentrations of other ions and dissolved gases that influence barite crystal habit and barite saturation gradients in barite-precipitating spring and sea water (such as Na^+ , Ca^{2+} , Mg^{2+} , Sr^{2+} , Cl^- , HCO_3^- , CO_2 , H_2S , CH_4 ; Bonny and Jones 2007; Aloisi et al., 2004). Nonetheless, the experimental precipitates have textural analogues in natural 'inorganic' and microbially-associated barite.

It has been demonstrated that barite crystal habit varies with solution chemistry, hydrodynamics, and degree of saturation (Sasaki and Minato, 1982; Shikazono, 1994; Radanovic-Guzvica, 1999; Su et al., 2002; Sanchez-Pastor et al., 2006). The stellate barite crystal rosettes formed in Experiment A, which are typical precipitates at air-water interfaces in barite-supersaturated solutions (Sermon et al., 2004), probably formed in the upper layers of the water in the experimental beaker soon after introduction of the sulphate solution. Anhydral microgranular barite, a product of rapid barite precipitation from extremely supersaturated solutions (Bala et al., 2005), probably formed most of the white 'cloud' produced when the sulphate solution was added to the barium solutions. Undissolved Na_2SO_4 and BaCl_2 particles can sometimes act as nuclei in laboratory barite precipitation experiments, and may have promoted precipitation of fine-grained, poorly crystalline barite (Blount, 1977). The scalloped and dendritic barite crystals formed in Experiments A and B are also typical of rapid precipitation (Shikazono, 1994; Stark et al., 2004) but form in solutions with limited ionic reactants, such that crystals 'scavenge' the solution by extending their crystal lattices to maximize reactive surface area (Saratovkin, 1959). Similar platy 'angel-wing' calcite (CaCO_3) crystals form in hot spring flow paths where rapid CO_2 degassing has established an excess of CO_3^{2-}

compared to Ca^{2+} (Jones and Renault, 1998). In these experiments, an excess of Ba^{2+} relative to SO_4^{2-} established by precipitation of microgranular barite, may have promoted secondary precipitation of angel-wing barite crystals.

In contrast to the barite precipitates formed rapidly in solution, euhedral tabular barite crystals generally form under conditions of lower supersaturation than scalloped and dendritic forms (Shikazono, 1994; Greinert et al., 2002). The 'bowtie' and tabular barite precipitated among bacterial streamers in Experiment B may have formed in microenvironments in EPS surrounding filaments that had a lower degree of barite supersaturation than the ambient solution as a result of retarded ionic diffusion to crystal growth faces through viscous EPS (cf. Buczynski and Chafetz, 1991; Arp et al., 1999).

In Experiment B, barite precipitation was not substrate selective, as it appears to have taken place in solution, in EPS, and on the surface of bacterial filaments. Nevertheless, precipitation of barite in EPS and on microbial cells indicates that these substrates were capable of hosting barite crystal nucleation. Above pH 4, the surfaces of filamentous sulphur bacteria and associated EPS usually carry an overall negative charge due to the presence of deprotonated carboxyl and phosphoryl groups, which attract divalent metal cations, like Ba^{2+} (Beveridge, 1989; Schultze-Lam et al., 1993; Sand et al., 1995; Podol'skaya et al., 2003; Teske and Nelson, 2005). Nucleation of barite in EPS and on microbial surfaces indicates that barium was probably adsorbed to negatively charged sites in the streamers, which provided localised sites for barite nucleation once sulphate was introduced.

Nucleation of barite on microbial substrates in Experiment C implies that barium was adsorbed to negatively charged sites on the outer cellular surface, similar to in Experiment B. The fact that barite microcrystals large enough for identification by petrographic microscope (i.e. $\sim 0.2 \mu\text{m}$ long) appeared only after sample desiccation, suggests that barium was retained by these charged sites through sample rinsing and provided a locus for precipitation of sulphate generated during desiccation. Sulphate may have been sourced from spontaneous oxidation of elemental sulphur trapped in the streamer samples (Brigmon et al., 1994), or from the bacterial filaments themselves. The fact that very little barite was found in associated EPS, which also adsorbs divalent cations and hosts elemental sulphur, argues for filament-sourced sulphate. This does not

imply that sulphate was produced by bacterial metabolism – it is, in fact, quite likely that desiccation of the filaments induced degradation of sulphur containing organic compounds in the filament walls (proteins and methylated sulphur compounds) and/or oxidation of vesicular intracellular sulphur (Stoner et al., 1994).

In Experiment D, sequential exposure of bacterial streamers first to barium, and then to unlimited sulphate, also produced barite crystals arranged on microbial substrates. Scalloped platy barite is typical of rapid barite precipitation from supersaturated solutions (Shikazono, 1994; Stark et al., 2004). Its presence around microbial filaments and associated EPS in experiment D indicates that significant amounts of barium were adsorbed by the bacterial streamers before immersion in sulphate solution.

The propensity of microbial streamers and biofilms to adsorb divalent cations in EPS and on cell walls is well established (e.g. Beveridge, 1989; Schultze-Lam et al., 1993; Arp et al., 1999), and exposure of barium-enriched biomass to sulphate has been implicated in localised barite precipitation among microbes growing in Antarctic lakes (Tazaki et al., 1997), Roman Catacombs (Sanchez-Moral et al., 2004), and around volcanic fumaroles (Glamoclija et al., 2004). In those natural settings, barite takes the form of subhedral to euhedral prisms (generally $\leq 10 \mu\text{m}$), which are generally distributed in EPS, rather than directly nucleated on microbial cells or filaments. The ‘bowtie’ and tabular barite produced in Experiment B might be considered counterparts to those crystals, with their anomalous morphology attributable to the low concentrations of foreign ions in the experimental solutions compared to natural spring and sea waters (cf. Blount, 1977).

Precipitation of barite on microbial filaments has only been documented from the dysoxic flow path of northern Canada’s Flybye Springs, where filamentous microbes are coated by subhedral barite microcrystals similar to those produced on filaments in experiment C (Bonny and Jones, 2007a). In this study, barite was preferentially localised on microbial substrates only in experiments C and D, where removal of samples from the barium solution ensured that barium adsorbed to microbes and EPS was the primary reactant once sulphate was added. Similarly, at Flybye Spring, barite forms preferentially on microbial cells only under conditions where sulphate and barium are dilute enough in solution that adsorptive concentration of barium to cell surfaces becomes important to

overcoming barite nucleation thresholds (Bonny and Jones, 2007a). For barium to adsorb to cellular surfaces, rather than precipitating in solution, sulphate concentrations must be ambiently low. The results of Experiment C indicate that, for barite precipitation to be restricted to cell surfaces sulphate must, further, be microbially sourced (either by metabolic sulphur oxidation, or by degradation of organo-sulphur compounds or intracellular elemental sulphur). In contrast, when barium-rich solutions oxidize rapidly (i.e. sulphate is not limiting), they precipitate laminated crystalline barites that lack biogenic textures (e.g. Sugauma, 1928; Sasaki and Minato, 1982; Younger, 1986).

At Flyby Springs, exposure of filaments with hosting barite microcrystals to dysoxic, sulphate-bearing waters results in precipitation of enveloping barite cements leading to the production of barite 'strings' up to 300 μm in diameter, which are preserved as biogenic textures in lithified barite (Bonny and Jones, *in press*). The strings of platy barite rosettes generated in experiment D also formed by crystallographic extension of barite nuclei precipitated on microbial filaments. Similar putatively biogenic strings of radially-arranged barite microcrystals with hollow and organic carbon-rich cores have been reported from barite chimneys formed around submarine cold seeps (Fu et al., 1994; Aloisi et al., 2004), indicating that microbial surfaces are suited to host barite precipitation, becoming basal to biogenic barite textures in diverse environmental settings.

The precipitation of mixed-oxidation state barite/FeS sandwiches in Experiments B and D indicates that dysoxic conditions were locally maintained in the bacterial streamers, despite the fact that they were immersed in oxidized solutions. Localised dysoxia may have been maintained by delayed oxygen diffusion through EPS and/or by consumption of oxygen via spontaneous oxidation of elemental sulphur. To the authors' knowledge, rosettes of intergrown barite/FeS sandwiches are a novel product of these precipitation experiments, but mixed-oxidation state sulphur assemblages are well known in the geologic record. Fluctuating redox boundaries around hydrothermal vents, methane seeps, and in marine sediments commonly produce barite deposits that host reduced sulphur minerals (e.g. pyrite or marcasite) and/or amorphous sulphides (FeS_x) (Fu et al., 1994; Fortin et al., 1998; Kastner, 1999). In ambient temperature deposits, sulphide mineral inclusions generally form around degrading organic matter or as a byproduct of

bacterial sulphur reduction (Shen et al., 2001; Huston and Logan, 2004). Precipitation of mixed-oxidation state barite/FeS sandwiches found in experiments B and D demonstrates that these redox fluctuations can occur along micrometric gradients.

Biogenic barite textures and barite-hosted sulphides have high potential for diagenetic resistance because of barite's insolubility through oxic diagenesis (Karnachuk et al., 2002). Putative biogenically textured barites, including barite stromatolites, have been reported from Recent (Fu et al., 1994; Greinert et al., 2002; Aloisi et al., 2004), Paleozoic (Graber, 1988; Carroue, 1996), and Precambrian (Buick et al., 1981; Kiyokawa et al., 2006) strata, and pyrite preserved in barite provides some of the earliest geochemical evidence for bacterial metabolism (Shen et al., 2001). Further investigation of barite precipitation in the presence of microbes in natural and laboratory settings is required to facilitate accurate palaeoenvironmental and palaeoecological interpretation of these and other low temperature barite deposits (Torres et al., 2003; Riedinger et al., 2006). The preliminary results of this study, however, have interesting implications for prospecting low temperature barite deposits for biogenic textures, or 'biomarkers.' If barite coatings on microbial filaments (which become basal to biogenic textures in lithified barite) form preferentially where barium and sulphate are limiting, focus should be placed on barite precipitated below redox interfaces.

In many barite deposits, potential biomarker zones may be spatially set apart from volumetrically dominant laminated crystalline barite precipitates. For example, biogenic textures might appear in barite formed in microbially maintained dysoxic horizons below the sediment water interface at cold methane seeps (Larkin and Henk, 1996; Huston and Logan, 2004; Riedinger et al., 2006), or in sulphate-limited niches proximal to anoxic hydrothermal and hydrocarbon vents (Graber, 1988; Fu et al., 1994; Greinert et al., 2002; Aloisi et al., 2004). In contrast, Precambrian (and extraterrestrial) barite deposits, formed where volcanogenic sulphate mixes with reduced, barium-bearing sea or ground water (Huston and Logan, 2004), may be more likely to preserve biogenic textures in their distal reaches. Sulphate oxidizing bacteria are not thought to have evolved until 0.64-1.5 Ga (Canfield and Teske, 1996), but filamentous bacteria and associated EPS were present as early as 3.5 Ga (Brocks et al., 1999; Shen et al., 2001) and likely had similar ability to adsorb barium and facilitate the development of biogenic textures in barite.

Conclusions

Precipitation of barite among bacterial streamers demonstrated that: (1) multiple barite crystal habits can co-precipitate in close-proximity; (2) sulphur oxidizing bacteria and associated EPS are suitable substrates for barite precipitation; (3) localization of barite precipitates on the outer cell surface of bacteria is facilitated by adsorption of barium; and that (4) barite precipitation is restricted to microbial substrates only when they are exposed to barium while sulphate is limiting, or are the source of sulphate in a sulphate-limited system. These results suggest that biogenic textures will be best developed in natural barites precipitated under anoxic-dysoxic conditions.

References

- Aharon, P. 2000. Microbial processes and products fueled by hydrocarbons at submarine seeps. In: Riding, R., Awramik, S.M. (Eds.), *Microbial Sediments*, Springer-Verlag, Heidelberg Germany, pp. 270-281.
- Aloisi, G., Wallmann, K., Bollwerk, S.M., Derkachev, A., Bohrmann, G. and Suess, E. 2004. The effect of dissolved barium on biogeochemical processes at cold seeps. *Geochimica et Cosmochimica Acta*, 68: 1735-1748.
- Arp, G., Theil, V., Reimer, A. Michaelis, W., and Reitner, J. 1999. Biofilm exopolymers control microbialite formation at thermal springs discharging into the alkaline Pyramid Lake, Nevada, USA. *Sedimentary Geology*, 126: 159-176.
- Bains, S., Norris, R.D., Cornfield, R.M., and Faul, K.L. 2000. Termination of global warmth at the Palaeocene/Eocene boundary through productivity feedback. *Nature*, 407: 171-174.
- Bala, H., Fu, W., Zhae, J., Ding, X., Jiang, Y., Yu, K., and Wang, X. 2005. Preparation of BaSO₄ nanoparticles with self-dispersing properties. *Colloids and Surfaces A*, 252: 129-134.
- Baldi, F., Pepi, M., Burrini, D., Kniewald, G., Scali, D., and Lanciotti, E. 1996. Dissolution of barium from barite in sewage sludges and cultures of *Desulphobibrio desulphuricans*. *Applied and Environmental Microbiology*, 62: 2398-2404.
- Beveridge, T.J., 1989, Role of cellular design in bacterial metal accumulation and mineralization: *Annual Reviews in Microbiology*, 43:147-171.
- Blount, C.W. 1977. Barite solubilities and thermodynamic quantities up to 300 °C and 1400 bars. *American Mineralogist*, 62: 942-957.
- Bonny, S. and Jones, B. *in press*. Barite (BaSO₄) biomineralisation at Flybye Springs, a cold sulphur spring system in Canada's Northwest Territories. *Canadian Journal of Earth Sciences*, 20 pp.
- Bonny, S. and Jones, B. 2007. Diatom-mediated barite precipitation in microbial mats calcifying at Stinking Springs, a warm sulphur spring system in Northwester Utah, USA. *Sedimentary Geology*, 194: 223-244.
- Brigmon, R.L., Martin, H.W., Morris, T.L., Bitton, G., and Zam, S.G. 1994. Biogeochemical ecology of *Thiothrix* spp. in underwater limestone caves. *Geomicrobiology Journal*, 12: 141-159.
- Brocks, J.J., Logan, G.A., Buick, R., and Summons, R.E. 1999. Archean molecular fossils and the early rise of Eukaryotes. *Science*, 285: 1033-1036.
- Buczynski, C. and Chafetz, H.S. 1991. Habit of bacterially induced precipitates of calcium carbonate and the influence of medium viscosity on mineralogy: *Journal of Sedimentary Petrology*, 61: 226-233.
- Buick, R., Dunlop, J.S.R., and Grooves, D.I. 1981. Stromatolite recognition in ancient rocks: an appraisal of irregularly laminated structures in an Early Archaean chert-barite unit from North Pole, Western Australia. *Alcheringa*, 5: 161-181.
- Canfield, D.E. and Teske, A. 1996. Late Proterozoic rise in atmospheric oxygen concentration inferred from phylogenetic and sulphur-isotope studies. *Nature*, 382: 127-132.

- Carroue, J-P. 1996. Une presentation originale de la barytine ou des stromatolithes de poids. *Mineraux et Fossiles*, 246: 21-22.
- Douglas, S. and Douglas, D.D. 2001. Structural and geomicrobiological characteristics of a microbial community from a cold sulphide spring. *Geomicrobiology Journal*, 18: 201-422.
- Fortin, D., Ferris, F.G., and Scott, S.D. 1998. Formation of Fe-silicates and Fe-oxides on bacterial surfaces in samples collected near hydrothermal vents on the Southern Explorer Ridge in the northeast Pacific Ocean. *American Mineralogist*, 83: 1399-1408.
- Fu, B., Aharon, P., Byerly, G.R., and Roberts, H.H. 1994. Barite chimneys on the Gulf of Mexico slope; initial report of their petrography and geochemistry. *Geo-Marine Letters*, 14: 81-87.
- Glamoclija, M., Garrel, L., Berthon, J., and Lopez-Garcia, P. 2004. Biosignatures and bacteria diversity in hydrothermal deposits of Solfatara Crater, Italy. *Geomicrobiology Journal*, 21: 529-541.
- Gonzalez-Munoz, M.T., Fernandez-Luque, B., Martinez-Ruiz, F., Chekroun, K.B., Arias, J.M., Rodriguez-Gallego, M., Martinez-Canamero, M., de Linares, C., and Paytan, A. 2003. Precipitation of Barite by *Myxococcus xanthus*: Possible Implications for the Biogeochemical Cycle of Barium. *Applied and Environmental Microbiology*, 69: 5722-5725.
- Graber, K.K. 1988. Stratigraphy and petrography of bedded barite in phosphatic Devonian Slaven chert, Toquima Range, Nye County, central Nevada [Unpublished MSc Thesis]: Houston, Texas, University of Houston, 294 pp.
- Greinert, J., Bollwerk, S.M., Derkachev, A., Bohrmann, G., and Suess, E. 2002. Massive barite deposits and carbonate mineralisation in the Derugin Basin, Sea of Okhotsk: Precipitation processes at cold seep sites. *Earth and Planetary Science Letters*, 203: 165-180.
- Hanor, J.S. 2000. Barite-celestine geochemistry and environments of formation. *Reviews in Mineralogy and Geochemistry*, 40: 193-275.
- Huston, D.L. and Logan, G.A. 2004. Barite, BIFs and bugs - evidence for the evolution of the Earth's early hydrosphere. *Earth and Planetary Science Letters*, 220: 41-55.
- Jones, B. and Renaut, R.W. 1998. Origin of platy calcite crystals in hot-spring deposits in the Kenya Rift Valley. *Journal of Sedimentary Research*, 68: 913-927.
- Karnachuk, O.V., Kurochkina, S.Y., and Tuovinen, O.H. 2002. Growth of sulphate-reducing bacteria with solid-phase electron acceptors. *Applied Microbiology and Biotechnology*, 58: 482-486.
- Kastner, M. 1999. Oceanic minerals - Their origin, nature of their environment, and significance. *Proceedings of the National Academy of Science*, 96: 3380-3387.
- Kiyokawa, S., Ito, T., Ikehara, M., and Kitajima, F. 2006. Middle Achaean volcano-hydrothermal sequence: Bacterial microfossil-bearing 3.2 Ga Dixon Island Formation, coastal Pilbara terrane, Australia. *Geological Society of America Bulletin*, 118: 3-22.
- Larkin, J.M. and Henk, M.C. 1996. Filamentous sulphide-oxidizing bacteria at hydrocarbon seeps of the Gulf of Mexico. *Microscopy Research and Technique*, 33: 23-31.

- Lu, Z.C., Liu, C.Q., Liu, J.J., and Wu, F.C. 2004. The bio-barite in witherite deposits from Southern Qinling and its significance. *Progress in Natural Science*, 14: 889-895.
- Paytan, A. Mearon, S., Cobb, K., and Kastner, M. 2002. Origin of marine barite deposits - Sr and S isotope characterization. *Geology*, 30: 747-750.
- Phoenix, V.R., Martinez, R.E., Konhauser, K.O., and Ferris, F.G. 2002. Characterization and implications of the cell surface reactivity of *Calothrix* sp. Strain KC97. *Applied and Environmental Microbiology*, 68: 4827-4834.
- Podol'skaya, V.I., Ermolenko, A.E., Yakubenko, L.N., U'berg, Z.R., 2003, Role of electro-surface properties of Thiobacteria and galenite in ore microbial leaching: *Colloid Journal*, 65: 482-487.
- Radanovic-Guzvica, B. 1999. The average structural density of barite crystals of different habit types: *Geologia Croatia*, 52: 59-65.
- Riedinger, N., Kasten, S., Groger, J., Franke, C., and Pfeifer, K. 2006. Active and buried authigenic barite fronts in sediments from the Eastern Cape Basin. *Earth and Planetary Sciences Letters*, 241: 876-887.
- Sakorn, P., Rakariyatham, N., Niamsup, H., and Nognkunsarn, P. 2002. Rapid detection of myrosinase-producing fungi - a plate method based on opaque barium sulphate formation. *World Journal of Microbiology and Biotechnology*, 18: 73-74.
- Sanchez-Moral, S., Luque, L., and Canaveras, J.C. 2004. Bioinduced barium precipitation in St. Callixtus and domitilla catacombs. *Annals of Microbiology*, 54: 1-12.
- Sanchez-Pastor, N., Pina, C.M., and Fernandez-Diaz, L. 2006. Relationships between crystal morphology and composition in the (Ba, Sr) SO₄-H₂O solid solution-aqueous solution system. *Chemical Geology*, 225: 266-277.
- Sand, W., Gerke, T., Hallmann, R., Schippers, A., 1995, Sulfur chemistry, biofilms, and the (in)direct attach mechanism – a critical evaluation of bacterial leaching: *Applied Microbiology and Technology*, 43: 961-966.
- Saratovkin, D.D. 1959. Dendritic crystallization: New York, Consultants Bureau, 126 pp.
- Sasaki, N. and Minato, H. 1982. Relationship between lattice constants and strontium and calcium contents of hokutolite. *Mineralogical Journal*, 11: 62-71.
- Schultze-Lam, S., Douglas, T., Thompson, J.B., and Beveridge, T.J. 1993. Metal ion immobilization by bacterial surfaces in freshwater environmental. *Water Pollution Research Journal of Canada*, 28: 51-81.
- Senko, J.M., Campbell, B.S., Henriksen, J.R., Elshahed, M.S., Dewers, T.A., and Krumholz, L.R. 2004. Barite deposition resulting from phototrophic sulphide-oxidizing bacterial activity. *Geochimica et Cosmochimica Acta*, 68: 773-780.
- Sermon, P.A., McLellan, N.M., and Collins, I.R. 2004. Formation of BaSO₄ nanoribbons from a molecular mangle. *Crystal Engineering Communications*, 6: 469-473.
- Shen, Y., Buick, R., and Canfield, D.E. 2001. Isotopic evidence for microbial sulphate reduction in the early Achaean era. *Nature*, 410: 77-81.

- Shikazono, N. 1994. Precipitation mechanisms of barite in sulphate-sulphide deposits in back-arc basins. *Geochimica et Cosmochimica Acta*, 58: 2203-2213.
- Stark, A.I.R., Wogelius, R.A., Collins, I.R., and Vaughan, D.J. 2004. Kinetic and thermodynamic controls on the precipitation and morphology of barite (BaSO_4), Extended abstract: Goldschmidt conference proceedings, Copenhagen. Theme 2: The dynamic interface, p. A148.
- Stoner, D.L., Burbank, N.S., and Miller, K.S. 1994. Anaerobic Transformation of Organosulphur Compounds in Microbial Mats from Octopus Springs. *Geomicrobiology Journal*, 12: 195-202.
- Su, H-Y., Lee, J-S., and Yu, S-C. 2002. Dopant effect on hokutolite crystals synthesized with hydrothermal process. *Western Pacific Earth Sciences*, 2: 301-318.
- Suganuma, I., 1928, On the constituents and genesis of a few minerals produced from hot springs and their vicinities in Japan. I. The Akita Hokutolite: *Journal of the Chemical Society of Japan*, 3: 69-73.
- Tazaki, K., Webster, J., and Fyfe, W.S. 1997. Transformation processes of microbial barite to sediments in Antarctica: *Japanese Journal of Geology*, 26: 63-68.
- Teske, A. and Nelson, D.C. 2005. The genera *Beggiatoa* and *Thiothrix*. in Dworkin, M. (Ed.) *The Prokaryotes – an evolving online resource for the microbiological community*, M BETA Release 3.20: http://141.150.157.117:8080/prokPUB/chaphtm/432/01_00.htm
- Torres, M.E., Bohrmann, G., Dube, T.E., and Poole, F.G. 2003. Formation of modern and Paleozoic stratiform barite at cold methane seeps on continental margins. *Geology*, 31: 897-900.
- Van Everdingen, R.O. 1972. *Thermal and Mineral Spring in the Southern Rocky Mountains of Canada: Water Management Service, Department of the Environment, Environment Canada*, 151 pp.
- Wher, J.D. and Sheath, G. 2003. *Freshwater Algae of North America: Ecology and Classification: San Diego, Academic Press*, 950 pp.
- Yee, N., Phoenix, V.R., Konhauser, K.O., Benning, L.G., and Ferris, F.G. 2003. The effect of cyanobacteria on silica precipitation at neutral pH - implications for bacterial silicification in geothermal hot springs. *Chemical Geology*, 199: 83-90.
- Younger, P. 1986. Barite travertine from southwestern Oklahoma and west-central Colorado [Unpublished M.Sc.Thesis]: Oklahoma State University, Stillwater, USA, 163 pp.

Chapter 7 **Conclusions**

There are literally thousands of mineral springs around the world (Waring, 1965), each of which represents an endpoint to a subterranean aquifer. Although some spring waters are augmented by magmatic fluids (Hedenquist and Lowenstern, 1994), most are derived from meteoric waters (rain, snowmelt, flood water, and glacial runoff) that have made their way into the earth by percolating down through permeable strata and/or descending along faults and fissures (Grasby and Hutcheon, 2001). The circuit that spring waters travel, into and out of the Earth, has metaphorical resonance with spiritual narratives of death and rebirth, of descent and arising. The poet Dylan Thomas (1952) likened the force that “drives the water through the rocks” to the force that drives the “red blood” of life through our veins. Scientists generally describe this force more mundanely as ‘hydrologic pressure,’ but do approach springs with reverence for the opportunities they provide to learn about Earth’s hydrologic cycles, and water-rock and mineral-microbe interactions. To scientist-poet Constantine Rafinesque (1836), springs are pores for “the sweat and moisture of this globe” and the wonder in them lies not in the mystical realm, but in their hydrologic and chemical variety:

“How various and unsteady in their sizes
 Contents and functions? Few are always pure
 But liquid fluids of many kinds they throw,
 Sweet or impure, both cold and tepid, warm
 Or hot; that gently rise, or bubbling boil,
 Nay spout on high. Now nearly dry becoming,
 Or full their basins filling to the brim.
 Not only water flows from earthly springs,
 But mineral fluids, holding sulphur, iron,
 Acids and gases, lime, and many salts.”

Carbonate, silica, and iron oxide are by far the most common precipitates from spring water (Pentecost, 2005), but at select springs barite precipitates from waters that have scavenged barium and sulphur deep in the conduits of anoxic aquifers. Rafinesque (1836) would, no doubt, have included spring-precipitated barite among his “stony gems”, arisen “fair and pure of atoms form’d in series superposed,” and all the more wondrous for their global rarity. The three barite-precipitating springs examined in this study yielded important results about physiochemical and biological influences on barite

precipitation, which advance current knowledge of barium's geochemical cycle and have widespread applicability for interpreting barite in the geological record.

Examination of inorganic barite precipitation at Flybye and Twitya Springs, NWT, and Stinking Springs, Utah, revealed that in low temperature ($< 40^{\circ}\text{C}$) depositional environments:

- (1) Microenvironmental parameters, including spring water oxidation rate, barium and sulphate concentrations, the presence of organic acids, and physio-hydrologic conditions, influence the distribution and habit of inorganically precipitated barite crystals.
- (2) Microbial streamers and mats commonly trap inorganically precipitated barite and can act as substrates for precipitation.
- (3) Microbes that colonize the surfaces of substrate-attached 'inorganic' barite crystals may be engulfed by continued crystal growth, and produce moldic porosity when they degrade.

Microbes growing in ambient-temperature spring flow paths commonly initiate, facilitate and/or organize the growth of mineral precipitates (Pentecost, 2005). Microbes can mediate mineral saturation gradients both actively, through bioaccumulation of reactive ions and/or metabolic adjustment of local redox and/or pH conditions (e.g. Arp et al., 1999), and passively, by acting as templates for mineralisation (e.g. Jones et al., 1998). The relative importance of active and passive processes to 'biogenic' mineral precipitation has been demonstrated to vary widely between different microbial species assemblages, and with changing physiochemical conditions, mineralogies, and precipitate habits, i.e. macrocrystalline versus microcrystalline versus amorphous (e.g. Arp et al., 1999; Konhauser et al., 2003; Jones and Renaut, 2007). Investigation of biologically mediated barite precipitation at Flybye, Twitya and Stinking Springs, combined with barite precipitation experiments, generated the following important conclusions regarding the role of microbes in ambient-temperature barite precipitation:

- (1) Chemosynthetic microbes assert influence on barite saturation gradients by establishing and maintaining macroenvironmental redox boundaries in ponded water

and in layered microbial mat communities, as well as microenvironmental redox boundaries around individual microbial cells.

- (2) Diverse microbial groups, including sulphur metabolizing bacteria, cyanobacteria, diatoms, and fungi, can act as passive hosts for barite precipitation.
- (3) Barite precipitation on microbial substrates is favoured by adsorption of barium to extracellular surfaces and extracellular polymeric substances (EPS).
- (4) Barite precipitation inside cell walls and in cellular cavities, first documented in this study, is promoted by active microbial processes including barium bioaccumulation, intracellular sulphur storage, and facultative and nonfacultative sulphur oxidation.
- (5) Differences in metabolic strategy and cellular structure between microbial genera lead to differences in the distribution and microtexture of barite precipitates. Specifically, barite precipitation is more common in and around degrading diatoms than cyanobacteria in carbonate-rich water at Stinking Springs; *Beggiatoa* and *Oscillatoria* cell walls are more readily permineralized by barite than those of *Thiothrix* and *Thioploca* at Flybye Springs; and *Penicillium* is preferentially coated by barite near its hyphal tips, whereas filamentous cyanobacteria and sulphur oxidizing bacteria are coated nonspecifically along their lengths at Flybye Springs.
- (6) Barite precipitation is restricted to microbial biomass only when barium and sulphate are limiting such that spontaneous 'inorganic' barite precipitation is not favoured in solution.

Microbially-mediated mineral precipitation (or biomineralisation) has been investigated intensively in calcium carbonate- (hereafter, carbonate), opaline silica- (hereafter, silica), and iron oxide-precipitating springs, producing information that has had direct application for the interpretation of microbial textures and microfossils in ancient chemical sediments (Walter and Des Marais, 1993). Outstanding questions remain, however, concerning the origin of differential preservation of microbes in these minerals, and the relative importances of environmental versus metabolic influences on microfossil taphonomy (Knoll et al., 2005). Comparison of biomineralisation in barite with biomineralisation in carbonate, silica, and iron oxide expands the geochemical frame of reference of this dialogue, and contributes the following new points for consideration:

- (1) Barite precipitation around dead microbes is facilitated not only by adsorption of cations to extracellular surfaces, but also by release of bioaccumulated barium during cellular decay. Silica, iron and calcium are all bioaccumulated to varying degrees by different microbial groups. Whereas silica is generally precipitated in the skeletal/structural components of silica bioaccumulators (cyst-forming algae, diatoms, radiolarians), iron and calcium are also incorporated into soft tissues and cytoplasm. Release of calcium and iron in purge fluids is not, however, commonly factored into textural interpretations of microfossils in carbonate or iron oxide (cf. Andres et al., 2006; Jones and Renault, 2007). Indeed, calcium and iron bioaccumulation are probably not overly important to initiating precipitation of carbonate on microbes (since ambient calcium and iron concentrations would probably be high, respectively, in carbonate and iron oxide depositing environments), but it might have a microenvironmental role in determining the textural details of microfossils.
- (2) Barite precipitation that is mediated by active metabolic processes is more texturally variable than barite precipitated passively on extracellular microbial templates. Like barite, carbonate and iron oxide saturation gradients are influenced by microbial metabolism (mainly by photosynthesis and sulphur and iron chemosynthesis; Pentecost, 2005), but no metabolic influences have been identified that promote extracellular silica precipitation. This suggests that carbonate, iron oxide and barite microfossils may have higher potential to preserve micro-textural evidence of how the microbe interacted with its chemical environment than microfossils preserved in silica.
- (3) Some micro-textural details of barite precipitation around microbes at Flybye Springs (such as selective permineralisation of *Beggiatoa* and *Oscillatoria* cell walls) are attributable to differences in cellular structure, rather than metabolic strategy. This highlights the fact that microbial taphonomy does not have equal fidelity between genera, which implies that the microfossil record is badly skewed (cf. Walter and DesMarais, 1993). To assess the relationship between similar sized microfossils preserved in chemical sediments of differing mineralogy, it would be useful to

investigate if the same microbial genera are equally prone to fossilization by different minerals.

- (4) In silica and iron oxide springs, high levels of supersaturation can lead to rapid precipitation of amorphous minerals, and are associated with superb microfossil preservation (Konhauser et al., 2003; Jones and Renault, 2007). In contrast, strongly barite and calcium carbonate supersaturated spring waters precipitate inorganic crystalline deposits that can locally preserve casts of microbes but rarely contain body microfossils (Sasaki and Minato, 1982; Jones and Renault, 1996). Rapid mineral precipitation is favoured by steep physiochemical gradients, whereas slower mineral precipitation is favoured by prolonged physiochemical disequilibrium.

Slow precipitation of opaline silica generates low fidelity microfossils (Konhauser et al., 2003), and slow precipitation of iron oxide leads to the formation of crystalline deposits that lack body microfossils (Jones and Renault, 2007). Slow precipitation of barite and calcium carbonate, however, promotes the formation of amorphous and subhedral microcrystals, which are associated with preservation of texturally complex microfossils (Arp et al., 2001; this study). These comparisons therefore suggest that silica and iron oxide are most likely to preserve fossils of extremely niche-limited, (potentially extremophilic) microbes. In terms of understanding Earth's palaeoecological evolution, carbonates and barite may, thus, provide a more useful microfossil record, because they are more likely to preserve fossils of microbes representative of wide-spread, ambient environments (e.g. tidal flats, marshes, and submarine seep fields, rather than restricted haloes around spring and hydrothermal vents).

- (5) The importance of EPS to passive biomineralisation is poorly constrained. The chemistry and viscosity of EPS varies between genera, and with environmental parameters including ionic strength, pH, and % hydration (Schultze-Lam et al., 1993) making EPS a 'wild card' for geochemical modeling of microbially colonised waters (Fein et al., 2001). In some cases adsorption of reactive ions to EPS inhibits mineral precipitation (e.g. Arp et al., 1999); in other systems, adsorption of reactants to EPS leads to precipitation of minerals on and/or within it (e.g. Tazaki et al., 1997). At Stinking Springs, EPS surrounding diatoms limits diffusion of barium released from

decaying diatoms, thus promoting barite precipitation; but adsorption of barium to EPS elsewhere in the Stinking Springs microbial mats may actually inhibit barite precipitation by reducing ambient Ba^{2+} concentrations (cf. Arp et al., 1999). At Twitya Spring, EPS surrounding microbial filaments houses and acts as a substrate for T3 barite, indicating that adsorption of barium to EPS may be important to facilitating barite precipitation. At Flybye Springs, adsorption of barium to the EPS sheaths of pond-dwelling *Thioploca* results in passive barite precipitation around filament bundles; but in nearby flow paths, non-attached EPS remains unmineralized while *Beggiatoa* filaments within it become permineralised and/or filled by barite precipitates. The different influences of sheath and non-attached EPS on mineral precipitation at the springs examined in this study demonstrates that the importance of EPS to passive biomineralisation is highly environmentally specific. Resolving the importance of EPS to the passive biomineralisation of microfossils and authigenic minerals in the geologic record will require microscale constraint of depositional geochemistry, which necessitates continued development of an analogue database from geochemically diverse modern environments where passive biomineralisation takes place in the presence of EPS formed by mixed microbial communities.

Petrographic analysis of relict barite tufa from Flybye Springs produced the first comprehensive description of low temperature subaerially-deposited barite. The co-deposition of 'inorganic' and 'biogenic' lithotypes in the Flybye barite tufa mound indicates that barite's textural development is highly sensitive to fluctuations in the physiochemical and biological context of its depositional environment. Particularly important conclusions regarding the textural development of barite that have direct relevance to the interpretation of barite deposits in the geologic record include the following:

- (1) Biogenic lithotypes form preferentially in barium- and sulphate-limited solutions, whereas inorganic lithotypes form in more strongly barite supersaturated solutions.
- (2) Inorganic lithotypes can form in microbially colonised environments, so they should not be interpreted as indicators of uninhabitable palaeoenvironmental conditions.

- (3) Both biogenic and inorganic lithotypes develop by initial precipitation of fine or microcrystalline barite crystals which act as a textural scaffold for the precipitation of coarser barite cements.
- (4) Both inorganic and biogenic barites precipitated in the presence of microbes have the potential to preserve biomarkers, including microfossils and organic carbon-rich laminae, and should, therefore, be considered potential reservoirs of palaeoecological information.

Important insights regarding the general textural development of chemical sediments gained by comparison of the Flybye barite tufa to carbonate, silica and iron oxide spring deposits, include that:

- (1) Physical and hydrological conditions can, locally, be more important to determining textural lithotype than specific physiochemical or biological parameters. For example, saltation of nuclei can produce coated grains in carbonate, silica, iron oxide or barite (or pyrite); thin mineral rafts will form at low turbulence air-water interfaces when equilibration (of heat, oxygen or gaseous content) between the precipitating solution and atmosphere increases the concentration of one or more precipitate reactant; and, mineralisation of gas bubbles is, similarly, favoured by low turbulence and by disequilibrium between the gas phase and surrounding solution.
- (2) Texturally convergent 'biogenic' lithotypes can form in chemically and mineralogically distinct spring systems because community growth patterns (filamentous streamers, laminar mats, bubbly mats, biofilms) are congruent between microbial genera with widely differing metabolic strategies and physiochemical tolerances.
- (3) Environmental restrictions placed on the growth of macrophytes by thermal spring waters can be mimicked by high sulphur content (and other chemical extremes) in ambient temperature and cold spring flow paths. Chemical sediments should not, therefore, be classified using physiochemically-indicative nomenclature (such as 'thermogene' versus 'metogene'; or thermal 'travertine' versus cold water 'tufa' – Pentecost, 2005) on the basis of textural criteria.

Particulate marine barite provides a proxy record of palaeoproductivity and is useful for analytic reconstruction of trends in ocean redox, Ba/Sr ratios, $^{87}\text{Sr}/^{86}\text{Sr}$ and $\delta^{34}\text{S}$ in both unconsolidated and lithified marine sediments (Kastner, 1999). Barite may prove to be especially useful when it is preserved unaltered in isotopically readjusted carbonates, but will not achieve its full potential utility until the controls on its occurrence are fully constrained. Investigation of barite precipitation and preservation in calcite travertine and tufa, at Stinking Springs and Twitya Spring, respectively, provided the following conclusions:

- (1) Barite crystal habit is influenced by the substrate on which it precipitates; anhedral to subhedral habits form in the presence of microbial biomass, whereas barite precipitated in solution and on calcite crystal phases is euhedral. This finding supports the idea that barite crystal habit may be correlated to specific precipitation mechanisms.
- (2) Biogenic barite crystals (precipitated in direct association with live or degrading biomass) can be co-deposited with inorganic barite. This highlights the importance of microbes in establishing chemically distinct micro-environments, and indicates a role for microbes in determining the abundance and distribution of barite hosted in carbonates.
- (3) Precipitation of barite at Stinking Springs is favoured by bioaccumulation of barium in diatoms. Biogenic (particulate marine) barites in the geologic record may not, therefore, necessarily have Ba/Sr ratios that reflect ambient seawater or porewater compositions.
- (4) Selective precipitation of barite around diatoms (and not around cyanobacteria) at Stinking Springs indicates that all genera of microbes are not equally suited to facilitating precipitation of barite. This raises the possibility that particulate marine barite crystals are not, in fact, a true palaeoproductivity proxy, but rather reflect the selective productivity of diatoms, or other microbial groups that have similar capability to catalyse barite precipitation.
- (5) At Twitya Spring, the abundance and distribution of barite crystals is influenced by the growth rate of co-precipitating calcite. This indicates that barite formation and

preservation in carbonates may take place under controls distinct from those operative in better studied siliclastic sediments.

As noted by Kastner (1999) and Knoll et al. (2005), chemical sediments have limited usefulness for palaeoenvironmental and palaeoecological reconstructions if they experience chemical and textural changes during diagenesis. Superb microfossils preserved in silica spring deposits, for example, commonly lose microtextural details during early diagenetic transformation of opal-A silica to opal-CT silica or microcrystalline quartz (Herdinanita et al., 2000). Microfossils in iron oxides can preserve excellent details, but are commonly geologically ephemeral, because iron oxide is highly soluble and prone to recrystallization (Knoll et al., 2005). Calcium carbonate spring deposits are also prone to early diagenetic recrystallization and sparmicritization, and to dissolution by meteoric waters, all of which can erase or overprint primary depositional textures and microfossils (Pentecost, 2005). These changes can happen rapidly (in less than 50 years – Herdinanita et al., 2000; Pentecost, 2005), complicating comparison of fresh precipitates with Recent relict precipitates, and even more so with their ancient counterparts (Walter and Des Marais, 1993; Konhauser et al., 2003).

Biogenic textures and preserved organic carbon are more diagenetically resistant, however (Walter, 1976; Grotzinger and Knoll, 1999; Altermann and Kazmierczak, 2003), and, despite the apparent improbability of primary microfossil textures surviving diagenesis, there are many examples of Paleozoic carbonates and silica that do preserve taxonomically identifiable microfossils (Birnbaum et al., 1986; Grotzinger and James, 2000; Petrov and Semikhatov, 2001), and several putative examples in Archean silica and silica-replaced carbonates (Awramik, 2004). Barite microfossils from Flyby Springs have persisted through early diagenetic changes, including deposition of cements and aggradational neomorphism. Barring late-diagenetic recrystallization under burial pressure, or exposure to reducing pore fluids, barite has excellent geologic persistence (Buick et al., 1981; Shen et al., 2001; Knoll et al., 2005), and may be better suited to preserving primary textures than carbonate, iron oxide or opaline silica.

Peculiarly, however, there have been very few reports of microfossils, or even biogenic textures preserved in geologic barite (Graber, 1988; Fu et al., 2004; Aloisi et al.,

2004). This may be partly explained by the fact that many large, low-temperature barite deposits formed by Paleozoic cold methane seepage were originally interpreted as high temperature hydrothermal deposits (Torres et al., 2003; Aloisi et al., 2004) and thus overlooked as sources of palaeoecological information (Graber, 1988). The importance of microbes as a barium source has been recognized in the formation of particulate marine barite (Bishop et al., 1981; Ganeshram et al., 2003), but has not yet been applied to the interpretation of stratiform barites formed in vent and seep fields where barite precipitation is also likely to be microbially mediated (cf. Reidinger et al., 2006).

Until recently, research into mineral-microbe interactions in the barium-sulphur-sulphate system has been hindered not only by the inaccessibility of marine barite-precipitating environments, but also by misinformation regarding the abundance of accessible barite-precipitating subaerial springs. The inconsistent nomenclature of barium sulphate (barite, baryte, radiobarite, radiobaryte, hepatite and hokutolite), has led to a perception among geologists that subaerial precipitation of barium sulphate is incredibly rare, with the result that the few documented barite-precipitating springs have been understudied compared to their carbonate, silica and iron oxide counterparts. Springs that precipitate barite as a dominant or accessory mineral phase provide important opportunities to investigate controls on barite precipitation. The textural responsiveness of barite precipitated at the Flybye, Twitya and Stinking Springs provides an exciting indication that petrographic analysis of low and ambient temperature barite in the geologic record will, in time, provide a robust means to investigate Earth's palaeoenvironmental and palaeoecological history. If recent reports of massive sulphate deposits on Mars and Europa are true (Dalton et al., 2005; Knoll et al., 2005; Andrews-Hanna et al., 2007), constraint of both inorganic and biological influences on subaerial barite precipitation may also be a precondition to understanding the geochemical, atmospheric and potential biological evolution of other planetary systems.

References

- Andres, M.S., Sumner, D.Y., Reid, R.P. and Swart, P.K. 2006. Isotopic fingerprints of microbial respiration in aragonite from Bahamian stromatolites. *Geology*, 34: 973-976.
- Andrews-Hanna, J.C., Phillips, R.J., and Zuber, M.T. 2007. Meridiani Planum and the global hydrology of Mars. *Nature*, 446: 163-166.
- Aloisi, G., Wallmann, K., Bollwerk, S.M., Derkachev, A., Bohrmann, G. and Suess, E. 2004. The effect of dissolved barium on biogeochemical processes at cold seeps. *Geochimica et Cosmochimica Acta*, 68: 1735-1748.
- Arp, G., Theil, V., Reimer, A., Michaelis, W. and Reitner, J. 1999. Biofilm exopolymers control microbialite formation at thermal springs discharging into the alkaline Pyramid Lake, Nevada, USA. *Sedimentary Geology*, 126: 159-176.
- Bishop, J.K.B. 1988. The barite-opal-organic carbon association in oceanic particulate matter. *Nature*, 332: 341-343.
- Dalton, J.B., Prieto-Ballesteros, O., Kargel, J.S., Jamieson, C.S., Jolivet, J., and Quinn, R. 2005. Spectral comparison of heavily hydrated salts with disrupted terrains on Europa. *Icarus*, 177: 472-490.
- Fein, J.B., Martin, A.M., and Wightman, P.G., 2001. Metal adsorption to bacterial surfaces: Development of a predictive approach. *Geochimica et Cosmochimica Acta*, 65: 4267-4273.
- Fortin, D. and Langley, S. 2005. Formation and occurrence of biogenic iron-rich minerals. *Earth-Science Reviews*, 72: 1-19.
- Fu, B., Aharon, P., Byerly, G.R., and Roberts, H.H. 1994. Barite chimney on the Gulf of Meico slope: Initial report on their petrography and geochemistry. *Geo-Marine Letters*, 14: 1432-1457.
- Ganeshram, R.S., Francois, R., Commeau, J. and Brown-Leger, L. 2003. An experimental investigation of barite formation in seawater. *Geochimica et Cosmochimica Acta*, 67: 2599-2605.
- Graber, K.K. 1988. Stratigraphy and petrography of bedded barite in phosphatic Devonian Slaven chert, Toquima Range, Nye County, central Nevada [Unpublished MSc Thesis]: Houston, Texas, University of Houston, 294 pp.
- Grasby, S.E., and Hutcheon, I. 2001. Controls on the distribution of thermal springs in the southern Canadian Cordillera. *Canadian Journal of Earth Sciences*, 38: 427-440.
- Hedenquist, J.W., and Lowenstern, J.B. 1994. The role of magmas in the formation of hydrothermal ore deposits. *Nature*, 370: 519-527.
- Herdianita, N.R., Browne, P.R.L., Rodgers, K.A., and Campbell, K.A. 2000. Mineralogical and textural changes accompanying ageing of silica sinter. *Mineralium Deposita*, 35: 48-62.
- Huston, D.L. and Logan, G.A. 2004/ Barite, BIFs and bugs: evidence for the evolution of the Earth's early hydrosphere. *Earth and Planetary Science Letters*, 220: 41-55.
- Jones, B. and Renaut, R.W. 1996. Morphology and growth of aragonite crystals in hot spring travertines at Lake Bogoria, Kenya Rift Valley. *Sedimentology*, 43: 323-340.

- Jones, B., Renaut, R.W. and Rosen, M.R. 1998. Microbial biofacies in hot-spring sinters: a model based on Ohaaki Pool, North Island, New Zealand. *Journal of Sedimentary Research*, 68: 413-434.
- Kastner, M. 1999. Oceanic minerals: Their origin, nature of their environment, and significance. *Proceedings of the National Academy of Science, USA*, 96: 3380-3387.
- Knoll, A.J., Carr, M., Clark, B., Marais, D.D., Farmer, J.D., Fischer, W.W., Grotzinger, J.P., McLennan, S.M., Malin, M., Schroder, C., Squyres, S., Tosca, N.J., and Wdowiak, T. 2005. An astrobiological perspective on Meridiani Planum. *Earth and Planetary Science Letters*, 240: 179-189.
- Konhauser, K.O., Jones, B., Reysenbach, A-L., and Renaut, R.W. 2003 Hot spring sinters; keys to understanding Earth's earliest life forms. *Canadian Journal of Earth Sciences*, 40: 1713-1724.
- Paytan, A., Kastner, M., Martin, E.E., Macdougall, J.D., and Herbert, T. 1993. Marine barite as a monitor of seawater strontium isotope composition. *Nature*, 366: 445-449.
- Pentecost, A. 2005. *Travertine*. Springer-Verlag, Heidelberg, 429 pp.
- Rafinesque, C.S. 1836. Chapter four, Mineral Springs and Volcanoes. *In The World, or Instability, a poem with notes and illustrations*. Philadelphia and London, 248 pp.
- Riedinger, N., Kasten, S., Groger, J., Franke, C., and Pfeifer, K., 2006. Active and buried authigenic barite fronts in sediments from the Eastern Cape Basin. *Earth and Planetary Sciences Letters*, 241: 876-887.
- Sasaki, N. and Minato, H. 1982. Relationship between lattice constants and strontium and calcium contents of hokutolite. *Mineralogical Journal*, 11: 62-71.
- Schultze-Lam, S., Douglas, T., Thompson, J.B., and Beveridge, T.J., 1993, Metal ion immobilization by bacterial surfaces in freshwater environmental: *Water Pollution Research Journal of Canada*, v. 28, p. 51-81.
- Tazaki, K., Webster, J., and W.S. Fyfe. 1997. Transformation processes of microbial barite to sediments in Antarctica. *Japanese Journal of Geology*, 26: 63-68.
- Thomas, D. 1952. The force that through the green fuse drives the flower. *In Collected poems of Dylan Thomas*, 6th Edition. New York, New Directions Publishing Corporation, p. 43.
- Torres, M.E., Bohrmann, G., Dube, T.E. and Poole, F.G. 2003 Formation of modern and Paleozoic stratiform barite at cold methane seeps on continental margins. *Geology*, 31: 897-900.
- Walter, W.R., Des Marais, D.J. 1993. Preservation of biological information in thermal spring deposits; developing a strategy for the search for fossil life on Mars, *Icarus*, 101: 129-143.

Appendix 1. Field notes and preliminary data from mineral springs in the Sahtu Settlement Area, NWT (reported to the Aurora Research Institute and Sahtu Renewable Resource Board, June 2006).

| Name | Type | Spring Mound? | Latitude | Longitude | T (°C) | pH | Dissolved Oxygen (mg/L) | Minerals* | Notable Biota |
|--|------------------------|---------------|------------|-------------|--------|------|-------------------------|---|-------------------------------------|
| Flybye Springs (Willow Camp Lick) | cold sulphur | yes | 64°17.837 | 130°33.223 | 8 | 7.3 | 0.5 | sulphur, barite, diatom silica, framboidal pyrite | bacteria, cyanobacteria, caribou |
| BR Spring | hot sulphur | no | 63°59.097 | 130°27.452 | 41.2 | 7 | - | sulphur, gypsum, framboidal pyrite | bacteria, fungi |
| Beaver Dammed | cold sulphur (?) | yes | 63°56 | 130°17 | - | - | - | - | beavers |
| Cold Sulphur Stream | cold sulphur | no | 64°16.961 | 130°14.993 | 8 | 7 | - | sulphur, gypsum | bacteria, cyanobacteria |
| Hailstone Creek Spring | cold sulphur | no | 63°54.114 | 129°49.300 | - | - | - | - | - |
| Stan Stevens Cabin Springs | cold carbonate-sulphur | yes | 64°38.906 | 129°12.367 | 8.5 | 8.01 | 0.75 | calcite, sulphur, gypsum | bryophytes, cyanobacteria |
| Moonscape Springs | cold carbonate | yes | 64°31'53.3 | 129°15'08.9 | 10.5 | 7.46 | 1.31 | calcite, diatom silica, dolomite (detrital?) and amorphous FeOH | cyanobacteria, diatoms, chironimids |
| Landing Strip Iron Springs | cold carbonate-iron | yes | 64°17.099 | 129°42.807 | 10.2 | 7.66 | 1.11 | calcite, dolomite | bryophytes, cyanobacteria |
| Twitya Springs | hot carbonate-sulphur | yes | 63°48.202 | 129°51'53.8 | 23.6 | 7.81 | 0.61 | calcite, barite, sulphur, silica | bacteria, cyanobacteria |
| Sculpin Hot Springs | hot carbonate-sulphur | yes | 63°56'12.1 | 129°18'53.7 | 16.7 | 7.49 | 0.95 | calcite, gypsum, barite, silica | bryophytes, brine shrimp, snails |
| Limnae Springs | hot carbonate-sulphur | yes | 64°08'48.3 | 128°25'53.6 | 20.8 | 7.56 | 1.84 | calcite, gypsum, silica | charophytes, bryophytes |
| Salt Flats | cold salt | no | 64°51'03.5 | 127°14'18.6 | - | - | - | halite, gypsum | - |

*Determined by powder X-ray analysis, listed in decreasing abundance

Appendix 2 Spring water chemistry and mineral saturation modeling – an evaluation of methods

The physiochemistry of waters from Flybye and Twitya Springs, NWT, was determined by field measurement of pH, conductivity, temperature, and dissolved oxygen (as described in Chapters 2, 4 and 5). This appendix elaborates upon and evaluates methods used for further characterization of water samples – it is divided into three parts: (1) sample collection, (2) analytical methods, and (3) SOLMINEQ88 saturation indices.

- (1) **Sample collection:** Water samples were collected through sterile syringes fitted with 45 μm FisherBrand membranes. The syringes were ‘contamination cleansed’ by rinsing with spring water before sample collection. Collected water were stored in sterile 250 ml Nalgene containers filled to a positive meniscus (to minimize potential for exchange between water and gas trapped in headspace).

Evaluation—While filtering is beneficial to prevent inadvertent collection of organic and inorganic detritus, it is problematic in that it inevitably results in (at least partial) cooling, oxidation of reduced chemical species, and release of dissolved gases. These changes may induce precipitation of mineral phases within the Nalgene container.

- (2) **Analytical Methods:** Two methods of geochemical analysis were used to determine the chemical constituents in the collected spring waters. It is worth noting that, while water analyses are important to characterize the nature of spring waters, the error of any analytical method is likely to be far exceeded by temporal variations in spring water composition (see Tables 2-1 and 4-1).

(a) Inductively Coupled Plasma Mass Spectrometry (ICP-MS)

Water samples were analysed by ICP-MS at the University of Saskatchewan (<http://www.usask.ca/geology/icpms.html>). ICP-MS analysis requires only several milliliters of solution, which are removed from sample containers by pipette. The water samples are nebulized and suspended in a carrier argon gas before ionization and mass separation. The mass spectrometer identifies ions with different mass by their differential deflection under an ion beam, and is sensitive enough to identify elements in concentrations ranging from nanograms to milligrams per litre (8 orders of magnitude). Data generated include the number and absolute abundance of elements present in a sample. Three subsamples of each water sample (four from Flybye Springs, two from Twitya Spring) were run in sequence at the University of Saskatchewan to assess analytical precision. The ICP-MS has precision of +/- 1.7% when peak detection limits have been calibrated to standards that have elemental concentrations within two orders of magnitude of the sample in question (Faires, 1993).

Evaluation—ICP-MS is a fast and well-tested method for characterizing the chemistry of water samples. It has the benefit that it can detect multiple elements in single runs, and is thus extremely efficient and cost effective. Limitations of the method for analysis of spring water include the fact that spring waters commonly have anomalous chemistry compared to instrument calibration standards designed for

surface or ground water analysis (see Chapter 2 for discussion of barium determination by ICP-MS), and that it provides *elemental* rather than *ionic* data. ICP-MS data are commonly reported as ions, however, based on speciation predicted by the pH, temperature and Eh at the time of sample collection. Due to the possibility that sample methods may alter some or all of these parameters, field measurements may not accurately reflect the character of samples provided for ICP-MS analysis. For this reason, redox and pH sensitive elemental speciations (e.g. bicarbonate vs. carbonate, sulphide vs. sulphate, and reduced vs. oxidized iron) reported in this thesis and other literature should be considered 'most probable', rather than quantitative, if they have been determined by ICP-MS. A further limitation of the ICP-MS method is that it cannot identify elements that may have precipitated from sample solutions between collection and analysis.

(b) Neutron Activation Analysis (NAA)

Neutron activation analysis detects the concentration of specific elements in a sample by first producing excited radioisotopes (by introduction of the sample to the radiation field of a nuclear reactor), and then using a gamma spectrometer to detect element specific radioactive decay patterns emitted as the isotopes revert to stable form. This method can be used for determination of elements in solid, fluid or mixed state samples, and has the advantage that it is nondestructive, extremely sensitive, and precise (0.3-0.6 wt. %, or better than 1% dissolved solutes). Seven mat and water samples from Flybye Springs were analysed at the University of Alberta SLOWPOKE facility (<http://www.ualberta.ca/~slowpoke/NAA.htm>) for barium, strontium and manganese.

Evaluation— In contrast to ICP-MS, NAA involves whole-sample analysis so it will detect both dissolved and precipitated spring water constituents. Limitations of the method include that it can only identify elements that have readily excitable radioisotopes (excluding C, H, O, Pb, N, and P), and that it is time-consuming (dependent upon the half-lives of the radioactive elements being measured). Additionally, since the gamma spectrometer must be calibrated to detect certain decay signatures, NAA may require some pre-existing knowledge of what may be in the sample.

- (3) **SOMINEQ88 saturation indices:** SOLMINEQ88 is a geochemical modeling program that determines mineral saturation indices for over 270 inorganic and 80 organic aqueous species and 214 minerals (Perkins et al., 1990). It has a thermodynamic database capable of modeling water-rock reactions up to 350°C, and has algorithms to adjust element activity ratios to changes in ionic concentration (via the Pitzer activity coefficient model), pressure, and ongoing equilibrium mineral precipitation (Perkins et al., 1990). Saturation indices reported in Chapters 2, 4 and 5 were calculated from input data generated by ICP-MS analysis using field measurements to set pH, temperature, and Eh parameters.

Evaluation— Saturation indices are useful in that they predict the thermodynamic propensity of certain mineral phases to precipitate or dissolve. They do not, however, accommodate kinetic restrictions to mineral precipitation, nor do they accommodate non-equilibrium conditions. For these reasons, they have limited value for predicting

the behaviour of spring systems. None of the spring waters examined in this thesis are in redox or gaseous equilibrium with the atmosphere into which they emerge. Nonequilibrium influences are also introduced to mineral precipitation by adsorption of dissolved ions to microbial biomass, and bioaccumulation of ions within living microbes (see Discussion, Chapter 5). Saturation indices are, nonetheless, included in this thesis because:

- They provide a quantitative measure of the 'relative likelihood' that various mineral phases will precipitate in a spring flow path.
- Since they do not accommodate biological influences on mineral precipitation, they provide an 'abiological' comparison against which to gauge the importance of biomineralisation processes (cf. Parraga et al., 1998).
- Provision of saturation indices has become standard practice in geochemical and springs literature and their omission would limit evaluation of similarities and differences between the Flybye and Twitya Springs and published descriptions of other spring systems.

References

- Faires, L.M. 1993. Methods of analysis by the US Geological Survey National Water Quality Laboratory – Determination of metals in water by inductively coupled plasma mass spectrometry. USGS Open-File Report 92-634, 28 pp.
- Parraga, J., Rivadeneyra, M.A., Delgado, R., Iniguez, J., Soriano, M., Delgado, G. 1998. Study of biomineral formation by bacteria from soil equilibria. *Reactive and Functional Polymers*, 36: 265-271.
- Perkins, E.H., Kharaka, Y.K., Gunter, W.D., DeBraul, J.D. 1990. Geochemical modeling of water-rock interactions using SOLMINEQ88. *Chemical Modeling of Aqueous Systems II*. American Chemical Society, Washington, DC, p. 117-127.

| Flybye Springs, NWT | | 64°17.837 130°33.223 |
|----------------------------|--|---|
| Fby (2004) - | | (barite, sulphur, diatom silica, framboidal pyrite, gypsum) |
| 2 | | stromatolitic layer |
| 3 | | heavily cemented bubble/sheety tufa |
| 4 | | cobble of sheety tufa with root weathering |
| 5 | | bubbly/stromatolitic |
| 6 | | stromatolitic |
| 11 | | conglomerate |
| 12 | | conglomerate/stromatolitic |
| 13 | | bubbly |
| 15 | | weathered barite above D4 |
| 16 | | fresh sulphur/gypsum coating on stromatolitic tufa chips |
| 17 | | streamers below D1 |
| 18 | | streamers below D1 |
| 20 | | streamers on dense stromatolitic lamina |
| 21 | | sheety |
| 24 | | bubbly |
| 26 | | lithoclast conglomerate |
| 27 | | convex stromatolitic laminae |
| 30 | | stromatolitic |
| 31 | | lithoclast conglomerate |
| 41 | | bubbly conglomerate with coated grains |
| 46 | | dense stromatolitic layer with topside streamers |
| 49 | | stromatolitic with topside streamers |
| F (2005) - | | |
| 4 | | loose sediment from D4 flow path |
| 5 | | bubbles/sheets/pillars |
| 8 | | sheets and curved porosity |
| 9 | | sheets/stromatolitic |
| 10 | | undulatory sheets |
| 11 | | coated grains |
| 12a | | sheety |
| 12 | | conglomerate |
| 13 | | streamers |
| 16 | | platy tufa |
| 18 | | streamers from top of mound |
| 19 | | sheety/stromatolitic |
| 20 | | weathered platy tufa, 2nd cements |
| 21 | | stromatolitic/undulatory sheets |
| 27 | | fresh mat and sulphur coating on border of wallow |
| 28 | | frost spalded chips from crown of mound |
| 30 | | stromatolitic cobble with fine barite strings spanning porosity |
| 33 | | bubbly/sheety cobble |
| 41 | | isopachous cements in porous conglomerate |
| 43 | | encrusting streamers on chip of conglomerate |
| 45 | | pendant cements 'popcorn' on stromatolitic cobble |
| 46 | | bubbly/sheety porous stromatolitic laminae |
| 47 | | fresh sulphur encrustation in flow path of D2 |
| 51 | | stromatolitic/bubbly |

| Stinking Springs, NW Utah | | 41.577° 112.235° |
|----------------------------------|--|---|
| S (2003)- | | (calcite, barite, clay, sulphur, silica, diatom silica) |
| 1 | | loose sediment from flow path |
| 2 | | relict tufa - layered mats, crusts, spongy textures |
| 3 | | relict tufa with plant casts |
| 4 | | soft sediment cobbles |
| 5 | | relict tufa - plant/stem casts |
| 6 | | relict tufa with stem casts |
| 7 | | relict tufa - lithified fragments |
| 8 | | crusts from side of flow path |
| 9 | | relict tufa - lithified mat & crust fragments |
| 10 | | relict tufa - spongy texture |
| 11 | | relict tufa - lithified crust fragments |
| 12 | | fresh crusts (> 3cm ²) |
| 13 | | barite cements in fragmented calcite tufa |
| 15 | | fresh crusts (fragmented) |
| 16 | | relict tufa with stem casts |
| 17 | | layered relict tufa - young, near levees |
| 19 | | fresh crusts from main flow path |

| | |
|----|--|
| 25 | crusts with distinct surface nodes |
| 29 | semi-cohesive mat over loose sediment, near levees |
| 32 | mat from upper flow path |
| 34 | mat at levee 2 |
| 36 | lithified fragments bound by mat, 1 m beyond levee |
| 37 | mat on terrace 1 - mid flow |
| 38 | mat on terrace 1 - edge of flow - surface nodes |
| 39 | mat on terrace 2 - mid flow path |
| 45 | lithified crust with nodes near SS44 |

Twitya Springs, NWT 63°48.202 129°51'53.8

| | |
|-------------------|---|
| T (2005) - | (calcite, barite, sulphur, clay) |
| 1 | coating on cobble from basal stream |
| 2 | crystallographic dendrites and splaying calcite rinds on lithic nucleus, upper flow, zone 2 |
| 3 | crystallographic dendrites, coating branch, zone 3 |
| 4 | "", zone 2/3 (~ 5 m) |
| 5 | noncrystallographic dendrites, travertine mound |
| 6 | layered dendrites, behind travertine mound (zone 3/4) |
| 7 | layered dendrites, surface weathered travertine mound (z4) |
| 8 | layered dendrites, surface weathered travertine mound (z4) |
| 9 | noncrystallographic dendrites, travertine mound |
| 10 | noncrystallographic dendrites, travertine mound |
| 11 | hydrated green portion of travertine mound |
| 12 | crystallographic and noncrystallographic dendrites, zone 3 |
| 13 | cemented landslide debris, zone 1 |
| 14 | dense dendrites from pool on travertine mound, zone 4 |
| 15 | coated cobble from mid-lower flow path, zone 3 |
| 16 | " |
| 17 | feather' dendrites with visible midline, apex of mound |
| 18 | thin calcite rinds, upper middle flow path, zone 3 |
| 19 | fragmented calcite rinds on landslide debris, upper middle flow path, zone 2 |
| 20 | abutting dendrite fans, topside of travertine mound |
| 21 | abutting dendrite laminae, convoluted crown of travertine mound |
| 22 | abutting dendrite laminae, weathered portion of travertine mound |
| 23 | crystallographic dendrites, coating branch, zone 3 |
| 24 | dense cemented travertine, central, front face of travertine mound |
| 25 | " |
| 26 | rubble of dendrites from basal channel |